https://DOI.org/10.15388/vu.thesis.262
https://orcid.org/0000-0002-1777-9781

VILNIUS UNIVERSITY

Ieva

GENDVILIENĖ

Development and evaluation of the innovative 3D printed scaffolds for bone regeneration *in vitro* and *in vivo*

DOCTORAL DISSERTATION

Medicine and Health Science,

Medicine (M 001)

VILNIUS 2021

This dissertation was written between 2015 and 2021 in Vilnius University, Faculty of Medicine. The research was supported by Research Council of Lithuania.

Academic supervisor –
Prof. Dr. Vygandas Rutkūnas (Vilnius University, Medicine and Health Science, Odontology, M 002).

Academic consultant –
Dr. Virginija Bukelskienė (Vilnius University, Natural Sciences, Biochemistry, N 004).

This doctoral dissertation will be defended in a public meeting of the Dissertation Defence Panel:
Chairman – Prof. Dr. Tomas Linkevičius (Vilnius University, Medicine and Health Science, Odontology, M 002).

Members:
Assoc. Prof. Dr. Arūnas Barkus (Vilnius University, Medicine and Health Science, Medicine, M 001);
Prof. Dr. Gintaras Janužis (Lithuanian University of Health Sciences, Medicine and Health Science, Odontology, M 002);
Assoc. Prof. Dr. Francesca Mangione (University of Paris (France), Medicine and Health Science, Odontology, M 002);
Prof. Dr. Saulius Šatkauskas (Vytautas Magnus university, Natural Sciences, Biochemistry, N 004).

The dissertation shall be defended at a public meeting of the Dissertation Defence Panel at 15:00 on December 17, 2021 in the main hall of the Faculty of Medicine.
Address: 21 M.K. Čiurlionio Street, Vilnius, Lithuania
Phone No.: +370 686 12017; email: mf@mf.vu.lt

The text of this dissertation can be accessed at the libraries of (name of the institutions granted the right to conduct doctoral studies in alphabetical order), as well as on the website of Vilnius University:
www.vu.lt/lt/naujienos/ivykiu-kalendorius

https://DOI.org/10.15388/vu.thesis.262
https://orcid.org/0000-0002-1777-9781

VILNIAUS UNIVERSITETAS

Ieva

GENDVILIENĖ

Inovatyvių 3D spausdintų karkasų, skirtų kaulinei regeneracijai, sukūrimas ir įvertinimas *in vitro* ir *in vivo*

DAKTARO DISERTACIJA

Medicinos ir sveikatos mokslai,

Medicina (M 001)

VILNIUS 2021

Disertacija rengta 2015–2021 metais Vilniaus universiteto Medicinos fakultete.
Mokslinius tyrimus rėmė Lietuvos mokslo taryba.

Mokslinis vadovas:
prof. dr. Vygandas Rutkūnas (Vilniaus universitetas, medicinos ir sveikatos mokslai, odontologija, M 002).
Mokslinė konsultantė:
dr. Virginija Bukelskienė (Vilniaus universitetas, gamtos mokslai, biochemija, N 004).

Gynimo taryba:
Pirmininkas – **prof. dr. Tomas Linkevičius** (Vilniaus universitetas, medicinos ir sveikatos mokslai, odontologija – M 002).
Nariai:
doc. dr. Arūnas Barkus (Vilniaus universitetas, medicinos ir sveikatos mokslai, medicina M 001).
prof. dr. Gintaras Janužis (Lietuvos sveikatos mokslų universitetas, medicinos ir sveikatos mokslai, odontologija – M 002).
doc. dr. Francesca Mangione (Paryžiaus universitetas (Prancūzija), medicinos ir sveikatos mokslai, odontologija – M 002).
prof. dr. Saulius Šatkauskas (Vytauto Didžiojo universitetas, gamtos mokslai, biochemija – N 004).

Disertacija ginama viešame Gynimo tarybos posėdyje 2021 m. gruodžio 17 d. 15:00 val. Vilniaus universiteto Medicinos fakulteto Didžiojoje auditorijoje. Adresas – M. K. Čiurlionio g. 21, Vilnius, Lietuva, tel. 8 686 12 017; el. paštas mf@mf.vu.lt.

Disertaciją galima peržiūrėti bibliotekose ir Vilniaus universiteto interneto svetainėje adresu*: https://www.vu.lt/naujienos/ivykiu-kalendorius*

Acknowledgements

This thesis becomes a reality with the kind support and help of many people. I want to extend my sincere thanks to all of them:

My supervisor, Prof. Dr. Vygandas Rutkūnas, who made this work possible. Your insightful feedback pushed me to sharpen my thinking and brought my work to a higher level.

My academic consultant, Dr. Virginija Bukelskienė, for the consultations and help to prepare the dissertation.

Prof. Dr. Reinhilde Jacobs for the consultations, kind help and co-operation throughout my studies.

My colleagues from Institute of Odontology, Faculty of Medicine, Vilnius University; Department of Biological Models, Institute of Biochemistry, Life Sciences Center, Vilnius University – especially Dr. Milda Alksnė, Dr. Egidijus Šimoliūnas; Laser Research Center, Department of Quantum Electronics, Faculty of Physics, Vilnius University; Prof. K. Barsauskas Ultrasound Research Institute, Kaunas University of Technology; UAB „3D Creative"; National Center of Pathology, Affiliate of Vilnius University Hospital Santaros Klinikos and all DIGITORUM team for their wonderful collaboration, comments, help with creating 3D printed innovative scaffolds, analysing the results, thinking out of the edge, even when things seemed very complicated.

My students – Milda Vitosytė and Eglė Marija Jonaitytė for assisting me in the surgeries, good mood, and enthusiasm throughout the research.

My family and friends for the endless support, believing in me and providing happy distractions to rest my mind outside my research.

CONTENTS

THE LIST OF ABBREVIATIONS

ABBM – anorganic bovine bone mineral

ALP – alkaline phosphatase

ASC – adipose tissue-derived stem cells

BG – bioglass 45S5

Bio-Oss – Geistlich Bio-Oss®

BMA – bone marrow aspirate

BMAC – bone marrow aspirate concentrate

BMP – bone morphogenetic proteins

BMSC – bone marrow-derived mesenchymal stromal cells

CAD/CAM – computer-assisted design and manufacturing

CAF – coronally advanced flap

CCPC – coralline carbonated calcium phosphate cement

cECM – cell-derived extracellular matrix

CT – computed tomography

DBM – demineralized bone matrix

DIW – direct ink writing

DMC – dimethyl carbonate

DPL – digital projection lithography

DPBS – Dulbecco's phosphate-buffered saline

DPSC – dental pulp stem cells

ECM – extracellular matrix

EDTA – ethylenediaminetetraacetic acid

EMD – enamel matrix derivative

FDA – Food and Drug Administration

FDM – fused deposition modelling

FFF – fused filament fabrication

GAG – glycosaminoglycans

GBR – guided bone regeneration

HA – hydroxyapatite

HME – Hot-melt extrusion

HU – Hounsfield units

IL – interleukin

IMDM – Iscove's Modified Dulbecco's Medium

MDS – melt-deposition system

MSC – mesenchymal stem cells

nECM – natural extracellular matrix

OCN – osteocalcin

P – porosity

PBS – phosphate-buffered saline

PDC – periosteum-derived cells

PDGF-AB – platelet-derived growth factor AB

PEEK – polyether ether ketone

PLA – polylactic acid

PLLA – poly(l-lactide) acid

PLDA – poly(d-lactide) acid

PMMA – polymethylmethacrylate

PPP – acellular plasma layer

PRF – platelet-rich fibrin

PRP – platelet-rich plasma

RBC – red blood cell

rhBMP-2 – recombinant bone morphogenetic proteins-2

RUNX2 – runt-related transcription factor 2

SCTG – subepithelial connective tissue graft

SEM – scanning electron microscopy

SLS – selective laser sintering

TCP – tricalcium-phosphate

TGF- β – Transforming Growth Factor Beta

VEGF – vascular endothelial growth factor

3D – three-dimensional

1. INTRODUCTION

1.1. RELEVANCE OF THE STUDY

Nowadays, the number of performed bone augmentation surgeries in various fields of medicine is growing due to an ageing population, improved life quality, and the increase in life expectancy [1,2]. Therefore, the need for bone substitutes and biomaterials is rising in various clinical situations such as cranioplasty or spinal fusion in neurosurgery, fracture nonunions or foot and ankle surgeries in orthopaedics, alveolar bone grafting in oral and maxillofacial surgeries [3–5].

Bone augmentation is performed by restoring a bone defect with various bone substitutes, ideally replacing a lost bone volume and structure, providing good mechanical stability, achieving a graft's predictable vascularisation, and subsequently remodelling subject to the augmented site requirements [6]. Although autologous bone grafts have been considered the *gold standard* and have shown excellent clinical success, their use is associated with some significant disadvantages: postoperative discomfort, chronic donor site pain, fracture, infection, hernia formation, sensory disturbances, bleeding, bruising, a limited number of donor sites and volume [5,7,8]. Moreover, existing bone substitutes (allogenic, xenogenic, alloplastic) fail to match all the ideal bone graft criteria and are usually characterized by osteoconductive features instead of osteoinductive ones [9,10]. Therefore, the research and development in bone augmentation may have played a significant role in accepting tissue engineering as a feasible treatment choice in medicine and dentistry [11,12].

One of the most advanced alternatives to bone substitutes is a three-dimensional (3D) composite scaffold that could control cell microenvironment, proliferate, and migrate during the development of a new bone [13,14]. Various organic and inorganic biomaterials may be used alone or in different combinations to develop an ideal bone scaffold [14,15]. Moreover, these osteoconductive scaffolds may be enhanced with various cell- or growth-factor-based tissue engineering techniques to promote osteogenesis and enhance scaffolds with osteoinductive features [1]. However, the composition of materials and scaffold decoration techniques are not the only essential features for producing a substitute suitable for bone tissue regeneration. Studies have shown that mechanical properties and biological performance are strongly affected by the morphology of a scaffold (porosity, pore size, interconnectivity) [16]. Therefore, fused deposition modelling (FDM) is one of the most promising, easiest and low-cost technologies, providing good mechanical properties and highly controllable porosity meeting the

requirements for a bone graft [17]. Currently, such an ideal bone scaffold with certified clinical indications has not yet been developed [5,18]. Therefore, the limitations of existing bone grafting procedures and bone substitutes have led to a strong clinical need to develop and evaluate newly designed biomaterials.

1.2. AIM OF THE STUDY

To develop an innovative topologically-ordered scaffold for bone regeneration and evaluate its properties *in vitro* and *in vivo*.

1.3. OBJECTIVES OF THE RESEARCH

1. To evaluate the morphology, printing accuracy, porosity of 3D scaffolds printed from industrial polylactic acid (PLA) filaments with different FDM 3D printers.
2. To produce suitable diameter filaments from PLA particles, composite filaments from PLA and hydroxyapatite (HA), PLA and bioglass 45S5 (BG) by hot-melt extrusion.
3. To evaluate the morphology, printing accuracy, and porosity of produced PLA, PLA/HA and PLA/BG scaffolds and compare the results with industrial PLA scaffolds.
4. To evaluate bone tissue regeneration in osteoconductive scaffolds (*in vivo* stage I) using the Wistar rat critical-size calvarial defect model.
5. To evaluate bone tissue regeneration in innovative osteoinductive 3D scaffolds from osteoconductive ones enhanced with dental pulp stem cells (DPSC) or their extracellular matrix (ECM) (*in vivo* stage II) using the Wistar rat critical-size calvarial defect model and compare the obtained results with the samples of *in vivo* stage I.

1.4. SIGNIFICANCE OF THE STUDY

Recently, the majority of bone augmentations in clinical practice have been performed using autogenous, allogeneic, or xenogeneic bone grafts, as no composite 3D scaffolds that could meet most of the ideal bone substitute requirements have been developed. In this study, innovative topologically ordered 3D scaffolds were created using the combination of HME and FDM technologies. Furthermore, insights and recommendations are provided,

noting which parameters affect printing accuracy, how these parameters can be improved by achieving the targeted scaffold morphology parameters.

For the first time, micro-CT and bone histological analysis results of bone tissue regeneration using various osteoconductive and osteoinductive scaffolds in the Wistar rat critical-size calvarial defect model were analysed in the same study. Moreover, the obtained results were compared with one of the most well-known and widely used xenogeneic materials in clinical practice – Bio-Oss. The gained knowledge is critical to assess whether the results of the created scaffolds are comparable to the provided results of the materials currently used in clinical practice. This study showed that PLA/HA ECM, PLA/BG, PLA/BG DPSC, PLA/BG ECM positively affected a new bone formation, while the obtained results were similar to Bio-Oss.

Recent studies have particularly favoured the technology of decorating osteoconductive frameworks with cells or their ECM. However, the results obtained in this study showed that there was no statistically significant difference between the osteoconductive scaffolds and their biodecorated constructs 8 weeks after surgery, although increased new bone formation was seen in biodecorated groups. This knowledge is essential for future research, and further investigation is needed for more extended post-surgery healing periods, and in large animals. In addition, researchers need to assess whether these decorating technologies significantly improve bone regeneration and are worth further development, considering the increased cost of the procedure, the time required, and new advanced technologies.

The *in vitro* and *in vivo* knowledge obtained in this study is essential for tissue engineering and "OSSEUM 4D" artificial bone tissue development.

1.5. STATEMENTS TO DEFEND

1. The morphology and accuracy of 3D printed scaffolds depend on 3D FDM printing technology and parameters.
2. Composite filaments created with hot-melt extrusion may be used to print 3D scaffolds with FDM technology resulting in the morphology and accuracy comparable to those obtained with industrial PLA filaments.
3. Composite 3D scaffolds positively impact new bone formation in critical-size defects in rats.
4. 3D scaffolds enhanced by DPSC or their ECM increase the amount of a newly formed bone in critical-size defects in rats.

5. The generated innovative topologically-ordered 3D scaffolds are suitable for bone tissue regeneration and further artificial bone development.

1.6. APPROBATION OF THE RESEARCH

Original publications (Clarivate Analytics Web of Science)

1. Gendviliene I., Simoliunas E., Rekstyte S., Malinauskas M., Zaleckas L., Jegelevicius D., Bukelskiene V., Rutkunas V. Assessment of the morphology and dimensional accuracy of 3D printed PLA and PLA/HAp scaffolds. *J Mech Behav Biomed Mater*. 2020;104:103616. DOI: 10.1016/j.jmbbm.2020.103616.
2. Gendviliene I., Simoliunas E., Alksne M., Dibart S., Jasiuniene E., Cicenas V., Jacobs R., Bukelskiene V., Rutkunas V. Effect of extracellular matrix and dental pulp stem cells on bone regeneration with 3D printed PLA/HA composite scaffolds. *Eur Cell Mater*. 2021; 41:204-215. DOI: 10.22203/eCM.v041a15.

Related co-authored publications (Clarivate Analytics Web of Science) that were used for another dissertation:

1. Alksne M., Simoliunas E., Kalvaityte M., Skliutas E., Rinkunaite I., Gendviliene I., Baltriukiene D., Rutkunas V., Bukelskiene V.The effect of larger than cell diameter polylactic acid surface patterns on osteogenic differentiation of rat dental pulp stem cells. J Biomed Mater Res A. 2018; 107(1):174-86. DOI: 10.1002/jbm.a.36547.
2. Alksne M., Kalvaityte M., Simoliunas E., Rinkunaite I., Gendviliene I., Locs J., Rutkunas V., Bukelskiene V. In vitro comparison of 3D printed polylactic acid/hydroxyapatite and polylactic acid/bioglass composite scaffolds: Insights into materials for bone regeneration. J Mech Behav Biomed Mater. 2020;104:103641. DOI: 10.1016/j.jmbbm.2020.103641.

Presentations

Oral

1. Gendviliene I., Bukelskiene V., Alksne M., Malinauskas M., Rutkunas V. "Evaluation of Bone tissue regeneration in vivo". “Laboratory animals in scientific research", Lithuania, 2015.

2. Gendviliene I. Will we print bone tissue with a 3D printer? Baltijos jūros regiono šalių odontologų dienos, Lithuania, 2019.
3. Gendviliene I. Bone tissue regeneration using 3D printed scaffolds. Aktualijos periodontologijoje, Lithuania, 2020.
4. Gendviliene I., Vitosyte M., Jonaityte E.M., Alksne M., Jacobs R., Borusevicius R., Bukelskiene V., Rutkunas V. Effect of extracellular matrix on bone healing with 3D printed Polylactic acid/Bioglass scaffolds, EAO Digital days, 2020. https://DOI.org/10.1111/clr.17_13643.
5. Gendviliene I. Innovative bone regeneration techniques in dentistry. Odontologijos naujoves. Vanagupe 2020, Lithuania, 2020.
6. Gendviliene I. Alksne M. 3D printed bone: an innovative solution for bone regeneration. NBCM 2020, Lithuania, 2020.
7. Gendviliene I. 3D BIO printing in dentistry. LOOD conference „Ortopedinė odontologija 4.0", Lithuania, 2021.

Poster

1. Skliutas E., Gendviliene I., Rutkunas V., Malinauskas M. „Fused filament farbrication of biodegradable polylactic acid three-dimensional microstuctures". „Open Readings 2016", Vilnius, Lithuania, 2016.
2. Alksne M., Gendviliene I., Simoliunas E., Barasa P., Kalvaityte M., Skliutas E., Malinauskas M., Baltriukiene D., Bukelskiene V., Jarasiene-Burinskaja R., Rutkunas V. „The effect of ordered 3D printed PLA scaffold micro-structurization on DPSC osteogenic differentiation *in vitro* and new bone formation *in vivo*". Termis conference „European Chapter Meeting of the Tissue Engineering and Regenerative Medicine International Society 2017" Switzerland, 2017.
3. Gendviliene I., Alksne M., Rekstyte S., Simoliunas E., Skliutas E., Malinauskas M., Dibart S., Bukelskiene V., Rutkunas V. „Effect of 3d PLLA, PLLA/HAP scaffolds on new bone formation". CED-IADR/NOF conference „Oral health research congress" Austria, 2017.
4. Gendviliene I., Rekstyte S., Borusevicius R., Simoliunas E., Alksne M., Skliutas E., Grybauskas S., Vaitiekunas M., Bukelskiene V., Rutkunas V. Assessment of 3D printed PLLA and PLLA/Hap scaffolds geometry. Micro-CT User Meeting 2018, Belgium, 2018.

5. Gendviliene I., Simoliunas E., Alksne M., Rekstyte S., Skliutas E., Malinauskas M., Dibart S., Bukelskiene V., Rutkunas V. Effect of 3d printed scaffolds on new bone formation. IADR/PER conference, United Kingdom, 2018.
6. Vitosyte M., Gendviliene I., Simoliunas E., Alksne M., Rekstyte S., Jacobs R., Bukelskiene V., Rutkunas V. "Effect of 3D printed PLA/HAP and their decellularized scaffolds on new bone formation". "European association for osseointegration", Portugal, 2019.
7. Vitosyte M., Gendviliene I., Simoliunas E., Alksne M., Rasteniene R., Zaleckas L., Bukelskiene V., Rutkunas V. Effect of extracellular matrix on bone regeneration with 3D printed polylactic acid scaffolds. EAO Digital days 2020. https://DOI.org/10.1111/clr.90_13644.

Awards

1. Gendviliene I., Legrand P., Nicolielo L. F. P., Sinha D., Spaey Y., Politis C., Jacobs R. The best doctoral poster presentation „Conservative management of large mandibular dentigerous cysts with a novel approach for treatment follow up" The 8th Baltic Morphology scientific conference, 2015, Lithuania, 2015.
2. Gendviliene I. NOF travel grant (The Scandinavian Association for Dental Research) CED-IADR/NOF, Austria, 2017.
3. Gendviliene I. First place in the Falling Walls Lab Lithuania - "Breaking the wall of bone insufficiency". Final presentation in Germany, 2018. https://www.youtube.com/watch?v=SWsaA18oGFc
4. Gendviliene I. NOF travel grant (The Scandinavian Association for Dental Research) IADR/PER, United Kingdom, 2018.

Participation in the research projects

1. MIP – 046/2015 project „Construction of composite bone scaffold material and in vivo evaluation of biocompatibility and osteopromotion" Research Council of Lithuania.
2. Intelligence. Science-business project J05-LVPA-K-02-0002 „Development of a new bioactive 3D printed scaffold technology for bone regeneration" Lithuania.

2. LITERATURE REVIEW

2.1. NEED FOR BONE SUBSTITUTES

Currently, the number of clinical situations where physiological bone regeneration is impaired or insufficient [2], and bone grafting procedures are required, has been increasing. In 2001, over 2 million bone grafting procedures were performed in the world [19,20]. However, the number of surgeries done could be even higher due to the rapidly growing market for dental implants and bone substitutes [22]. The global bone grafts and substitutes market will reach $3.912 million by 2025 [23], increasing by 4.8% annually. Although the dental bone substitutes market is just a part of the global bone substitutes market, it is one of the fastest growing with an annual rise of 9.8% [22]. Bone substitutes are used in various fields of medicine, such as neurosurgery, orthopaedics, oral, and maxillofacial surgery specialities.

2.1.1. BONE SUBSTITUTES IN NEUROSURGERY

Neurosurgeons diagnose and treat potentially surgical remediable conditions of central (intracranial and spinal) and peripheral nervous systems [24]. Technological advances (image-guidance devices, clinical neurophysiology devices, operating microscopes, endoscopes, neuromodulation devices, and miscellaneous) made neurosurgery one of the most developing surgical specialities [25]. Leading surgeries using bone substitutes are cranioplasty and spinal fusion [26]. Cranioplasty aims to reconstruct a cranium reducing contour irregularities and improving function and aesthetics [3]. Mostly, cranioplasty is performed after decompressive craniectomy or ischemic intracranial complication, as a bone flap replacement after an osteitis or removal of a tumour-invaded bone flap [26]. In 2010, the number of performed cranioplasties reached 20-25 per million inhabitants (in Europe, the Middle East, and Africa) [27]. Spinal fusion aims to permanently connect two or more vertebrae into one solid bone using bone substitutes or internal fixation [28]. Spinal (cervical and lumbar) fusions are often used to treat various degenerative conditions, trauma, infection, and neoplasia [29,30]. More than 200,000 spine fusions are performed each year in the United States, and this number continues to increase annually [28]. The global spinal fusion devices market is anticipated to reach $7,435 million by 2022 [31].

An ideal material used for cranioplasty must entirely close a skull and maintain mechanical stability and protection for an underlying brain until sufficient bone regenerates [26,32]. Then, the physiological environment of the

brain and intracranial pressure between 5 and 10 mmHg can be maintained [33]. Moreover, cranioplasty substitutes should be resistant in trauma cases, especially when a sharp object penetrates into an unprotected area [32]. Furthermore, bone substitutes should be biocompatible, adaptable, radiolucent, non-toxic, reasonably priced, and ensure an excellent aesthetic result, mainly when a bone defect is located in a frontal region [26,27]. Autologous bone grafts (calvarium, rib), allografts (cadaveric skull, cartilage), metals (titanium, vitallium, tantalum, stainless steel mesh), polymethylmethacrylate (PMMA), ceramics (HA, coralline carbonated calcium phosphate cement (CCPC), porous polyethylene (Medpore), and polyether ether ketone (PEEK) may be used for cranioplasty [3,26]. Allografts and xenografts are a poor choice for cranioplasty and are not widely used due to the high rate of infection, bone resorption, and reactions to a foreign substance [34,35].

Although autologous bone grafts are considered as *a gold standard* in cranioplasty, their use may be limited in large cranial defects (>16 cm^2) [3,26]. Moreover, they demonstrate a high resorption rate, mainly when a rib is used [3]. Other disadvantages that must be taken into account are subsequent decrements in strength and aesthetic contour, poor malleability, infection complication, and variable donor-site morbidity [3,27]. Furthermore, computer-assisted design and manufacturing (CAD/CAM) prefabricated titanium implants show positive results when they are used for large cranial defects [36]. However, titanium implants may potentially break a surrounding bone. Thus, an overlapping margin should be considered [36]. Nevertheless, PMMA is one of the most frequently used cranial bone graft substitutes because of its similar strength and biocompatibility to a bone, easy contouring after hardening [3]. However, the use of PMMA is limited in full-thickness defects as it has exothermic properties and generates large amounts of heat during hardening [36]. Other disadvantages of PMMA are post-placement shrinkage, lack of osseointegration and osteoinductive properties, low resistance to a traumatic injury directly applied to a plate [36].

Prefabricated HA implants are among the most promising ceramic materials for cranioplasty because they have good osteoconduction and osteoinduction features, no foreign body reaction, good aesthetic results, low risk of infection, and low posttraumatic fracture rate [3,26]. However, the cost of patient-specific HA implants is about €8,000, and they are more expensive at least by €3,945 compared to autologous implants [26]. Moreover, high complication rates of developing seromas, chronic drain fistulas, and persistent oedema were observed when HA cementum used intraoperatively contacted sinus mucosa [37]. Furthermore, HA cementum is not highly resistant

to mechanical stress and can easily break [35]. Another promising material for cranioplasty is PEEK as it is inert, durable, easily removable, and radiolucent [3]. Moreover, PEEK may be CAD/CAM prefabricated, and it has strength and elasticity similar to a cortical bone [38]. Although the success rate of this material is counted by about 93.7%, and the complication rate is similar to PMMA, the high cost has to be taken into consideration [39]. Therefore, further research is needed to reduce the cost of the alloplastic materials and increase compatibility and integration in a bone [39].

An ideal bone graft for optimum spinal fusion enhancement should be non-immunogenic, have good osteoinductive, osteoconductive, and stable biomechanical properties, and promote osteogenesis [40,41]. Constantly used spinal fusion materials are autografts, allografts, allograft stem cells, demineralized bone matrix (DBM), bone marrow aspirate (BMA), ceramics (β-Tricalcium phosphate (TCP), HA) and growth factors (bone morphogenetic proteins (BMP)) [30,40]. Autografts are superior for spinal fusion due to their excellent osteogenic, osteoinductive, and osteoconductive properties [41]. Usually, autografts can be harvested from a local bone (laminectomy bone), iliac crest, fibula, or ribs [41]. The biggest disadvantage of the local bone graft is a small amount of available bone volume [41]. The iliac crest autograft is considered a gold standard because of the associated excellent fusion rates as high as 92% [41,42]. However, a prolonged pain, hypersensitivity, and buttock anaesthesia are the most common complications at an iliac crest donor site [29,43]. Almost all patients feel a postoperative pain in iliac crest donor sites during the first week [43]. In addition, muscle weakness, compartment syndrome, and neurovascular injuries often occur after harvesting from a fibula [41].

Allografts are highly osteoconductive, however variably osteoinductive [44]. Allografts are often used in conjunction with BMA, autologous bone, or BMP due to a lack of osteogenic properties [45]. Moreover, pathogen transmission, including human immunodeficiency virus (HIV), Clostridium difficile, Hepatitis B, and bacterial infections, is a rare but severe complication [45]. DBM shows reasonable fusion rates as high as 86% but they are lower than those of autografts [44,45]. They are commercially available in various forms, however, lack structural strength and stable biomechanical properties. Thus, DBM cannot be used alone in spinal fusion [44]. BMA contains pluripotent mesenchymal stem cells (MSC), which release cytokines and growth factors within an autograft, allograft, ceramics, or DBM [45]. The advantages of BMA are osteoinductive and osteogenic properties, a less invasive procedure compared to autograft taking, and a lower harvest site morbidity [46]. However, the older age of a patient negatively affects the rate of

colony-forming unit fibroblasts and osteoblast, especially in women [46]. TCP takes shorter time for biodegradation and resorption and has greater osteoconductive properties than HA because of total porosity and large pores but lesser mechanical strength [45]. Thus, TCP is recommended for cervical spine fusions, however, the findings for lumbar spine fusion have been still controversial [44].

Recombinant BMP-2 (rhBMP-2) are currently approved by the Food and Drug Administration (FDA) for anterior lumbar spine fusion [45]. Moreover, they show comparable efficacy to the gold standard autologous iliac crest bone graft in cervical and lumbar spine fusions for adults. Contrarily, there is a lack of data to support the use of recombinant BMP-2 in pediatric spinal fusion [44]. Furthermore, rhBMP-2 must be used in conjunction with the carrier matrix, otherwise, they quickly diffuse from a fusion site [47]. However, hematoma formation, heterotopic ossification, retrograde ejaculation, and a higher risk of cancer are the complications of rhBMP-2 applications and have to be considered before use [45,48]. In conclusion, the field of various bone graft materials is expanding and entering the market without providing proper evidence-based studies [44]. Therefore, it is difficult for neurosurgeons to choose the optimal bone graft material for spinal fusion [30]. Moreover, none of the alternative bone graft substitutes has demonstrated better results than iliac crest autograft, which remains the gold standard for spinal fusion [44]. New innovational technologies such as gene therapy and tissue engineering show promising results in spinal fusion animal models [47]. Future studies must further evaluate the clinical relevance and efficacy of these emerging fields and investigate the best available options specific to the patient population [45].

2.1.2. BONE SUBSTITUTES IN ORTHOPAEDICS

New surgical techniques, procedures, metal alloy biomaterials, and orthobiologics have been the leading advancements in orthopaedic surgery over the last 20 years [49,50]. Orthobiologics are a group of biological materials and substrates (bone grafts, bone substitutes, growth factors, stem cells) that promote the healing of a bone, cartilage, ligament, and tendon injuries [51]. They are used to reduce the need for surgery in orthopaedic trauma and improve the effectiveness of existing orthopaedic implants and surgical techniques [4]. Orthobiologics used for bone regeneration and augmentation must be osteoinductive, osteoconductive, and/or osteogenic [52]. The use of particular material depends on the problem at hand, the properties of a material, comorbidities and contraindications, country-specific regulations, and a

cost [51, 53]. Bone orthobiologics are often used to treat adult fracture nonunions or during foot and ankle surgeries [4,54,55].

Nonunion rates of all fractures vary between 1.9 to 10% due to different anatomic regions, fracture type, soft tissue injury, fracture fixation principles used for treatment, and patient-dependent factors such as age, nutrition, drug therapies (NSAID use), congenital bone disorders, and systemic diseases (e. g., diabetes) [56–58]. This diagnosis is established after a minimum of 9 months following a trauma, with no signs of healing for 3 months [56]. Nonunions will not heal without additional intervention, regardless of elapsed time [59]. Only a few non-operative treatment strategies (pulsed low-intensity ultrasound, extended immobilization) are available to treat nonunions [60]. Operative treatment depends on the type of nonunions: improved mechanical stability with internal fixation is used for hypertrophic nonunions, biologic stimulation (autografts, DBM, allografts, BMAC, BMSC, platelet-rich plasma (PRP), BMP) and mechanical stability – for atrophic or oligotrophic nonunions [60]. Although autografts are considered the gold standard against which all other bone substitutes are measured, the healing success rate is counted only up to 80% to treat nonunions [57]. Some alternatives promoted commercially consist of an allograft conductor and DBM inductor mixture [61]. However, their success rate is lower than those of autografts, especially in large defects or when a prior contamination of a tissue bed persisted [57,61]. The overall contamination rate of allografts has been reported increasing by up to 10%, and an infection rate of implanted allografts – up to 12.2% [56].

BMA concentrate (BMAC) or bone marrow-derived mesenchymal stromal cells (BMSC) obtained from iliac crest aspiration is commonly used to treat delayed union or nonunion due to a decreased number of complications compared to autografts, easy handling of the procedure for orthopaedic surgeons [62,63]. The success rate of BMAC for nonunion healing is similar to this of autografts and counts up to 81% if used alone; the success rate for BMSC is up to 87% [62]. However, BMAC and BMSC independently may be insufficient for treating nonunions with large bone gaps or long bone nonunions, and the combination of these techniques with scaffolds should be considered [57,62]. Another problem with BMAC is that the level of osteoprogenitor cells in an aspirate is highly variable [64]. However, BMAC, PRP, and BMP may be used with percutaneous administration to decrease morbidity, cost, and hospitalisation time in nonunion treatment [64]. Although platelet concentrations can be achieved as desired, and several studies showed promising nonunions healing, careful patient selection for this treatment should be observed [65]. PRP for non-surgical treatment should be injected in

less than 11 months in fractures with near-total contact between fracture fragments [64].

BMP-2 and BMP-7 are the most widely used growth factors for orthopaedics from the BMP family because they induce ectopic bone formation [66]. U.S. FDA approved BMP-7 for treating the tibial nonunion [67] with a success rate varying from 75% to 90% [68]. BMP-2 is more effective at the stem cell level than BMP-7. However, BMP-7 is more effective at osteoblastic precursors level and better induces osteoporotic mesenchymal stem cells [66]. Although BMP-7 shows a similar success rate compared to autogenous grafts, several possible complications need to be considered, such as surgical site infection, heterotopic ossification, pseudoarthrosis, seroma formation [66]. Furthermore, a surgical site's irrigation after BMP application and contact with neurovascular structures should be avoided [68]. The BMP-2 usage in children or pregnant women has not yet been determined, and it is contraindicated for patients with an active infection at a surgical site [69].

Orthobiologics in foot and ankle surgery are used for primary arthrodesis of ankle, hindfoot, and midfoot joints or secondary surgeries when the nonunions, malunions or secondary trauma occur [70,71]. The golden standard in foot and ankle surgery is an autogenous bone block that can be cortical, cancellous (success rate of 93.7%) or combined (94.2%) depending on the defect and the type of surgery [72]. The most significant disadvantages of autografts are the limited quantity of graft material, mainly if local donor sites like calcaneus or distal tibial metaphysis are used [71]. Iliac crest bone can overgo some limitations. However, some disadvantages must be considered, such as separate incision requirements, the risk of damaging nerves or vessels at a harvest site, longer operating time, larger surgical team needed [70]. Therefore, alternative orthobiologics are being sought. Although allografts have a success rate of 86.9-93.3% for union in foot and ankle surgeries [73], they have only osteoconductive features as during the sterilisation process all live bone cells are killed and cytokines, BMP are lost [71]. One new exciting technique has been described in the literature – combining allografts with MSC with a success rate of 81-87% [71]. However, the union rate is not as high as the one of autografts. Some promising results show BMAC especially combined with PRP in patients having open wounds with chronic draining osteomyelitis (diabetic Charcot arthropathy) [71]. The main advantage of BMAC, PRP, BMP is that it is less invasive compared to autografts. However, BMP use is not approved by the FDA for foot and ankle applications. Moreover, there is a lack of evidence-based results that using orthobiologics gives statistically significant improvement than without them [70]. Further

research is needed to investigate orthobiologics use in foot and ankle surgeries, compare the materials with controls, and other orthobiologics so that precise indication for use could be given to surgeons [70].

2.1.3. BONE SUBSTITUTES IN ORAL AND MAXILLOFACIAL SURGERY

Bone defects in the maxillofacial region occur due to a trauma, congenital disorders, tumours, odontogenic, nonodontogenic cysts or tooth loss [5]. Various studies show that the percentage of edentulous persons aged 65 and older differs from 20 to 60% in multiple countries [74,75]. One of the most effective ways of treating tooth loss is by using dental implants. However, almost every second dental implant surgery needs bone augmentation due to existing bone deficiencies [76]. Therefore, bone substitutes used in maxillofacial surgery need to regenerate tissues structurally and functionally similar to those lost, and provide an adequate bone quantity and quality to allow dental implant insertion for prosthetic rehabilitation [5]. Alveolar bone grafting can be divided into ridge preservation and ridge augmentation (onlay, inlay grafting) [77]. In addition, block grafting, osteoperiosteal flaps, guided bone regeneration (GBR), maxillar sinus surgery are bone augmentation techniques for large alveolar bone defects treating with bone substitutes [8]. Therefore, these techniques will be discussed further as they are challenging in clinical practice due to insufficient blood supply, graft instability, exposure of graft material to the oral environment and infection [8].

Block grafting is one of the oldest alveolar ridge horizontal and vertical augmentation techniques [8]. The principle of the method is to fix bone blocks to recipient ridges with osteosynthesis screws or dental implants [8]. It is recommended to use at least two osteosynthesis screws to fix a graft to prevent micromovements. Otherwise, an avascular necrosis of the graft may occur due to malnutrition [78]. Block grafting may be done with autogenous, allogeneic, xenogenous or alloplastic blocks [79]. Autogenous bone blocks are considered the gold standard as they induce bone by the mechanisms of osteogenesis, osteoinduction, and osteoconduction [7]. Autogenous bone grafts may be trabecular, corticotrabecular or cortical. The trabecular component of grafts supplies osteogenic cells and osteogenesis [7,80]. The cortical part provides the majority of BMP, promotes osteogenesis, serves as a barrier to soft tissue invasion and allows blood vessels to penetrate the graft from the host bone for an extended time [7,80]. The donor sites for block grafts are extraoral such as an iliac crest, skull vault, fibula, rib and intraoral such as a mandibular ramus, mental region or coronoid process, maxillary tuberosity, tori and others [7,8].

According to the research, an autogenous iliac crest bone should serve as the gold standard for comparing all forms of alveolar grafts [80,81]. A graft can be harvested from an anterior or posterior iliac crest [80]. The success rate for iliac crest grafts for alveolar bone augmentation may be up to 99% [78]. Furthermore, the enormous benefit of this graft is a large amount of bone available for grafting up to 5x5 cm [77,82]. However, the main disadvantages of this method are a postoperative discomfort, high resorption rate (12-60%) before an implant placement and after loading, chronic donor site pain, fracture, infection, or hernia formation [5,8,80]. Moreover, some literature suggests that harvesting from the iliac crest was more painful than an oral wound possibly leaving a patient upset about a scar [82]. Furthermore, some cautions should be mentioned such as severely osteoporotic individuals, previous hip replacements, retained hardware from an earlier femur fracture [77]. The high resorption rate of the iliac crest graft may be due to the low cortical to the trabecular ratio in the graft, the memory of endochondral ossification and different osteoblast mechano-sensing between donor and recipient sites [8].

Less common extraoral donor sites for alveolar ridge augmentation with block grafts are cranial vault, fibula, rib, the second metatarsal due to the high morbidity associated with a donor site or complex surgeries [8]. However, a cranial vault is successfully used for orbital roof and floor reconstruction or covering cranial defects, while fibula - for large bone defects after tumour excision, reconstruction of mandibular defects or treating chronic osteomyelitis [32,83]. The advantages of a calvarial graft are mechanical characteristics, slow resorption rate (cortical bone), and a large amount ($\sim 8 \times 10$cm) of bone available for harvesting from a parietal region [32]. However, possible cautions for use are the risk of a dura injury, surface deformity at a donor or recipient site, a graft fracture during harvesting, a very rare intracranial haemorrhage [32]. Furthermore, one of the major considerations is the decreased strength of a skull at a cranial donation location. Therefore, it is recommended to choose another site for grafting [32]. Fibular grafts can provide a strong capacity for bone remodelling, sufficient blood supply to combat bony infections, repair mechanical and structural defects [83]. Possible complications are graft fracture (11.7%), infection (5.6%), ankle deformity (3.3%), peroneal nerve palsy (7.5%) etc. [84]. A proper surgical planning, the standardization of harvesting protocols are needed to cope with high postoperative complication rates [84].

Intraoral donor sites are more advantageous in comparison with extraoral sites due to an easy surgical access, reduced operating time, eliminated need for hospitalization, the contiguity between donor and recipient sites, the

absence of skin scars and minimum discomfort to a patient [5,85]. A mandibular ramus and symphysis are among the most readily accessible sources of intraoral bone grafts. One of the reasons is that mandible grafts are membranous, undergo less resorption, and revascularize more rapidly than endochondral bone [86,87]. Moreover, mandibular grafts represent minor volume loss and show good integration at a short healing time [87]. In addition, the mandibular ramus has sufficient bone volume to augment up to a 3 or even 4-teeth edentulous site. The maximum dimensions of the available bone graft from mandibular ramus are 4mm in thickness, 1.5cm in height, and 3cm in length [86]. The available bone graft dimensions from mandibular symphysis are 4mm in thickness, 1cm in height and 2cm in length, and may augment a 3-teeth edentulous site [88]. According to the literature, the postoperative pain of both bone grafting techniques is classified as slight to moderate. However, a symphysis graft causes more uncomfortable sensations for patients [85]. Moreover, temporary (40.5%) and permanent (13.5%) sensory disturbances are more frequent in harvesting bone graft from mandibular symphysis than ramus (16.2% and 2.3%, accordingly) [85]. The same is with temporary or permanent dental sensory alterations resulting in pulp necrosis [85]. Other complications such as bleeding, bruising, infection are rare for both bone grafting sites [85]. Thus, the mandibular ramus is preferable for bone harvesting due to a greater possible bone volume and fewer potential complications than mandibular symphysis.

Alternative intraoral donor sites to the mandibular symphysis and ramus may be a mandibular coronoid process, zygomatic body, anterior maxillary sinus wall, alveolar zygomatic buttress, tuberosity, incisive fossa, anterior nasal spine, palate, or torus [89]. The main disadvantage of the alternative donor sites is low bone quantities [89]. Therefore, these bone grafts are used only for small bone defect augmentation, usually for single-tooth edentulous site augmentation [89]. Currently, the tuberosity graft is gaining more attention for alveolar bone reconstruction, alveolar preservation, periodontal defects augmentation, and sinus elevation due to an easy clinical access, low incidence of complications, and high quantity of osteoprogenitor cells [89]. However, tuberosity graft is type IV bone and provides poor bone quality, consistency, and structure. In addition, the limitation of available bone volume is the Schneiderian membrane, and one of the most common complications is its perforation [89]. Another beneficial source of cortical or corticocancellous bone grafts is a torus, an exostosis occurring at a characteristic site, either in the midline of a palate or on the lingual surface of a mandible [90]. This bone graft is easy to access and results in a non-anatomical or aesthetic deficiency.

However, one torus is enough to augment a single-tooth edentulous site, and possible complications of a surgery may be a lingual nerve damage, infection, and bleeding [90]. Nevertheless, new regenerative techniques are currently being developed to reduce the quantity of an autogenous bone needed to regenerate more extensive size defects [89].

Allografts are a promising alternative to autogenous bone blocks due to unlimited supply, decreased operative trauma and blood loss, absence of donor site morbidity [8,79]. Allografts are tissues obtained from human cadavers, preserving a natural bone tissue architecture and extracellular proteins [91]. Allograft blocks may be cortico-cancellous or cancellous with excellent osteoconductive and integrative properties, good mechanical characteristics comparable to an autologous bone [92]. However, the origins of a donor material are heterogeneous, affecting biological behaviour and the rate of allografts resorption [93]. Furthermore, allografts have variable osteoinductive properties because of the varying remaining BMP concentration depending on the used processing technique, and poor osteogenic properties due to the lack of living cells [92]. In addition, a different allograft issue poses a risk of disease transmission or an immunological response after the transplantation of the same species tissues [44]. This issue may be eliminated by removing a tissue's cellular component by freeze-dried and fresh-frozen processing [44]. Moreover, successful alveolar ridge augmentation results are described in the literature, especially for single-tooth edentulous site augmentation comparable to the results achieved with type II-IV autogenous bone blocks [79]. However, histologically the results of allogenic grafts are doubtful and show some issues achieving vascularization of the grafted region [8,93]. Finally, an ever increasing shortage of tissue donors are reported each year. In addition, allografts are often abandoned in clinical practice due to increasing regulatory limitations, especially in Europe, and the new medical device legislation [94].

As the number of tissue donors decreases each year, xenografts may be suitable for replacing autografts and allografts due to shorter surgery time, unlimited availability, lower morbidity, and lower risk of neurosensory disturbances [95]. Xenografts are mostly inorganic, mineral components of bone stripped of their protein composition and acting as osteoconductive fillers [96]. According to the literature, xenograft bone blocks achieved results comparable to autogenous bone blocks for horizontal alveolar ridge augmentation in patients with severe atrophic jaws, and even better results for vertical alveolar ridge augmentation due to a lower resorption rate [95]. Moreover, the failure rate of augmented sites, when blocks needed to be removed, was almost the same as for autogenous blocks, primarily associated with block dehiscences [95]. However, implant survival rate was lower by

10-20% in augmented sites with xenografts compared to autogenous bone blocks [95]. In addition, the critical step in obtaining xenografts is eliminating all the immunogenic components of donor tissues (e.g. cells or cell remnants) without impairing their inherent biological characteristics [10]. However, independent research has found that histologically xenograft blocks contained organic / cellular remnants, although the manufacturers of the materials stated otherwise. These remnants could provoke an undesired immune response inducing a foreign body reaction [10]. Therefore, future research is needed to clarify the manufacturing technology, clinical outcomes and indications of xenograft block augmentation [10,95].

An osteoperiosteal flap is an alveolar ridge bone augmentation technique when a vascularized segmental osteotomy is performed on an alveolar bone [8]. The critical factor for this technique is the maintenance of vascularization in bone fragments from a periosteum [8]. The osteoperiosteal flap is combined with inlay grafts and is increasingly used for dental implant site development in atrophic ridges [8]. Interpositional grafts are beneficial for a mobilized bone fragment stabilisation and mechanical support [97]. Several techniques of segmental osteotomies are used for bone augmentation: sandwich osteotomies, alveolar split osteotomies, and island bone flap approaches [98]. The main advantages of the methods are the preservation of an attached gingiva and even papillae, crestal bone stability, and a relatively uneventful recovery [8,98]. Moreover, vertical ridge augmentation results using osteotomies are comparable to the effects of distraction osteogenesis [8]. However, osteotomies for vertical augmentation are surgically sensitive and may result in a torn pedicle, causing the complete loss of a bone segment and soft tissue [98]. Moreover, the sandwich grafting is not a good choice when an alveolar ridge is thin (4mm or less) [98]. However, a successful vertically approached osteoperiosteal flap gains up to 8-10mm, while a guided bone regeneration only achieves modest vertical gains [97]. Horizontal alveolar ridge augmentation may be done with alveolar split osteotomy that widens the alveolar ridge from 2 to 5mm and may be done with simultaneous implant placement [97]. However, this technique is unsuitable for highly atrophic alveolar ridges, where 5mm and more gain is needed. In addition, surgeons should maintain an osseous facial plate thickness of at least 2mm. Otherwise, the plate may undergo replacement by granulation tissue and resorb away [97]. Future research is needed to determine which bone substitutes suit best as interpositional grafts for the osteoperiosteal flaps [97,99].

Guided bone regeneration (GBR) is used for horizontal and vertical alveolar ridge augmentation with particulate graft materials separated from surrounding soft tissues by non-resorbable or resorbable membranes [8].

Membranes are needed to stabilise the graft material, lower graft resorption, and act as an occlusive barrier to surrounding soft tissue ingrowth [8]. Successful GBR needs a good primary wound closure, proper angiogenesis, space maintenance and stability of the wound [77]. It is known that minor self-containing defects may be restored with the graft materials used alone. However, barrier membranes combined with particulate bone substitutes result in more predictable clinical outcomes [8]. The main problems associated with GBR are a high bone graft resorption rate, anatomical limitations for graft containment, and postsurgical infection [8,77]. In addition, vertical GBR has shown limited clinical success due to a wound dehiscence, the exposure of a non-resorbable membrane, and a fibrous tissue ingrowth [8]. Autologous, allogeneic, xenogeneic, or alloplastic bone substitutes may be used for GBR.

Interestingly, autologous bone blocks show better results for an alveolar ridge augmentation than GBR with autogenous bone chips and barrier membranes gaining only maximum of 5.03-5.68mm of a new bone [100]. Therefore, various combinations of bone substitutes and barrier membranes are being searched for a lesser graft resorption rate and more predictable results for large alveolar ridge defects [100]. The most practiced mixtures are 50:50 autogenous/allogenic bone particles (corticocancellous / cancellous bone chips sized 100-400μm) or 50:50 autogenous / xenogenous bone particles [101,102]. Anorganic bovine bone mineral (ABBM) is the most well-documented xenogenous material for GBR due to cancellous and cortical bone construction and geometric form closely resembling the bone [102].

Geistlich Bio-Oss® (Geistlich Pharma AG, Wolhusen, Switzerland) (Bio-Oss) is the most well-known, widely used and reliable ABBM in dentistry, with positive preclinical and clinical outcomes [103]. The graft is made up of alkaline hydroxyapatite and heat treatment (300°C) to remove organics from a bone. Bio-Oss was investigated in 1996, and it was discovered that this material supported bone ingrowth when implanted into a rabbit muscle. Afterwards, it was found that Bio-Oss resorbed and underwent normal physiologic bone remodelling after a graft implantation [104]. Furthermore, Bio-Oss is featured by good biocompatibility and osteoconductivity due to a porous structure and physical characteristics comparable to a human bone [103,105]. Therefore, the material facilitates the attachment of bone-forming cells, supports the formation of a new bone, and maintains the original defect space [103,105]. Various studies confirm that Bio-Oss particles mixed with autogenous chips for GBR grafting showed good incorporation with a newly formed bone and predictable results for dental implants osseointegration [102]. Moreover, new studies show that the gained amount of the newly formed bone is comparable between Bio-Oss alone or with different mixtures of Bio-Oss and

an autogenous bone, and even with autogenous bone blocks [106]. The most common complication is postoperative dehiscence that appeared in 57% of cases augmented with Bio-Oss alone. However, the amount of the newly formed bone did not seem to be compromised by this complication [106]. However, these beneficial results are related with short-term clinical outcomes. Therefore, long-term clinical and radiographic studies on the final implant treatment outcome are needed for further conclusions [106].

The edentulous alveolar ridge of a posterior maxilla is a challenging site for dental implantation due to insufficient bone quality and low bone volume caused by ridge resorption and maxillary sinus pneumatization [107]. One of the most predictable ways to restore alveolar ridge volume in the posterior maxilla is maxillary sinus augmentation with or without bone substitutes [107]. Bone substitutes occasionally used for maxillary sinus augmentation are autogenous, allogenic or xenogenic. Currently, autogenous grafts are not favoured in open sinus lift surgeries due to donor site morbidity, needs for general anaesthesia during a surgery and a considerable resorption rate of the material (up to 40%) [108]. Furthermore, allogenic bone grafts are also unpopular as histologically, a fibrous connective tissue with no evidence of ossification is found in the centre of a graft even two months after a surgery [108]. However, if a surgeon decides to use an allograft, small-particle allogenic grafts are preferred to cover a significantly higher bone area than with large-particles [108]. On the other hand, xenografts are occasionally used in open sinus lift surgeries due to a prolonged resorption rate, bone volume stability, and high initial pull-out forces of dental implants [108]. Furthermore, many articles showed comparable results between Bio-Oss xenograft and the mixture of Bio-Oss and autogenous bone in bone regeneration, dental implants survival rates for one year, bone-to-implant contact [109]. In addition, histologically, Bio-Oss showed proper incorporation in a newly formed bone [109].

Currently, there is an increasing interest in using alloplastic materials, PRF, or maxillary sinus augmentation without using bone substitutes [107]. HA, β-TCP are among the most common alloplastic materials due to high biocompatibility and integration rate of particles within a newly formed bone [110]. In addition, animal studies confirmed no significant difference between HA and the autogenous graft in bone-to-implant contact [108]. PRF has several advantages: simple, low-cost, low-resource technique, improved healing period, bone regeneration, promotion of angiogenesis [111]. However, there is no high-quality evidence for using only PRF to augment a sinus floor or that the achieved new bone volume is comparable to an autologous bone or other biomaterials [111]. Furthermore, the addition of PRF to other biomaterials

provides only several beneficial effects: a slightly higher percentage of a new bone formation and a lower portion of residual bone substitute material compared to the biomaterials alone [111]. However, no benefits are achieved in the augmented bone height, percentage of soft tissue area, implant survival rate, or implant stability [111].

Graftless maxillary sinus elevation with dental implantation is a new technique based on space-maintaining between dental implants and the Schneiderian membrane [112]. This technique gives space for a stable blood clot formation, initiating a wound-healing cascade and promoting bone regeneration [112]. However, some precautions should be mentioned such as primary dental implants stability, low bone quality, and volume [111,112]. In addition, at least 5mm of a vertical bone height are needed to provide a proper dental implant stability and successful performance of this technique [112]. Moreover, long-term clinical trials are required to support new strategies and prepare evident clinical indications [111,112]. Therefore, there is a high research demand for clarifying the clinical indications on various bone augmentation techniques and bone substitutes. Furthermore, considering all different clinical bone deficiency situations in oral and maxillofacial surgery, future studies should evaluate newly designed biomaterials or enhance the existing biomaterials and surgical techniques [5].

2.2. BONE STRUCTURE AND MORPHOLOGY

Bone is a mineralized connective tissue consisting of 50-70% mineral, 20-40% organic matrix, 5-10% water, and less than 3% lipids [113]. Bone extracellular matrix (ECM) is composed of a mineral component, which is mostly hydroxyapatite [Ca10(PO4)6(OH)2], and an organic matrix. The organic part of the bone tissue is predominately collagen type I. Noncollagenous proteins, including osteocalcin, osteonectin, osteopontin, fibronectin, growth factors, and bone morphogenetic proteins (BMP), compose up to 15% of total bone proteins. The organic matrix forms a scaffold for hydroxyapatite deposition, provides elasticity and flexibility to the bone, ensures bone homeostasis, and regulates the activity of bone cells. Meanwhile, the mineral component grants rigidity and the load-bearing strength of the bone [113,114]. Multiple cell types are found in the bone: stromal lineage of osteogenic, adipogenic and chondrogenic derivatives, the hematopoietic origin of an erythroid, myeloid and lymphoid lineage. Furthermore, the microenvironment consists of endothelial, perivascular, and neural baseline cells that collectively maintain skeletal integrity and assist in skeletal repair following an injury [115].

Four types of cells can be found in a bone tissue: osteoblasts, osteocytes, osteoclasts, and bone lining cells. Osteoblasts develop from mesenchymal stem cells and perform a bone-forming function. The Runx2 gene and BMP are the critical elements for osteoblast differentiation [116]. First, mesenchymal stem cells differentiate to preosteoblasts, which exhibit alkaline phosphatase (ALP) activity [117]. Afterwards, preosteoblasts mature to osteoblasts leading to secretion of bone ECM [114]. Thus, bone ECM is formed in two stages: synthesising organic matrix proteins by osteoblasts and a subsequent mineralization of the matrix [114]. The expression of alkaline phosphatase and noncollagenous proteins such as osteocalcin, osteopontin, and bone sialoprotein, indicates ECM maturation [113]. Later, osteoblasts become osteocytes or bone lining cells, or undergo apoptosis [116]. Osteocytes are the most abundant bone cells [118]. They are surrounded by mineralized bone ECM, detect mechanical loads, and control skeletal adaptation to daily forces. Therefore, osteocytes are thought to play a significant role in bone remodelling by affecting the activity of osteoblasts and osteoclasts [119]. Osteoclasts differentiate from mononuclear cells of a hematopoietic stem cell lineage [114]. The most studied function of osteoclasts is bone resorption. However, they also produce cytokines, which regulate osteoblast activity during bone remodelling and influence hematopoietic stem cells and immune cells [120]. Bone lining cells reside on surfaces where neither bone resorption nor bone formation is present. Their functions are not entirely clear but are thought to be removing bone collagen, which is left after bone resorption by osteoclasts so that bone formation may begin [121].

In the adult human skeleton, 80% of bone is cortical and 20% is trabecular [113]. The cortical bone surrounds a bone marrow space. It is dense and exhibits porosity usually less than 5%. The trabecular bone, on the other hand, is a porous bone with a spongy appearance. The trabecular bone struts and plates form a scaffold for interspersed bone marrow [113]. However, the trabecular bone is characterized by a high surface to volume ratio, and its microarchitecture is arranged to withstand a mechanical load transfer. The trabecular bone has active metabolism and remodelling. Therefore it is less mineralized than the cortical bone [122]. The outer surface of the cortical bone is covered by fibrous connective tissue – the periosteum. Inside the bone, the endosteum shields the inner surface of the cortical bone, the trabecular bone, and blood vessels [113].

2.2.1. Maxilla and mandible morphological features

Substantial differences in structure and bone biology exist between a maxillary and mandibular bone tissue. The maxillary bone tissue develops by intramembranous ossification and a mandible by endochondral and intramembranous ossifications [123]. The maxilla consists of a pyramid-shaped body and alveolar, frontal, zygomatic, and palatine processes. The body of the maxilla contains maxillary sinuses, and it is a part of the bony orbit, nasal cavity, and infratemporal fossa. The mandible is the largest and strongest facial bone. It comprises two major components – the mandible body and two rami [124]. Moreover, the maxilla is highly vascularized, while the mandible shows more centralized vascularization [123].

Microscopically lamellar bone builds up 46% of the bone tissue in the maxilla and 63% in the mandible. The maxilla is richer in bone marrow compared to the mandible, 23% and 16%, respectively. The bone marrow in the anterior segment of the maxilla occupies approximately 4 % [125]. Multiple studies reveal that bone density is more significant in the mandible than in the maxilla. In addition, the bone in the anterior areas of the jaws is denser than in the posterior regions. The anterior mandible has the greatest density values followed by the anterior maxilla, the posterior mandible, and the posterior maxilla [126,127]. The densest bone in the anterior parts of the jaws can be explained by the food-tearing function of the anterior teeth since more bone support is needed to withstand substantial lateral forces [126]. The cortical crest is more than twice wider in the mandible than the maxilla, with the widest point at the mandibular symphysis [125]. Knowledge of the bone density in the maxillofacial region is essential for dental research and clinical practice. Bone density in jaws has five main types based on the number of Hounsfield units (HU) classified by Misch CE, Kircos LT [128]. This classification is helpful for dental implant treatment planning, bone augmentation procedures, and observation of augmented sites, e.g. augmented sites resorption, correlation between the density of bone block and resorption rate, or orthodontic treatment planning [128].

With age, cortical porosity of the mandible increases, leading to lower cortical bone mass, however, the mass of the trabecular bone does not correlate with age [129]. Moreover, bone metabolism is affected by osteoporosis and other systemic diseases, menopause, smoking, alcohol consumption, and hormone intake. It had been recently discovered that a moderate or severe chronic periodontitis significantly decreased the bone density in the mandible and have some associations with skeletal bone mineral density [130]. In addition, after teeth extraction, the mandibular alveolar ridge undergoes greater and

faster resorption than the maxillary alveolar ridge [131]. Moreover, the resorption of the jaws' alveolar process is more significant in the horizontal dimension and occurs mainly on the facial aspect of the ridge followed subsequently by vertical mid-facial and mid-lingual changes. An average alveolar bone loss of 1.5-2mm (vertical) and 3.8mm (40-50%) (horizontal) was recorded within 6 months after teeth extraction [8,95]. However, the sites presenting a thick facial bone plate (>1mm) show less horizontal resorption than those with a thin plate (≤1mm) [132]. Thus, bone tissue is characterized by a complex internal and external structure. Therefore, progressive tissue engineering techniques and their combinations are needed to create 3D scaffolds with controllable outer and inner shapes.

2.3. MANUFACTURING METHODS OF TOPOLOGICALLY-ORDERED POROUS SCAFFOLDS

The repair of maxillofacial region defects often requires custom-made, personalized and anatomically shaped bone scaffolds [18]. Therefore, topologically-ordered porous scaffolds are a promising treatment strategy in bone tissue engineering due to distributed, interconnected pores, controlled porosity and pore size [18]. There are two leading 3D fabrication technologies: conventional and rapid prototyping. The rapid prototyping or additive manufacturing is overcoming some issues of the conventional technologies such as limited ability to control outer and inner shapes and geometries, or the use of organic solvents [18]. Therefore, the additive manufacturing or 3D printing becomes one of the essential tissue engineering methods to produce scaffolds with orderly-arranged pores. According to different characteristics, 3D printing methods used for porous scaffolds production can be classified into three categories: powder-, ink-, and polymerization-based [18].

2.3.1. Powder-based 3D printing

The powder-based 3D printing method uses powder bound together in the required shape by various binder materials (polymer glues or thermal fusion methods) [133]. The remaining unused powder is cleaned off the storage tank, recycled after the 3D printing is finished and the printed object is removed. To date, several different powder-based 3D printing techniques can be distinguished: binder jetting and selective laser sintering (SLS) [133].

In SLS, a solid scaffold structure is formed by a high-powered laser, which fuses small powder particles. The laser beam, controlled by a computer-aided platform, moves according to the scaffold model CAD file. Then a new

layer of powder is spread on top of the previous layer, and the process is repeated until the object is completed [134]. The broad spectrum of materials (polymers, ceramics, and metals) can be adapted for SLS 3D printing. This diversity of the materials makes it possible to manufacture artificial constructs matching the mechanical properties of a desired tissue / organ. An object's mechanical properties and structure can also be controlled by varying other SLS parameters: powder particle size, scan speed, laser power, etc. Another advantage of SLS is printing resolution. The diameter of the smallest object can reach even 5-10μm [135]. In addition, unused particles beyond the heat-affected zone can be re-used, resulting in the reduction in the cost of this method. The main disadvantages of SLS: all materials used for printing should be in powder form; trapped materials / material leftovers are difficult to remove from a printed object; printed objects have a rough surface, low mechanical strength; not compatible with cell bioprinting [133].

Binder jetting is another powder-based 3D printing method. This 3D technique was developed at the Massachusetts Institute of Technology and patented in 1993 by Emanuel Sachs [136]. The main difference between SLS and the binder jetting is that in the latter method, powder materials are selectively joined into the desired layer shape with a binder (typically a polymeric liquid) instead of a laser beam. The object may then be heated to cure the binder if needed [137]. However, this method's accuracy is limited due to the difficulty to control the size of the binder droplet. Moreover, the binder materials need to be carefully selected. For the application in the medical area, the binder should be non-toxic and toxic residue-free when heated [138].

2.3.2. Polymerization-based 3D printing

The polymerization-based technique is based on the projection of direct light (i.e. UV, laser) on a viscous photosensitive polymer solution to cross-link it and, thus, promote its solidification. After repeating this process layer by layer, the final 3D object can be manufactured [138]. The oldest but still widely used version of this technique is SLA. It uses a low-power UV light to cure photocurable polymers. However, new techniques such as projection micro-stereolithography, also called digital projection lithography (DPL), have been developed recently. The main difference of DLP is the use of a visible light source (such as a liquid crystal display panel and an arc lamp) for the polymer's polymerisation induction [139]. Both polymerization-based technologies demonstrate high accuracy and precision [140] . However, free radicals often form during the photopolymerization process. They, in turn, can

affect cell membrane, protein, and nucleic acids. Therefore, it is essential to apply a cytocompatible photo-initiator to use SLA or DPL 3D printing method for tissue engineering [141]. Moreover, the uncured photoinitiators are cytotoxic. Thus, scaffolds prepared by these methods should be thoroughly washed before use in tissue engineering applications [140].

2.3.3. Ink-based 3D printing

In the ink-based method, fluidic raw material is ejected by a nozzle (an extruder) steered through a mechanical or electromagnetic actuator. The extruded material deposits layer by layer and thus forms a printing object. For ink-based methods, the layer thickness is critical in the 3D printing process. It is known that a standard 3D incremental layer with a thickness of 150mm or less is recommended to minimize vertical z-steps and optimize interlayer communication in tissue engineering [142]. The diameter of the nozzle, in principle, controls the layer thickness, which represents the upper limit of the pore strut height. By changing the layer structure from single- to double-layer printed versions, the direct 3D printing technique can generate scaffolds of various layer thicknesses [143]. It was found that the double-layer printed scaffolds with smaller layer thickness could produce a higher osteogenic capacity for a long period of time (8-12 weeks), higher cell density in the scaffold's sidewall region, potentially promoting previous and final bone-forming [144]. Two main ink-based 3D printing techniques can be distinguished: direct ink writing (DIW) and FDM.

In the DIW method, the viscoelastic materials are extruded out of the nozzle by the pressure from a piston, a screw, or pneumatic force. Thus, DIW allows the extrusion at low temperatures (e.g. room temperature). This specific advantage of DIW enables the printing of cells without affecting their viability, which is impossible when using FDM [145,146]. As a result, DIW is one of the most studied techniques in bioceramic scaffolds fabrication. One of the benefits of this 3D printing method is its versatility to print almost any type of bioceramics: calcium phosphates, bioactive glasses, calcium silicates, etc. However, it is challenging to print multi-material structures using DWI as it often leads to nozzle clogging [140].

In FDM applications, the material, usually synthetic thermoplastics, is heated at high temperatures (140-250°C) to the melt state and then extruded to prepare a 3D structure. The main advantages of the FDM method in tissue engineering are low cost, ease of use, a variety of biomaterials and additional solvents. In addition, it provides good mechanical properties and highly controllable porosity due to the laydown pattern [17]. However, the main

disadvantage is that it cannot be combined with cells inside a filament when preparing scaffolds due to the high manufacturing temperature [139]. Therefore, one method is insufficient to design 3D bone scaffolds with multiple components and functions concerning all techniques, weaknesses, and advantages. Hot-melt extrusion (HME) could be a valuable supportive method for creating 3D composite scaffolds with FDM technology.

2.3.3.1. Hot-melt extrusion for bone engineering

HME technique has been used in food and plastics industries since 1930. Joseph Brama invented it for the manufacturing of lead pipes. Since then, HME has been a great succeess in plastic, rubber, pharmaceutical, and food industries to produce items ranging from pipes to sheets, bags or even drugs. In general, HME is a process in which filaments or amorphous solid dispersions from different materials (by shredding, mixing and melting) are produced [147]. The critical components of the HME technique are: feeder system for adding materials; barrel and screws for mixing the materials; heating elements for melting; motor for controlling the screw speed; extruder for filament / dispersion formation. According to an extruder type, the HME can be classified into a single-screw extruder and twin-screw extruder. Single-screw extruders are commonly used for filaments or films production. The twin-screw extruder is used for amorphous solid dispersions or pharmaceutical co-crystals [148].

In application areas of this method, artificial bone engineering is no exception. As an alternative technique, HME is usually used for composite filament preparation. Filaments for bone scaffold production are manufactured by mixing various polymers (PLA, PCL, etc.) with different concentrations of ceramic (HA, TCP, BG, etc.). With the proper selection of these materials' formulation and processing conditions, HME can produce suitable quality thermoplastic composite filaments printed by various FDM 3D printers [149]. In summary, HME is a relatively low-cost, fast, and easy to handle composite filament production method. However, sometimes it is not easy to obtain a precise, uniform filament's diameter with HME technology. According to the studies, it was observed that a varying filament diameter could further affect scaffold printing quality resulting in its topography inaccuracies compared to the initial model [150]. Still, it remains debatable what deviations of a filament diameter may affect the 3D printing results.

2.4. TISSUE ENGINEERING. REQUIREMENTS FOR AN IDEAL BONE SUBSTITUTE

Tissue engineering refers to the practice of combining scaffolds, cells, and growth factors into functional tissues [151]. It aims to restore, sustain, or improve a damaged tissue. Although not all tissue engineering approaches involve using all three components, a scaffold is necessary to provide the architectural cues for the regeneration of large bony defects. The ideal scaffold should be biodegradable with a controllable degradation rate; produce non-toxic degradation products; be capable of sterilization without loss of bioactivity; be biocompatible in terms of lack of toxicity and inflammatory reactions, cell attachment, migration, and proliferation; provide favourable mechanical properties to bear weight during bone regeneration period and promote bone cell migration into the scaffold (osteoconductive); be capable of eluting bioactive molecules, support and promote osteogenic differentiation (osteoinductive), and have suitable microarchitecture (pore size, pore shape, interconnected pore network, high porosity) for cell migration, nutrients, and waste transfer, angiogenesis [11,12].

Scaffold microarchitecture (porosity, pore size, and interconnected pores) is essential for achieving cell viability and promoting tissue regeneration. Porosity promotes cell movement through the scaffold and increases the surface area available for cell-scaffold binding and tissue contact. Scaffolds with sufficient total porosity have been shown in multiple research to facilitate osteogenesis while retaining mechanical properties [12,142]. Even so, several recent studies have shown that 30-50% of total scaffold porosity can achieve better cell proliferation, maintain good mechanical features and perform equally well in terms of cell proliferation and osteoconduction as compared to scaffolds with higher porosity [152,153]. Another important feature of 3D printed scaffolds is the size of the pores. 3D printing has been used to make scaffolds with custom pore sizes more often than any other fabrication process [154]. Scaffold vascularization has been shown to improve with the pore size. In both mathematical and laboratory models, pore sizes between 160 and 270μm resulted in substantial vessel development [154]. Pore size affects osteoblast proliferation and migration via scaffolds. Bigger pores (about 300μm and higher) result in larger cell numbers across the scaffold due to an easy passing for the cells through the length of scaffold without binding between the cells or the surface-adsorbed proteins [154–157].

The impact of pore configuration and geometry on bone regeneration is also essential. For example, bone cells opt for concave surfaces for migration and proliferation compared to flat and convex regions of the scaffolds [157].

Moreover, cell bridging occurs faster in hexagonal pores than rectangular and triangular pores due to the higher number of corners and the short distance between the two arches in the corners [157–159]. Furthermore, scaffolds with hierarchical porous architectures have recently received a lot of recognition due to their ability to enhance cell viability, binding, proliferation, and differentiation [160]. Apart from the importance of the macro and microarchitecture of the scaffolds, the materials for the scaffolds must be safe and biocompatible. Therefore, materials implanted in the human body should have a *medical grade* designation, which is earned after the US Pharmacopeial Convention (USP) or ASTM International testing, or meet the International Organization for Standardization (ISO) 10993 standard. The most often used osteoconductive organic and inorganic materials and their various compositions, osteoinductive materials and cell combinations in bone tissue engineering are discussed further.

2.4.1. Organic materials used for bone tissue engineering

Biodegradable polymers are materials with physical, chemical, and mechanical properties similar to biological tissues. These polymers break down into biologically acceptable molecules by hydrolysis of ester bonds by biodegradation [161]. The degradation time of different polymers varies [162]. The rate of polymer degradation may affect cell proliferation, extracellular matrix synthesis, and host response [163]. The most broadly used biodegradable synthetic polymers are aliphatic polyesters: PLA, poly(glycolic acid) (PGA), poly(ε-caprolactone) (PCL). These polymers have been extensively investigated for tissue engineering purposes because of their biocompatibility and biodegradability [164]. Polymers' physical, mechanical, and thermal properties differ and depend on chemical structure, molecular weight, crystallinity, glass transition temperature, etc. Higher glass transition temperature and a higher degree of crystallinity result in a more rigid and thermally stable but brittle material. The amorphous regions of a polymer provide elasticity and impact resistance [164]. The degradation behaviour of polymers depends on molecular weight and crystallinity. Lower molecular weight polyesters are degraded faster than those with higher molecular weights [165]. The degradation rate also increases with a higher degree of crystallinity [166].

PLA, PGA, and PCL are all thermoplastic materials that readily soften when heated and can be easily moulded. Therefore, they are suitable for 3D printing. The attractiveness of these plastics is also driven by their relatively

low cost. One of the most beneficial aspects of polyesters is the possibility to combine them with ceramic materials, tailoring the properties of the scaffold to fit the specific requirements needed for tissue engineering. These characteristics make PLA, PGA, and PCL popular choices as scaffold fabrication materials [15].

2.4.1.1. Polylactic acid. Advantages and disadvantages

PLA is a polymer with a high molecular weight (1.8×105 to 5.3×105). It was first synthesized in 1932 and later patented by Carothers (DuPont). To this day, PLA has been recognized by the US Food and Drug Administration (FDA) and European regulatory authorities as safe for all food packaging applications and some surgical applications [167,168]. PLA was initially introduced for resorbable sutures, resorbable medical plates, and screws, which were applied in maxillofacial trauma surgery, orthognathic surgery, and pediatric surgery [169]. In the late 1980s, Bos et al. demonstrated successful bone union in 10 patients with zygomatic fracture after fixation with PLLA plates and screws [170]. Further, PLA has been studied for drug delivery applications, leading to several pharmaceutical products such as vaccines, antagonistic, and anti-inflammatory treatments [171,172]. Lately, PLA scaffolds are being widely investigated for musculoskeletal, cardiovascular, nervous, and cutaneous tissue engineering purposes [173]. Many of these scaffolds have been analysed *in vitro* studies and require further evaluation *in vivo*.

PLA is derived from natural resources such as corn starch, potatoes, and cassava roots. Therefore, PLA can be produced in an environmentally friendly manner [161]. Usually, PLA is synthesized from lactic acid by polycondensation or ring-opening polymerization [174]. PLA has stereoisomers: poly(l-lactide) (PLLA), poly(d-lactide) (PDLA), and poly(dl-lactide) [173]. The stereochemistry influences PLA crystallinity and physical properties such as mechanical, thermal properties, and degradation characteristics [175]. The L stereoisomer constitutes the main fraction of PLA [176]. In addition, PLLA is found in most lactic acid, derived from renewable sources [168]. PLLA content higher than 90% tends to be crystalline, which decreases the rate of degradation [166,168]. PLLA tensile modulus (2.7-4.14 GPa) is similar to that of bone (0.5 GPa to 20 GPa), making it an attractive material for bone regeneration [173,175,177]. PLLA scaffolds may provide sufficient mechanical support to facilitate bone regeneration while reducing the stress shielding effect as well[178].

After several months of exposure to moisture, PLA biodegrades by hydrolysis to carbon dioxide and water, excreted during respiration, or

molecules used in glycogenesis [179]. The molecular mass of PLA in laboratory rats is reduced threefold in 32 weeks (from 14,100 g/mol to 4,300 g/mol), and PLA is fully metabolised in 72 weeks [180]. PLA degradation time in humans ranges from 1 to 7 years depending on stereoisomers percentage in the polymer with an average of 3 years, which provides good stability and allows complete bone healing [169]. PLA melting temperature is between 120-180°C. Therefore, PLA is one of the most common plastics used for 3D printing [168,181].

However, the main limitation of PLA is the formation of acidic by-products during degradation, which lowers the pH of the extracellular matrix and induces mild inflammatory and foreign body reactions [173,182]. Moreover, PLA is hydrophobic, making it more resistant to hydrolysis, and might complicate cell adhesion and proliferation [169,183]. However, lactic acid has been shown to have antioxidative properties, which may protect cells from damage caused by free radicals, naturally produced throughout a cell's life cycle [184,185]. Furthermore, sufficient thickness of PLA is required to achieve favourable mechanical strength, which may cause aesthetical complications in the maxillofacial area [186].

2.4.1.2. Polyglycolic acid. Advantages and disadvantages

PGA is the first biodegradable synthetic polymer commercially successful for sutures in medical applications [169]. PGA has a lower than PLA molecular weight (2.0×104 to 1.45×105), higher melting temperature (about 224°C), and a high degree of crystallinity [169]. PGA is synthesized by the polycondensation process of glycolic acid. PGA exhibits a high rate of degradation, which leads to rapid mechanical strength loss of about 2-7 weeks (an insufficient duration to allow complete bone healing) after scaffold implantation *in vivo* [161]. In addition, when used for fracture fixation, PGA implants were associated with foreign body reactions such as swelling at the implantation site, fluid accumulation, and sinus formation [187]. Due to these limitations, pure PGA was rarely used in the maxillofacial area.

2.4.1.3. Polycaprolactone. Advantages and disadvantages

PCL is a semi-crystalline polymer with molecular weight varying from 5.3×105 to 6.3×105 [188]. The PCL degree of crystallinity is up to 69%, resulting in high elongation at break as its amorphous parts are in the rubbery state [189]. PCL glass transition temperature is −60°C, melting point range 58-65°C [161]. Therefore, it is one of the softest aliphatic polyesters at room

temperature, making PCL convenient for 3D printing. There are two main pathways to produce PCL. The first one is the polycondensation of 6-hydroxyhexanoic acid under vacuum conditions. However, the preferred method is ring-opening polymerisation as it gives a polymer with a higher molecular weight [188, 189]. PCL is FDA-approved for tissue engineering applications [190]. Being a biocompatible and chemically inert material, PCL has been successfully used for sutures, wound dressing, cardiovascular, neural, and bone tissue engineering [188].

Among the polyesters, PCL is characterized by the slowest degradation [191]. Slow scaffold degradation causes a less acidic environment, resulting in greater cell viability [192]. The PCL-based polymer scaffold's degradation took about 3-4 years in rabbits and rats [193]. In humans, PCL degrades during a two-phase hydrolysis process that takes more than 4 years. During the first phase of degradation, lasting for about 3 years, the implant's mass and volume remain unchanged and interfere with bone formation [194]. The limitation of PCL is its hydrophobicity and absence of functional groups, which causes poor cell attachment and proliferation [15,195]. In addition, PCL exhibits lower than PLA tensile strength and might lack the mechanical properties needed for bone regeneration [196].

2.4.2. Inorganic materials used for bone tissue engineering

The primary constituent of bone is an inorganic component. Bone consists of up to 65% calcium-phosphate minerals, specifically, hydroxyapatite [197]. Therefore some calcium-phosphate formulations, which are sintered to form a ceramic, have been developed and investigated for their bioactivity: tricalcium-phosphate (TCP), synthetic HA. Due to their similarity to natural bone mineral CaP based ceramics possess excellent osteoconductivity [198,199]. However, these ceramics differ in their chemical formula and the Ca/P ratio, which impact the material rate of resorption and osteoconductivity. In addition, bioglass is another type of osteoconductive material capable of forming direct bonding with bone. However, the major limitation of inorganic materials is their brittleness, which prevents their use in the regeneration of large bone defects [200]. Nowadays, various forms of HA and β-TCP (putties, granules, porous scaffolds) make up the majority of the synthetic bone graft substitutes available commercially for dental and orthopaedic applications.

2.4.2.1. Tricalcium phosphate. Advantages and disadvantages

There are two forms of TCP: β-TCP (β-tricalcium phosphate, β-Ca3(PO4)2) and α-TCP (α-tricalcium phosphate, α-Ca3(PO4)2). α-TCP is usually obtained from β-TCP by heating above 1125ºC. Both TCPs have the same chemical composition but a different crystallographic structure, which affects solubility [201]. β-TCP is more stable and less soluble than α-TCP [202]. Pure α-TCP has a quick resorption rate, limiting its application for bone regeneration purposes [203]. On the contrary, β-TCP has been broadly studied since its biocompatibility was reported a century ago. In 1920, it was described for the first time as a bone graft in a rabbit's radius [204]. Later, β-TCP was commercialized as a bone substitute, metallic prosthesis coating, cement, composite material, and polishing agent in toothpastes.

β-TCP can be prepared by bone calcination or using chemical preparation routes, usually by thermal conversion of amorphous calcium phosphate or calcium-deficient hydroxyapatite [203,205]. β-TCP has a Ca/P ratio of 1.5; therefore, it has a high dissolution rate that accelerates its resorption [206]. β-TCP's 0.7-1.4mm particles are almost entirely resorbed over 8 weeks after implantation in intraosseous defects in minipigs [207]. The resorption of 8mm diameter and 13mm length cylinders of β-TCP was shown to take over 24 weeks after the implantation in the cancellous sheep bone [208]. β-TCP is resorbed by osteoclastic cell-mediated degradation, and part of the calcium ions released during resorption is used for bone formation [209,210]. During the degradation, surfaces of the implants become rough, and the bone grows into surface irregularities causing mechanical interlocking between the bone and implant. However, no apatite layer is present at the interface of β-TCP [211]. Nevertheless, β-TCP possesses osteoconductive properties and might even show higher bone-bonding strength than HA [212,213]. Studies have shown β-TCP to be highly osteoinductive and have similar performance to autologous bone regarding bone formation [214]. Although fast degradation is beneficial for osteoinduction, a stable surface is required for bone formation to occur. This obstacle can be overcome by combining β-TCP with polymers.

2.4.2.2. Hydroxyapatite. Advantages and disadvantages

Since its introduction in the mid-1980s, hydroxyapatite with a general formula of Ca10(PO4)6(OH)2 has been widely used as a biomedical material [215]. Due to its similarity to the inorganic part of bone and teeth, HA particles have been widely used in orthopaedics and oral surgery for bone defect filling, bioactive coating for titanium implants, and as particles in the

toothpaste. It has also been studied for drug delivery, cell targeting, and diagnosis [216,217]. HA may be derived from natural sources such as corals, eggshells, seashells, mussel shells, mammalian bones (bovine, camel, horse, pig), fish bones or scales, limestones, fruit peels, wood [218]. The usage of HA from natural sources can be considered environmentally friendly, sustainable, and positively contributing to the economy since these materials are available in large quantities [218]. However, such HA has different characteristics: particle sizes ranging from 5 μm to 10.4 μm, low or high crystallinity (depending on the method of extraction), different Ca/P ratio or presence of trace elements (Mg, Na, Zn, Sr, Ba, Fe, Al, K, Zn) [218]. In addition, HA may be produced synthetically using calcium and phosphate precursor salts with different wet (precipitation, hydrothermal synthesis, sol-gel, ultrasonic synthesis, microemulsion) or dry (solid-state reaction) methods [219,220]. The benefit of synthetic HA is the crystalline phase, which is similar to natural HA found in bones [221].

HA crystals can be easily sintered to HA ceramics to enhance mechanical properties [222]. Moreover, HA can be prepared as a nanoscale powder to combine with other biomaterials, including polymers [223]. The pure HA Ca/P molar ratio is 1.67, making it the most stable calcium phosphate salt at room temperature and under physiological pH [224]. HA possesses excellent biocompatibility, and no adverse local, systemic toxicity, or foreign body reaction has been reported [215]. When HA comes into contact with the blood serum or hematoma at the early stages of healing shortly after implantation, Ha creates carbonated HA on the surface, which is the central aspect of the bioactivity [221]. After the implantation, the regenerating bone binds directly to HA through a carbonated calcium-deficient apatite layer followed by cell adhesion and migration [203,225]. Moreover, HA has positive effects on the differentiation of osteoblasts and exhibits osteoconductive properties [221]. Because of its low solubility, the osteoinductive properties of HA are debatable. While some studies claim HA to be osteoinductive, others believe the osteoinductive properties highly depend on the microporosity and geometry of the scaffold [226,227]. Therefore it is usually called *intrinsically osteoinductive* [228].

The major weakness of HA is insufficient mechanical strength and brittleness when used in load-bearing locations [225]. However, the mechanical properties of HA scaffolds are superior to β-TCP scaffolds prepared by the same method and with the same porosity [229]. Artificial HA ceramics are slightly soluble, thus challenging to resorb and even being regarded as non-degradable, as their degradation takes decades [201,215]. Various approaches, such as synthesis of calcium-deficient or calcium-rich HA, amorphous HA,

poorly crystalline HA, or adding other calcium-based materials, are studied to increase the degradation rate of HA [230–234].

2.4.2.3. Bioglass. Advantages and disadvantages

There are several types of bioactive glass: silicates, phosphate-based glasses, and borate-based glasses. Phosphate-based and borate-based glasses exhibit fast dissolution and are studied for soft tissue healing [235]. The conventional silicate bioactive glasses are amorphous and compound of different proportions of SiO2, CaO2, P2O5, and Na2O [236]. The composition of the bioactive glasses determines their bioactivity and bonding to bone or soft tissue. The original bioactive glass composition, 45S5 Bioglass (BG) (45 wt% SiO2, 24.5 wt% CaO, 24.5 wt% Na2O, and six wt% P2O5) was discovered in 1969 by Hench [237]. The first bioactive glass-based product received FDA approval in 1985. Since then, several commercially available bone substitutes based on bioactive glass such as NovaBone or S53P4 Bioglass BonAlive [238,239] have been proposed and showed promising results comparable to autogenous bone [240].

Bioactive glasses are biocompatible and do not induce inflammatory or toxic responses upon implantation [241]. In addition, they have antibacterial properties against clinically essential bacteria species, e.g.,Streptococcus spp attributed to the pH increase caused by cation release during degradation [242]. Within an hour of the implantation of bioactive glasses, its surface precipitates hydroxycarbonate apatite crystals, which form a bond with bone collagen fibres [243]. In fact, within 6 weeks after implantation, the bond between bioactive glass and bone gets stronger than the host bone itself [244]. The hydroxycarbonate apatite crystals layer absorbs extracellular matrix proteins and facilitates osteoblast attachment and bone matrix deposition [245]. Bioactive glass can also bond to soft tissues; therefore, it has been used for middle ear replacement prostheses [246].

BG is considered an A class bioactive material, which means it possesses osteoconductive and osteoinductive properties [247]. When implanted, BG releases soluble silica and calcium ions in a controllable manner having positive intracellular effects on bone tissue proliferation [247]. Consequently, within 48 hours after implantation, several families of genes are upregulated, and the synthesis of growth factors, which affect the osteoblasts' cell cycle, is initiated [237]. For example, the expression of insulin-like growth factor II (IGF-II), which aids in osteoblasts proliferation, is increased by up to 320% [248]. Particles of BG have also been suggested to induce osteogenic differentiation of bone-marrow-derived mesenchymal stem cells into osteoblast-like cells [249].

Moreover, silicic acid released from BG stimulates collagen production by osteoblasts [250]. Because of these effects, BG can induce ectopic bone formation [251]. Studies have also shown that BG can stimulate fibroblasts to secrete vascular endothelial growth factor (VEGF), which induces angiogenesis [252]. However, it is speculated that the potent bioactivity of BG can cause soft tissue calcification. More studies are needed to investigate this issue [253].

The limitation of bioactive glasses is the difficulty of producing porous scaffolds [254]. Scaffolds must be sintered to fuse glass particles, making them crystallize. This structure transformation from amorphous to crystalline reduces the bioactivity of the glass [254]. Various modifications of bioactive glass composition that prevent crystallization during sintering, e.g. adding magnesium, are being studied [255]. Sintering is also required to fuse bioactive glass particles with a polymer template. The polymer template improves the porous scaffold's mechanical properties compensating for bioactive glass brittleness [256].

2.4.3. Composite materials. Advantages and processing strategies

Bone is a mineralized connective tissue [114]. From a material science perspective, the bone matrix is a heterogeneous composite substance composed of a polymer-ceramic lamellar fibre-matrix [257]. Therefore, two or more biocompatible materials can be combined into a composite to fulfil multiple requirements for the ideal scaffold for bone regeneration [13,14]. Organic-inorganic composites combine the ductility of a polymer phase with the stiffness and strength of an inorganic component to have mechanical properties similar to native bone and improve tissue interaction [14]. Furthermore, the addition of polymers facilitates the production and control of the microarchitecture of the porous scaffold. In turn, bioceramics such as hydroxyapatite and bioactive glass enhance the scaffold's osteoconductive and osteoinductive properties, counteract the acidic degradation of biodegradable polymers, increase the hydrophilicity and water absorption of the hydrophobic polymer matrix [14]. In addition, a targeted degradation rate of the scaffold can be achieved by modifying the percentage of organic-inorganic parts. Usually, the percentage of inorganic materials in the porous scaffolds' ranges are 10-50 wt. % for HA, 10-50 wt. % for BG, and 10-40 wt. % for TCP [14]. Although there are various possible combinations of organic and inorganic materials in the scaffolds, the PLA/HA and PLA/BG combinations will be discussed further. These composites are suitable for the FDM technique and are the main focus of the research.

2.4.3.1. PLA/HA composite material

PLA/HA composites have been studied as the scaffolds for bone regeneration, carriers for drug delivery into the host, and commercially available bone fixation devices [258–260]. Stimulation of stem cells to differentiate into the osteoblasts, a better stem cell attachment, proliferation, and migration may be achieved when a new composite PLA/HA material is created [261,262]. One of the advantages of combining PLA and HA is the neutralization of the acidity degradation products of PLA by the alkalinity catabolite of HA [261,263]. Regular activity of osteoblasts is achieved during PLA/HA biodegradation as the degradation products of the composite do not change the media's pH value [263]. The composition of the PLA/HA composite strongly affects its rate of biodegradation. The degradation is more pronounced in scaffolds with higher HA percentages due to enhanced wettability and the dissolution of the smaller amount of polymer between the HA particles in the *in vitro* studies [264,265].

Although PLA/HA composites exhibit better mechanical properties than PLA, the percentage of HA in the PLA/HA biocomposites, PLA molecular weight, and HA's dispersion within the PLA matrix influence the composite's mechanical properties. [266,267]. In some studies, HA concentration of 40 wt% in the PLA/HA composites increased the bending strength, 15 wt% of HA improved the crack resistance of PLA during cyclic loading [268]. In addition, HA content of 20 wt% demonstrated better mechanical performance and thermal stability than 10 or 30 wt% of HA under the same experimental conditions (tensile strength 48.3 MPa, tensile modulus 3.44 GPa) [266]. The composite's thermal stability is improved as the thermal energy is efficiently distributed over several bonds [267]. However, poor dispersion and incorporation of HA within the PLA matrix may lead to undesirable premature failure at the PLA/HA composite interface and lower mechanical properties. This uneven dispersion of HA was discovered in the PLA/HA composite with 20 wt% of HA [267]. It was found that 10 wt% of HA increased the mean stiffness of the composite PLA/HA scaffold, tensile strength and tensile modulus were improved by about 18-25%, flexural strength and flexural modulus were increased by about 20% compared to PLA scaffolds [267]. However, to achieve the scaffold's higher elastic modulus, which can be statistically comparable to human cortical bone, HA content ranging 70-85 is required with better HA and interfacial adhesion [264,267,268].

Regarding biocompatibility studies, HA concentration of 10 wt% improved osteogenic potential, with no measurable changes to cellular compatibility or the mechanical shear strength of the composite [269]. PLA/HA scaffold with 15 wt% of HA showed better results than pure PLA scaffolds in

cell viability, significantly higher initial cell attachment, and proliferation on the scaffolds [270]. Moreover, the expression of alkaline phosphatase in 7 days of culturing was significantly higher on the PLA/HA composite than on the pure PLA, confirming HA significance in the bone regeneration [270]. Wan et al. confirmed that PLA/HA composites exhibit biocompatibility toward a wide range of cell lines, including L929 fibroblasts and MC3T3-E1 osteoblasts, and induce expression of osteocalcin, a bone-specific marker [266]. Zhang et al. have chosen a melt-deposition system (MDS) method to produce PLA (85 wt%) and HA (15 wt%) composite scaffolds and compared them to the demineralized bone matrix (DBM) and β-TCP. They found no significant difference in local cellular inflammatory reaction between all experimental groups and control. The expression of osteogenic-related genes was upregulated on PLA/HA scaffolds compared to β-TCP scaffolds but lower than DBM scaffolds. However, the relative newly formed bone area in PLA/HA scaffolds was greater than in the DBM scaffolds group, however, lower than the β-TCP group in 4 and 8 weeks after implantation [259].

2.4.3.2. PLA/BG composite material

BG was combined with metals, ceramics, and polymers for hard and soft tissue engineering to produce highly bioactive materials and overcome its inherent brittleness and low strength [271]. BG can be incorporated in PLA scaffolds by the melt-deposition system or polymer dissolution in chloroform, 1,4-dioxane or dimethyl carbonate (DMC) [272–277]. Recent studies using additive manufacturing methods, combining BG with high elastic modulus polymers (PLA), have shown the composite scaffolds' improved compressive strength and repairing ability in critical-size defects in load sites [278]. PLA in composite scaffolds reduces the effective load on the BG and limits the initiation or growth of cracks [278]. Another research has confirmed the increase of the tensile strength of the composites from 56.7 MPa (pure PLA) to 69.2 MPa by loading PLA scaffolds with 4 wt% of BG [275]. Moreover, it is known that an addition of 5 wt% BG to PLA scaffolds enhances the compressive strength of the scaffolds roughly 1.5 times [277]. Eldesoqi et al. studied larger BG concentration impact on discs' mechanical properties consisting of PLA and 20 wt% BG, or PLA and 40 wt% BG. Three points bending test showed an increased ultimate load of scaffolds with BG particles [276]. Zhang et al. compared 9 and 29 wt% BG PLA/BG scaffolds. Mechanical tests revealed the elastic modulus increase with increasing BG content, however, tensile strength and break strain decreased [273]. They also showed that

3-aminopropyltrimethoxysilane pretreatment might enhance elastic modulus and prevent the decrease in tensile strength with larger glass content [273].

Multiple *in vitro* biodegradability studies demonstrated that PLA/BG composites induce the formation of an apatite layer on the scaffold surfaces [272,273,275,277,279,280]. The presence of BG particles was found to decrease the composite's degradation rate compared to pure PLA [272,277]. During the first 2 weeks of *in vitro* degradation, PLA/BG scaffold weight loss was higher than pure PLA scaffold, followed by a decrease in degradation rate between weeks 4 and 6. PLA scaffold weight loss, on the other hand, began within 2 weeks and progressed more quickly than PLA/BG at 8 weeks, reaching 8% (versus 4.5% weight loss of PLA/BG) [277]. Human adipose-derived stem cells, bovine annulus fibrosus cells, fetal osteoblasts, and human BMSC have been utilized to assess the biocompatibility and bioactivity of PLA/BG composites containing different BG percentages from 0 to 40 wt% [274,281–283]. PLA/BG composites have been shown to support cell attachment, growth, proliferation, and osteogenic differentiation, confirmed by increased alkaline phosphatase (ALP) activity and osteocalcin protein synthesis [281–283]. However, Yang et al. found that 5 wt% BG concentration was more effective in enhancing cell differentiation than 40 wt% BG. They suggested that higher BG concentrations increase and prolong ion release, which might cause medium alkalinisation, cytotoxic to osteoblasts [281]. In another study, 30 wt% PLA/BG foams stimulated collagen and sulphated glycosaminoglycans (sGAG) production by bovine annulus fibrosus cells [274]. Moreover, it was found that 5 wt% and 40 wt% PLA/BG composites significantly increased extracellular matrix mineralization compared to pure PLA [282].

In vivo study in rats suggests excellent biocompatibility of PLA, PLA/BG 20 wt%, and PLA/BG 40 wt% scaffolds. These scaffolds did not cause any behavioural changes, visible signs of neurological toxicity, organ damage, long-term systemic inflammatory reactions, or tumour formation during a 3-month observation period [276]. The presence of BG in the composite implant promoted bone formation in a rat skull critical size bone defect at the contact area of the implant and the skull and towards the centrum of the defect [276]. 5 wt% and 40 wt% PLA/BG composites have also been shown to induce ectopic bone formation, confirming BG osteoinductive properties [283]. The vascularization pattern of PLA/BG composites with BG content of 5, 10 and 20 wt% and pure PLA has been studied *in vitro* [284]. Vascular endothelial growth factor secreted by human fibroblasts in contact with scaffolds was recorded to be 5 times bigger with 20 wt% PLA/BG composites than pure PLA [2844]. A rat model was chosen to analyse the vascularisation of the

scaffolds *in vivo*. PLA/BG scaffolds with 5 wt% of BG demonstrated greater vascularisation than PLA scaffolds in 8 weeks after implantation [277].

2.4.4. Osteoinductive materials in bone tissue engineering

Over the last few decades, a lot of research has been conducted on osteoinductive bone grafting materials. Osteoinduction has historically been described as the mechanism by which one tissue, or a substance extracted from it, causes a second undifferentiated tissue to differentiate into bone due to physicochemical effect or contact with another tissue [287,288]. One of the first osteoinductive proteins regulating chemotaxis, mitosis, differentiation, callus, and bone formation was found in 1971 and called BMP [287]. It is known that BMP induce bone-forming via an endochondral pathway, while biomaterials are intramembranous [1]. Although the exact mechanism of osteoinduction by biomaterials is unknown, osteoinductive properties depend on their macrostructure, microstructure, and chemical composition [1]. The osteogenic differentiation *in vitro* of undifferentiated mesenchymal stem cells or osteoprogenitor cells in contact with new materials can show the osteoinductive potential before *in vivo* investigation [288]. However, injecting the agent or placing the biomaterials into non-osseous sites (muscle pouch) is the safest way to demonstrate osteoinduction properties and differentiate them from osteoconduction [1]. So far, two main strategies for adding osteoinductivity to bone grafting materials have been developed: adding osteoinductive agents (various growth factors, BMP, PRP, Emdogain) and seeding scaffolds with stem cells to create bone tissue-engineered constructs [288].

2.4.4.1. Emdogain

Emdogain is composed of enamel matrix derivative (EMD), a family of hydrophobic proteins secreted by Hertwig's epithelial root sheet. The purified fraction of the proteins is derived from the enamel layer of porcine unerupted tooth buds. Hammarstrom et al. was the first research group to find that EMD induced periodontal regeneration [289]. They compared the healing of surgically created recession defects in the animal model treated with either coronally advanced flap (CAF) alone or with EMD. After 8 weeks, the histological evaluation revealed the formation of acellular cementum, periodontal ligament, and alveolar bone formation in all EMD group defects. In comparison, healing by forming a long junctional epithelium occurred in the CAF alone group [289]. The basis of EMD's biological effect is thought to be

through mimicking odontogenesis by stimulating local growth factor secretion and cytokine expression, influencing mesenchymal cell differentiation, stimulating migration and viability of osteoblasts [201–292]. Over 20 years of research, more than 60 randomized clinical trials of EDM use were carried out. No studies reported any adverse events or patient allergic reactions [293]. However, concerns have been raised regarding EDM use for patients with premalignant or malignant mucosal lesions [294].

One of the EMD applications is root coverage procedures. Treatment of root recessions with CAF combined with EDM led from 12% to 15% improvements than CAF alone [295]. However, subepithelial connective tissue graft (SCTG) provided significantly superior long-term outcomes than CAF combined with EDM. Treatment with SCTG resulted in the development of a long junctional epithelium, while the formation of new cementum, alveolar bone, and periodontal ligament occurred in EMD procedures [295]. Moreover, oral mucosa wound healing might be improved by EDM application. In rats, EMD treatment significantly increased the number of blood vessels and the collagen fibres in the connective tissue by enhancing the expression of various growth factors [296]. Furthermore, EMD application for pulp regeneration and healing of replanted teeth has been evaluated. However, recent systematic reviews found EMD application results in endodontic treatments highly variable [297]. In most cases, EMD treatment promoted an ingrowth of hard tissues into a root canal space and induced the formation of a cementum-like tissue at the apical region of the root's external surface [298].

A meta-analysis showed that EMD treated sites for the treatment of intrabony defects displayed statistically significant probing attachment level improvements and pocket depth reductions compared to placebo or control-treated sites [299]. However, a high degree of heterogeneity was observed among trials. Comparing EDM with guided bone regeneration (GBR), significantly more postoperative complications occurred in the GBR group. The review concluded that the actual clinical advantages of using EMD are unknown [300]. Moreover, various studies looked at whether EMD promotes bone regeneration alone or in combination with other biomaterials. Many *in vivo* studies agreed that EMD has more *osteopromotive* properties than osteoinductive [291,292] and that EMD shows a lack of osteoregenerative potential in critical-size bone defects [301]. The main problems are the gelatinous nature of EMD as it is ineffective in preserving the space for new bone formation and low concentrations of amelogenins with osteogenic potential [292,302]. Furthermore, EMD was combined with various osteoconductive materials or membranes to maintain the space for bone regeneration. Most of these studies show slight but insignificant improvement of combined

techniques compared to biomaterials alone [292,302,303]. However, EMD combined with biomaterials seems to be more effective in periodontal regenerative therapy than bone regeneration alone as it positively affects cementum and periodontal fibres [292,301,302]. Furthermore, it is essential to mention that EMD positively affects bone formation over 36 months after its use. However, most *in vivo* studies expect for the bone regeneration results earlier with the healing process not yet completed [302].

2.4.4.2. Bone morphogenetic proteins

BMP are osteoinductive proteins from the transforming growth factor-beta (TGF-β) family that induce endochondral bone development from mesenchymal cells *in situ* [304]. BMP enhance chemotaxis, mesenchymal and osteoprogenitor cell proliferation and differentiation, angiogenesis, and mediated extracellular matrix synthesis [305]. There are more than 20 human BMP identified [306]. Based on a detailed review, BMP-2/-6/-9 of the 14 forms of BMP molecules were described as the most influential factors inducing MSC differentiation into osteoblasts. Another study confirmed that BMP heterodimers, such as BMP-4/-7 and BMP-2/-7, have better osteoinductive activity and more effectively control the differentiation and proliferation of MSC towards osteoblasts *in vitro* and *in vivo* [307]. Moreover, the FDA has licensed BMP-2 in single-level anterior lumbar interbody fusion, tibial nonunions, and oral and maxillofacial reconstructions [308,309]. On the other hand, the BMP-related side effects in animal studies include induction of inflammation [310]. Moreover, these proteins can stimulate bone formation in many other non-osseous tissues, have short half-lives, and remain a costly procedure with a relatively limited outcome [311]. Also, a low concentration of BMP will stimulate MSC to differentiate into adipocytes instead of osteoblasts [307]. As a result, BMP are only used as the ultimate treatment option [308]. They often require a transportation system (e.g. collagen sponge) to hold them sequestered, and the appropriate concentration, species-specific for bone osteoinduction [308].

After FDA approval, BMP-2 with 1.5 mg/ml concentrations are among the most often clinically used osteoinductors and alternatives to autografts [285]. The research showed that BMP-2 result in shorter operating times (25 min) and shorter hospital stays (0.75 days) than autografts in single-level degenerative disk disease patients [312]. However, some bias was reported in the initial industry-sponsored publications with no clear advantages of BMP-2 use compared to the iliac crest bone graft [308]. Up to date, studies have shown that higher concentrations (1.5 mg/ml) of BMP-2 are more effective in bone

healing in humans, as it is revealed in extraction socket augmentation in terms of extraction socket thickness and implant positions than the concentration of 0.75 mg/ml [308]. Furthermore, *in vivo* research confirmed that higher concentrations of the BMP-2 group had the most successful bone regeneration in the calvarial defects and showed near-complete healing [313]. Unfortunately, side effects are often associated with the higher dosages of BMP [308].

Moreover, BMP-2 are one of the primary inductors of the signalling cascade that start periosteal progenitor proliferation and differentiation during bone repair and regeneration [314]. *In vivo* studies revealed that periosteal progenitors would remain quiescent, and healing would not be initiated in the absence of BMP-2 [314]. *In vitro* study showed that BMP-2 improved cell adhesion and proliferation with no signs of significant cytotoxicity or apoptosis/necrosis [315]. However, some adverse effects or complications that range from 20% to 70% of clinically treated patients need to be mentioned [308]. Animal studies revealed the elevation of various cytokines and chemokines, including IL-1, IL-6, IL-10, IL-18, TNF-α, when treated with high doses of BMP-2 [310]. Several reports have demonstrated that BMP-2 stimulate osteoclastic activity *in vitro* and *in vivo* by activating receptor activators of nuclear factor-kb ligands that promote osteoclastic development [316,317]. The main complications in spinal fusions are an increased risk for implant displacement, subsidence, infection, urogenital events, radiculitis, ectopic bone formation, and osteolysis. BMP-2 in cervical spine fusion is prohibited due to the risk of cervical swelling and corresponding dyspnea, dysphagia [308]. Moreover, the exact effect on cancer risk or proper indications for application in pediatric population are still unknown [308]. However, despite these concerns, no suitable alternative has been found similar or superior to the BMP-2 in terms of osteoinduction [308].

2.4.4.3. Platelet concentrates

Recent research has focused on platelet concentrates on bone osteoinduction. Platelet concentrates are produced from an autologous platelet suspension derived from a patient's blood using centrifugation techniques [318]. Platelets have osteoinductive properties due to their high concentration of growth factors. Platelet alpha granules explicitly produce and release a variety of growth factors: platelet-derived growth factor AB (PDGF-AB), TGF-β, vascular endothelial growth factor (VEGF), epidermal growth factor, fibroblast growth factor, and insulin-like growth factor 1, which can promote cell migration, proliferation, matrix remodelling, and angiogenesis [318,319]. In addition, the dense granules of platelets contain bioactive factors: serotonin,

histamine, dopamine, calcium, and adenosine, which can increase membrane permeability and modulate inflammation [320]. Blood plasma is made up not only of water. It also contains from 8% to 9% of solids: coagulants (fibrinogen), various plasma proteins (albumin, globulin), electrolytes (sodium, potassium, bicarbonate, chloride, calcium), immunoglobulins, enzymes, hormones, and vitamins [321]. Platelet-rich plasma (PRP) is prepared from extracted blood with an anticoagulant. It is immediately or within an hour centrifuged to separate whole blood into 3 layers: a top acellular plasma layer (PPP), middle leukocyte and platelet layer, and bottom red blood cell (RBC) layer [322]. The aim is to collect a concentrate of platelets and discard the RBC and the PPP layers [322]. Platelet-rich fibrin (PRF) concentrates obtained by centrifugation without anticoagulants are exclusively autologous [323]. Four main platelet preparations depend on their cell content and architecture: pure or leukocyte-poor PRP (P-PRP), leukocyte-rich PRP (L-PRP), pure or leukocyte-poor PRF, and leukocyte-rich PRF (L-PRF) [319].

P-PRP is the standard platelet concentrate used in orthopaedics and has demonstrated promising effects in bone regeneration [322]. P-PRP combined with autografts has been used extensively to restore craniofacial deformities facilitating quicker maturation of autologous bone grafts and improving new bone development in mandibular defects [319]. Animal studies confirmed that too high (more than 30%) platelet concentration has inhibitory and even cytotoxic effects on osteoblasts. A significant increase in osteoblasts proliferation was achieved with platelet concentrations ranging from 1% to 5% [319]. However, the benefits of P-PRP in osteogenesis are debatable, and some experiments have shown that when P-PRP is used, bone maturation fails [325]. Moreover, P-PRP use is limited in oral and maxillofacial surgery due to complicated handling (liquid), the need to be used with other biomaterials, and quick release of growth factors [325]. The leucocytes in L-PRP played an essential role in the early stages of inflammation and influenced bone wound healing effectiveness [326]. However, the effect on osteogenesis tended to be more harmful than positive due to the suppression of BMP-2 and increasing TGF-β1 activity [326]. *In vivo* study demonstrated that bone defects in rats treated with L-PRP had lower new bone deposition than autograft or no grafting material groups, resulting in appendicular bone with thinner trabeculae and an expanded medullary region consisting of adipose cells [327].

According to the literature, the P-PRF method is very unpopular - firstly P-PRP should be created, and then $CaCl_2$ added. This kind of PRF preparation remains challenging and is expensive in daily practice [322]. Other problems identified in the literature are poorly described preparation protocols and results of PRP or PRF, without specifying they are pure or containing

leucocytes [328]. Despite the gaining of different platelet concentrations, the vitality of the cells is essential. Evidence in the literature shows that some centrifuges produced PRF-like materials with a damaged and almost destroyed cell population using the standard protocols [319]. The speed and angulation of the tubes are critical factors when choosing a centrifuge [319]. L-PRF is more manageable, more cost reasonable to prepare than PRP or P-PRF as it does not require direct activation with external factors (e.g. bovine thrombin or extrinsic anticoagulants) [325]. L-PRF stores cytokines and growth factors in a 3D fibrin scaffold achieving better cell attachment, migration due to its fibrous nature [319]. *In vivo*, L-PRF breaks down more slowly than PRP, creating a rigid fibrin matrix that slowly remodels in the manner of a blood clot. Platelets and cytokines are effectively stored and progressively released over a 10-day cycle, allowing migration and proliferation of the stem cells to be more effective for the duration of their growth cycle [325]. It must be mentioned that L-PRF cannot be used as allograft material as it is donor-specific due to antigenic plasmatic molecules and immune cells [319]. The literature confirms that L-PRF can stimulate the proliferation of most cell types (fibroblasts, keratinocytes, pre-adipocytes, osteoblasts, BMSC) and the differentiation of stem cells (e.g. DPSC) towards osteoblasts [322,329].

L-PRF showed promising results in bone regeneration, especially in the early stages of healing, and combined with various osteoconductive materials, e.g. polylactic-co-glycolic acid, β-TCP scaffolds, or bone substitutes [319,330]. L-PRF combined with TCP showed better results than TCP/BMP-2 mixture in sinus lift augmentation [319]. Moreover, L-PRF combined with osteoconductive materials shortened the healing time and showed promising healing in periodontal intrabony defects, alveolar cleft reconstructions [319]. Although L-PRF combined with bone substitutes may result in volume reduction, several advantages like angiogenesis, stem cell attraction, and migration of osteoprogenitor cells to the centre of the graft are induced [319]. The use of L-PRF improves bone healing, reduces infection better than covering post-extraction sites with the membranes [325]. Further research is needed to compare BMP-2 with L-PRF in clinical trials. Low cost, autologous source, and easy handling make L-PRF ideal biomaterial worth further investigation across various surgical procedures [325].

2.4.5. Stem cells in bone regeneration

Stem cells are undifferentiated cells capable of proliferation, self-renewal, and possess proliferation and multilineage differentiation [331]. Adult stem cells are found in bone marrow, periosteum, muscle, adipose tissue,

brain, and skin. Studies have shown that these cells' differentiation ability and plasticity might be higher than only one tissue where the stem cells are found [12,331]. Various growth factors or osteoinductive biomaterials can be used to achieve osteogenic differentiation *in vitro* [332]. However, several recent studies have shown that stem cells may spontaneously differentiate from osteoblasts due to the appropriate 3D surface morphology [333,334]. Cell-based tissue regeneration relies on a patient stem cells' isolation, expansion, and seeding on the scaffolds to produce an extracellular matrix *in vitro* [12]. Finally, the scaffolds with differentiated cells or decellularized scaffolds are implanted to patient bone defects [335]. The disadvantages of these tissue regeneration techniques are the need for two surgical procedures, an increased risk of scaffold contamination when cells are cultured *ex vivo*, and the necessity of rigorous sterilization techniques [12]. The main groups of stem cells used for bone regeneration are bone marrow, periosteum-derived, adipose tissue, and dental pulp stem cells. In addition, new sources (periodontal ligament, periapical cyst, the apical papilla, the dental follicle) of the stem cells are investigated and show some promising results for bone regeneration. Still, more preclinical evidence is needed [336 – 338].

2.4.5.1. Bone marrow stem cells

BMSC are pluripotent cells found in the bone marrow, which can differentiate into mesenchymal origin cells [12]. These cells can be obtained from the patient by a bone marrow aspiration, isolated and expanded in culture, and induced *in vitro* to form bone, cartilage, tendon, muscle, fat, skin, and other mesenchymal origin tissues [339,340]. Another essential advantage of BMSC is the ability to be cultured *in vitro* for many passages without spontaneous differentiation [341]. However, some studies report that BMSC may lose their bone-forming efficiency after multiple passages [342]. Furthermore, hundreds of clinical trials use human BMSC *in vivo* [340]. Besides BMSC differentiation potential, they secrete bioactive molecules, promoting new tissue formation, and modulating a host's immune response [340,343]. In addition, BMSC cells injected in the diseased or injured sites secrete bioactive factors that are immunomodulatory and trophic (regenerative) and stimulate a patient's site-specific and tissue-specific resident stem cells to construct the new tissue [340]. Moreover, BMSC can support the survival of the surrounding tissue through the release of the paracrine factors. Moreover, the newly-formed bone expresses significantly higher bone differentiation markers (e.g. alkaline phosphatase, RUNX2 (runt-related transcription factor 2), and OCN (osteocalcin)) [103,115].

A recent systematic review has found that BMSC are among the most used cell types in bone tissue regeneration studies [344]. The main treatment strategies to regenerate the bone are endogenous activation of BMSC through bioactive molecules or scaffolds/hydrogels and exogenous BMSC delivery systemically or locally with or without the scaffolds [115]. The main challenges of the endogenous BMSC activation and direction to the injured site are a short half-life and high expenditure of directly injected factors [345]. This treatment technique's main target is to create more specific biomaterial designs and incorporate the selected homing factors in the constructs [345]. On the other hand, exogenous BMSC delivery by injection of cell suspensions directly into the injured site has several disadvantages: insufficient cell supply, poor engraftment, the spread of injected cells to surrounding healthy tissue, and loss of cell fate control [345]. Therefore, most new studies focus on new bone formation *in vivo* through enhancement by combining different scaffolds with BMSC and applying them locally [115]. This technique showed better results in bone regeneration than scaffolds alone [103,115,344]. However, several limitations associated with painful collection methods, donor site damage, and lower proliferation / differentiation capacities with advancing donor age should be considered in clinical practice [103].

Clinical trials in the maxillofacial region use BMSC for alveolar socket preservation, lateral ridge augmentation, and sinus augmentation [345]. A randomised clinical trial stage I/II has shown that transplanted BMSC for alveolar socket preservation accelerated the regeneration of the osseous tissue and significantly reduced the need for secondary bone grafting at the time of oral implant placement compared to GBR-treated sites [346]. Moreover, a few clinical trials used bone marrow aspirate to aid lateral ridge augmentation [347–349]. The combination of BMSC and allogeneic bone grafts resulted in higher alveolar bone gain and density in the graft's peripheral regions than allografts alone [347,349]. The researchers suggested that an autologous bone marrow aspirate can increase allografts' regenerative potential in patients with severe alveolar ridge volume deficiency in the anterior maxilla [347,349]. A combination of BMSC and xenograft showed an increased mineralization trend in the anterior maxilla yet similar healing results as the xenograft alone [348]. A meta-analysis revealed that cell-based therapies resulted in higher alveolar bone gain than control groups with considerable heterogeneity between the results [345]. Another clinical trial did not find statistically significant differences in new bone formation between BMSC with xenograft and autogenous bone and xenograft mixture for maxillary sinus augmentation procedure [350]. Although *in vitro* and *in vivo* studies show promising BMSC use in bone regeneration, long-term clinical trials are needed [115].

2.4.5.2. Periosteum-derived cells

The periosteum is a specialized, highly vascularized connective tissue that envelopes bone surfaces [314]. It is composed of 2 layers: an external fibrous layer containing elastic fibres and microvessels and an inner layer where periosteum-derived cells (PDC), fibroblasts, and sympathetic nerves reside [351]. Periosteum plays an essential role in bone elongation and modelling, bone fracture healing, and callus formation [123,352] due to PDC capability to differentiate to osteoblasts and chondrocytes [353,354]. These cells have a higher proliferation rate following injury and proliferate faster than BMSC in a cell culture [123,341]. PDC potential for proliferation and differentiation might persist throughout life as studies show that PDC grafted from the elderly show comparable results to cells obtained from younger patients [355,356]. One reason why PDC keep their potential to proliferate and differentiate could be good telomeres stability and telomerase activity, e. g. telomere lengths after 24 population doublings similar to the parental population [314]. Animal trials report PDC' ability to induce new bone formation at heterotopic sites with a greater newly formed bone percentage than BMSC or alveolar bone cells [357,358]. However, the newly formed bone area in dogs' peri-implant defects was similar in groups treated with PDC and BMSC with carriers [359].

One of the unique PDC features is the initiation of endochondral bone formation, maintained even when cells have been expanded *ex vivo* [351]. Therefore, the autologous periosteum graft has been used in orthopaedic surgeries as a covering layer in autologous chondrocyte transplantation to treat nonunion fractures as a graft to reconstruct the patellar articulation [314]. Although PDC show promising results in treating non-healing and previously resistant nonunions, bone fractures, and large bone defects, several limitations should be considered [314,351]. The regenerative potential of PDC may be affected by a harvest site, donor conditions, resection methods (the use of forceps), and cell isolation procedure [351]. It is known that loadbearing bones have a more osteogenic periosteum than flat bones [351]. Even if the PDC regenerative features are maintained, several disadvantages are surgery-related such as donor site morbidity, seroma, transient paraesthesia, or iatrogenic femoral fracture [351]. Preoperative CT angiography could help avoid the complications and provide valuable information on the 3D assessment of the defect and vasculature surrounding. However, it cannot be used routinely due to radiation exposure, and plain radiographs used by most surgeons [351].

Craniofacial bone tissue *ages* more slowly and has higher levels of osteoblastic markers than appendicular skeletal bone tissue [123]. PDC can be obtained from the upper vestibule, lower vestibule, and hard palate in the

maxillofacial region, allowing rapid *in situ* engraftment [356]. However, different anatomical sources affect the transcriptomic signature of PDC and *in vivo* differentiation [123]. A couple of clinical trials used autogenous PDC for alveolar ridge augmentation and maxillary sinus lift [360,361]. In these studies, PDC were mixed with autogenous bone and platelet-rich plasma. No adverse events were reported. The addition of PDC boosted bone anabolic activity, and increased augmented bone density. Therefore, the insertion torque during implant placement was increased compared to autogenous bone and platelet-rich plasma alone. The authors concluded that PDC could improve dental implants' primary fixation [361]. Besides, PDC promoted faster autogenous cortical bone remodelling, suggesting that the waiting time for implant placement could be reduced when using PDC [360]. Although PDC harvested from the jaws are a promising source for bone tissue engineering, harvest morbidity, subsequent characterization, and patient acceptance should be considered before choosing the appropriate cell source [314].

2.4.5.3. Adipose tissue stem cells

Adipose tissue is another source of multipotent stem cells. Adipose tissue-derived stem cells (ASC) can be isolated from human subcutaneous lipoaspirate, peritoneal, omentum, and inguinal fat pads, allowing safer and easier stem cell isolation [362,363]. The high abundance of adipose tissue within the body lets obtain a much higher ASC than MSC [364]. The number of stem cell progenitors isolated from adipose tissue is tenfold higher than from bone marrow of equivalent amount [365]. When cultured in specific culture media, ASC can differentiate into osteoblast, chondrocyte, adipocyte, neuronal, and myocyte lineages [366]. The proliferation rate of isolated ASC is by one-third faster than MSC, which may decrease *ex vivo* culturing time [366]. Research shows that ASC can secrete cytokines such as interleukin-6 (IL-6) and transforming growth factor-β (TGF-β) 1, suggesting the immunomodulatory effects of ASC. Further, a lower amount of ASC has been shown to achieve the same level of immunomodulation as MSC and can be a promising alternative for immunomodulatory therapy [367].

Lee et al. were the first to isolate ASC, differentiate them into osteoblasts *in vitro*, and aid in bone formation implanted subcutaneously into Lewis rats [368]. Further studies used ASC seeded on apatite-coated poly(lactic-co-glycolic acid) scaffolds to test its effect on healing critical-size mouse calvariae defects. After 12 weeks, a complete bony bridging was seen by X-ray analysis, bone histological analysis, and live macromolecular imaging [369]. A couple of

studies compared the osteogenic potential of MSC, PDC, and ASC [370,371]. Stockmann et al. reported no statistically significant differences among test groups in volume and mineralization of a newly formed bone in monocortical calvarial bone defects in domestic pigs [371]. However, when Hayashi et al. implanted a composite of hydroxyapatite ceramics with different stem cells subcutaneously into laboratory rats, only new bone formation in composites seeded with MSC and PDC but not with ASC was detected [370]. A split-mouth design clinical study applied a stromal vascular fraction of adipose tissue with calcium phosphate ceramics to increase maxillary bone height for dental implants. No adverse reactions were reported in 3 and more year follow-up. Micro-CT or histomorphometric evaluations reported higher bone volumes in the test group [372]. The research concludes that ASC may be a promising and possibly more effective alternative to MSC [364].

2.4.5.4. Dental pulp stem cells

The dental pulp of human exfoliated deciduous and permanent teeth is another promising source of stem cells. In 2000, Gronthos et al. were the first group to isolate, characterize, and explore the differentiation potential of dental pulp stem cells (DPSC) [373]. The authors concluded that DPSC are highly proliferative, clonogenic, forming ectopic dentin and associated pulp tissue. Later, the same research group showed that DPSC could differentiate into adipocytes and neural-like cells [373]. DPSC originate from the neural crest during embryo development. Therefore, DPSC secrete neuroprotective growth factors and are broadly investigated for neural regeneration [374]. Further studies revealed DPSC' ability to differentiate to odontoblasts, neural progenitors, osteoblasts, chondrocytes, and adipocytes [375,376]. Along with stem cells from other sources, DPSC possess immune-suppressive properties by secreting anti-inflammatory cytokines such as Interleukin-8 (IL-8), IL-6, TGF-β [377]. DPSC also express angiogenic genes, secret vascular endothelial growth factor, and platelet-derived growth factor A [378]. Furthermore, DPSC also secret osteogenic markers such as alkaline phosphatase, collagen type I, osteocalcin, and osteopontin [9]. Moreover, DPSC can survive *in vitro* longer than BMSC, exhibit a higher growth rate, and produce an extracellular matrix with less immunosuppressive activity [103]. Besides the characteristics mentioned above, easy accessibility from dental tissues of both adults (wisdom teeth extraction) and children, *ex vivo* expansion of DPSC make them an attractive source of mesenchymal stem cells for tissue regeneration [103,379]. Stem cells from human exfoliated deciduous teeth (SHED) exhibit a higher

proliferation rate than DPSC with good osteoinduction properties *in vivo* but fail to induce a dentin-pulp complex formation [380].

A recent systematic review has analysed the studies that employed DPSC for *in vivo* bone regeneration [379]. They found 52 animal studies and 4 human studies for DPSC or SHED evaluation for bone tissue regeneration. Subcutaneous implantation of DPSC or SHED with an osteoconductive scaffold showed ectopic bone formation [379]. de Mendonça Costa et al. were the first research group to investigate new bone formation when DPSC with collagen scaffolds were implanted in critical-size cranial bone defects [381]. They found DPSC's ability to contribute to more mature bone formation in 1 month after surgery. Afterwards, various preclinical studies' evidence has shown the positive effect of DPSC combined with synthetic bone scaffolds superior to scaffolds alone for bone defect reconstruction and craniofacial bone regeneration [103,382]. However, although DPSC with the scaffolds significantly increased bone formation compared to the scaffolds alone, the autogenous bone group at all time points was superior to test groups [383]. Furthermore, it must be mentioned that the optimal number of DPSC, 3D structures with specific ECM components are essential for successful cell transplantation [338]. It is known that TCP enhances the differentiation of DPSC into osteoblast-like cells, and HA improves DPSC adhesion, proliferation, and differentiation toward the osteogenic lineage [338].

DPSC with collagen sponges were used to fill in an injury site after extracting mandibular third molars in humans [375]. On 3-month examination, alveolar bone has gained optimal vertical height, and a complete restoration of periodontal tissue was observed. Moreover, DPSC resulted in a more mature and cortical bone gain, as revealed by a histology analysis [375]. The same patients were assessed 3 years after the procedure. The bone was entirely compact in DPSC and collagen group; bone volume and vertical height were superior to the collagen alone group [384]. Another research found that DPSC seeded on collagen-polyvinylpyrrolidone sponges in a patient's left lower premolar region with the periodontal disease increased bone density and decreased tooth mobility, periodontal pocket depth, and the bone defect area [338]. Moreover, the combination of DPSC with hydroxyapatite-collagen scaffolds resulted in satisfactory bone regeneration of the alveolar defects for cleft lip and palate patients [338]. Despite the remaining challenges, the encouraging effectiveness of early new bone formation in animal models and promising results in humans should be considered for innovative bone defect treatment protocols in future trials on human models [382].

2.4.6. Extracellular matrix in bone regeneration

The ECM is a non-cellular component of every human organ or tissue composed of water, proteins, and polysaccharides [385]. The ECM proteins may be structural (collagens, elastin, fibronectin) or non-structural (laminin, tenascin, various growth factors, matrix metalloproteinases) [385]. Mainly, collagens are responsible for a tissue's tensile strength, cell adhesion, and migration [385,386]. In addition, different fibril arrangement of collagens assures to withstand different required mechanical stresses such as tension, shear, and pressure [385]. Thus, the main functions of ECM are anchorage, migration barrier, migration track, a signal reservoir of growth factors and matrix metalloproteinases, low-affinity co-receptor, signal presenter, and biomechanical force [385]. These functions are essential to support tissue morphogenesis, differentiation, and homeostasis [387]. Furthermore, each tissue has tissue-specific ECM with a unique physical, topological, and biochemical composition and topology generated during tissue development [386].

Bone tissue ECM has compact and rigid fibril-forming collagen-matrix due to many intra- and intermolecular cross-links [387]. Moreover, bone ECM is rich in BMP and angiogenic growth factors such as VEGF released in a controlled manner [388]. However, the predominant difference between bone ECM and other connective tissues is mineralization capacity. Bone ECM contains 99% of body calcium, mainly in the shape of HA crystals [387]. The prominent functions of bone ECM are skeletal development and repair / regeneration after the bone injury (trauma, tumours, skeletal deformities) [387]. Therefore, the use of ECM in bone tissue engineering could lead to osteoinductive materials superior to single osteoinductive molecules due to their multi-component structure with various cell-activating ligands [389]. Two main techniques developed in ECM have enhanced bone tissue engineering: obtaining ECM from tissue *in vivo* or producing it by autologous cells *in vitro* combined with decellularization [388]. The decellularisation technique minimizes the risk of transmission of infections and ensures low immunogenicity of scaffolds [390,391]. Interestingly, the remaining proteins and associated factors in ECM could be well-conserved even across species [388].

Natural ECM (nECM) can be collected from a donor, a cadaver, or animal bones. However, any cellular material must be removed from the obtained nECM to reduce the risk of disease transmission [388,392]. The main advantage of such nECM is a perfect structure and architecture matching the bone biophysical requirements and making an adequate template for host cells [388]. Various methods have been proposed to decellularize ECM. However, maximal removal of cellular components without damaging EMC

architecture remains a challenge [393]. Currently, demineralization is used in most bone decellularisation techniques [388,394]. Demineralised nECM is called DBM and is used in clinical practice as powders or granules to fill in bone cavities as it does not provide structural support [388]. Moreover, the osteoinductive properties of DBM are highly variable and depend on a donor species, site, and sterilization technique [388]. One way to overcome demineralized nECM limits is combining it with 3D-printed scaffolds and producing composite scaffolds [394]. A recent study showed that the composite scaffold of DBM with PCL/β-TCP scaffolds successfully induced stem cell proliferation and osteogenic differentiation *in vitro* and new bone formation *in vivo* [394]. Moreover, micro-CT evaluation revealed that Hounsfield Units (HU) values of newly regenerated bone in the PCL/β-TCP/DBM group were similar to those of cortical bone [394]. Another advanced attempt is to produce nECM from a non-bone tissue [395]. One study combined decellularized human adipose tissue hydrogel with adipose-derived stem cells, resulting in higher new bone formation compared to the negative control group in critical-size defects [395]. However, all advantages gained from nECM rely on the successful preservation of bioactive factors derived from a donor. Even then, they may not match the set of instructive signals required to induce *de novo* bone formation [388].

One of the most progressive tissue engineering treatment strategies is creating cell-derived decellularized ECM (cECM)-ornamented natural or synthetic 3D scaffolds *in vitro* [396]. This technique can lead to osteoinductive scaffolds with favourable mechanical properties [396]. However, ECM structure and functions depend on the specific stem cell cultures used to produce ECM [396]. Several research groups have combined organic-inorganic scaffolds with cECM to address *in vitro* stem cells differentiation and *in vivo* new bone formation. Pati et al. used PCL, PLGA, and β-TCP scaffolds with cECM formed by human nasal inferior turbinate tissue-derived mesenchymal stromal cells. The scaffolds supported newly seeded stem cells osteoblastic differentiation *in vitro* by upregulating osteoblastic genes. After ectopic implantation in rats, scaffolds ornamented with cECM induced more accomplished bone formation than bare scaffolds [262]. Another research group examined a PLGA/PLA mesh scaffold coated with cECM formed by human umbilical cord blood-derived mesenchymal stem cells [397]. *In vitro* results revealed stem cell proliferation and osteogenic differentiation with high alkaline phosphatase (ALP) activity and expression of osteogenic markers. They concluded that scaffolds with cECM provide a better microenvironment for osteogenesis [397]. Another study showed excellent biocompatibility and enhanced cellular adhesion, proliferation, and differentiation of stem cells *in*

vitro and more new bone formation with no apparent inflammation *in vivo* in the 3D printed calcium silicate, PCL/cECM from MG63 cells scaffolds [398]. Although these studies reveal promising results that cECM may enhance osteogenic differentiation of stem cells without additional exogenous growth factors and increase bone regeneration *in vivo*, further research is needed to find the best scaffolds and stem cell culture combinations in bone tissue engineering.

3. MATERIALS AND METHODS

3.1. RAW MATERIALS

Materials used for the fabrication of the scaffolds: PLA1 filament (PLA filament; DR3D Filament Ltd, UK, natural, diameter 2.85 mm), PLA2 filament (PLA filament; DR3D Filament Ltd, UK, natural, diameter 1.75 mm). The raw materials used for the preparation of the filaments created with HME equipment were PLA beads (STP Chem Solutions Co., Ltd., Thailand) having a particle size of 100–800 μm and a molecular weight of 42,700 (g/mol), 50 μm size HA particles (Riga Technical University, Latvia [399]), and Bioactive Glass 45S5 (XL Sci-Tech, Inc., USA) having a particle size of 38–75 μm. Geistlich Bio-Oss® (Geistlisch Pharmaceutical, Wolhusen, Switzerland) granules 0.25–1 mm in diameter were used as a positive control for *in vivo* investigation.

Materials used for cell research: Iscove's Modified Dulbecco's Medium (IMDM) (Gibco); Penicillin and streptomycin (Gibco); Phosphate-Buffered Saline (PBS) (Gibco); Ethylenediaminetetraacetic acid (EDTA) (Sigma-Aldrich Co.); Trypsin (Gibco); Dexamethasone (Sigma-Aldrich Co.); β-Glycerophosphate (Sigma-Aldrich Co.); L-Ascorbic acid-2-phosphate (Sigma-Aldrich Co.); Ethanol 96 % (Vilniaus Degtinė); Ammonium hydroxide solution ~10 % in H2O (Sigma-Aldrich Co.); Collagenase, Type I (Sigma-Aldrich Co.); Hyaluronidase (Sigma-Aldrich Co.); BSA (AppliChem GmbH); Dulbecco's phosphate-buffered saline (DPBS) (10x) (Gibco); Goat Anti-Mouse IgG coated Magnetic Beads (New England Biolabs, Inc.); primary mouse antibodies to CD45, CD54, CD14, CD90 (Merck Millipore), CD44 (Cell Signaling Technology), CD13 (Santa Cruz Biotechnology, Inc.), CD31 (Abcam, Inc.); Goat anti-Mouse IgG Secondary Antibody, RPE conjugated (Invitrogen); Mouse IgG2a Isotype Control (Abcam, Inc.). All materials were used as received.

3.2. PREPARATION OF THE FILAMENTS

A desktop extruder (Filabot Original, Filabot HQ, Barre VT, USA) equipped with a 1.75 mm nozzle was used to fabricate the filaments. Pure PLA filament was produced from PLA beads. The composite materials were acquired by thoroughly mixing the PLA and HA powders or PLA and BG powders at a ratio of 9:1. Before extrusion, the mixtures were stored in a sealed bag with silica gel pellets to absorb all the moisture from the materials.

Otherwise, the extrusion process was hard to control due to bubble formation in the filaments. Then the extruder was pre-heated to 140°C for the preparation of PLA filament, 145°C for creating PLA/HA filament, and 142°C for the preparation of PLA/BG filament. Afterwards, the composite materials or pure PLA beads were poured inside the hopper, and the feed screw was turned on. A self-made spooler with adjustable spooling speed was used to wind the filament onto the reel. During the extrusion process, the extruder's temperature was manually adjusted to 140°C for PLA filament creation, in the range of 140–145°C for PLA/HA filament creation and 137–142°C for PLA/BG filament creation. As a result, the PLA filament diameter varied from 1.67 to 1.75 mm, the composite PLA/HA filament varied from 1.28 to 1.45 mm, and the PLA/BG filament diameter – from 1.6 to 1.75 mm.

3.3. THERMOGRAVIMETRIC ANALYSIS OF PLA/HA FILAMENTS

Additional investigation is performed for the evaluation of HA concentration in the composite filament. Alumina crucibles heated until constant weight four times at 1000°C for 5 hours at a heating rate of 5°C/min. Ten PLA/HA mixture samples were placed in crucibles and heated at 800°C for 5 hours at a heating rate of 1°C/min.

3.4. FABRICATION OF SCAFFOLDS

Five scaffold groups from different materials were included in the study: PLA, PLA1, PLA2, PLA/HA, and PLA/BG scaffolds. PLA1 scaffolds were printed with a FDM 3D printer (Ultimaker Original, Ultimaker, USA). The printing head was computer-controlled in three axes of delta mode (x, y, z with an xyz speed of 50 mm/s). A gear system guided the filaments into the printing head, which was heated at a temperature above the melting point of PLA (the temperature near the nozzle was 210°C). The melted PLA filaments were extruded through a brass nozzle with a diameter of 0.4 mm onto a printing plate heated at 50°C. STL file for Ultimaker Original printer was sliced with Ultimaker Cura 3.6 (Ultimaker, USA).

PLA, PLA2, PLA/HA, and PLA/BG composite scaffolds were fabricated with a FDM 3D printer (Pharaoh XD 20, Mass Portal, Latvia). The printing head was computer-controlled in three axes of delta mode (x, y, z with an xyz speed of 35 mm/s). Other parameters were the same as described earlier. Slicer software used to prepare the STL file for Pharaoh XD 20 printer was open-source Slic3r 1.2.8 software.

According to the STL production file, all scaffolds were designed with an average pore size of 450 μm, with total porosity of 48 %. The width and height of the logs were 0.4 and 0.2 mm, respectively, and there were eight layers of logs (Fig. 1 A and B).

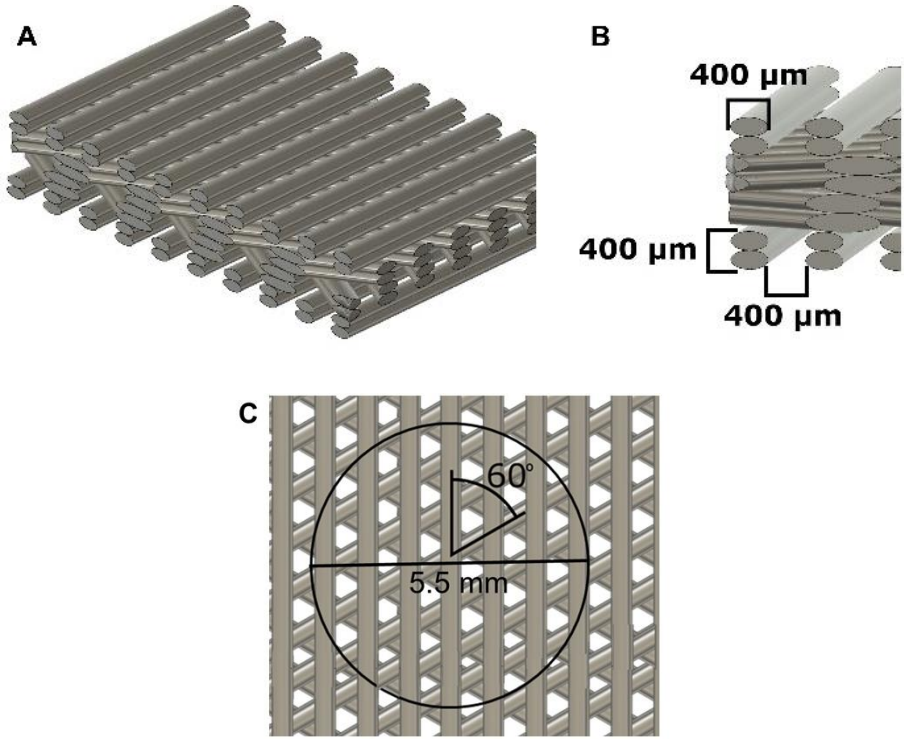

Fig. 1. The morphology of the scaffolds from the STL file: A – the scaffold from the side; B – the diameter of the woodpiles; C – the top view of the scaffold: micro-logs are rotated 60° angle, 5.5 mm circular cutting zone.

The geometry of the scaffolds was composed of 3D micro-structured woodpiles with threads rotated at an angle of 60° in respect to the two ones of the previous layer to create a hexagonal inner geometry (Fig. 1 C). Dimensions of the scaffolds were 3 cm×3 cm×0.16 cm for the *in vitro* study. Necessary 5.5 mm circles for the *in vivo* study were formed with laser light filament fabrication (Fig.1 C).

3.5. SCANNING ELECTRON MICROSCOPY ANALYSIS

A Hitachi TM-1000 tabletop scanning electron microscope (SEM) was used to evaluate the printing accuracy and morphology of five independent samples from the scaffold groups: PLA, PLA1, PLA2, PLA/HA, and PLA/BG. The sides of the prepared scaffolds (3 cm×3 cm×0.16 cm) were cut out from a rectangular woodpile (Fig. 2) with laser light filament fabrication technology 10 mm away from the sides.

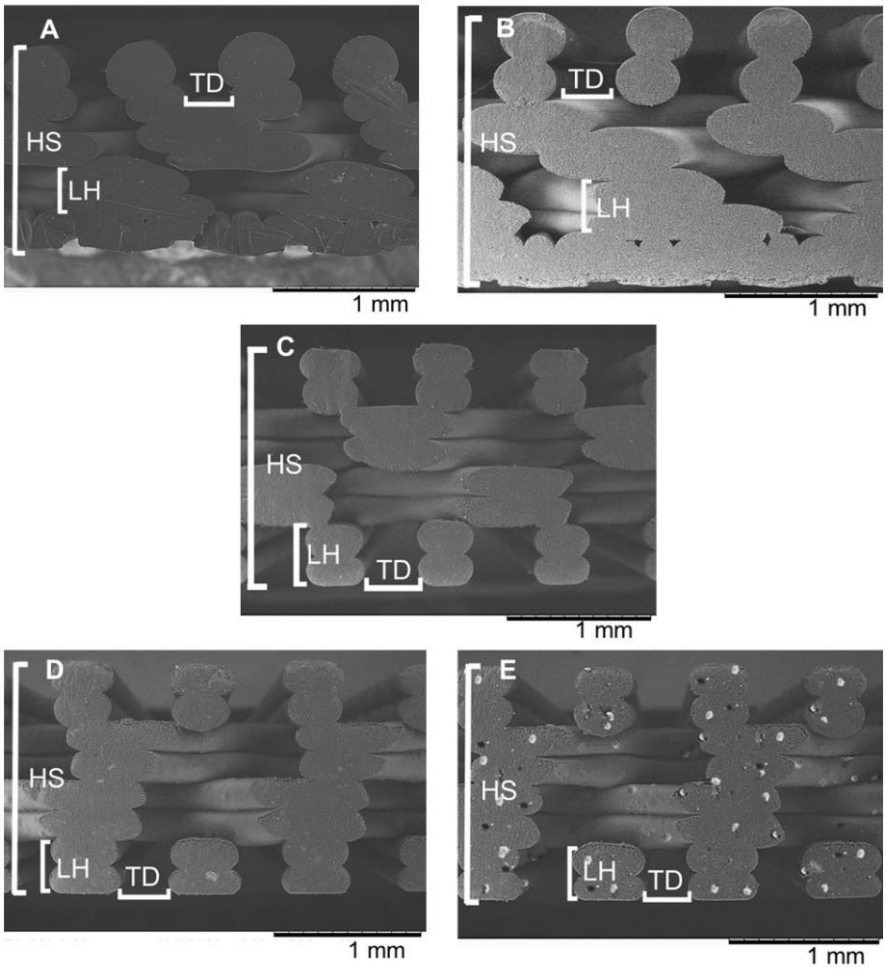

Fig. 2. Side views of the scaffolds obtained with SEM: A – PLA, B – PLA1, C – PLA2, D – PLA/HA, E – PLA/BG.

Scaffolds were scanned edgewise (5 images from each sample, 25 images in total for each group). The height of layers (LH), the distance between

threads (TD), and the height of scaffolds (HS) were measured using ImageJ 1 .8.0_112 image analysis software [401].

3.6. TOTAL POROSITY: GRAVIMETRIC METHOD

The total porosity (P) of PLA1, PLA2, and PLA/HA scaffolds were determined by the gravimetric method using the bulk and true density of the material. The gravimetric method is a simple and fast method, where $\rho_{material}$ is the density of the material, which can be determined by the Archimedes method. The volume of scaffolds was calculated by measuring the length, width, and height of the samples. A rough estimation of the porosity of specimens was carried out by using the following equations:

$$\rho_{scaffold} = \frac{mass}{volume}$$

$$\text{Total porosity} = 1 - \frac{\rho_{scaffold}}{\rho_{material}}$$

3.7. OPEN POROSITY: LIQUID DISPLACEMENT METHOD

The porosity of PLA1, PLA2, and PLA/HA scaffolds was also measured using a displacement liquid that is not a solvent of the polymers, for example, ethanol, which can penetrate the pores easily but does not cause shrinking or swelling of the material being tested. Open porosity can be calculated using the following equation:

$$\text{Porosity} = \frac{v_1 - v_3}{v_2 - v_3}$$

where V1 is the known volume of ethanol used to submerge the scaffold, V_2 is the volume of the ethanol and ethanol-impregnated scaffold, and V_3 is the remaining ethanol volume when the ethanol-impregnated scaffold is removed. The liquid displacement method is another simple technique that can be performed easily, but it is an indirect way of measuring porosity [402].

3.8. MICRO-CT ANALYSIS AND SUPERIMPOSITION *IN VITRO*

PLA1, PLA2, and PLA/HA scaffolds were scanned with a micro-CT Skyscan 1178 (Bruker microCT, Belgium). X-ray tube potential was 65 kV, and the tube current was 615 µA. The scanning mode was slow (80 µm pixels,

82 mm FOV). The acquired dimensions of image XY were 1024x1024 with about 400–500 slices in direction Z. Scaffolds sizes in image pixels were approximately 360x360x20. Due to the low scanning resolution (voxel size – 0.08495x0.08495x0.08495 mm) compared to the dimensions of the scaffold structure (approximately 5 pixels for one layer), micro-CT scan images were additionally processed using digital image processing methods to get sharper images. Image segmentation was also performed to get surface STL models to compare with the original 3D printing model. For this, a Fiji image processing software package based on ImageJ [401], MeshLab [403], and Geomagic Control X software packages (3D Systems, Canada) was used.

Deconvolution of the images was performed to improve the quality of the CT scan. The point spread function of the micro-CT system was determined to be Gaussian, and its size was chosen to be 17x17x17 with sigma equal to 3 as estimated from the sharp edges of the scans. For the deconvolution, the Richardson-Lucy algorithm with total variation regularization [404] was chosen. The parameters of the algorithm were set at seven iterations and a regularization factor of 2·10-3. The Deconvlab2 software plugin [405] for Fiji was used for deconvolution. Fig. 3 shows the deconvolution and segmentation process of the micro-CT scan.

For 3D segmentation, a method based on global thresholding was chosen. Due to the high variability of scaffold samples, the segmentation of the intensities of the CT scan image was performed using statistically computed thresholds for each scan. Thresholds were calculated using a method that preserved the statistical moments of image stacks [406]. Then 3D segmentation was performed using the computed threshold and converted to STL format (Fig. 3).

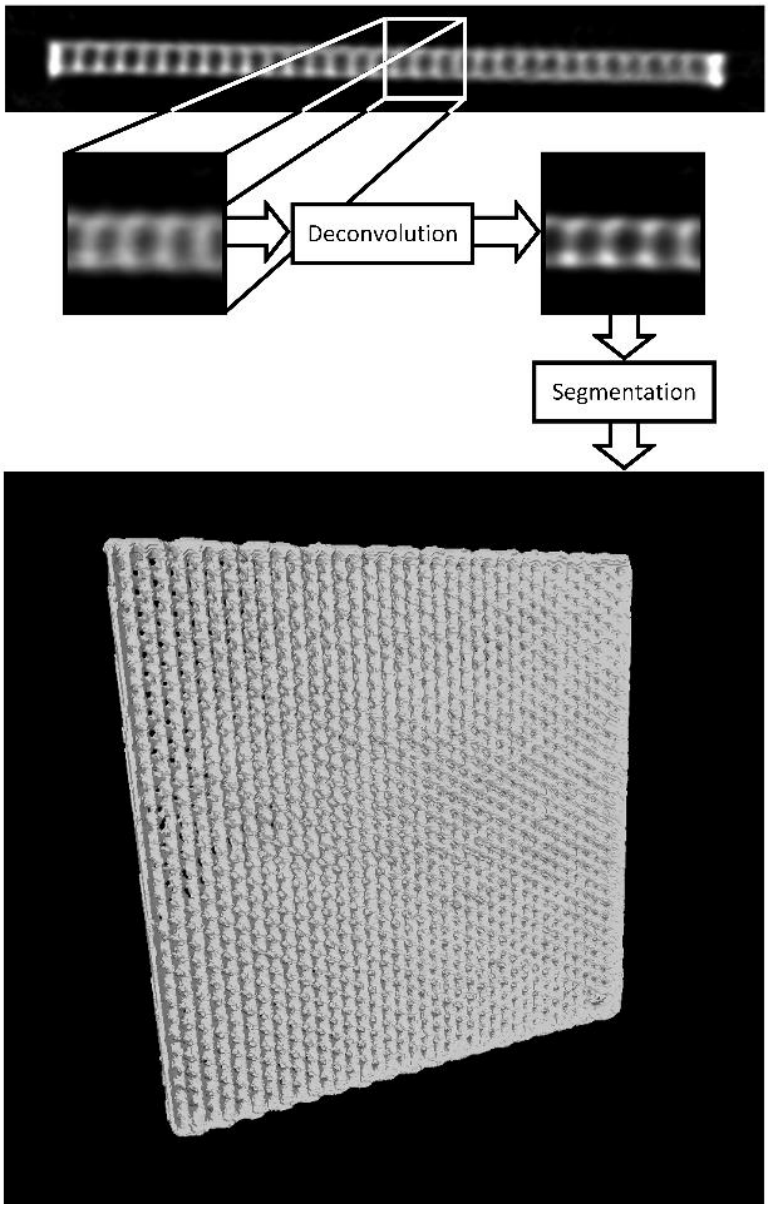

Fig. 3. The deconvolution and segmentation process of micro-CT scan.

To estimate the deviation between the reference scaffold model and the segmentations of the obtained micro-CT scans, 3D Geomagic Control X (3D Systems, USA) software was used. The superimposition of reference and tomographic models was done with transform alignment using a manual N points method followed by best-fit alignment.

3.9. STEM CELL ISOLATION

DPSC were isolated from the dental pulp of incisors of 3 months old three Wistar rats (n = 4 pulp samples in each extraction). Cell isolation and characterization were performed, as previously described [334]. Briefly, dental pulp samples were washed several times with IMDM supplemented with 100 μg/mL Primocin and mechanically minced into <1 mm^3 fragments, which were transferred to the digestive solution (0.5 % collagenase type 1, 0.3 % hyaluronidase, 0.25 % trypsin, and 0.02 % EDTA) and were shaken for 30–45 min at 37°C. Later on, IMDM supplemented with 10 % PBS and antibiotic: (penicillin – 100 U/mL, streptomycin 100 mg/mL), referred as growth medium (GM), was added and centrifuged twice at 1500 rpm for 10 min (CL10 centrifuge Thermo Scientific). The supernatant was removed, and the cells were seeded in GM. When cell monolayers reached 70–80 % confluence, it was dispersed and CD44-positive cells were extracted using magnetic beads coated with antibodies against the CD44 antigen. This separation procedure was performed according to BioLab's magnetic beads recommendations using the KingFisher™ mL (Thermo Scientific) purification system. Cells used in the experiments were up to 12 passages. Cells were cultivated in IMDM supplemented with 10 % FBS and antibiotics: penicillin – 100 U/mL, streptomycin 100 mg/mL at 37°C, 5 % CO2 environment.

3.10. PRODUCTION OF CELLULARIZED AND DECELLULARIZED SCAFFOLDS

The production of cellularized and decellularized scaffolds was prepared according to a previous *in vitro* study [400]. For the production of scaffolds, DPSC were seeded on PLA, PLA/HA, and PLA/BG scaffolds at a density of 4000 cells/cm^2 and grown in an osteogenesis-inducing medium composed of GM enriched with 50 nM dexamethasone, 25 μg/mL ascorbic acid, and 10 mM β-glycerophosphate. The medium was changed every second/third day for 21 days (Fig. 4).

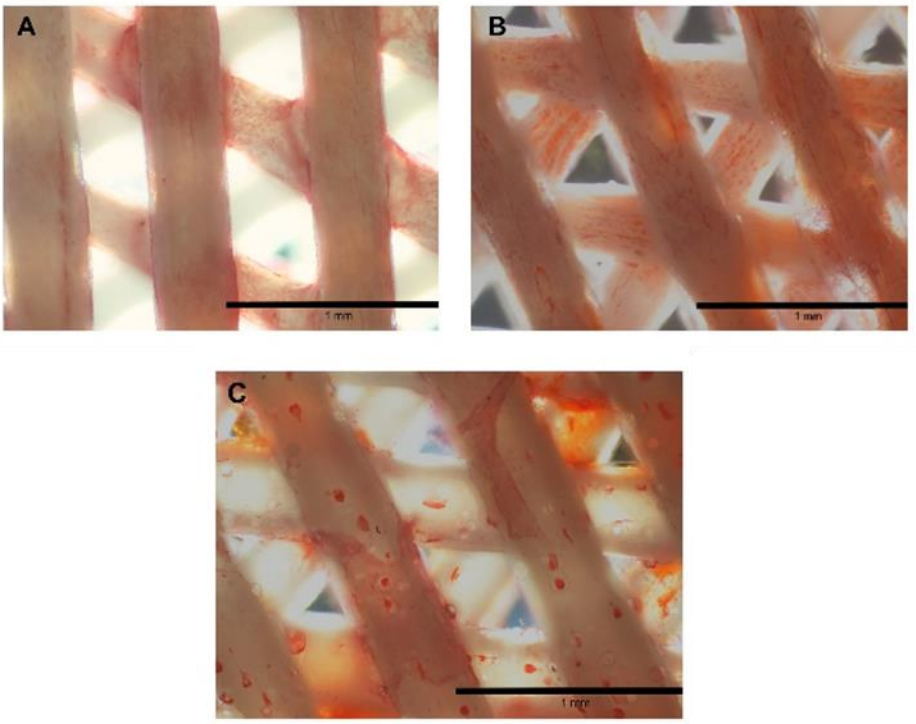

Fig. 4. The typical findings of osteogenically differentiated DPSC grown on the scaffolds for 21 days. Red colour depicts calcium deposits in cells formed ECM (stained with Alizarin Red S): A – PLA scaffold; B – PLA/HA scaffold; C – PLA/BG scaffold.

After this differentiation period, cellularized scaffolds were directly used for Wistar rats' bone defect regeneration. Decellularized scaffolds were produced from cellularized ones. For this purpose, cells grown on scaffolds were washed twice with PBS and then frozen at –80°C. Afterwards, scaffolds were allowed to defrost and washed with deionized water, then frozen again. In summary, 5 freeze-thaw cycles with deionized water washing were performed. Then scaffolds were incubated in 25 mM NH_4OH for 20 min to wash out any remaining DNA. Finally, scaffolds were washed six times with deionized water, and then they were ready for use in surgery.

3.11. ANIMALS

Forty-eight four months old Wistar rats (approximate weight 300 g) were used in the research. Approval of the Ethics Committee and permission for the experimentation were received from the State Food and Veterinary Service of Lithuania, No G2-40, 2016-03-18 (S 1). Wistar rats were obtained by inbreeding from the Department of Biological Models at Vilnius University, Life Sciences Center, Institute of Biochemistry (Vilnius, Lithuania). The animal experiments were carried out on the same premises. The sample size was calculated with the Gpower software (one-way ANOVA test with a priori analysis: α – 0.05, power 0.8, effect size f – 0.75). There were four female and four male animals in each group (8 animals per group). During the whole experimental period, the rats were kept in a monitored environment (21°C; 12:12 h light cycle) and received a standardized diet and water *ad libitum*.

The *in vivo* study was performed in two stages. First of all, the influence of the six samples of different materials on new bone formation in a critical-sized defect model was investigated (Fig. 5). Negative and positive (Bio-Oss) controls were allocated to the first group, PLA and PLA/HA scaffolds – to the second, PLA2 and PLA/BG – to the third.

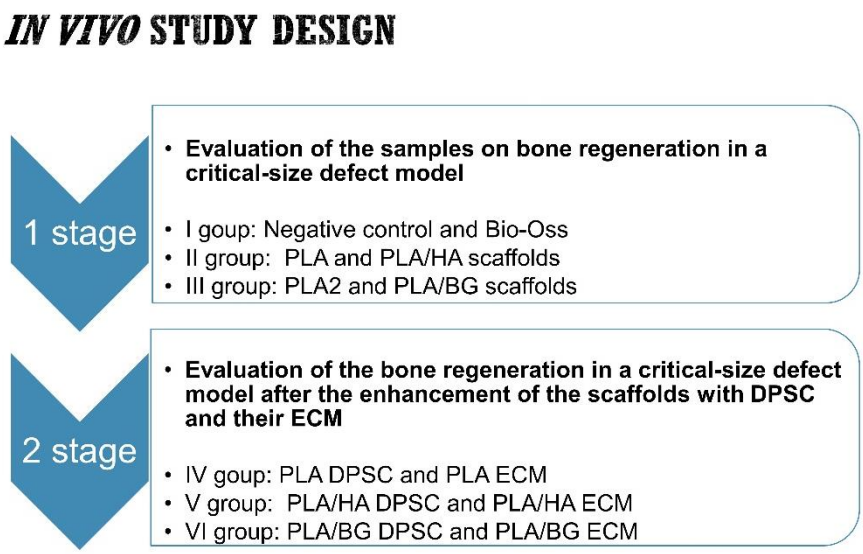

Fig. 5. The explanation of the two stages of the *in vivo* research.

Afterwards, PLA, PLA/HA, and PLA/BG scaffolds were enhanced with DPSC, and their produced ECM and their influence on bone regeneration was evaluated. PLA cellularized with DPSC, and PLA ECM scaffolds formed the

fourth group, PLA/HA DPSC and PLA/HA ECM – the fifth, and PLA/BG DPSC and PLA/BG ECM – the sixth group.

3.12. SURGICAL PROCEDURES

Animals were anaesthetized with an intraperitoneal injection of Ketamine hydrochloride (100 mg/mL; Rotex Medica GMBH, Tritau, Germany) 2.4 mL/kg and Xylazine (2 %; Alfasan, Woerden, The Netherlands) 5 mg/kg. The dorsal part of the cranium was shaved and aseptically prepared with Octenidine dihydrochloride (Octenisept, Schülke & Mayr GmbH, Germany). Local anaesthesia was done by injecting 0.25 mL of 2 % lidocaine (20 mg/mL; Baxter Holding B.V., Utrecht, the Netherlands) subcutaneously along the sagittal midline of the skull. One vertical incision was made in the middle of the posterior part of the cranium, and a full-thickness flap was reflected to expose the parietal and frontal bones (Fig. 6 A). The 5.5 mm circular critical size defects (2 per animal) with at least 1.5 mm bone bridge between them were made with a calibrated trephine burr (Hager & Meisinger GmbH, Germany) mounted on a contra-angle and irrigated with saline solution (Fig. 6 B). Scaffolds were randomly implanted as inlay-onlay grafts at the defect sites in all groups (Fig. 6 C, E). After implantation, the flap was closed, and the periosteum and skin were sutured with resorbable sutures (Vicryl 5/0, Ethicon®, Johnson&Johnson, Amersfoort, the Netherlands) (Fig. 6 D).

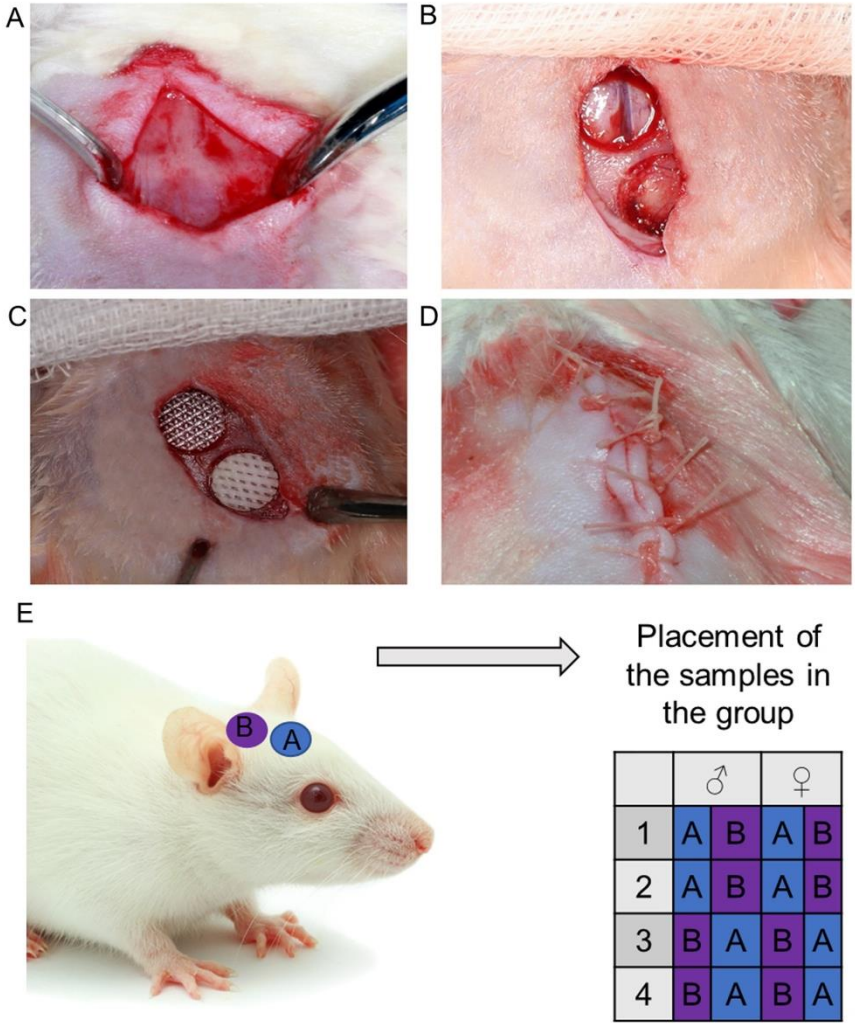

Fig. 6. Surgical procedure: A – surgical site; B – two 5.5 mm circular defects; C – implanted PLA and PLA/HA scaffolds; D – sutured wound; E – scheme of sample position variation in the skull of one group. A and B mean the identification of the samples in the group. I group: A – negative control, B – Bio-Oss; II group: A – PLA, B – PLA/HA; III group: A – PLA2, B – PLA/BG scaffolds; IV group: A – PLA DPSC, B – PLA ECM; V group: A – PLA/HA DPSC, B – PLA/HA ECM; VI group: A – PLA/BG DPSC, B – PLA/BG ECM.

After the surgery, the rats were transferred to the cages and housed singly for eight weeks. The first dose of Buprenorphine HCl 0.01 mg/kg (0.3 mg/mL; Richter Pharma AG, Wels, Austria) was given 3 hours after the surgery subcutaneously and then two times per day, three days for postoperative

analgesia. After eight weeks, specimens were harvested and were immediately fixed in 10 % (v/v) neutral buffered formalin. The defects were evaluated by micro-computed tomography and histological analysis.

3.13. MICRO-CT ANALYSIS *IN VIVO*

Micro-CT analysis *in vivo* was carried out in the Prof. K. Barsauskas Ultrasound Research Institute, Kaunas University of Technology (Kaunas, Lithuania). X-ray 3D computer tomography device RayScan 250 E (RayScan Technologies GmbH, Germany) with 10 – 230 kV microfocus X-ray source was used to evaluate bone defect regeneration. In order to collect 3D data of investigated objects, the X-ray source irradiates the test object with the cone beam, and a 2D image at the flat panel detector with 2048x2048 pixels is recorded (Fig. 7). During each measurement, the object was rotated, and 1800 projections were acquired at a 100 kV voltage and 200 μA current with the 666 ms integration time. As a result, a voxel size of 20 μm was achieved.

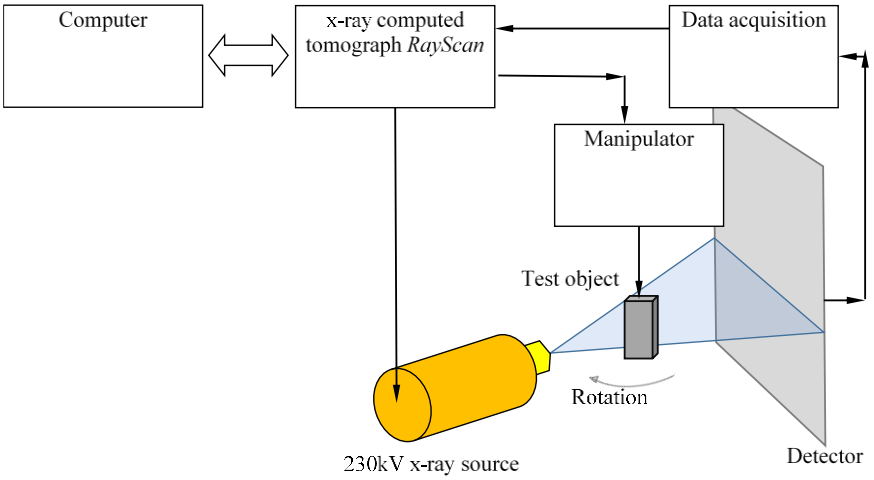

Fig. 7. The experimental set-up for X-ray computed tomography

The dimensional analysis was carried out with Avizo for Industrial Inspection 9.70 (FEI-SAS, Thermo Fischer Scientific Inc.) software. A special algorithm was developed for the regenerated bone volume calculation from the CT data. Regenerated skull bone calculation algorithm includes finding the perpendicular vector to the trepanation zone plane. Then parallel to this vector, the 5.5 mm diameter zone is cut using a cylindrical template, and later for analysis, only the material limited inside this cylinder was used. It includes

soft tissues, new bone, and artificial implants used to improve the bone regeneration process. These three material groups differed by their density and were separated using this parameter. Soft tissue and PLA grey values lay up to 20 000, new bone values are from 20 000 to 44 000, and Bio-Oss, HA, and BG values are above 44 000. Knowing these values allows the calculation of voxel count. According to their value, voxels were attributed to one of three groups. Later, each group's voxel sum is multiplied by the voxel volume, which produces the cut region's overall material volume. Based on the micro-CT results, bone volume (mm^3) of the regenerated bone was calculated.

3.14. BONE HISTOLOGICAL ANALYSIS

After micro-CT analysis, bone specimens were decalcified in 10 % EDTA – 10 % formalin solution, pH 7.0 – 7.4 (Laboratory of National Center of Pathology, Vilnius, Lithuania) for two weeks. Slices were obtained from the central part, 1.3 mm and 2.6 mm apart from the centre of each healed bone defect, embedded in paraffin, sectioned longitudinally into five histological sections (3 μm thick) and stained with hematoxylin and eosin stains. The stained preparations were examined under a light microscope (Olympus BX41TF, Olympus Optical Co. LTD, Japan), and the entire section was evaluated for qualitative analysis: new bone, connective tissue, presence of lymphocytes, foreign body reaction. Images were obtained of each section with ScanScope XT (Aperio, USA). The new bone area in the defect site was determined as the bony area (mm^2) using the software Aperio ImageScope (Leica Biosystems Imaging, USA).

3.15. STATISTICAL ANALYSIS

For data analysis and presentation, RStudio 1.1.453 statistical analysis software (RStudio, USA) was used. Five independent samples were used for SEM experiments and 22 for micro-CT *in vitro* experiments. The Shapiro-Wilk test and Levene's test were first performed to check the normality and equal variance assumptions of the data. Data are presented as mean ± standard deviation. One-way ANOVA parametric statistical analysis was used for the evaluation of *in vitro* results. Differences between groups were evaluated by performing the Tukey post hoc test. Statistically significant differences *in vivo* between the gender groups were determined using a t-test, between the sample groups – one-way analysis of variance (ANOVA) and Tukey post-hoc test. Differences were considered statistically significant when the *p*-value was <0.05.

4. RESULTS

4.1. OVERALL

PLA filament was created from PLA beads, and composite filaments were prepared by mixing PLA beads with HA or BG at a ratio of 9:1 using a desktop extruder (Filabot Original). The research used two FFF 3D printers – Ultimaker Original and Pharaoh XD 20 to print the same STL files. 3D micro-structured weaves with threads rotated at an angle of 60° were printed (Fig. 8).

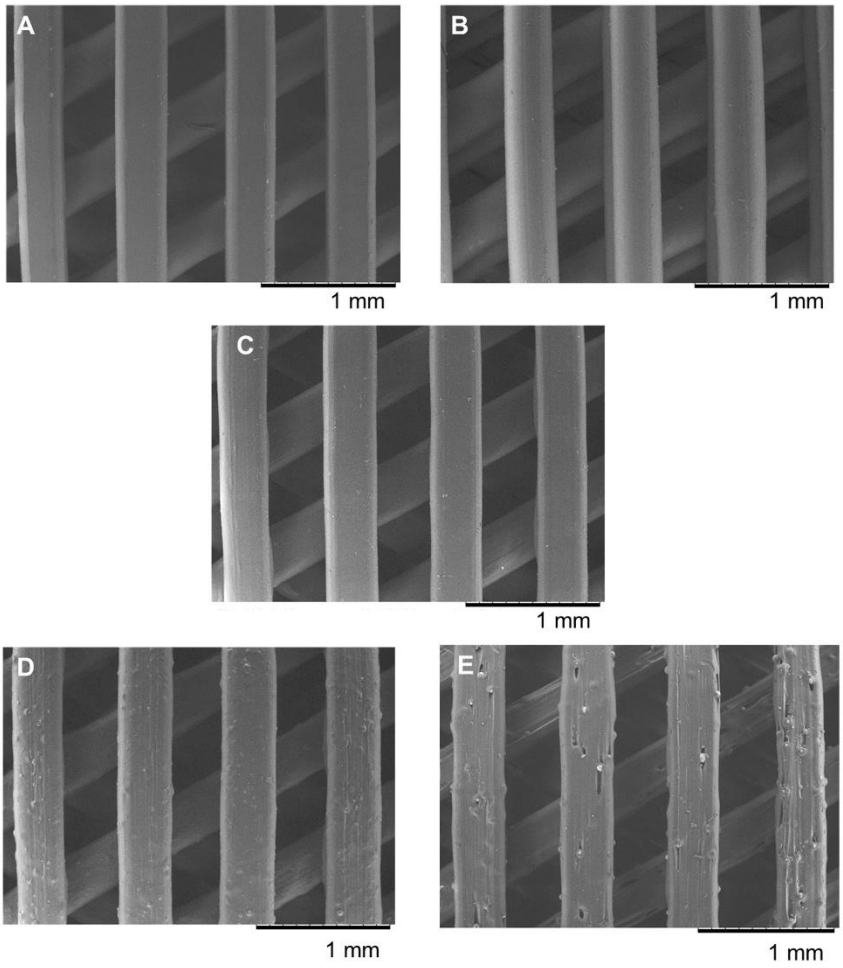

Fig. 8. The top views of the 3D printed scaffolds obtained with SEM, threads are rotated at 60° angle: A – PLA, B – PLA1, C – PLA2, D – PLA/HA, E – PLA/BG.

Thermogravimetric analysis revealed that the mean amount of HA in the composite PLA/HA filament was 10.43 % ± 0.03 (data not shown). PLA, PLA/HA, PLA/BG scaffolds cellularized with DPSC and PLA ECM, PLA/HA ECM, PLA/BG ECM scaffolds were prepared according to a previous *in vitro* study [400]. All animals survived for the duration of the study without complications. There were no clinical signs of infection, hematoma, or necrosis at the defect sites at eight weeks. The scaffolds were stable and did not move from the created defects.

4.2. *IN VITRO RESULTS*

4.2.1. Scanning electron microscopy evaluation

Printed scaffolds were analyzed with SEM. Several dimensions were evaluated: the height of layers, the distance between the threads, and scaffold height. The heights of scaffold layers made with the Ultimaker Original 3D printer varied the most. The means and deviations of the thickness of each layer in different groups are represented in Fig. 9.

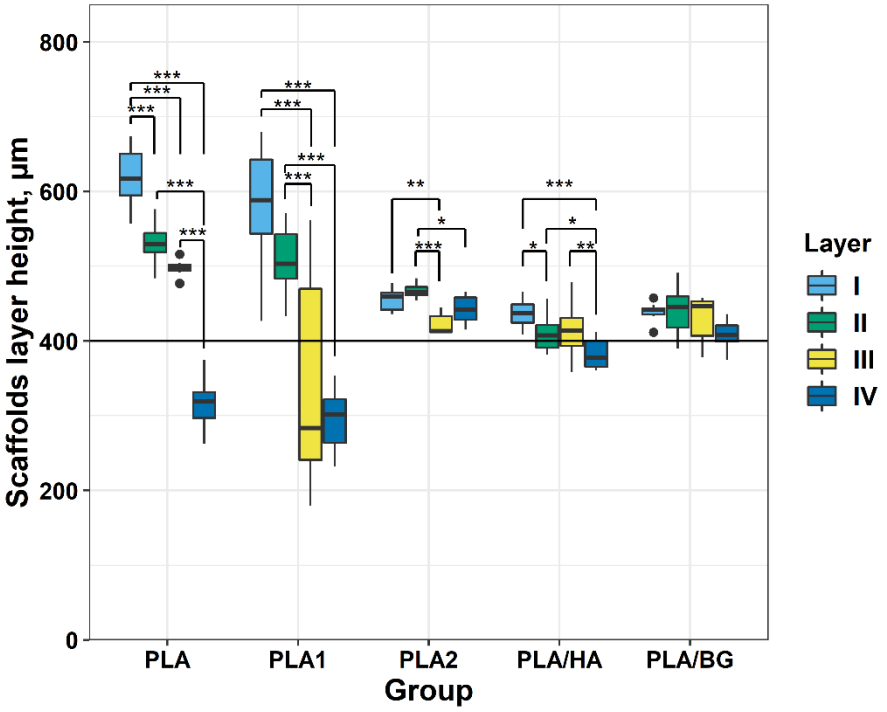

Fig. 9. Box plot of heights of scaffold layers. The black horizontal line marks the theoretical dimension of the prepared layer – 400 µm. *, ** and *** mark the statistically significant differences between the groups: $p < 0.05$, $p < 0.01$ and $p < 0.001$ respectively.

The bottom layers of PLA1 scaffolds were compressed, ranging from 250 to 400 μm (layers 3 and 4), and the top ones were more dispersed, ranging from 500 to 600 μm (layers 1 and 2). The Pharaoh XD20 3D printer compressed only the fourth layer (ranging from 270 to 370 μm) of the PLA scaffolds and dispersed the rest of the layers. However, this effect wasn't seen in the PLA2 and composite scaffolds. The evenest layers were printed with the Pharaoh XD20 3D printer from the PLA/BG filament. There was no statistically significant difference between the printed layers in the PLA/BG scaffolds.

The means of the distances between the threads in PLA (328 μm) and PLA1 (335 μm) groups were lower than 400 μm (Fig. 10).

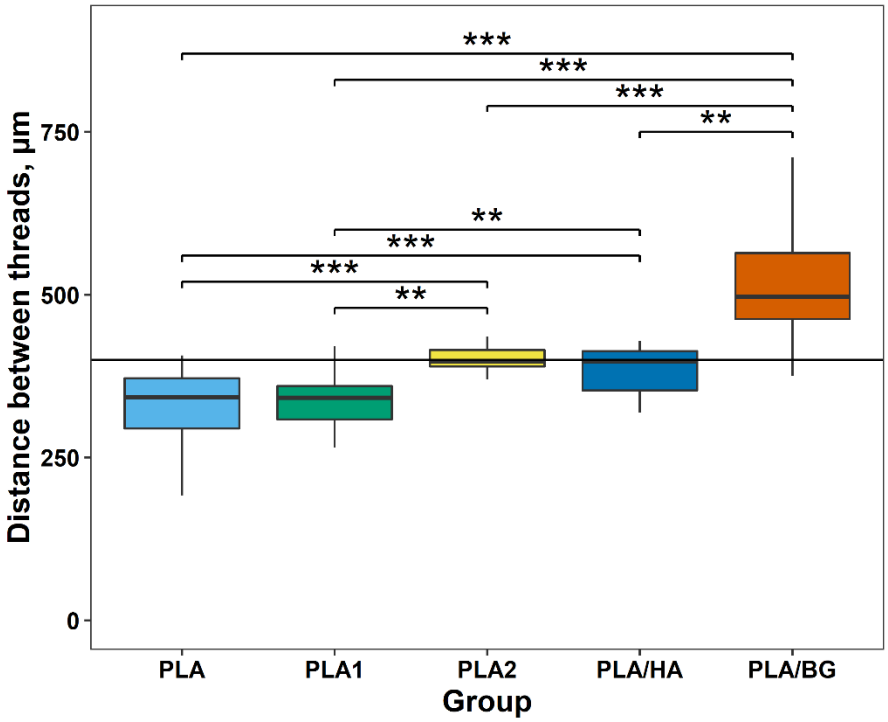

Fig. 10. Box plot of distance between scaffold threads. The black horizontal line marks the theoretical dimension of the distance between scaffold threads – 400 μm. *, ** and *** mark the statistically significant differences between the groups: $p < 0.05$, $p < 0.01$ and $p < 0.001$ respectively.

The distances between the threads of these two groups statistically significantly differed from the PLA2, PLA/HA, PLA/BG scaffolds, and theoretical distance between the threads gained from the STL file. The Pharaoh XD20 printer laid threads more accurately in PLA2 and PLA/HA

scaffolds. However, there was a statistically significant difference between PLA/BG and the rest of the scaffolds and the theoretical distance between the threads gained from the STL file. Interestingly, composite filaments affected the distance between threads that deviated from the STL model more than in the group of scaffolds printed with PLA filament (PLA2).

Despite the considerable variation in layer heights, both the Ultimaker Original and Pharaoh XD 3D printers produced similar heights of scaffolds while printing with PLA, PLA1, and PLA2 filaments (Fig. 11).

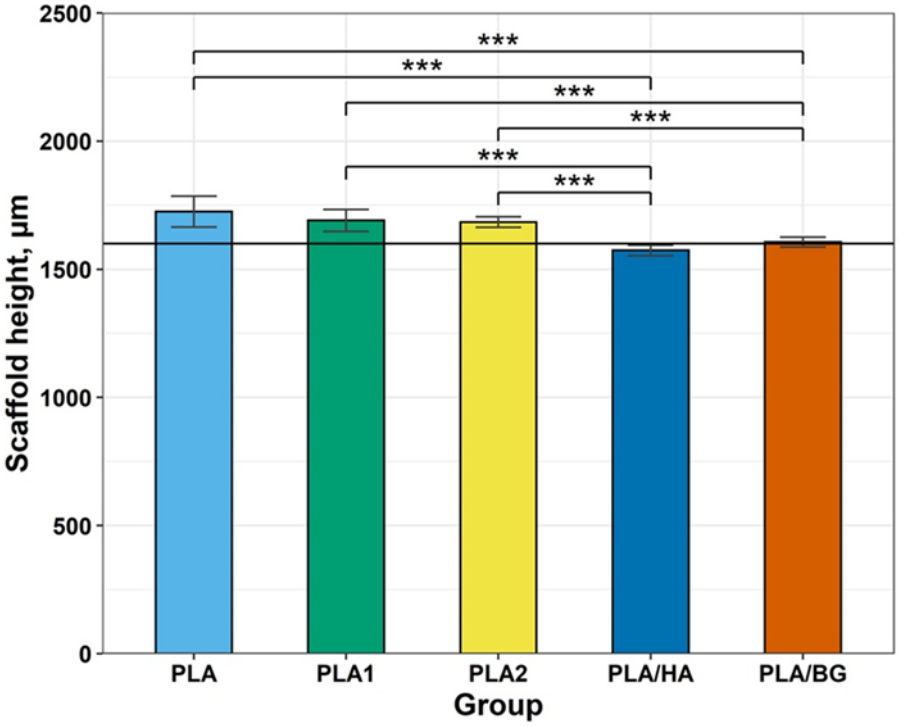

Fig. 11. Scaffolds heights. The black horizontal line marks the theoretical dimension of the scaffold height – 1600 µm. *, ** and *** mark the statistically significant differences between the groups: $p < 0.05$, $p < 0.01$ and $p < 0.001$ respectively.

PLA/HA and PLA/BG scaffolds' height significantly differed from PLA, PLA1, and PLA2 scaffolds. Nonetheless, the height of PLA/HA and PLA/BG scaffolds deviated the least from the STL model. Thus, SEM results indicate that the Pharaoh XD20 3D printer was more accurate while printing composite scaffolds in separate layers and the overall height of the scaffolds.

4.2.2. Porosity evaluation

The theoretical assessment of P (total porosity) was 48 %. Gravimetric and liquid displacement methods showed that the average P of printed PLA/HA scaffolds had the closest value to the original STL model: 48.15 % ± 0.01 and 50.6 % ± 0.06 accordingly (Fig. 12).

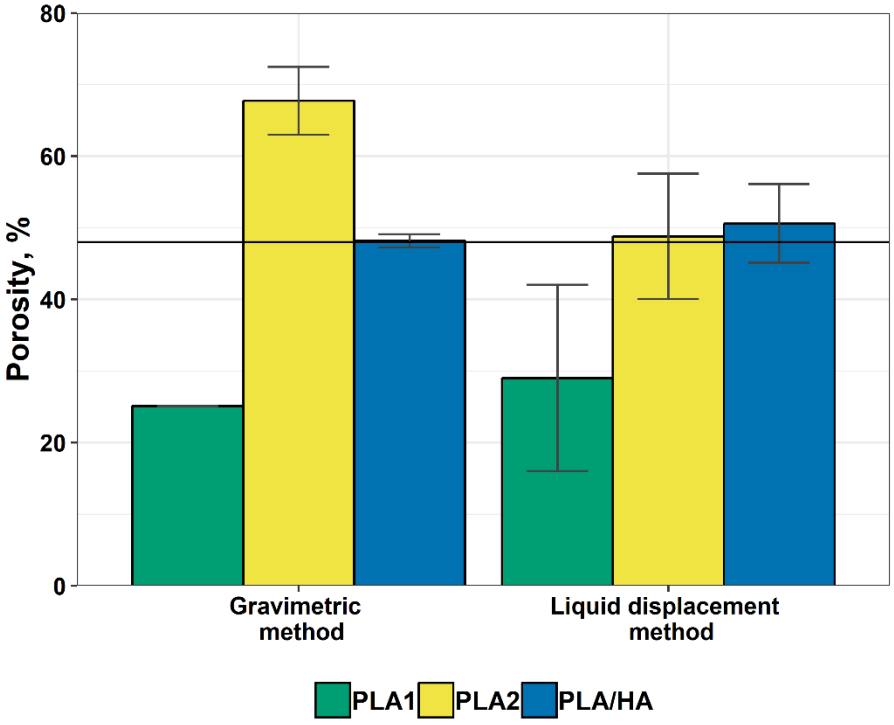

Fig. 12. The average total porosity of the scaffolds (%) for different analysis techniques compared with theoretical porosity – 48 %.

Although P of PLA1 and PLA2 scaffolds deviated more from the STL file, there were no statistically significant differences found between scaffold groups ($p > 0.05$) or between the porosity of scaffolds and the porosity of the original STL file ($p = 0.64$ and $p = 0.31$).

4.2.3. Micro-ct evaluation *in vitro*

The material volume of the original STL file was calculated to be 753.23 mm^3. Micro-CT and superimposition analysis showed that the mean volume was 1057.32 ± 87.46 mm^3 in the PLA1 group, 956.37 ± 34.21 mm^3 in the PLA2 group, 960.19 ± 114.54 mm^3 in the PLA/HA group (Fig. 13).

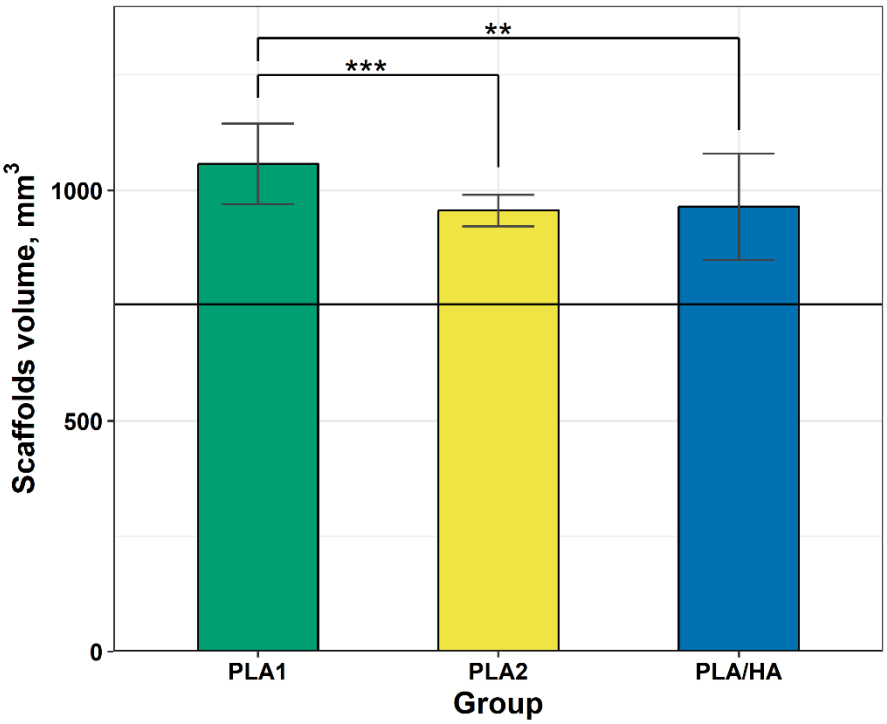

Fig. 13. The volume of the scaffolds (mm^3) micro-CT and superimposition results. The black horizontal line marks the theoretical dimension of the volume of the scaffolds – 753.23 mm^3. *, ** and *** mark the statistically significant differences between the groups: $p < 0.05$, $p < 0.01$ and $p < 0.001$ respectively.

The means of all scaffold groups differed from the volume of the original STL file ($p < 0.05$). The difference in volume was statistically significant between the PLA1 and PLA2 ($p < 0.001$) groups and the PLA1 and PLA/HA groups ($p < 0.01$). On the other hand, no statistically significant difference was found between the PLA2 and PLA/HA scaffold groups ($p > 0.05$).

4.3. *IN VIVO* RESULTS

4.3.1. Micro-ct evaluation *in vivo*

The acquired micro-CT data was processed using a developed algorithm to determine the volume of bone formation in the regions of interest. The images from the micro-CT after eight weeks of healing are shown in Fig. 14 and 15.

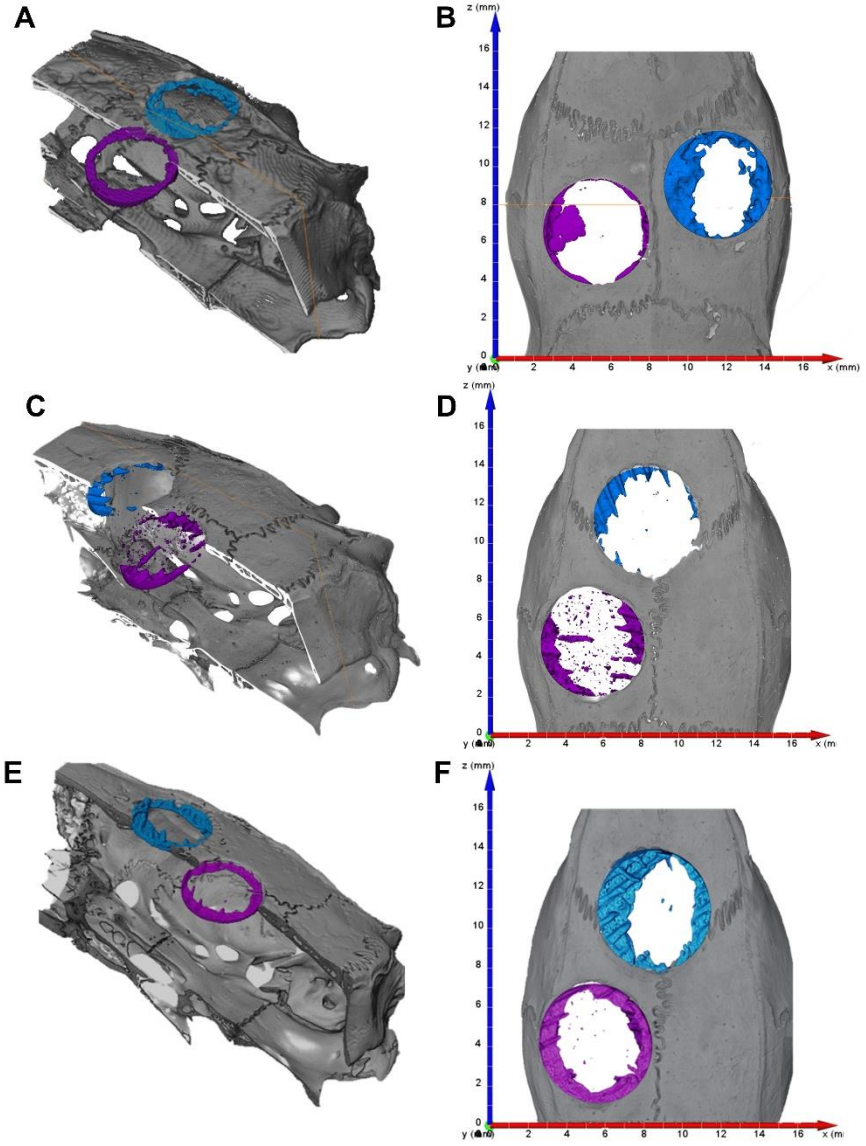

Fig. 14. Processed micro-CT images of stage 1 groups were taken with an X-ray 3D Computer tomograph RayScan 250E. A, B – Negative control (purple) and Geistlich Bio-Oss® (blue). C, D – PLA (blue) and PLA/HA (purple) scaffolds. E, F – PLA/BG (blue) and PLA2 scaffolds (purple).

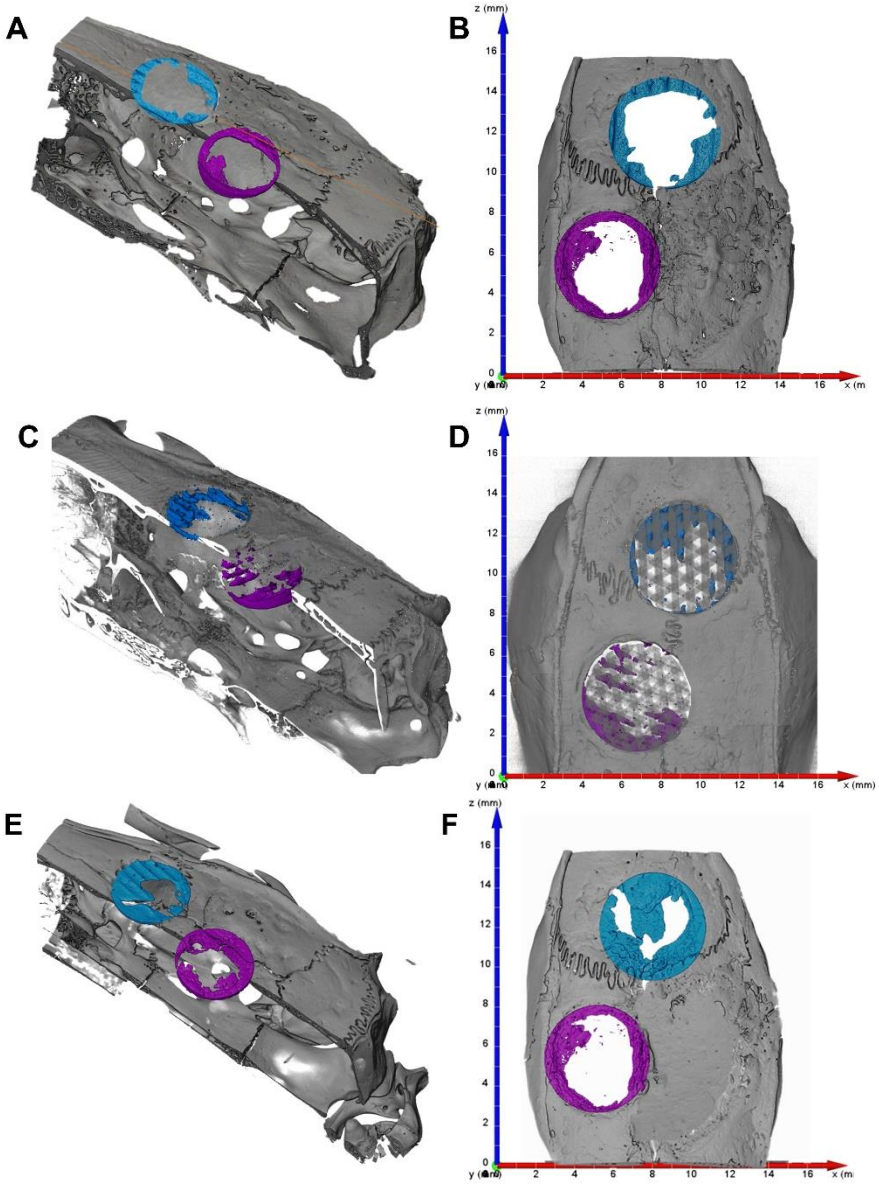

Fig. 15. Processed micro-CT images of stage 2 groups were taken with an X-ray 3D Computer tomograph RayScan 250E. A, B – PLA DPSC (purple) and PLA ECM (blue). C, D – PLA/HA ECM (blue) and PLA/HA DPSC (purple) scaffolds. E, F – PLA/BG ECM (blue) and PLA/BG DPSC scaffolds (purple).

Micro-CT evaluation showed that the best results were achieved with PLA/BG (6.27 ± 1.58 mm^3) and PLA/BG ECM (5,34 ± 0.59 mm^3) groups (Fig.16).

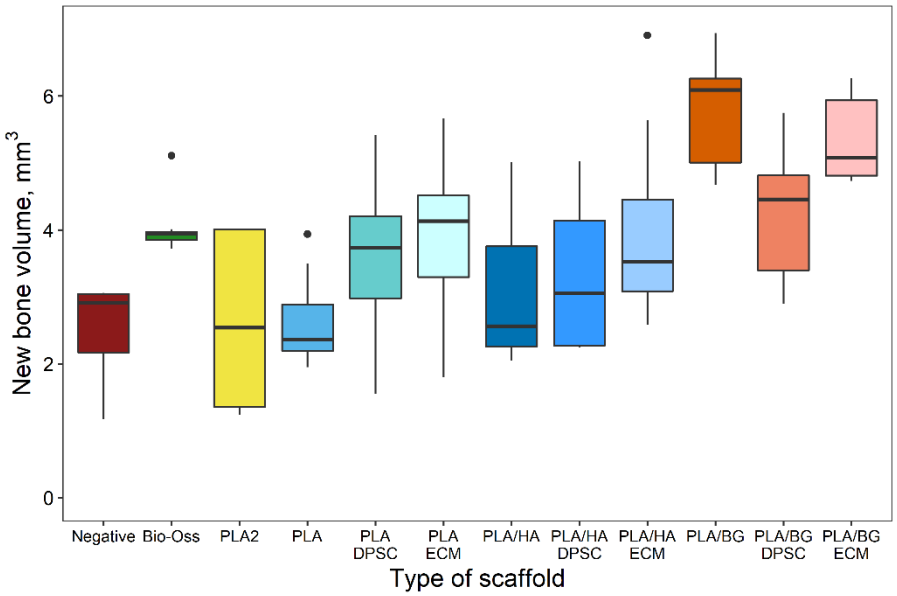

	Negative	Bio-Oss	PLA2	PLA	PLA DPSC	PLA ECM	PLA/HA	PLA/HA DPSC	PLA/HA ECM	PLA/BG	PLA/BG DPSC	PLA/BG ECM
Negative												
Bio-Oss	-											
PLA2	-	-										
PLA	-	-	-									
PLA DPSC	-	-	-	-								
PLA ECM	-	-	-	-	-							
PLA/HA	-	-	-	-	-	-						
PLA/HA DPSC	-	-	-	-	-	-	-					
PLA/HA ECM	-	-	-	-	-	-	-	-				
PLA/BG	***	**	***	***	***	**	***	***	**			
PLA/BG DPSC	-	-	-	-	-	-	-	-	-	*		
PLA/BG ECM	***	-	***	***	0.09	-	**	*	-	-	-	
Group	Negative	Bio-Oss	PLA2	PLA	PLA DPSC	PLA ECM	PLA/HA	PLA/HA DPSC	PLA/HA ECM	PLA/BG	PLA/BG DPSC	PLA/BG ECM

Fig. 16. *In vivo* micro-CT results. Box plots representing newly formed bone volume (BV, mm^3), according to sample groups. *, ** and *** mark the statistically significant differences between the groups at $p < 0.05$, $p < 0.01$ and $p < 0.001$, respectively.

Micro-CT evaluation showed a statistically significant difference between PLA/BG and all other tested samples, except PLA/BG ECM group. There was no statistically significant difference between PLA/BG ECM, PLA/HA ECM, and PLA ECM groups ($p > 0.05$). However, PLA/BG ECM showed statistically significantly better results than Negative control, PLA2, PLA, PLA/HA, PLA/HA DPSC, and almost PLA DPSC ($p = 0.09$). PLA and PLA/HA scaffolds improved with DPSC, or their produced ECM showed an improvement in gained new BV; however, no statistically significant difference was found.

Further results were analysed according to the *in vivo* stages, comparing the results between the groups in genders and between the genders (Fig. 17 and 18).

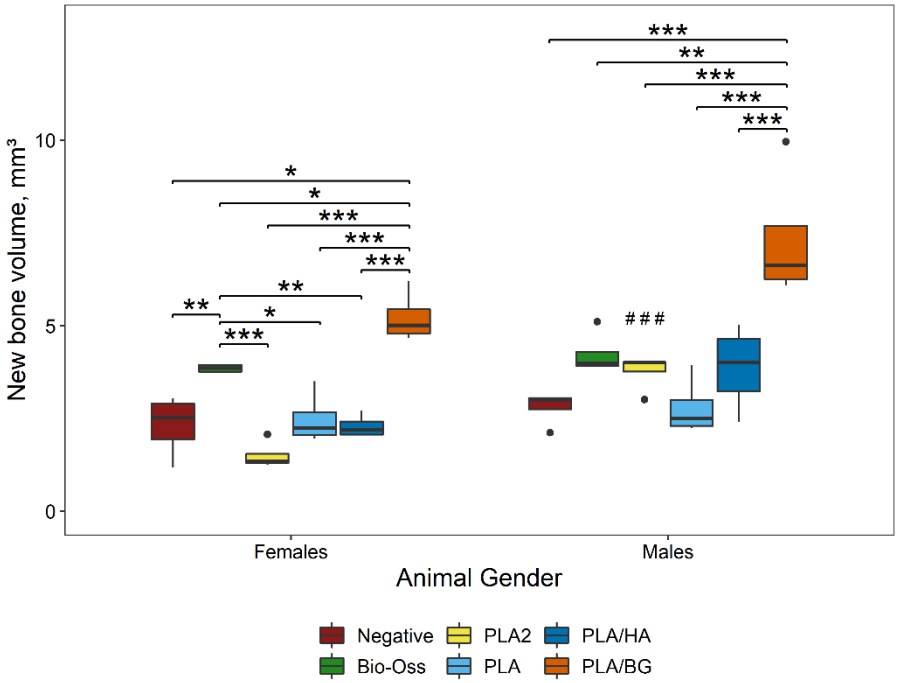

Fig. 17. Stage 1 micro-CT results. Box plots representing newly formed bone volume (BV, mm^3), according to sample groups and gender. *, ** and *** mark the statistically significant differences between the groups at $p < 0.05$, $p < 0.01$ and $p < 0.001$, respectively. #, ## and ### mark the statistically significant differences between the gender in the same sample group at $p < 0.05$, $p < 0.01$, and $p < 0.001$, respectively.

A statistically significant gender-specific difference was detected only in the PLA2 group ($p < 0.001$) (Fig. 17). New bone volume formed in the created

critical-size defects of the PLA/BG group was statistically higher than all other sample groups in Stage 1 in both genders. A statistically significant difference was found between the Bio-Oss group and all other sample groups, except PLA/BG group in females.

A statistically significant gender-specific difference was detected in the PLA DPSC and PLA/HA DPSC groups ($p < 0.05$) in Stage 2 investigation (Fig. 18). More new BV was statistically significantly gained in males in these two groups. PLA/BG ECM gained the most significant new bone volume in Stage 2 investigation compared to PLA DPSC, PLA/HA DPSC, and PLA/HA ECM groups in females. There was no statistically significant difference between the tested groups in Stage 2 in males. Scaffolds improved with ECM showed better results than scaffolds improved with DPSC, except the PLA group in males. However, no statistically significant differences were found between the same scaffold DPSC and ECM groups.

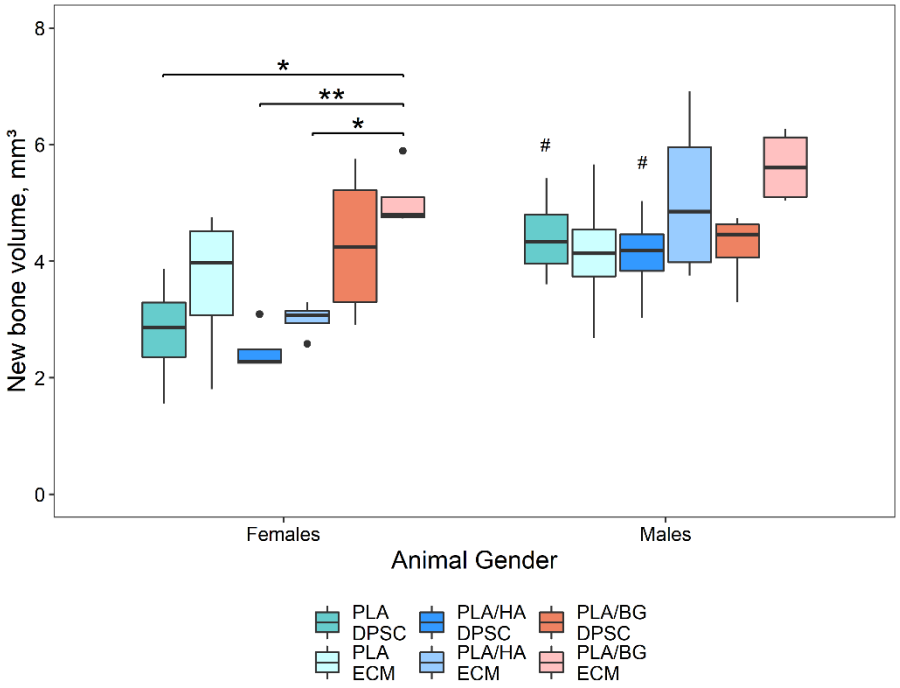

Fig. 18. Stage 2 micro-CT results. Box plots representing newly formed bone volume (BV, mm^3), according to sample groups and gender. *, ** and *** mark the statistically significant differences between the groups at $p < 0.05$, $p < 0.01$ and $p < 0.001$, respectively. #, ## and ### mark the statistically significant differences between the gender in the same sample group at $p < 0.05$, $p < 0.01$, and $p < 0.001$, respectively.

4.3.2. Qualitative bone histological analysis

The histological slides were obtained in cooperation with researchers from the National Center of Pathology, Affiliate of Vilnius University Hospital Santaros Klinikos, Lithuania. The histological slides for all groups after eight weeks of healing are shown in Fig. 19 and 20.

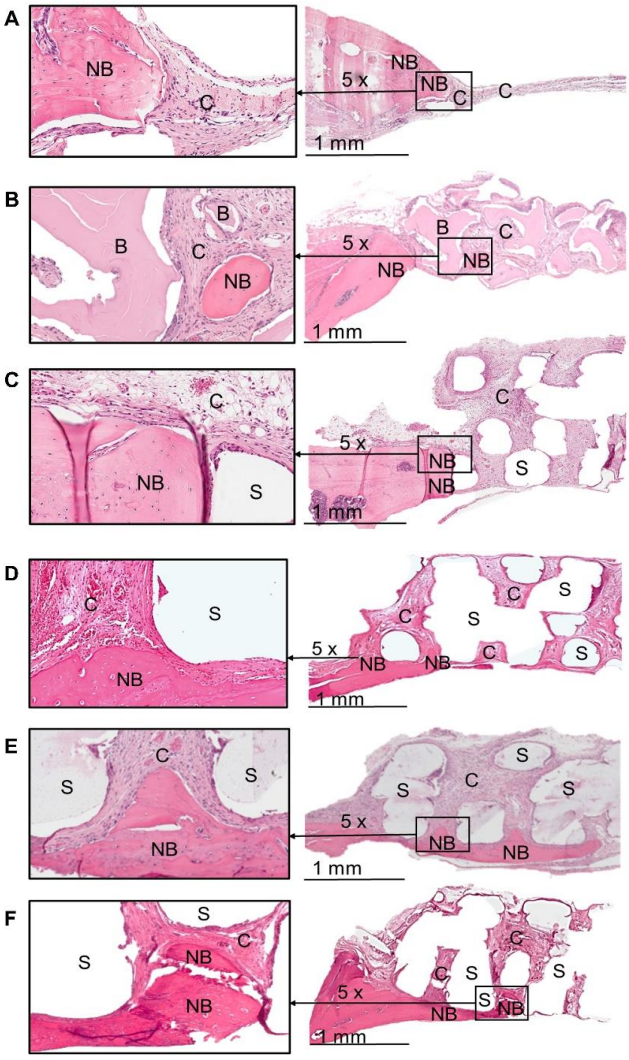

Fig. 19. Histological sections of the calvarial bone at the eighth week of healing (hematoxylin and eosin staining). The sections are taken at the centre of the defect (5.5 mm). The left sides of the sections are shown for the typical findings of the samples for both genders in Stage 1 groups. NB – newly formed bone, B – Bio-Oss, C – connective tissue, S – scaffold (original magnification 2×). A – Negative control; B – Bio-Oss particles. C – PLA2 group; D – PLA group; E – PLA/HA; F – PLA/BG scaffolds.

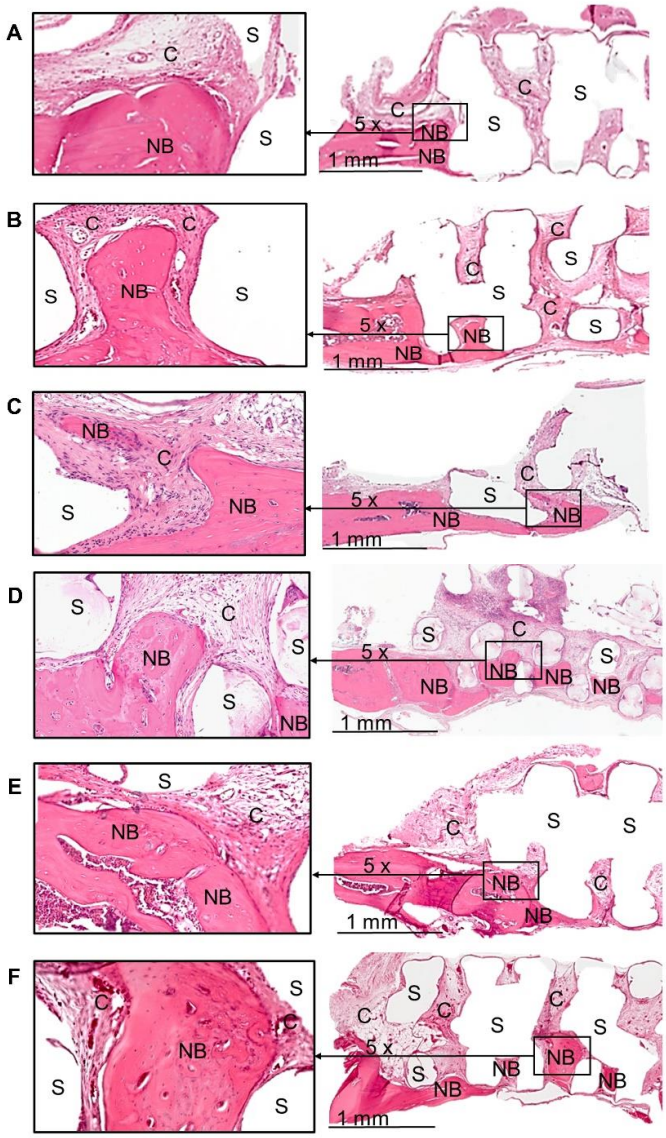

Fig. 20. Histological sections of the calvarial bone at the eighth week of healing (hematoxylin and eosin staining). The sections are taken at the center of the defect (5.5 mm). The left sides of the sections are shown for the typical findings of the samples for both genders in Stage 2 groups. NB – newly formed bone, C – connective tissue, S – scaffold (original magnification 2×). A – PLA DPSC; B – PLA ECM; C – PLA/HA DPSC; D – PLA/HA ECM; E – PLA/BG DPSC; F – PLA/BG ECM scaffolds.

Histologically, the analysed biopsy contained connective tissue, residual grafting material, and newly-formed bone. None of the defects of all groups was wholly healed after eight weeks (Fig. 19 and 20). The formation of thin connective tissue was observed up to 0.3 mm in the negative control group (Fig. 19 A). The connective tissue thickness varied from 1.0 mm to 2.0 mm in the other sample groups of both stages (Fig. 19 B – F, 20). Lymphocytes were found mainly in the PLA and PLA2 groups (Fig. 19 C, D). More new bone was forming towards the centre of the defect in the negative control group than in other sample groups (Fig. 19 A). However, the layer of the new bone was thinner, varying in thickness from 0.1 to 0.3 mm. The new bone formed a thicker layer ranging from 0.3 mm to 1.0 mm in the other sample groups, but it was less developed towards the centre of the created defects (Fig. 19 B – F, 20). Some sections of PLA/BG, PLA/HA DPSC, PLA/HA ECM, PLA/BG DPSC, and PLA/BG ECM scaffolds showed bridged new bone formation from one side to another with ingrowth between the scaffold layers (Fig. 19 F, 20 C – F). Furthermore, the new bone islands were found in the centre of defects of the Bio-Oss, PLA/HA ECM, PLA/BG ECM scaffolds. (Fig. 19 B, Fig. 20 D, F). These new bone islands formed separately from the newly formed bone at the defect edges.

4.3.3. Quantitative bone histological analysis

Histological evaluation showed that the best results were achieved with Bio-Oss (3.75 ± 0.6 mm^2), PLA/BG DPSC (3.9 ± 0.34 mm^2 and PLA/BG ECM (3.86 ± 0.27 mm^2) groups (Fig. 21). Statistically significant difference was found between those three groups and Negative control, PLA2, PLA, PLA DPSC, PLA ECM, and PLA/HA groups. PLA/BG (3.60 ± 0.31 mm^2) showed a statistically significant difference with the sample groups mentioned earlier, except PLA/ECM scaffold group. PLA/HA ECM showed statistically significantly better results than Negative control, PLA2, PLA, PLA DPSC, and PLA/HA groups.

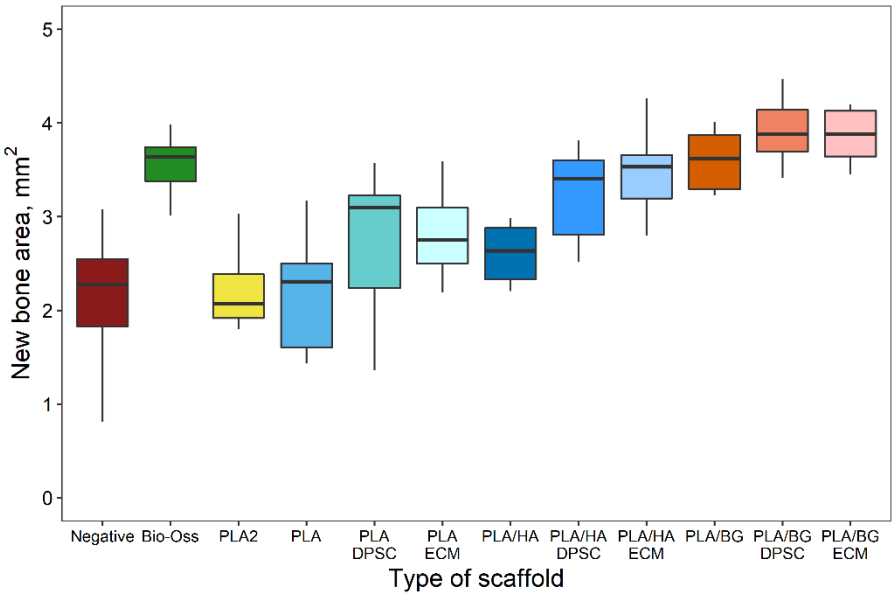

Negative												
Bio-Oss	***											
PLA2	-	***										
PLA	-	***	-									
PLA DPSC	-	**	-	-								
PLA ECM	-	*	-	-	-							
PLA/HA	-	**	-	-	-	-						
PLA/HA DPSC	**	-	**	**	-	-	-					
PLA/HA ECM	***	-	***	***	-	-	0.07	-				
PLA/BG	***	-	***	***	*	-	*	-	-			
PLA/BG DPSC	***	-	***	***	**	**	***	-	-	-		
PLA/BG ECM	***	-	***	***	**	**	***	-	-	-	-	
Group	Negative	Bio-Oss	PLA2	PLA	PLA DPSC	PLA ECM	PLA/HA	PLA/HA DPSC	PLA/HA ECM	PLA/BG	PLA/BG DPSC	PLA/BG ECM

Fig. 21. Quantitative bone histological analysis results of the area (mm^2) of newly formed bone according to sample groups. *, ** and *** mark the statistically significant differences between the groups at $p < 0.05$, $p < 0.01$ and $p < 0.001$, respectively. #, ## and ### mark the statistically significant differences between the gender in the same sample group at $p < 0.05$, $p < 0.01$ and $p < 0.001$, respectively.

Further results were analysed according to the *in vivo* stages, comparing the results between the groups in genders and between the genders (Fig. 22 and 23).

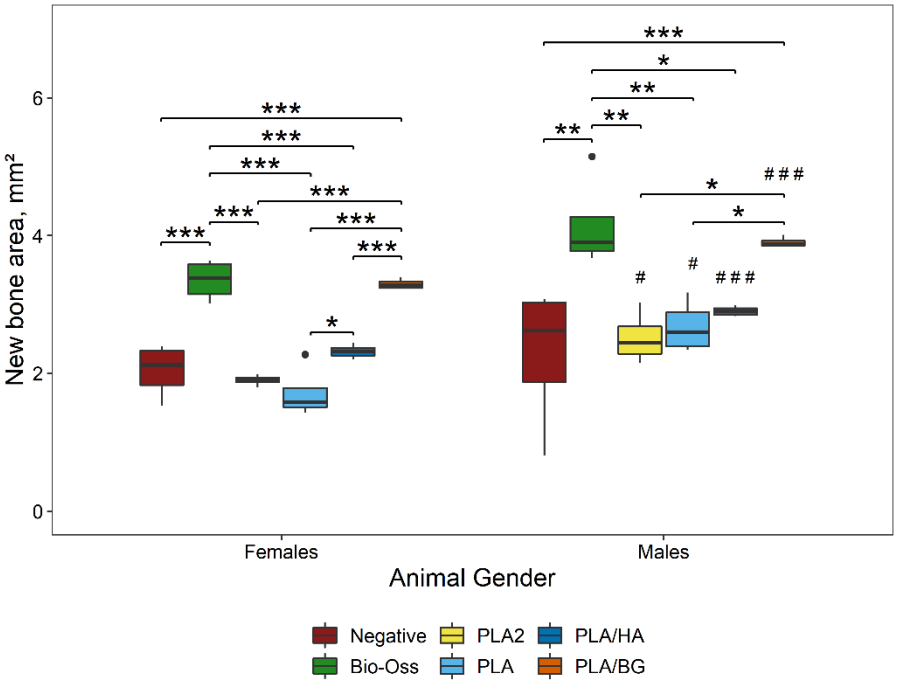

Fig. 22. Stage 1 quantitative bone histological analysis results of the area (mm^2) of newly formed bone according to sample groups and gender. *, ** and *** mark the statistically significant differences between the groups at $p < 0.05$, $p < 0.01$ and $p < 0.001$, respectively. #, ## and ### mark the statistically significant differences between the gender in the same sample group at $p < 0.05$, $p < 0.01$, and $p < 0.001$, respectively.

Histological evaluation showed no significant gender-specific differences in new bone formation of negative control and Bio-Oss groups ($p > 0.05$) (Fig. 22). However, gender-specific differences were found in all experimental groups. Moreover, Bio-Oss and PLA/BG showed statistically significantly more new bone areas than all other tested groups in females. On the other hand, there was no statistically significant difference between PLA/BG and PLA/HA groups in males.

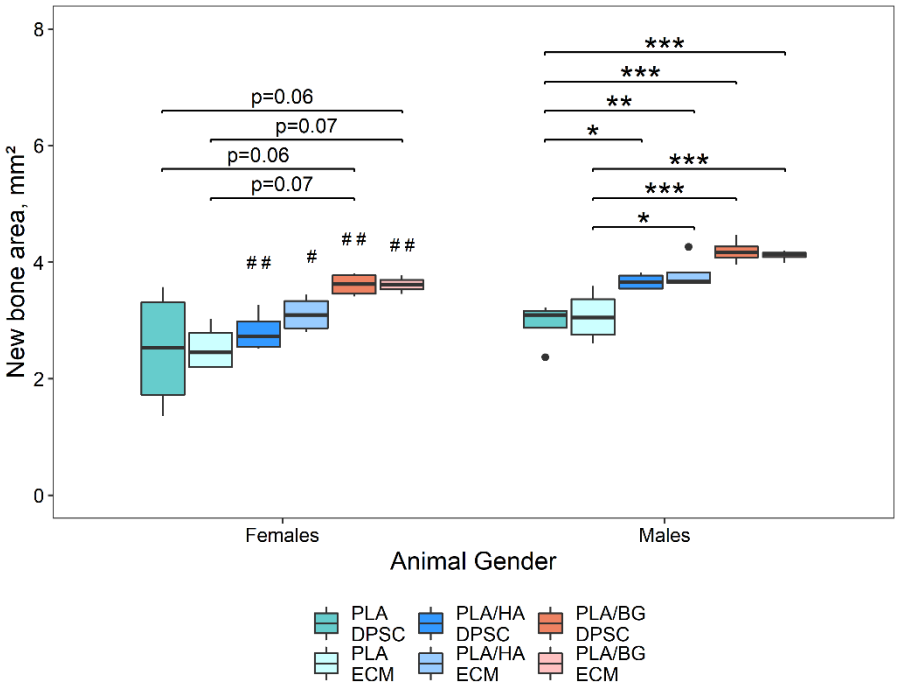

Fig. 23. Stage 2 quantitative bone histological analysis results of the area (mm^2) of newly formed bone according to sample groups and gender. *, ** and *** mark the statistically significant differences between the groups at $p < 0.05$, $p < 0.01$ and $p < 0.001$, respectively. #, ## and ### mark the statistically significant differences between the gender in the same sample group at $p < 0.05$, $p < 0.01$, and $p < 0.001$, respectively.

Histological evaluation showed no significant gender-specific differences in new bone formation of PLA DPSC and PLA ECM groups ($p > 0.05$) (Fig. 23). However, gender-specific differences were found in PLA/HA, and PLA/BG scaffold groups improved with DPSC and ECM. Although no statistically significant differences were found between the sample groups in females, some results were close to significance. PLA/HA ECM, PLA/BG DPSC, and PLA/BG ECM showed statistically significantly more new bone areas than PLA DPSC and PLA ECM groups in males. In addition, PLA/HA DPSC group showed statistically significantly more new bone area than the PLA DPSC group in males.

5. DISCUSSION

5.1. *IN VITRO* RESULTS

The restoration of bone defects remains one of the most challenging bone grafting surgeries in various fields of medicine: neurosurgery, orthopaedics, oral and maxillofacial surgery specialities [19]. However, bone tissue engineering is a new and promising treatment strategy [262]. Bone is a mineralized connective tissue [114] with a highly specialised organic-inorganic architecture classified as micro and nanocomposite tissue [257]. It is known that the mechanical properties of bone depend on its composition (porosity, mineralization, etc.) and structural organization (trabecular or cortical bone architecture, collagen fibre orientation, fatigue damage, etc.) [257]. It is, therefore, essential to mimic these bone properties when creating scaffolds for bone regeneration or replacement. Various bone augmentation techniques are based on understanding how the bone heals and regenerates after injury. Direct bone healing occurs if a correct anatomical reduction of the fracture ends and a stable fixation [407]. If the gap between bone ends is less than 0.01 mm and interfragmentary strain is less than 2 %, the fracture unites by so-called contact healing. Gap healing occurs if the gap is less than 800 μm to 1 mm [407]. Therefore, the accuracy of the 3D printing of bone scaffolds is critical since the scaffold needs to match the defect's shape closely.

First of all, two FDM 3D printers were chosen for this research: an Ultimaker Original and a Pharaoh XD 20. According to the specifications, both printers are compatible with PLA filaments. The ultimate layer resolution of the Ultimaker Original printer is 20 to 200 μm [408]. Filaments with a 2.85 mm diameter are used with this printer. The ultimate layer resolution of the Pharaoh XD 20 printer is 100 μm [408], and it uses 1.75 mm diameter filaments for printing. Therefore, we decided to check the printing accuracy of these two 3D printers using the same printing parameters from the same company‘s filaments before fabrication of custom-made filaments. The printing accuracy and morphology of the scaffolds were assessed by SEM, gravimetric and liquid displacement methods, and micro-CT evaluation. SEM results showed that it was challenging to produce even layers at 400 μm with an Ultimaker Original printer. On the other hand, the Pharaoh XD 20 printer laid threads with industrial PLA filament (PLA2 group) more accurately than the Ultimaker Original (PLA1 group). Moreover, the distance between the threads was maintained more accurately to original STL file dimensions in the PLA2 group and statistically significantly differed from the PLA1 group. Although the total porosity of the scaffolds showed no statistically significant

difference between the two groups or compared to original STL file porosity, PLA2 scaffolds showed more considerable porosity. Furthermore, micro-CT evaluation showed a statistically significant difference in volume between the PLA1 and PLA2 groups.

These statistically significant differences between two FDM 3D printers could have occurred due to different hardware or software. Moreover, the Pharaoh XD printer had an automatic calibration for keeping a more accurate distance between the printing head and bed. It is known that automatic levelling improves bed adhesion and printing accuracy. However, some manual adjustments sometimes need to be done [410]. Slicer 1.2.8 software was used with the Pharaoh XD 20 printer and Ultimaker Cura 3.6 software with the Ultimaker Original printer. Although there is no statistically significant evidence among the two software used in the research, there is evidence that different slicer software can generate different results from the exact initial specifications [411]. According to the results of this study, it was decided to create custom-made 1.75 mm diameter filaments with HME and print the experimental scaffolds with the Pharaoh XD 20 printer.

HME is one of the most widely applied processing technologies in the plastic, rubber, food, and pharmaceutical industries [412]. This method was recently introduced as an alternative technique for filament preparation in bone regeneration applications [413]. The Filabot Original extruder system produced composite filaments from PLA with approximately 10 % HA or 10 % BG concentrations. The distributions of the HA and BG in the composite filaments were controlled through thorough manual mixing and selecting the similar size of HA or BG and PLA particles. 10 % concentrations of inorganic materials in the composite filaments were chosen because lower concentrations of HA can be considered too low to have measurable effects on the outcome with the cell cultures *in vitro* or bone regeneration *in vivo*. According to the literature, a 10 % concentration of HA improves new bone formation *in vitro* and *in vivo* [269]. Although a concentration of 5 % BG in the composite filaments showed ectopic bone formation [283], positive effect on vascularisation [277], or extracellular matrix mineralization [282], it was believed that 10 % of BG might increase these effects. Moreover, higher concentrations (15 %, 20 %) were also produced in this research. However, they resulted in a less controllable extrusion process, and the filaments turned out to be too brittle for fabrication with FDM 3D printers. In addition, the diameters of the prepared filaments through all their lengths varied (PLA – from 1.67 to 1.75 mm, PLA/HA – from 1.28 to 1.45 mm, PLA/BG – from 1.6 to 1.75 mm). It was observed that the middle portions of the created filaments resulted in having minor deviations in diameter and were adequate to produce the

experimental specimens. However, according to the literature, varying filament diameters can cause severe complications during extrusion. Still, it remains debatable whether minor deviations in diameter can affect the 3D printing result and the morphology of the created scaffolds [150].

The PLA group was printed first and evaluated with SEM. It was noticed that uneven layers were laid, and the results were similar to the PLA1 group. According to the achieved results, the Pharaoh XD 20 printer parameters (bed levelling, first layer height) were adjusted before printing the scaffolds from PLA/HA and PLA/BG filaments. Afterwards, the evaluation with SEM was done to compare the composite scaffolds with PLA groups. According to SEM results, scaffolds printed from PLA/HA and PLA/BG filaments showed equal or even better accuracy in printing layers and scaffold heights than all PLA groups. Interestingly, SEM images showed that PLA/BG scaffolds laid the evenest threads with no statistically significant difference between the layers. Possibly, this effect helped to maintain the most extended distances between threads in PLA/BG scaffolds. Moreover, theoretical porosity could be counted for PLA/BG scaffolds because it displayed the threads evenly, and the deviation of distance between threads was minimal. For this reason, gravimetric and liquid displacement methods, micro-CT evaluation were not performed for PLA/BG scaffolds.

The further morphological analysis compared PLA/HA scaffolds with the PLA2 group because PLA/HA scaffolds were the most difficult to print due to the filament brittleness and most varying diameter. Moreover, SEM images showed statistically significant differences between the different layers of the PLA/HA scaffolds. Therefore, it was essential to find the total porosity and volume of PLA/HA scaffolds because it could affect the results *in vivo*. Despite the difficulties in printing the scaffolds, porosity evaluation showed that PLA/HA scaffolds achieved 48 – 50 % of the average total porosity and showed the closest values to the original STL model compared to the PLA2 group. The research in the literature confirms that 50 % porosity in the scaffolds induces cell proliferation and migration and positively influences bone regeneration [152]. Additionally, micro-CT results showed that PLA2 and PLA/HA scaffolds printed with the Pharaoh XD 20 printer displayed accurate 3D morphology. However, the volumes of the scaffold groups were not equal to the volumes of the original STL files.

Overall, HME was confirmed to be a valuable tool to create custom-made composite filaments. However, further research is needed to improve the uniformity of the diameter of the filaments. This goal could be achieved by employing smart filament extruders with online diameter control, which measures the filament diameter and adjusts the extrusion parameters

accordingly (temperature, speed, etc.). It is difficult to say which of these parameters (varying diameter or filament composition) had a more significant effect on the final morphology of the scaffolds. We think composite filaments had a higher specific heat capacity and cooled slower because of the HA and BG. The viscosity of the composite filaments was also higher. Presumably, this allowed to lay the threads more evenly and get more accurate volumetric dimensions (better representing the production STL file) than the PLA groups. Furthermore, we suggest that 10 wt% of HA and BG could increase mechanical properties and enhance dimensional stability before setting the material. This effect was reported with 15 wt% of HA added in PLA/HA filament [414]. In the literature, a positive effect of 10 wt% of HA on the stiffness, tensile strength and modulus, flexural strength, and modulus was also confirmed [267]. Additionally, various studies confirmed the positive outcome of the BG in the composite scaffolds on compressive strength [277,278], tensile strength with 4 wt% of BG [275], ultimate loading with 20 wt% of BG [276], elastic modulus with 9 wt% of BG [273].

Several techniques (SEM, gravimetric and liquid displacement methods, micro-CT) were obtained to get more accurate imaging of the scaffolds in this research. SEM enables qualitative assessment of the scaffolds' surface morphology but not an internal structure [16]. Thus, other techniques to assess 3D morphology are also needed. In addition, total porosity was analysed with gravimetric and liquid displacement methods. According to the literature, the interconnected porosity of the scaffold and pore size are essential to measure for reproducible and predictable scaffold properties and optimal scaffold functions, such as mechanical support, the transportation of nutrients and oxygen, cell growth and proliferation, and the removal of waste [262,402]. Furthermore, studies show that micro-CT could improve the efficiency of *in vitro* testing because numerous parameters like pore shape, pore size, layer thickness, even closed pores, scaffold volume could be counted. However, the recommended micro-CT scanning resolution should vary from 1 to 50 μm [16]. Since the Skyscan 1178 micro-CT had a relatively low scanning resolution, the micro-CT scan images were additionally processed using digital image processing methods to get sharper images. Low scanning resolution could affect the precision of volume measurement, but it was a valuable tool to compare the 3D morphology of different scaffolds.

The results achieved from assessing the scaffolds' accuracy and morphology helped better understand the 3D printing process. The critical message based on this study is that the dimensions and morphology of the 3D printed scaffolds can differ from the original STL file. Thus, it may be very important in medical applications, e.g.,visual-tactile aids for surgery

preplanning, anatomically-matched surgical guides, or patient-specific implants [415]. Therefore, we recommend checking the first-time 3D printed product's measurements and final morphology and comparing the results with the original STL file. If differences in the measurements occur, an STL file should be adopted to get a more accurate final product, especially for medical applications [407].

5.2. *IN VIVO* RESULTS

Bone regeneration is a complex process where new biomaterials play a pivotal role in filling bone defects and restoring the bone's functions [11]. Recently, several studies showed that 3D printed composite bone scaffolds are among the most promising bone grafting strategies [13,14]. However, their efficiency should be evaluated through reliable and comparable methods before adopting them in clinical practise [416]. In addition, some standardised assessments of biomaterials like cytotoxicity, biocompatibility, biological activity, the immunogenicity of specific compounds, mechanical and morphological properties may be successfully evaluated *in vitro* [417,418]. In this study, after successfully printing PLA, PLA/HA and PLA/BG scaffolds, further evaluation with cell cultures *in vitro* was done by Milda Alksne [334,400]. When the screening of the biomaterials *in vitro* was finished, promising candidates were further evaluated *in vivo* to assess the material/host interaction and the regenerative efficacy.

The rodent models are well described in the literature, highly reproducible and broadly used in similar studies studying bone healing and regeneration [417]. In this study, Wistar rats were chosen and obtained by inbreeding because they were relatively inexpensive, easy to house and manipulate. Inbred animals are genetically similar and respond to external and internal stimuli similarly, allowing for a more reliable evaluation of new bone regeneration strategies [417]. Additionally, the usage of homozygous animals reduced the number of rats for DPSC isolation and production of cellularized and decellularized scaffolds. Furthermore, bone regeneration was estimated equally in male and female rats in this study. Literature showed that female rats have lower regenerative capacity than males due to lower mesenchymal stem cell numbers found in their bone marrow [418]. Equality of the animal gender in the sample groups is also crucial because males become larger than females in neurocranial length and width measurements at 120 days [419]. Thus, the results of bone regeneration could be affected because of different animal growth.

The femora, spine, mandible and calvarium of the rodents are the most often used anatomical sites to investigate bone regeneration [420]. The primary goal of this research was to evaluate the bone regenerative potential of the created scaffolds for the treatment of oral and maxillofacial region bone defects. Therefore, the mandible and calvarium critical-size defect models were of interest in this study because they were suitable for investigating intramembranous bone formation [420]. Although the mandibular defect model showed the potential to be used in this research, significant disadvantages of this defect model were poor visibility, complex handling during surgical procedures, the risk to damage important adjacent anatomical structures (nasal bones, sinus, veins, and arteries) [421]. Moreover, studies showed that the operated animals might be in severe pain and unable to feed after the surgery, significantly affecting the healing results [421].

Meanwhile, the calvarial critical-size defect model allows researchers to test the bioactivity of different materials (granular, bulk or scaffold) and compare the results with existing data [417]. This aspect was essential for choosing a calvarial site in this study because Bio-Oss was a granular bone substitute and the created samples were scaffolds. Furthermore, calvarial surgery is easy to perform, as there is no need for external fixation of the biomaterials. The evaluation of the healing process is done by micro-CT and bone histological analysis [417]. On the other hand, it is impossible to test the performance of the biomaterial under physiological mechanical loads or interactions with implant surfaces [422]. However, considering all advantages and disadvantages of the models, the calvarial model was suitable for *in vivo* investigation of bone regeneration for craniomaxillofacial reasons [420].

Controversial data of critical-size defects in the calvarial rat model exist considering 8.0 mm or 5.0 mm to be critical size [417,423]. In the current study, circular 5.5 mm calvarial defects were made with at least a 1.5 mm bone bridge between them. In the pilot study, we have found that a smaller bridge between the two defects may be resorbed and affect the healing results. Furthermore, the defects were created in an oblique line because the thickness of the calvarial bones is the biggest in the sagittal suture and more homogenous laterally [419]. Therefore, a more prominent bone bridge between the created defects could be achieved. In addition, the samples were placed equally in upper and lower defects in male and female rats to minimise the source of bias in the study. Moreover, none of the created defects throughout the study healed spontaneously, so the term “critical-size defect” can be used [424]. This surgical technique was beneficial because the samples were analysed in the critical-size defect model. The number of animals was reduced,

remaining more consistent with the 3Rs concept (refinement, reduction, replacement).

The euthanasia term varies among studies [422]. In this study, the evaluation of bone regeneration using micro-CT and bone histological analysis were done eight weeks after the surgery because it is the best time to investigate new bone formation in the rat model [425]. If the defects had been left for a longer healing time, it would have been possible that more significant differences could have occurred between the PLA2, PLA, PLA/DPSC, PLA/ECM and all PLA/HA, PLA/BG and Bio-Oss groups due to PLA biodegradation products [261]. According to the literature, both inorganic components in the created composite scaffolds decrease the degradation rate of the scaffolds and neutralise the acidity of PLA degradation products [261,263,272,277]. Moreover, it is possible that biodecorated constructs with DPSC or their ECM would have shown better results through longer healing time in critical-size bone defect regeneration than scaffolds alone due to their osteoinductive features [338].

It is a well-known fact that scaffold architecture is of critical importance for bone regeneration. The optimal pore size, ranging from 200 to 500 μm, is ideal for bone regeneration and vascularisation [155]. In this study, the scaffolds were designed with macropores having the average theoretical pore size of 450 μm. In consonance with the literature, the macropores of the scaffolds cannot be smaller than 350 μm because the space is needed for the cell migration to the site of the defect and bone production [154,156]. Moreover, created macropores of the scaffolds in this study were also suitable for vascularisation [154]. The pore configuration and geometry are also essential for bone cell migration and proliferation [157]. Therefore, the scaffold threads should form hexagonal or octagonal shapes or be composed with an angle of 60° to each other [158]. Such an internal structure was adopted in our created scaffolds. The thickness of the average rat calvarial bones was about 1 mm, so the scaffolds were implanted into the defects using the "over-inlay" surgical technique. Therefore, it was possible to create the 3D structure to satisfy the requirements of the bone scaffold architecture.

Bio-Oss is one of the most commonly used inorganic bovine bone xenografts in regenerative bone procedures due to its adequate new bone formation, low reabsorption rate, osteoconductive characteristics, and compensation for the natural bone resorption caused by remodelling [156]. In addition, recent research in bone regeneration of the oral and maxillofacial region showed that Bio-Oss induced new bone formation comparably to autogenous bone blocks that are considered to be „the golden standard" [106]. Therefore, Bio-Oss was chosen as the material for positive control in this study because it was essential to understand whether the results of the created

scaffolds are competitive compared to the provided results of the materials currently used in clinical practice. In this study, micro-CT and histological results revealed that only Bio-Oss and negative control groups showed no significant gender-specific differences in new bone formation. Interestingly, during the first stage of *in vivo* evaluation, histological results showed that all experimental sample groups had gender-specific differences. Therefore, we hypothesised that it might be due to lower mesenchymal stem cell numbers found in females bone marrow [418]. PLA, PLA/HA and PLA/BG scaffolds were decorated with DPSC or their ECM, respectively, hoping to improve the healing process. However, biodecoration failed to improve new bone formation between genders in the same group. Gender-specific differences were identified in new bone formation of all stage II *in vivo* experimental groups‘ results obtained from either micro-CT or quantitative bone histological analysis.

According to the literature, another possible gender-specific reason for lower bone regeneration properties in females may be differences in sex or growth hormones levels found in animal and human studies [426]. Therefore, further research is needed to analyse these effects in bone regeneration and the interaction between the host and the biomaterials. Furthermore, the universal scaffold composition was not found in this study because the created scaffolds didn‘t improve critical-size bone defect healing in both genders. Therefore, further research is needed to improve the osteoconductivity of the created scaffolds by using more advanced printing technologies and achieving more inorganic materials in the composite scaffolds. The osteoinductive properties of the scaffolds could also be improved with osteoinductive materials like BMP or PRF [1]. However, this information could have been missed if only male animals had been included in the research. Then PLA/BG and their biodecorated constructs, PLA/HA biodecorated constructs would have shown better results than even the Bio-Oss group. Therefore, the results would be misinterpreted and distorted, as the gender effect would not be evaluated. Moreover, there is an ongoing discussion in the literature that research involving only male animals can't represent the actual outcome in particular species [427]. Unfortunately, even 80 % of the articles include only males in the research, and only 1 % of papers analyzed results by sex for surgical research in rodents [427]. Therefore, it is essential to have an equal number of males and females per study group.

Despite the achieved gender-specific differences in new bone formation of the experimental groups, when the results were counted in total, micro-CT results revealed that the best bone regeneration abilities were demonstrated by PLA/BG and PLA/BG ECM groups. Furthermore, PLA/BG scaffolds showed

statistically significantly better new bone formation than all other groups from stage I and stage II *in vivo* investigation, except PLA/BG ECM group in males. The possible reason for such a great result could be that BG is very active from the first contact with the host bone defect. BG surface precipitates hydroxycarbonate apatite crystals within an hour of the implantation [243]. Furthermore, within 48 hours after implantation, the synthesis of growth factors is initiated, affecting the osteoblast proliferation [237,248]. Various *in vivo* studies showed that PLA/BG scaffolds were superior to pure PLA in inducing bone regeneration [276], ectopic bone formation [283], vascularization [277,284] eight weeks after implantation.

However, some controversial results exist in the literature that Bio-Oss and BG (Biogran) in the GBR model gained less bone than the negative control and arrested bone formation [428]. These results should be carefully interpreted because the skeletal bones of rats continue remodelling throughout the whole life of the animal. Thus, bone formation might be higher in negative controls of rodents than other animal species [420,422]. Moreover, different surgical techniques influence bone defect healing, and critical-size defect models are more relevant because spontaneous bone healing through all the defects won‘t occur [417]. Moreover, if the materials' chemical properties (molecular weight, particle size, etc.) are changed, their degradation, mechanical and bone regeneration properties may change accordingly [429]. Thus, the results of Biogran can‘t be compared to the PLA/BG scaffolds used in this study. Furthermore, long term *in vivo* experiments are needed in large animal bone regeneration models for further PLA/BG scaffolds investigation, evaluation of bone regeneration, the interaction between biomaterial and hormones, growth factors and host answer.

Histologically, PLA/HA ECM, PLA/BG, PLA/BG DPSC, PLA/BG ECM scaffolds showed the best results in new bone formation in this study. The obtained results were comparable to Bio-Oss with no statistically significant difference between the groups. Moreover, qualitative histology showed that the new bone islands were found in the centre of the defects only in Bio-Oss, PLA/BG ECM and PLA/HA ECM groups. ECM-coated scaffolds have increased interest in bone tissue regeneration due to retained native biological molecules, which enhance cellular adhesion, proliferation, migration, and differentiation but reduce inflammation [398]. The decellularisation procedure used in the current study was sufficient, and an evenly dispersed ECM network remained on the PLA, PLA/HA, and PLA/BG ECM scaffolds. Histologically, ECM-coated scaffolds showed better bone regeneration results than cellularized scaffolds and scaffolds alone. However, no statistically significant differences were observed between the

osteoconductive scaffolds and their biodecorated constructs eight weeks after the surgery. A possible reason could be that residual host bone stem cells had difficulties migrating into the centre of the bone defect because different fibril arrangements of collagen left after the decellularization process could work as the anchorage and migration barrier [385]. Further research should focus on the scaffold morphology and ECM interactions and long term *in vivo* investigations of bone regeneration.

In this study, the decellularized scaffolds showed slightly better results in bone regeneration than cellularized constructs, although cellularized scaffolds also had the remaining ECM. Possible reasons for the differences in the cellularized scaffolds' osteoconductivity could be due to the onset of DPSC death at the centre of the scaffolds because of malnutrition [430]. Moreover, some stem cells could have died during the implantation because of mechanical injury during the operation procedure [431]. Stem cells could also have been lost due to bleeding or insufficient blood circulation in bone defects [432]. Moreover, even if the stem cells survive transplantation, their viability still decreased significantly [432]. Thus, in most cases, usually, the cell death process occurs. While the cells are dying, the cellular materials (DNA, signalling molecules, etc.) are released into the extracellular fluid and promote inflammatory response [431]. Moreover, the released materials may even migrate to other organs of the body and cause side effects [430]. Thus, it leads to worse osteoconductivity results of the scaffolds with live cells than decellularized ones. However, many details in these processes are still unknown and require further research to characterise the role and the fate of grafted cells and how they interplay with resident cells at the edges of the bone defects [158]. Also, researchers need to assess whether the improved results of bone regeneration are worth the increased cost and time of the procedure.

Finally, in the current study, pure PLA scaffolds showed the most negligible effect on new bone formation in the created bone defects. The possible reason could be the pronounced inflammation reaction seen in the qualitative bone histological analysis and confirmed by other authors [158]. PLA biodegradation products could also be acidifying the microenvironment and causing additional stress to the healing tissue. HA and BG included in the composite scaffolds had a positive effect on prolonging PLA degradation, thus reducing the acidity of the biodegrading scaffold and increasing osteoconductivity of the created scaffolds [261,263,272,277]. It is known that PLA/HA and PLA/BG scaffolds with a ratio of 9:1 have a positive effect on new bone formation *in vitro* and *in vivo* [269,276]. However, an increase of inorganic concentration can be expected to provide better osteoconductive potential and be associated with higher levels of new bone formation [159,372].

Further studies should investigate the exact characterisation of ECM from DPSC, improve the morphology of the scaffolds and composition of the materials. Moreover, the mechanical properties and resorption rate of 3D printed materials should be evaluated in future research to increase the biologic outcomes of the 3D printed scaffolds.

6. CONCLUSIONS

Considering study limitations, the following conclusions can be drawn:

1. Based on SEM, micro-CT, and porosity evaluation methods, industrial PLA scaffolds printed with a Pharaoh XD printer were statistically significantly more accurate in layer height, the distance between the threads, scaffold height, volume, and had bigger total porosity than industrial PLA scaffolds printed with Ultimaker Original printer. 3D printer settings affect the morphology and accuracy of 3D scaffolds.
2. Filaments from PLA microbeads, composite filaments from PLA/HA and PLA/BG at a ratio of 9:1 may be created with hot-melt extrusion. The diameters of the produced filaments were not uniform and ranged from 1.28 to 1.75 mm, but were suitable for producing 3D scaffolds with the FDM 3D printer.
3. The achieved morphological parameters of the printed composite PLA/BG, and PLA/HA scaffolds at a ratio of 9:1 were similar to the STL model and just as accurate or even more accurate than industrial PLA scaffolds printed with the Pharaoh XD 20 printer.
4. The evaluation of the micro-CT results in both animal genders showed that statistically significantly more new bone formed in PLA/BG group than all other *in vivo* stage I groups. In addition, the quantitative bone histological analysis evaluation showed comparable results between PLA/BG and Bio-Oss on new bone formation in a rat calvarial critical-size defect 8 weeks after surgery. However, statistically significant gender-specific differences of new bone formation were found in all experimental groups.
5. The evaluation of the micro-CT and quantitative bone histological analysis results of *in vivo* stage II groups showed that PLA/HA ECM, PLA/BG DPSC, and PLA/BG ECM groups had a positive influence on new bone formation in a rat calvarial critical-size defect 8 weeks after surgery. In addition, the obtained bone regeneration results were comparable to Bio-Oss and PLA/BG according to the bone quantitative histological analysis. However, statistically significant gender-specific differences of new bone formation were found in the composite groups enhanced with DPSC or their ECM. Furthermore, based on qualitative bone histological analysis, only Bio-Oss, PLA/HA ECM, and PLA/BG ECM groups showed new bone islands formation separately from the newly formed bone at the defect edges. The results of micro-CT and quantitative bone histological analysis showed that there were no

statistically significant differences between the osteoconductive scaffolds and their biodecorated constructs. However, slightly greater new bone formation was seen in ECM-coated scaffolds in rat calvarial critical-size defects.

7. PRACTICAL RECOMMENDATIONS AND FUTURE PERSPECTIVES

1. We recommend checking the first-time 3D printed product's measurements and final morphology and comparing the results with the original STL file. If differences in the measurements occur, an STL file should be adopted to get a more accurate final product, especially for medical applications.
2. Further *in vivo* studies should be performed on animals of both genders to avoid misinterpretation of the results.
3. The results of this study are essential for the further development and improvement of 3D artificial bone tissue „OSSEUM 4D“.

ORCID

Ieva Gendviliene https://orcid.org/0000-0002-1777-9781

Vygandas Rutkunas https://orcid.org/0000-0001-5740-4573

Virginija Bukelskiene https://orcid.org/0000-0001-6215-2542

8. CURRICULUM VITAE

Name	Ieva
Surname	Gendvilienė
Date of birth	1987 01 06
Place of birth	Ukmergė
E-mail	ieva.gendviliene@gmail.com
Research activities website	https://www.researchgate.net/profile/Ieva-Gendviliene

Education

2006	Ukmergės Jonas Basanavičius secondary school
2011	Vilnius University, Faculty of Medicine, Institute of Odontology, *Master's Diploma*
2015	Vilnius University, Faculty of Medicine, Institute of Odontology, *Certificate of Specialist in Oral surgery*

Work experience

2011 – 2015	Dentist General Practitioner, Public and private practice
2015 – current	Oral surgeon, Private practice
2019 – current	Member of a scientific group DIGITORUM

9. SUPPLEMENTAL MATERIAL

Approval of the Ethics Committee

VALSTYBINĖ MAISTO IR VETERINARIJOS TARNYBA

LEIDIMAS ATLIKTI BANDYMO SU GYVŪNAIS PROCEDŪRŲ PROJEKTĄ

Vilniaus universiteto Raštinė
GAUTA
2016 -03- 2 3
Nr. 9A - 1030

2016-03-18 Nr. G2-40
Vilnius

Vadovaujantis Lietuvos Respublikos gyvūnų gerovės ir apsaugos įstatymo 16 straipsnio 4 dalimi, Mokslo ir mokymo tikslais naudojamų gyvūnų laikymo, priežiūros ir naudojimo reikalavimais, patvirtintais Valstybinės maisto ir veterinarijos tarnybos direktoriaus 2012 m. spalio 31 d. įsakymu Nr. B1-866 „Dėl Mokslo ir mokymo tikslais naudojamų gyvūnų laikymo, priežiūros ir naudojimo reikalavimų patvirtinimo“, Europos konvencija dėl eksperimentiniais ir kitais mokslo tikslais naudojamų stuburinių gyvūnų apsaugos (OL *2004 m. specialusis leidimas,* 15 skyrius, 4 tomas, p. 325) ir remiantis Lietuvos bandomųjų gyvūnų naudojimo etikos komisijos prie Valstybinės maisto ir veterinarijos tarnybos 2016-03-14 išvada Nr. 2 „Dėl leidimo atlikti bandymus su gyvūnais“,
l e i d ž i a m a

Vilniaus universiteto Biochemijos institutui,
(ūkio subjekto (-ų), kuriam (-iems) išduotas leidimas atlikti bandymo su gyvūnais procedūrų projektą,

Universiteto g. 3, Vilnius, 211950810,
adresas (-ai), kodas (-ai) Juridinių asmenų registre)

atlikti bandymo su gyvūnais procedūrų projektą

„Kompozitinių karkasų, skirtų kaulo regeneracijai, kūrimas, jų biosuderinamumo bei efektyvumo vertinimas *in vivo*“,
(bandymo su gyvūnais procedūrų projekto pavadinimas, vadovas, naudojamų gyvūnai)

projekto vadovė Virginija Bukelskienė, naudojant 61 žiurkę, 20 triušių,

Vilniaus universiteto Biochemijos institute, Universiteto g. 3, Vilnius.
(bandymo su gyvūnais procedūrų projekto atlikimo vietos pavadinimas, adresas)

Leidimas atlikti bandymo su gyvūnais procedūrų projektą galioja iki 2018 m. gruodžio 31 d.

LIETUVOS RESPUBLIKA VALSTYBINĖ MAISTO IR VETERINARIJOS TARNYBA

Direktoriaus pavaduotojas,
pavaduojantis direktorių Virginijus Jauga

BIBLIOGRAPHY

1. Habibovic P, de Groot K. Osteoinductive biomaterials-properties and relevance in bone repair. *J Tissue Eng Regen Med.* 2007;1(1):25–32.

2. Dimitriou R, Jones E, Mcgonagle D, Giannoudis PV. Bone regeneration: current concepts and future directions. *BMC Med.* 2011;9(1):66.

3. Goldstein JA, Paliga JT, Bartlett SP. Cranioplasty: indications and advances. *Curr Opin Otolaryngol Head Neck Surg.* 2013;21(4):400–9.

4. Wee J, Thevendran G. The role of orthobiologics in foot and ankle surgery. *EFORT Open Rev.* 2017;2(6):272–80.

5. Zizzari VL, Zara S, Tetè G, Vinci R, Gherlone E, Cataldi A. Biologic and clinical aspects of integration of different bone substitutes in oral surgery: a literature review. *Oral Surg Oral Med Oral Pathol Oral Radiol.* 2016;122(4):392–402.

6. Moussa NT, Dym H. Maxillofacial Bone Grafting Materials. *Dent Clin North Am.* 2020;64(2):473–90.

7. Chavda S, Levin L. Human Studies of Vertical and Horizontal Alveolar Ridge Augmentation Comparing Different Types of Bone Graft Materials: A Systematic Review. *J Oral Implantol.* 2018;44(1):74–84.

8. Sheikh Z, Sima C, Glogauer M. Bone Replacement Materials and Techniques Used for Achieving Vertical Alveolar Bone Augmentation. *Materials.* 2015;8(6):2953–93.

9. Yusof MFH, Zahari W, Hashim SNM, Osman ZF, Chandra H, Kannan TP, et al. Angiogenic and osteogenic potentials of dental stem cells in bone tissue engineering. *J Oral Biol Craniofacial Res.* 2018;8(1):48–53.

10. Ghanaati S, Barbeck M, Booms P, Lorenz J, Kirkpatrick CJ, Sader RA. Potential lack of "standardized" processing techniques for production of allogeneic and xenogeneic bone blocks for application in humans. *Acta Biomater.* 2014;10(8):3557–62.

11. Hutmacher DW. Scaffolds in tissue engineering bone and cartilage. *Biomaterials.* 2000;21(24):2529–43.

12. Porter JR, Ruckh TT, Popat KC. Bone tissue engineering: a review in bone biomimetics and drug delivery strategies. *Biotechnol Prog.* 2009;25(6):1539–60.

13. Turnbull G, Clarke J, Picard F, Riches P, Jia L, Han F, et al. 3D bioactive composite scaffolds for bone tissue *engineering*. *Bioact Mater.* 2018;3(3):278–314.

14. Rezwan K, Chen QZ, Blaker JJ, Boccaccini AR. Biodegradable and bioactive porous polymer/inorganic composite scaffolds for bone tissue engineering. *Biomaterials.* 2006;27(18):3413–31.

15. Siddiqui N, Asawa S, Birru B, Baadhe R, Rao S. PCL-Based Composite Scaffold Matrices for Tissue Engineering Applications. *Mol Biotechnol.* 2018;60(7):506–32.

16. Bertoldi S, Farè S, Tanzi MC. Assessment of scaffold porosity: the new route of micro-CT. *J Appl Biomater Biomech JABB.* 2011;9(3):165–75.

17. Raeisdasteh Hokmabad V, Davaran S, Ramazani A, Salehi R. Design and fabrication of porous biodegradable scaffolds: a strategy for tissue engineering. *J Biomater Sci Polym Ed.* 2017;28(16):1797–825.

18. Roseti L, Parisi V, Petretta M, Cavallo C, Desando G, Bartolotti I, et al. Scaffolds for Bone Tissue Engineering: State of the art and new perspectives. *Mater Sci Eng C.* 2017;78:1246–62.

19. Wang W and Yeung KWK. Bone grafts and biomaterials substitutes for bone defect repair: A review. *Bioact Mater.* 2017;2(4):224-47. DOI: 10.1016/j.bioactmat.2017.05.007.

20. de Grado GF, Keller L, Idoux-Gillet Y, Wagner Q, Musset AM, Benkirane-Jessel N, Bornert F, Offner D. Bone substitutes: a review of their characteristics, clinical use, and perspectives for large bone defects management. *J Tissue Eng.* 2018;9:2041731418776819. DOI: 10.1177/2041731418776819.

21. Garcia-Denche JT, Tamimi F, Alkhraisat MH, Prados-Frutos JC, López-Cabarcos E. Bone Substitutes. Implant Dentistry - The Most Promising *Discipline of Dentistry*, 2011. DOI: 10.13140/2.1.1825.2801.

22. Markets and markets. Dental bone graft substitutes market by type (synthetic bone grafts, xenografts, allografts, and demineralized

allografts), application (sinus lift, ridge augmentation, socket preservation, periodontal defect regeneration, and implant-bone regeneration), product (Biooss, Osteograf, Grafton, and others) – forecast to 2021. Available at https://www.marketsandmarkets.com/Market-Reports/dental-bone-graft-substitutes-market-159678690.html (Accessed: 17 April 2020).

23. Srivastava A., Jaiswal P. Bone grafts and substitutes market overview. Available at https://www.alliedmarketresearch.com/bone-graft-substitutes-market#toc (Accessed: 17 April 2020).

24. Tarnaris A, Arvin B, Ashkan K. Evolution in Practice: How has British Neurosurgery Changed in the Last 10 Years? *Ann R Coll Surg Engl.* 2008;90(6):508–12.

25. Marcus HJ, Hughes-Hallett A, Kwasnicki RM, Darzi A, Yang G-Z, Nandi D. Technological innovation in neurosurgery: a quantitative study. *J Neurosurg.* 2015;123(1):174–81.

26. Beuriat P-A, Lohkamp L-N, Szathmari A, Rousselle C, Sabatier I, Di Rocco F, et al. Repair of Cranial Bone Defects in Children Using Synthetic Hydroxyapatite Cranioplasty (CustomBone). *World Neurosurg.* 2019;129:e104–13.

27. van de Vijfeijken SECM, Münker TJAG, Spijker R, Karssemakers LHE, Vandertop WP, Becking AG, et al. Autologous Bone Is Inferior to Alloplastic Cranioplasties: Safety of Autograft and Allograft Materials for Cranioplasties, a Systematic Review. *World Neurosurg.* 2018;117:443-452.e8.

28. Boden SD. Overview of the Biology of Lumbar Spine Fusion and Principles for Selecting a Bone Graft Substitute. *Spine.* 2002;27(16S):S26.

29. Buser Z, Brodke DS, Youssef JA, Meisel H-J, Myhre SL, Hashimoto R, et al. Synthetic bone graft versus autograft or allograft for spinal fusion: a systematic review. *J Neurosurg Spine.* 2016;25(4):509–16.

30. Stark JR, Hsieh J, Waller D. Bone Graft Substitutes in Single- or Double-Level Anterior Cervical Discectomy and Fusion: A Systematic Review. *Spine.* 2019;44(10):618–28.

31. Tatkare D. Spinal fusion devices market by product (thoracolumbar devices, cervical fusion devices, and interbody fusion devices) and by surgery (open spine surgery and minimally invasive spine surgery) - global

opportunity analysis and industry forecast, 2014-2022. Available at https://www.alliedmarketresearch.com/spinal-fusion-devices-market (Accessed: 22 April 2020).

32. Elsalanty ME, Genecov DG. Bone Grafts in Craniofacial Surgery. *Craniomaxillofacial Trauma Reconstr.* 2009;2(3):125–34.

33. Mount CA, M Das J. Cerebral Perfusion Pressure. In: StatPearls [Internet]. Treasure Island (FL): StatPearls Publishing; 2020 [cited 2020 Apr 22]. Available from: http://www.ncbi.nlm.nih.gov/books/NBK537271/

34. Shah AM, Jung H, Skirboll S. Materials used in cranioplasty: a history and analysis. *Neurosurg Focus.* 2014;36(4):19.

35. Aydin S, Kucukyuruk B, Abuzayed B, Aydin S, Sanus GZ. Cranioplasty: Review of materials and techniques. *J Neurosci Rural Pract.* 2011;2(2):162–7.

36. Bonda DJ, Manjila S, Selman WR, Dean D. The Recent Revolution in the Design and Manufacture of Cranial Implants: Modern Advancements and Future Directions. *Neurosurgery.* 2015;77(5):814–24.

37. Garcia CM, Toms SA. A cautionary tale of hydroxyapatite cement use in frontal sinus obliteration. *Interdiscip Neurosurg.* 2020;21:100702.

38. Punchak M, Chung LK, Lagman C, Bui TT, Lazareff J, Rezzadeh K, et al. Outcomes following polyetheretherketone (PEEK) cranioplasty: Systematic review and meta-analysis. *J Clin Neurosci.* 2017;41:30–5.

39. Zhang J, Tian W, Chen J, Yu J, Zhang J, Chen J. The application of polyetheretherketone (PEEK) implants in cranioplasty. *Brain Res Bull.* 2019;153:143–9.

40. Guerado E, Fuerstenberg CH. What bone graft substitutes should we use in post-traumatic spinal fusion? *Injury.* 2011;42:64–71.

41. Jakoi AM, Iorio JA, Cahill PJ. Autologous bone graft harvesting: a review of grafts and surgical techniques. *Musculoskelet Surg.* 2015;99(3):171–8.

42. Epstein NE. Iliac crest autograft versus alternative constructs for anterior cervical spine surgery: Pros, cons, and costs. *Surg Neurol Int.* 2012;3 (3):143–56.

43. Sudhakar KNV, Mohanty R, Singh V. Evaluation of Donor Site Morbidity Associated with Iliac Crest Bone Harvest in Oral and Maxillofacial, Reconstructive Surgery. *J Clin Diagn Res JCDR*. 2017;11(6):28–33.

44. Kadam A, Millhouse PW, Kepler CK, Radcliff KE, Fehlings MG, Janssen ME, et al. Bone substitutes and expanders in Spine Surgery: A review of their fusion efficacies. *Int J Spine Surg*. 2016;10:33. DOI: 10.14444/3033. eCollection 2016.

45. Yoo JS, Ahn J, Patel DS, Hrynewycz NM, Brundage TS, Singh K. An evaluation of biomaterials and osteobiologics for arthrodesis achievement in spine surgery. *Ann Transl Med.* 2019;7:S168. DOI: 10.21037/atm.2019.06.80.

46. Chaput CD, Shar A, Jupiter D, Hubert Z, Clough B, Krause U, et al. How stem cell composition in bone marrow aspirate relates to clinical outcomes when used for cervical spine fusion. *Plos one*. 2018;13(9):e0203714.

47. Gupta A, Kukkar N, Sharif K, Main BJ, Albers CE, El-Amin III SF. Bone graft substitutes for spine fusion: A brief review. *World J Orthop*. 2015;6(6):449–56.

48. Carragee EJ, Chu G, Rohatgi R, Hurwitz EL, Weiner BK, Yoon ST, et al. Cancer risk after use of recombinant bone morphogenetic protein-2 for spinal arthrodesis. *J Bone Joint Surg Am.* 2013;95(17):1537–45.

49. Russell TA, Insley G. Bone Substitute Materials and Minimally Invasive Surgery. *Orthop Clin North Am.* 2017;48(3):289–300.

50. Roberts TT, Rosenbaum AJ. Bone grafts, bone substitutes and orthobiologics. *Organogenesis.* 2012;8(4):114–24.

51. Calcei JG, Rodeo SA. Orthobiologics for Bone Healing. *Clin Sports Med.* 2019;38(1):79-95. DOI: 10.1016/j.csm.2018.08.005.

52. Murphy RF, Mooney 3rd JF. Orthobiologics in Pediatric Orthopedics. *Orthop Clin North Am.* 2017;48(3):323-331. DOI: 10.1016/j.ocl.2017.03.007.

53. Murphy CP, Sanchez A, Peebles LA, Provencher MT. Incorporating Ortho-Biologics into Your Clinical Practice. *Clin Sports Med.* 2019;38(1):163-8. DOI: 10.1016/j.csm.2018.08.008.

54. Pierannunzii L, Zagra L. Bone grafts, bone graft extenders, substitutes and enhancers for acetabular reconstruction in revision total hip arthroplasty. *Efort open rev*. 2016;1(12):431–9.

55. Shafaghi R, Rodriguez O, Schemitsch EH, Zalzal P, Waldman SD, Papini M, et al. A review of materials for managing bone loss in revision total knee arthroplasty. *Mater Sci Eng C.* 2019;104:109941.

56. Rupp M, Biehl C, Budak M, Thormann U, Heiss C, Alt V. Diaphyseal long bone nonunions — types, aetiology, economics, and treatment recommendations. *Int Orthop*. 2018;42(2):247–58.

57. Emara KM, Diab RA, Emara AK. Recent biological trends in management of fracture non-union. *World J Orthop.* 2015;6(8): 623-8.

58. Palombella S, Lopa S, Gianola S, Zagra L, Moretti M, Lovati AB. Bone Marrow-Derived Cell Therapies to Heal Long-Bone Nonunions: A Systematic Review and Meta-Analysis—Which Is the Best Available Treatment? *Stem Cells Int.* 2019; 2019: 3715964. DOI: 10.1155/2019/3715964

59. Agarwal A. Nonunions: Diagnosis, Evaluation and Management. *Springer;* 2018:350.

60. Thomas JD, Kehoe JL. Bone Nonunion. In: StatPearls. Treasure Island (FL): *StatPearls Publishing*; 2020. Available from: http://www.ncbi.nlm.nih.gov/books/NBK554385/

61. Ziran BH, Smith WR, Morgan SJ. Use of Calcium-Based Demineralized Bone Matrix/Allograft for Nonunions and Posttraumatic Reconstruction of the Appendicular Skeleton: Preliminary Results and Complications. *J Trauma Acute Care Surg.* 2007;63(6):1324–8.

62. Palombella S, Lopa S, Gianola S, Zagra L, Moretti M, Lovati AB. Bone Marrow-Derived Cell Therapies to Heal Long-Bone Nonunions: A Systematic Review and Meta-Analysis-Which Is the Best Available Treatment? *Stem Cells Int*. 2019;2019:3715964.

63. Hernigou P, Desroches A, Queinnec S, Lachaniette CHF, Poignard A, Allain J, Chevallier N, Rouard H. Morbidity of graft harvesting versus bone marrow aspiration in cell regenerative therapy. *Int Orthop*. 2014;38(9):1855-60. DOI: 10.1007/s00264-014-2318-x.

64. Malhotra R, Kumar V, Garg B, Singh R, Jain V, Coshic P, et al. Role of autologous platelet-rich plasma in treatment of long-bone nonunions: a prospective study. *Musculoskelet Surg.* 2015;99(3):243–8.

65. Say F, Türkeli E, Bülbül M. Is platelet-rich plasma injection an effective choice in cases of non-union? *Acta Chir Orthop Traumatol Cech*. 2014;81(5):340–5.

66. Conway JD, Shabtai L, Bauernschub A, Specht SC. BMP-7 Versus BMP-2 for the Treatment of Long Bone Nonunion. *Orthopedics.* 2014;37(12):e1049-57. DOI: 10.3928/01477447-20141124-50.

67. Campana V, Milano G, Pagano E, Barba M, Cicione C, Salonna G, et al. Bone substitutes in orthopaedic surgery: from basic science to clinical practice. *J Mater Sci Mater Med.* 2014;25(10):2445–61.

68. Ronga M, Fagetti A, Canton G, Paiusco E, Surace MF, Cherubino P. Clinical applications of growth factors in bone injuries: Experience with BMPs. *Injury.* 2013;44(1):34-9.DOI:10.1016/S0020-1383(13)70008-1.

69. Garrison KR, Shemilt I, Donell S, Ryder JJ, Mugford M, Harvey I, Song F, Alt V. Bone morphogenetic protein (BMP) for fracture healing in adults. *Cochrane Database Syst Rev.* 2010;2010(6):CD006950. DOI: 10.1002/14651858.CD006950.pub2.

70. Greer N, Yoon P, Majeski B, Wilt TJ. Orthobiologics in Foot and Ankle Arthrodesis Sites: A Systematic Review. Washington (DC): Department of Veterans Affairs (US); 2020 [cited 2021 Jun 29]. (VA Evidence-based Synthesis Program Reports). Available from: http://www.ncbi.nlm.nih.gov/books/NBK558309/

71. Yeoh JC, Taylor BA. Osseous Healing in Foot and Ankle Surgery with Autograft, Allograft, and Other Orthobiologics. *Orthop Clin North Am*. 2017;48(3):359–69.

72. Wallace GF. Current Orthobiologics for Elective Arthrodesis and Nonunions of the Foot and Ankle. *Clin Podiatr Med Surg*. 2017;34(3):399–408.

73. Lareau CR, Deren ME, Fantry A, Donahue RMJ, DiGiovanni CW. Does autogenous bone graft work? A logistic regression analysis of data from 159 papers in the foot and ankle literature. Foot Ankle Surg Off J Eur Soc *Foot Ankle Surg*. 2015;21(3):150–9.

74. Sveikata K, Balciuniene I, Tutkuviene J. Needs for prosthetic treatment in Vilnius population at the age over 45 years old. *Stomatologija*. 2012;14(3):81–4.

75. Hopcraft MS, Morgan MV, Satur JG, Wright FAC. Edentulism and dental caries in Victorian nursing homes. *Gerodontology*. 2012;29(2):e512-519.

76. Cha H-S, Kim J-W, Hwang J-H, Ahn K-M. Frequency of bone graft in implant surgery. *Maxillofac Plast Reconstr Surg*. 2016;38(1):19.

77. Tolstunov L, Hamrick JFE, Broumand V, Shilo D, Rachmiel A. Bone Augmentation Techniques for Horizontal and Vertical Alveolar Ridge Deficiency in Oral Implantology. *Oral Maxillofac Surg Clin N Am.* 2019;31(2):163–91.

78. Sethi A, Kaus T, Cawood JI, Plaha H, Boscoe M, Sochor P. Onlay bone grafts from iliac crest: a retrospective analysis. *Int J Oral Maxillofac Surg*. 2020;49(2):264–71.

79. Kloss FR, Offermanns V, Kloss-Brandstätter A. Comparison of allogeneic and autogenous bone grafts for augmentation of alveolar ridge defects-A 12-month retrospective radiographic evaluation. *Clin Oral Implants Res*. 2018;29(11):1163–75.

80. Robinson BT, Metcalfe D, Cuff AV, Pidgeon TE, Hewitt KJ, Gibbs VN, et al. Surgical techniques for autologous bone harvesting from the iliac crest in adults. *Cochrane Database Syst Rev.* 2018;2018(4):CD011783.

81. Rawashdeh MA. Morbidity of iliac crest donor site following open bone harvesting in cleft lip and palate patients. *Int J Oral Maxillofac Surg.* 2008;37(3):223–7.

82. Eufinger H, Leppänen H. Iliac crest donor site morbidity following open and closed methods of bone harvest for alveolar cleft osteoplasty. *J Cranio-Maxillo-fac Surg Off Publ Eur Assoc Cranio-Maxillo-fac Surg*. 2000;28(1):31–8.

83. Barr ML, Haveles CS, Rezzadeh KS, Nolan IT, Castro R, Lee JC, et al. Virtual Surgical Planning for Mandibular Reconstruction With the Fibula Free Flap: A Systematic Review and Meta-analysis. *Ann Plast Surg*. 2020;84(1):117–22.

84. Landau MJ, Badash I, Yin C, Alluri RK, Patel KM. Free vascularized fibula grafting in the operative treatment of malignant bone tumors of the upper extremity: A systematic review of outcomes and complications. *J Surg Oncol.* 2018;117(7):1432–9.

85. Reininger D, Cobo-Vázquez C, Monteserín-Matesanz M, López-Quiles J. Complications in the use of the mandibular body, ramus and symphysis as donor sites in bone graft surgery. A systematic review. *Med Oral Patol Oral Cirugia Bucal*. 2016;21(2):e241-249.

86. Güngörmüş M, Yavuz MS. The ascending ramus of the mandible as a donor site in maxillofacial bone grafting. *J Oral Maxillofac Surg Off J Am Assoc Oral Maxillofac Surg*. 2002;60(11):1316–8.

87. Dolanmaz D, Esen A, Yıldırım G, İnan Ö. The use of autogeneous mandibular bone block grafts for reconstruction of alveolar defects. *Ann Maxillofac Surg.* 2015;5(1):71–6.

88. Sittitavornwong S, Gutta R. Bone graft harvesting from regional sites. *Oral Maxillofac Surg Clin N Am*. 2010;22(3):317–30, v–vi.

89. Reininger D, Cobo-Vázquez C, Rosenberg B, López-Quiles J. Alternative intraoral donor sites to the chin and mandibular body-ramus. *J Clin Exp Dent.* 2017;9(12):e1474–81.

90. Barker D, Walls AW, Meechan JG. Ridge augmentation using mandibular tori. *Br Dent J*. 2001;190(9):474–6.

91. Bow A, Anderson DE, Dhar M. Commercially available bone graft substitutes: the impact of origin and processing on graft functionality. *Drug Metab Rev*. 2019;51(4):533–44.

92. Shang F, Yu Y, Liu S, Ming L, Zhang Y, Zhou Z, et al. Advancing application of mesenchymal stem cell-based bone tissue regeneration. *Bioact Mater*. 2021;6(3):666–83.

93. Sanz M, Dahlin C, Apatzidou D, Artzi Z, Bozic D, Calciolari E, et al. Biomaterials and regenerative technologies used in bone regeneration in the craniomaxillofacial region: Consensus report of group 2 of the 15th European Workshop on Periodontology on Bone Regeneration. *J Clin Periodontol*. 2019;46(21):82–91.

94. Haugen HJ, Lyngstadaas SP, Rossi F, Perale G. Bone grafts: which is the ideal biomaterial? *J Clin Periodontol*. 2019;46(21):92–102.

95. Sánchez-Labrador L, Molinero-Mourelle P, Pérez-González F, Saez-Alcaide LM, Brinkmann JC-B, Martínez JL-Q, Martínez-González JM. Clinical performance of alveolar ridge augmentation with xenogeneic bone block grafts versus autogenous bone block grafts. A systematic review. *J Stomatol Oral Maxillofac Surg*. 2021;122(3):293-302. DOI:10.1016/j.jormas.2020.10.009.

96. Musson DS, Gao R, Watson M, Lin J-M, Park Y-E, Tuari D, et al. Bovine bone particulates containing bone anabolic factors as a potential xenogenic bone graft substitute. *J Orthop Surg.* 2019;14(1):60.

97. Jensen OT, Bell W, Cottam J. Osteoperiosteal flaps and local osteotomies for alveolar reconstruction. *Oral Maxillofac Surg Clin N Am*. 2010;22(3):331–46.

98. Jensen OT, Ringeman JL, Cottam JR, Casap N. Orthognathic and osteoperiosteal flap augmentation strategies for maxillary dental implant reconstruction. *Oral Maxillofac Surg Clin N Am.* 2011;23(2):301–19.

99. Choi B-H, Lee S-HR, Huh J-Y, Han S-G. Use of the sandwich osteotomy plus an interpositional allograft for vertical augmentation of the alveolar ridge. *J Cranio-Maxillo-fac Surg Off Publ Eur Assoc Cranio-Maxillo-fac Surg*. 2004;32(1):51–4.

100. Mendoza-Azpur G, de la Fuente A, Chavez E, Valdivia E, Khouly I. Horizontal ridge augmentation with guided bone regeneration using particulate xenogenic bone substitutes with or without autogenous block grafts: A randomized controlled trial. *Clin Implant Dent Relat Res*. 2019;21(4):521–30.

101. Cucchi A, Ghensi P. Vertical Guided Bone Regeneration using Titanium-reinforced d-PTFE Membrane and Prehydrated Corticocancellous Bone Graft. *Open Dent J*. 2014;8:194–200.

102. Urban IA, Nagursky H, Lozada JL, Nagy K. Horizontal ridge augmentation with a collagen membrane and a combination of particulated autogenous bone and anorganic bovine bone-derived mineral: a prospective case series in 25 patients. *Int J Periodontics Restorative Dent*. 2013;33(3):299–307.

103. Lee Y-C, Chan Y-H, Hsieh S-C, Lew W-Z, Feng S-W. Comparing the Osteogenic Potentials and Bone Regeneration Capacities of Bone Marrow and Dental Pulp Mesenchymal Stem Cells in a Rabbit Calvarial Bone Defect Model. *Int J Mol Sci.* 2019;20(20).

104. Richardson CR, Mellonig JT, Brunsvold MA, McDonnell HT, Cochran DL. Clinical evaluation of Bio-Oss: a bovine-derived xenograft for the treatment of periodontal osseous defects in humans. *J Clin Periodontol*. 1999;26(7):421–8.

105. Bae E-B, Kim H-J, Ahn J-J, Bae H-Y, Kim H-J, Huh J-B. Comparison of Bone Regeneration between Porcine-Derived and Bovine-Derived Xenografts in Rat Calvarial Defects: A Non-Inferiority Study. *Materials.* 2019;12(20):3412.

106. Aludden HC, Mordenfeld A, Hallman M, Dahlin C, Jensen T. Lateral ridge augmentation with Bio-Oss alone or Bio-Oss mixed with particulate autogenous bone graft: a systematic review. *Int J Oral Maxillofac Surg*. 2017;46(8):1030–8.

107. Ali S, Bakry SA, Abd-Elhakam H. Platelet-Rich Fibrin in Maxillary Sinus Augmentation: A Systematic Review. *J Oral Implantol*. 2015;41(6):746–53.

108. Browaeys H, Bouvry P, De Bruyn H. A literature review on biomaterials in sinus augmentation procedures. *Clin Implant Dent Relat Res.* 2007;9(3):166–77.

109. Starch-Jensen T, Aludden H, Hallman M, Dahlin C, Christensen A-E, Mordenfeld A. A systematic review and meta-analysis of long-term studies (five or more years) assessing maxillary sinus floor augmentation. *Int J Oral Maxillofac Surg.* 2018;47(1):103–16.

110. Mangano C, Sinjari B, Shibli JA, Mangano F, Hamisch S, Piattelli A, et al. A Human Clinical, Histological, Histomorphometrical, and Radiographical Study on Biphasic HA-Beta-TCP 30/70 in Maxillary Sinus Augmentation. *Clin Implant Dent Relat Res*. 2015;17(3):610–8.

111. Ortega-Mejia H, Estrugo-Devesa A, Saka-Herrán C, Ayuso-Montero R, López-López J, Velasco-Ortega E. Platelet-Rich Plasma in Maxillary Sinus Augmentation: Systematic Review. *Mater Basel Switz*. 2020;13(3):E622.

112. Parra M, Atala-Acevedo C, Fariña R, Haidar ZS, Zaror C, Olate S. Graftless Maxillary Sinus Lift Using Lateral Window Approach: A Systematic Review. *Implant Dent*. 2018;27(1):111–8.

113. Clarke B. Normal Bone Anatomy and Physiology. *Clin J Am Soc Nephrol CJASN*. 2008;3(3):S131–9.

114. Florencio-Silva R, Sasso GR da S, Sasso-Cerri E, Simões MJ, Cerri PS. Biology of Bone Tissue: Structure, Function, and Factors That Influence Bone Cells. *BioMed Res Int*. 2015;2015:421746.

115. Arthur A, Gronthos S. Clinical Application of Bone Marrow Mesenchymal Stem/Stromal Cells to Repair Skeletal Tissue. *Int J Mol Sci.* 2020;21(24).

116. Komori T, Yagi H, Nomura S, Yamaguchi A, Sasaki K, Deguchi K, et al. Targeted disruption of Cbfa1 results in a complete lack of bone formation owing to maturational arrest of osteoblasts. *Cell.* 1997;89(5):755–64.

117. Capulli M, Paone R, Rucci N. Osteoblast and osteocyte: games without frontiers. *Arch Biochem Biophys*. 2014;561:3–12.

118. Franz-Odendaal TA, Hall BK, Witten PE. Buried alive: how osteoblasts become osteocytes. *Dev Dyn Off Publ Am Assoc Anat.* 2006;235(1):176–90.

119. Dallas SL, Prideaux M, Bonewald LF. The osteocyte: an endocrine cell and more. *Endocr Rev*. 2013;34(5):658–90.

120. Charles JF, Aliprantis AO. Osteoclasts: more than "bone eaters." *Trends Mol Med.* 2014;20(8):449–59.

121. Everts V, Delaissé JM, Korper W, Jansen DC, Tigchelaar-Gutter W, Saftig P, Beertsen W. The bone lining cell: its role in cleaning Howship's lacunae and initiating bone formation. *J Bone Miner Res Off J Am Soc Bone Miner Res.* 2002;17(1):77–90. DOI: 10.1359/jbmr.2002.17.1.77.

122. Oftadeh R, Perez-Viloria M, Villa-Camacho JC, Vaziri A, Nazarian A. Biomechanics and Mechanobiology of Trabecular Bone: A Review. *J Biomech Eng*. 2015;137(1):0108021–01080215.

123. Groeneveldt LC, Herpelinck T, Maréchal M, Politis C, van IJcken WFJ, Huylebroeck D, et al. The Bone-Forming Properties of Periosteum-

Derived Cells Differ Between Harvest Sites. *Front Cell Dev Biol*. 2020;8:554984.

124. Soriano RM, M Das J. Anatomy, Head and Neck, Maxilla. In: StatPearls [Internet]. Treasure Island (FL): StatPearls Publishing; 2021 [cited 2021 Apr 22]. Available from: http://www.ncbi.nlm.nih.gov/books/NBK538527/

125. Lindhe J, Bressan E, Cecchinato D, Corrá E, Toia M, Liljenberg B. Bone tissue in different parts of the edentulous maxilla and mandible. *Clin Oral Implants Res*. 2013;24(4):372–7.

126. Di Stefano DA, Arosio P, Pagnutti S, Vinci R, Gherlone EF. Distribution of Trabecular Bone Density in the Maxilla and Mandible. *Implant Dent.* 2019;28(4):340–8.

127. Turkyilmaz I, Tözüm TF, Tumer C. Bone density assessments of oral implant sites using computerized tomography. *J Oral Rehabil*. 2007;34(4):267–72.

128. Chugh T, Jain AK, Jaiswal RK, Mehrotra P, Mehrotra R. Bone density and its importance in orthodontics. *J Oral Biol Craniofacial Res.* 2013;3(2):92–7.

129. von Wowern N, Stoltze K. Sex and age differences in bone morphology of mandibles. *Scand J Dent Res*. 1978;86(6):478–85.

130. Öztürk Tonguç M, Ş Büyükkaplan U, Fentoğlu Ö, A Gümüş B, S Çerçi S, Y Kırzıoğlu F. Comparison of bone mineral density in the jaws of patients with and without chronic periodontitis. *Dentomaxillofacial Radiol*. 2012;41(6):509–14.

131. Tallgren A. The continuing reduction of the residual alveolar ridges in complete denture wearers: a mixed-longitudinal study covering 25 years. *J Prosthet Dent.* 1972;27(2):120–32.

132. Couso-Queiruga E, Stuhr S, Tattan M, Chambrone L, Avila-Ortiz G. Post-extraction dimensional changes: A systematic review and meta-analysis. J *Clin Periodontol*. 2021;48(1):126–44.

133. Brunello G, Sivolella S, Meneghello R, Ferroni L, Gardin C, Piattelli A, et al. Powder-based 3D printing for bone tissue engineering. *Biotechnol Adv*. 2016;34(5):740–53.

134. Kolan KCR, Leu MC, Hilmas GE, Velez M. Effect of material, process parameters, and simulated body fluids on mechanical properties of 13-93 bioactive glass porous constructs made by selective laser sintering. *J Mech Behav Biomed Mater*. 2012;13:14–24.

135. Roy NK, Behera D, Dibua OG, Foong CS, Cullinan MA. A novel microscale selective laser sintering (μ-SLS) process for the fabrication of microelectronic parts. *Microsyst Nanoeng*. 2019;5(1):1–14.

136. Sachs EM, Haggerty JS, Cima MJ, Williams PA. Three-dimensional printing techniques [Internet]. US5204055A, 1993 [cited 2021 Jun 20]. Available from: https://patents.google.com/patent/US5204055A/en

137. Mostafaei A, Elliott AM, Barnes JE, Li F, Tan W, Cramer CL, et al. Binder jet 3D printing—Process parameters, materials, properties, modeling, and challenges. *Prog Mater Sci.* 2021;119:100707.

138. 3D Printing of Scaffolds for Tissue Engineering | IntechOpen [Internet]. [cited 2021 Jun 20]. Available from: https://www.intechopen.com/books/3d-printing/3d-printing-of-scaffolds-for-tissue-engineering

139. Gu BK, Choi DJ, Park SJ, Kim MS, Kang CM, Kim C-H. 3-dimensional bioprinting for tissue engineering applications. *Biomater Res*. 2016;20:12.

140. Lin K, Sheikh R, Romanazzo S, Roohani I. 3D Printing of Bioceramic Scaffolds—Barriers to the Clinical Translation: From Promise to Reality, and Future Perspectives. *Materials.* 2019;12(17):2660.

141. Devi MG, Amutheesan M, Govindhan R, Karthikeyan B. A Review of Three-dimensional Printing for Biomedical and Tissue Engineering Applications. Open Biotechnol J [Internet]. 2018 Sep 28 [cited 2021 Jun 24];12(1). Available from: https://openbiotechnologyjournal.com/VOLUME/12/PAGE/241/FULLTEXT/

142. Williams DF. On the mechanisms of biocompatibility. *Biomaterials.* 2008;29(20):2941–53.

143. Luo Y, Wu C, Lode A, Gelinsky M. Hierarchical mesoporous bioactive glass/alginate composite scaffolds fabricated by three-dimensional plotting for bone tissue engineering. *Biofabrication.* 2013;5(1):015005.

144. Shao H, Ke X, Liu A, Sun M, He Y, Yang X, et al. Bone regeneration in 3D printing bioactive ceramic scaffolds with improved tissue/material interface pore architecture in thin-wall bone defect. *Biofabrication*. 2017;9(2):025003.

145. Milazzo M, Negrini NC, Scialla S, Marelli B, Farè S, Danti S, et al. Additive Manufacturing Approaches for Hydroxyapatite-Reinforced Composites. *Adv Funct Mater*. 2019;29(35):1903055.

146. Jungst T, Smolan W, Schacht K, Scheibel T, Groll J. Strategies and Molecular Design Criteria for 3D Printable Hydrogels. *Chem Rev*. 2016;116(3):1496–539.

147. Zheng Y, Pokorski JK. Hot melt extrusion: An emerging manufacturing method for slow and sustained protein delivery. *Wiley Interdiscip Rev Nanomed Nanobiotechnol*. 2021;e1712.

148. Tan DK, Davis DA, Miller DA, Williams RO, Nokhodchi A. Innovations in Thermal Processing: Hot-Melt Extrusion and KinetiSol® Dispersing. *AAPS PharmSciTech*. 2020;21(8):312.

149. Nevado P, Lopera A, Bezzon V, Fulla MR, Palacio J, Zaghete MA, et al. Preparation and in vitro evaluation of PLA/biphasic calcium phosphate filaments used for fused deposition modelling of scaffolds. *Mater Sci Eng C Mater Biol Appl*. 2020;114:111013.

150. Cardona C, Curdes AH, Isaacs AJ. Effects of Filament Diameter Tolerances in Fused Filament Fabrication. *IU J Undergrad Res*. 2016;2(1):44–7.

151. Yu X, Tang X, Gohil SV, Laurencin CT. Biomaterials for Bone Regenerative Engineering. *Adv Healthc Mater*. 2015;4(9):1268–85.

152. Seidenstuecker M, Kerr L, Bernstein A, Mayr H, Suedkamp N, Gadow R, et al. 3D Powder Printed Bioglass and β-Tricalcium Phosphate Bone Scaffolds. *Materials*. 2017;11(1):13.

153. Gregor A, Filová E, Novák M, Kronek J, Chlup H, Buzgo M, et al. Designing of PLA scaffolds for bone tissue replacement fabricated by ordinary commercial 3D printer. *J Biol Eng*. 2017;11(1):31.

154. Murphy CM, Haugh MG, O'Brien FJ. The effect of mean pore size on cell attachment, proliferation and migration in collagen-glycosaminoglycan scaffolds for bone tissue engineering. *Biomaterials*. 2010;31(3):461–6.

155. Son S-R, Linh N-TB, Yang H-M, Lee B-T. In vitro and in vivo evaluation of electrospun PCL/PMMA fibrous scaffolds for bone regeneration. *Sci Technol Adv Mater*. 2013;14(1):015009.

156. Shamsoddin E, Houshmand B, Golabgiran M. Biomaterial selection for bone augmentation in implant dentistry: A systematic review. *J Adv Pharm Technol Res.* 2019;10(2):46–50.

157. Abbasi N, Hamlet S, Love RM, Nguyen N-T. Porous scaffolds for bone regeneration. *J Sci Adv Mater Devices*. 2020 1;5(1):1–9.

158. Maisani M, Pezzoli D, Chassande O, Mantovani D. Cellularizing hydrogel-based scaffolds to repair bone tissue: How to create a physiologically relevant micro-environment? *J Tissue Eng*. 2017;8:2041731417712073.

159. Han J, Ma B, Liu H, Wang T, Wang F, Xie C, et al. Hydroxyapatite nanowires modified polylactic acid membrane plays barrier/osteoinduction dual roles and promotes bone regeneration in a rat mandible defect model. *J Biomed Mater Res A*. 2018 ;106(12):3099–110.

160. Wang C, Zhao Q, Wang M. Cryogenic 3D printing for producing hierarchical porous and rhBMP-2-loaded Ca-P/PLLA nanocomposite scaffolds for bone tissue engineering. *Biofabrication.* 2017 7;9(2):025031.

161. Balaji AB, Pakalapati H, Khalid M, Walvekar R, Siddiqui H. 1 - Natural and synthetic biocompatible and biodegradable polymers. In: Shimpi NG, editor. Biodegradable and Biocompatible Polymer Composites. *Woodhead Publishing;* 2018:3–32.

162. Kundu J, Pati F, Jeong YH, Cho D-W. Chapter 2 - Biomaterials for Biofabrication of 3D Tissue Scaffolds. In: Forgacs G, Sun W, editors. *Biofabrication*. *Boston: William Andrew Publishing*; 2013: 23–46.

163. Babensee JE, Anderson JM, McIntire LV, Mikos AG. Host response to tissue engineered devices. *Adv Drug Deliv Rev*. 1998;33(1):111–39.

164. Tian H, Tang Z, Zhuang X, Chen X, Jing X. Biodegradable synthetic polymers: Preparation, functionalization and biomedical application. *Prog Polym Sci*. 2012;37(2):237–80.

165. Nishida H, Tokiwa Y. Effects of higher-order structure of poly(3-hydroxybutyrate) on its biodegradation. I. Effects of heat treatment on microbial degradation. *J Appl Polym Sci*. 1992;46(8):1467–76.

166. Tokiwa Y, Calabia BP. Biodegradability and biodegradation of poly(lactide). *Appl Microbiol Biotechnol*. 2006;72(2):244–51.

167. FDA — inventory of effective food contact substance (FCS) notifications no.178 [Internet]. 2002. Available from: http://www.accessdata.fda.gov/scripts/fcn/fcnDetailNavigation.cfm?rpt=fcsListing&id=178

168. Lasprilla AJR, Martinez GAR, Lunelli BH, Jardini AL, Filho RM. Poly-lactic acid synthesis for application in biomedical devices — A review. *Biotechnol Adv*. 2012;30(1):321–8.

169. On S-W, Cho S-W, Byun S-H, Yang B-E. Bioabsorbable Osteofixation Materials for Maxillofacial Bone Surgery: A Review on Polymers and Magnesium-Based Materials. Biomedicines [Internet]. 2020 Aug 21 [cited 2020 Dec 14];8(9). Available from: https://www.ncbi.nlm.nih.gov/pmc/articles/PMC7555479/

170. Bos RR, Boering G, Rozema FR, Leenslag JW. Resorbable poly(L-lactide) plates and screws for the fixation of zygomatic fractures. *J Oral Maxillofac Surg Off J Am Assoc Oral Maxillofac Surg.* 1987;45(9):751–3.

171. Wednesday, June 15, Share 2016. FDA's Regulatory Science Program for Generic PLA/ PLGA-Based Drug Products [Internet]. [cited 2021 Jan 4]. Available from:http://www.americanpharmaceuticalreview.com/Featured-Articles/188841-FDA-s-Regulatory-Science-Program-for-Generic-PLA-PLGA-Based-Drug-Products/

172. James R, Manoukian OS, Kumbar SG. Poly(lactic acid) for delivery of bioactive macromolecules. *Adv Drug Deliv Rev*. 2016;107:277–88.

173. Santoro M, Shah SR, Walker JL, Mikos AG. Poly(lactic acid) nanofibrous scaffolds for tissue engineering. *Adv Drug Deliv Rev*. 2016;107:206–12.

174. Garlotta D. A Literature Review of Poly(Lactic Acid). *J Polym Environ*. 2001;9(2):63–84.

175. Bigg DM. Polylactide copolymers: Effect of copolymer ratio and end capping on their properties. *Adv Polym Technol*. 2005;24(2):69–82.

176. Singhvi MS, Zinjarde SS, Gokhale DV. Polylactic acid: synthesis and biomedical applications. *J Appl Microbiol*. 2019;127(6):1612–26.

177. Van de Velde K, Kiekens P. Biopolymers: overview of several properties and consequences on their applications. *Polym Test*. 2002;21(4):433–42.

178. Engh CA, Bobyn JD, Glassman AH. Porous-coated hip replacement. The factors governing bone ingrowth, stress shielding, and clinical results. *J Bone Joint Surg Br*. 1987;69(1):45–55.

179. Lehtonen TJ, Tuominen JU, Hiekkanen E. Resorbable composites with bioresorbable glass fibers for load-bearing applications. In vitro degradation and degradation mechanism. *Acta Biomater*. 2013;9(1):4868–77.

180. Heidemann W, Jeschkeit S, Ruffieux K, Fischer JH, Wagner M, Krüger G, et al. Degradation of poly(D,L)lactide implants with or without addition of calciumphosphates in vivo. *Biomaterials*. 2001;22(17):2371–81.

181. Vroman I, Tighzert L. Biodegradable Polymers. *Materials*. 2009;2(2):307–44.

182. Bergsma EJ, Rozema FR, Bos RR, de Bruijn WC. Foreign body reactions to resorbable poly(L-lactide) bone plates and screws used for the fixation of unstable zygomatic fractures. *J Oral Maxillofac Surg Off J Am Assoc Oral Maxillofac Surg*. 1993;51(6):666–70.

183. Bellini D, Cencetti C, Sacchetta AC, Battista AM, Martinelli A, Mazzucco L, et al. PLA-grafting of collagen chains leading to a biomaterial with mechanical performances useful in tendon regeneration. *J Mech Behav Biomed Mater*. 2016;64:151–60.

184. Groussard C, Morel I, Chevanne M, Monnier M, Cillard J, Delamarche A. Free radical scavenging and antioxidant effects of lactate ion: an in vitro study. *J Appl Physiol Bethesda Md* 1985;89(1):169–75.

185. Lampe KJ, Namba RM, Silverman TR, Bjugstad KB, Mahoney MJ. Impact of lactic acid on cell proliferation and free radical-induced cell death in monolayer cultures of neural precursor cells. *Biotechnol Bioeng*. 2009;103(6):1214–23.

186. Kanno T, Sukegawa S, Furuki Y, Nariai Y, Sekine J. Overview of innovative advances in bioresorbable plate systems for oral and maxillofacial surgery. *Jpn Dent Sci Rev*. 2018;54(3):127–38.

187. Böstman O, Hirvensalo E, Mäkinen J, Rokkanen P. Foreign-body reactions to fracture fixation implants of biodegradable synthetic polymers. *J Bone Joint Surg Br*. 1990;72(4):592–6.

188. Mondal D, Griffith M, Venkatraman SS. Polycaprolactone-based biomaterials for tissue engineering and drug delivery: Current scenario and challenges. *Int J Polym Mater Polym Biomater*. 2016;65(5):255–65.

189. Mark JE. The Polymer Data Handbook. Second Edition. Oxford, New York: *Oxford University Press*; 2009. 1264 p.

190. Abedalwafa M, Wang F, Wang L, Li C. Biodegradable poly-epsilon-caprolactone (PCL) for tissue engineering applications: A review. Reviews on Advanced Materials Science. 2012;34(2):123-40.

191. Hao J, Yuan M, Deng X. Biodegradable and biocompatible nanocomposites of poly(ϵ-caprolactone) with hydroxyapatite nanocrystals: Thermal and mechanical properties. *J Appl Polym Sci*. 2002;86(3):676–83.

192. Sung H-J, Meredith C, Johnson C, Galis ZS. The effect of scaffold degradation rate on three-dimensional cell growth and angiogenesis. *Biomaterials*. 2004;25(26):5735–42.

193. Pitt CG, Chasalow FI, Hibionada YM, Klimas DM, Schindler A. Aliphatic polyesters. I. The degradation of poly(ϵ-caprolactone) in vivo. *J Appl Polym Sci.* 1981;26(11):3779–87.

194. Kim J. Isovolemic Degradation of Polycaprolactone Particles and Calculation of Their Original Size from Human Biopsy. Plast Reconstr Surg Glob Open [Internet]. 2020 Jun 26 [cited 2020 Dec 16];8(6). Available from: https://www.ncbi.nlm.nih.gov/pmc/articles/PMC7339322/

195. Dwivedi R, Kumar S, Pandey R, Mahajan A, Nandana D, Katti DS, et al. Polycaprolactone as biomaterial for bone scaffolds: Review of literature. *J Oral Biol Craniofacial Res*. 2020;10(1):381–8.

196. Van de Velde K, Kiekens P. Thermoplastic polymers: overview of several properties and their consequences in flax fibre reinforced composites. *Polym Test*. 2001;20(8):885–93.

197. Vallet-Regí M, González-Calbet JM. Calcium phosphates as substitution of bone tissues. *Prog Solid State Chem*. 2004;32(1):1–31.

198. Rodrigues CVM, Serricella P, Linhares ABR, Guerdes RM, Borojevic R, Rossi MA, et al. Characterization of a bovine collagen-hydroxyapatite composite scaffold for bone tissue engineering. *Biomaterials*. 2003;24(27):4987–97.

199. Chen K-Y, Shyu P-C, Dong G-C, Chen Y-S, Kuo W-W, Yao C-H. Reconstruction of calvarial defect using a tricalcium phosphate-oligomeric proanthocyanidins cross-linked gelatin composite. *Biomaterials*. 2009;30(9):1682–8.

200. Salgado AJ, Coutinho OP, Reis RL. Bone Tissue Engineering: State of the Art and Future Trends. *Macromol Biosci.* 2004;4(8):743–65.

201. Bohner M. Calcium orthophosphates in medicine: from ceramics to calcium phosphate cements. *Injury*. 2000;31:37–47.

202. Yin X, Stott MJ, Rubio A. α- and β-tricalcium phosphate: A density functional study. *Phys Rev B.* 2003;68(20):205205.

203. Dorozhkin SV. Calcium Orthophosphates in Nature, Biology and Medicine. *Materials*. 2009;2(2):399–498.

204. Albee Fh. studies in bone growth: Triple calcium phosphate as a stimulus to osteogenesis. *Ann Surg*. 1920;71(1):32–9.

205. Bohner M, Santoni BLG, Döbelin N. β-tricalcium phosphate for bone substitution: Synthesis and properties. *Acta Biomater*. 2020;113:23–41.

206. Fernández E, Gil FJ, Ginebra MP, Driessens FC, Planell JA, Best SM. Calcium phosphate bone cements for clinical applications. Part I: solution chemistry. *J Mater Sci Mater Med.* 1999 (3):169–76.

207. Jensen SS, Broggini N, Hjørting-Hansen E, Schenk R, Buser D. Bone healing and graft resorption of autograft, anorganic bovine bone and β-tricalcium phosphate. A histologic and histomorphometric study in the mandibles of minipigs. *Clin Oral Implants Res*. 2006;17(3):237–43.

208. von Doernberg M-C, von Rechenberg B, Bohner M, Grünenfelder S, van Lenthe GH, Müller R, et al. In vivo behavior of calcium phosphate scaffolds with four different pore sizes. *Biomaterials.* 2006 ;27(30):5186–98.

209. Le Huec JC, Clément D, Brouillaud B, Barthe N, Dupuy B, Foliguet B, et al. Evolution of the local calcium content around irradiated β-tricalcium phosphate ceramic implants: in vivo study in the rabbit. *Biomaterials.* 1998;19(7):733–8.

210. Roy M, Bose S. Osteoclastogenesis and osteoclastic resorption of tricalcium phosphate: Effect of strontium and magnesium doping. *J Biomed Mater Res A.* 2012;100A(9):2450–61.

211. Neo M, Kotani S, Fujita Y, Nakamura T, Yamamuro T, Bando Y, et al. Differences in ceramic-bone interface between surface-active ceramics and resorbable ceramics: a study by scanning and transmission electron microscopy. *J Biomed Mater Res*. 1992;26(2):255–67.

212. Kitsugi T, Yamamuro T, Nakamura T, Kotani S, Kokubo T, Takeuchi H. Four calcium phosphate ceramics as bone substitutes for non-weight-bearing. *Biomaterials.* 1993;14(3):216–24.

213. Rojbani H, Nyan M, Ohya K, Kasugai S. Evaluation of the osteoconductivity of α-tricalcium phosphate, β-tricalcium phosphate, and hydroxyapatite combined with or without simvastatin in rat calvarial defect. *J Biomed Mater Res A.* 2011;98A(4):488–98.

214. Yuan H, Fernandes H, Habibovic P, de Boer J, Barradas AMC, de Ruiter A, et al. Osteoinductive ceramics as a synthetic alternative to autologous bone grafting. *Proc Natl Acad Sci USA*. 2010;107(31):13614–9.

215. Kattimani VS, Kondaka S, Lingamaneni KP. Hydroxyapatite–-Past, Present, and Future in Bone Regeneration. *Bone Tissue Regen Insights.* 2016;7:BTRI.S36138.

216. Kozlova D, Chernousova S, Knuschke T, Buer J, Westendorf AM, Epple M. Cell targeting by antibody-functionalized calcium phosphate nanoparticles. *J Mater Chem*. 2011;22(2):396–404.

217. Lin K, Liu P, Wei L, Zou Z, Zhang W, Qian Y, et al. Strontium substituted hydroxyapatite porous microspheres: Surfactant-free hydrothermal synthesis, enhanced biological response and sustained drug release. *Chem Eng J*. 2013;222:49–59.

218. Mohd Pu'ad NAS, Koshy P, Abdullah HZ, Idris MI, Lee TC. Syntheses of hydroxyapatite from natural sources. *Heliyon*. 2019;5(5):e01588.

219. Hu J, Russell JJ, Ben-Nissan B, Vago R. Production and analysis of hydroxyapatite from Australian corals via hydrothermal process. *J Mater Sci Lett.* 2001;20(1):85–7.

220. Fathi MH, Hanifi A, Mortazavi V. Preparation and bioactivity evaluation of bone-like hydroxyapatite nanopowder. *J Mater Process Technol.* 2008;202(1–3):536–42.

221. Gotz W, Papageorgiou S. Molecular, Cellular and Pharmaceutical Aspects of Synthetic Hydroxyapatite Bone Substitutes for Oral and Maxillofacial Grafting. *Curr Pharm Biotechnol.* 2017;18(1):95–106.

222. Sadat-Shojai M, Khorasani M-T, Dinpanah-Khoshdargi E, Jamshidi A. Synthesis methods for nanosized hydroxyapatite with diverse structures. *Acta Biomater*. 2013;9(8):7591–621.

223. Li SH, De Wijn JR, Layrolle P, de Groot K. Synthesis of macroporous hydroxyapatite scaffolds for bone tissue engineering. *J Biomed Mater Res.* 2002;61(1):109–20.

224. Koutsopoulos S. Synthesis and characterization of hydroxyapatite crystals: A review study on the analytical methods. *J Biomed Mater Res.* 2002;62(4):600–12.

225. Lin K, Chang J. 1 - Structure and properties of hydroxyapatite for biomedical applications. In: Mucalo M, editor. Hydroxyapatite (Hap) for Biomedical Applications [Internet]. Woodhead Publishing; 2015 [cited 2021 Jan 14]. p. 3–19. (Woodhead Publishing Series in Biomaterials). Available from: http://www.sciencedirect.com/science/article/pii/B9781782420330000018

226. Hong Y, Fan H, Li B, Guo B, Liu M, Zhang X. Fabrication, biological effects, and medical applications of calcium phosphate nanoceramics. *Mater Sci Eng R Rep.* 2010;70(3):225–42.

227. Lin K, Xia L, Gan J, Zhang Z, Chen H, Jiang X, Jiang C. Tailoring the Nanostructured Surfaces of Hydroxyapatite Bioceramics to Promote Protein Adsorption, Osteoblast Growth, and Osteogenic Differentiation. *ACS Appl Mater Interfaces.* 2013;5(16):8008–17.

228. Rh Owen G, Dard M, Larjava H. Hydoxyapatite/beta-tricalcium phosphate biphasic ceramics as regenerative material for the repair of complex bone defects. *J Biomed Mater Res B Appl Biomater.* 2018;106(6):2493–512.

229. Wagoner Johnson AJ, Herschler BA. A review of the mechanical behavior of CaP and CaP/polymer composites for applications in bone replacement and repair. *Acta Biomater*. 2011;7(1):16–30.

230. Tadic D, Peters F, Epple M. Continuous synthesis of amorphous carbonated apatites. *Biomaterials.* 2002;23(12):2553–9.

231. Mavropoulos E, Rossi AM, da Rocha NCC, Soares GA, Moreira JC, Moure GT. Dissolution of calcium-deficient hydroxyapatite synthesized at different conditions. *Mater Charact.* 2003;50(2):203–7.

232. Dorozhkin SV. Amorphous calcium (ortho)phosphates. *Acta Biomater.* 2010;6(12):4457–75.

233. Lin K, Zhang M, Zhai W, Qu H, Chang J. Fabrication and Characterization of Hydroxyapatite/Wollastonite Composite Bioceramics with Controllable Properties for Hard Tissue Repair. *J Am Ceram Soc.* 2011;94(1):99–105.

234. Zhang Q, Wang W, Schmelzer E, Gerlach J, Liu C, Nettleship I. The degradation behavior of calcium-rich hydroxyapatite foams in vitro. J Biomed Mater Res A [Internet]. 2020 [cited 2021 Jan 15];n/a(n/a). Available from: http://onlinelibrary.wiley.com/DOI/abs/10.1002/jbm.a.37077

235. Neel EAA, Pickup DM, Valappil SP, Newport RJ, Knowles JC. Bioactive functional materials: a perspective on phosphate-based glasses. *J Mater Chem.* 2009;19(6):690–701.

236. Pecquet Goad ME, Goad DL. Biomedical Materials and Devices-ClinicalKey. In: Haschek and Rousseaux's Handbook of Toxicologic Pathology. *Third. Elsevier;* 2013:783–806.

237. Hench LL. The story of Bioglass. *J Mater Sci Mater Med.* 2006;17(11):967–78.

238. Ilharreborde B, Morel E, Fitoussi F, Presedo A, Souchet P, Penneçot G-F, et al. Bioactive glass as a bone substitute for spinal fusion in adolescent idiopathic scoliosis: a comparative study with iliac crest autograft. *J Pediatr Orthop.* 2008;28(3):347–51.

239. Heikkilä JT, Kukkonen J, Aho AJ, Moisander S, Kyyrönen T, Mattila K. Bioactive glass granules: a suitable bone substitute material in the operative treatment of depressed lateral tibial plateau fractures: a prospective, randomized 1 year follow-up study. *J Mater Sci Mater Med.* 2011;22(4):1073–80.

240. Rantakokko J, Frantzén JP, Heinänen J, Kajander S, Kotilainen E, Gullichsen E, et al. Posterolateral spondylodesis using bioactive glass S53P4 and autogenous bone in instrumented unstable lumbar spine burst fractures. A prospective 10-year follow-up study. *Scand J Surg SJS Off Organ Finn Surg Soc Scand Surg Soc.* 2012;101(1):66–71.

241. Wilson J, Pigott GH, Schoen FJ, Hench LL. Toxicology and biocompatibility of bioglasses. *J Biomed Mater Res.* 1981;15(6):805–17.

242. Munukka E, Leppäranta O, Korkeamäki M, Vaahtio M, Peltola T, Zhang D, et al. Bactericidal effects of bioactive glasses on clinically important aerobic bacteria. *J Mater Sci Mater Med.* 2008;19(1):27–32.

243. Beckham CA, Greenlee TK, Crebo AR. Bone formation at a ceramic implant interface. *Calcif Tissue Res.* 1971;8(2):165–71.

244. Piotrowski G, Hench LL, Allen WC, Miller GJ. Mechanical studies of the bone bioglass interfacial bond. *J Biomed Mater Res.* 1975;9(4):47–61.

245. LeGeros RZ. Calcium phosphate-based osteoinductive materials. *Chem Rev.* 2008;108(11):4742–53.

246. Merwin GE, Atkins JS, Wilson J, Hench LL. Comparison of ossicular replacement materials in a mouse ear model. *Otolaryngol--Head Neck Surg Off J Am Acad Otolaryngol-Head Neck Surg.* 1982;90(4):461–9.

247. Fiume E, Barberi J, Verné E, Baino F. Bioactive Glasses: From Parent 45S5 Composition to Scaffold-Assisted Tissue-Healing Therapies. J Funct Biomater [Internet]. 2018 Mar 16 [cited 2021 Feb 14];9(1). Available from: https://www.ncbi.nlm.nih.gov/pmc/articles/PMC5872110/

248. Xynos ID, Edgar AJ, Buttery LD, Hench LL, Polak JM. Ionic products of bioactive glass dissolution increase proliferation of human osteoblasts and induce insulin-like growth factor II mRNA expression and protein synthesis. *Biochem Biophys Res Commun*. 2000;276(2):461–5.

249. Bosetti M, Cannas M. The effect of bioactive glasses on bone marrow stromal cells differentiation. *Biomaterials.* 2005;26(18):3873–9.

250. Reffitt DM, Ogston N, Jugdaohsingh R, Cheung HFJ, Evans B a. J, Thompson RPH, et al. Orthosilicic acid stimulates collagen type 1 synthesis and osteoblastic differentiation in human osteoblast-like cells in vitro. *Bone.* 2003;32(2):127–35.

251. Schepers EJ, Ducheyne P. Bioactive glass particles of narrow size range for the treatment of oral bone defects: a 1-24 month experiment with several materials and particle sizes and size ranges. *J Oral Rehabil.* 1997;24(3):171–81.

252. Day RM. Bioactive glass stimulates the secretion of angiogenic growth factors and angiogenesis in vitro. *Tissue Eng.* 2005;11(5–6):768–77.

253. Baino F, Hamzehlou S, Kargozar S. Bioactive Glasses: Where Are We and Where Are We Going? J Funct Biomater [Internet]. 2018 Mar 19 [cited 2021 Feb 3];9(1). Available from: https://www.ncbi.nlm.nih.gov/pmc/articles/PMC5872111/

254. Bellucci D, Sola A, Gazzarri M, Chiellini F, Cannillo V. A new hydroxyapatite-based biocomposite for bone replacement. *Mater Sci Eng C Mater Biol Appl.* 2013;33(3):1091–101.

255. Moimas L, Biasotto M, Lenarda RD, Olivo A, Schmid C. Rabbit pilot study on the resorbability of three-dimensional bioactive glass fibre scaffolds. *Acta Biomater.* 2006;2(2):191–9.

256. Hench LL, Jones JR. Bioactive Glasses: Frontiers and Challenges. Front Bioeng Biotechnol [Internet]. 2015;3. Available from: https://www.ncbi.nlm.nih.gov/pmc/articles/PMC4663244/

257. Henkel J, Woodruff MA, Epari DR, Steck R, Glatt V, Dickinson IC, et al. Bone Regeneration Based on Tissue Engineering Conceptions - A 21st Century Perspective. *Bone Res.* 2013;1(3):216–48.

258. Paul W, Sharma CP. Development of porous spherical hydroxyapatite granules: application towards protein delivery. *J Mater Sci Mater Med.* 1999;10(7):383–8.

259. Zhang H, Mao X, Du Z, Jiang W, Han X, Zhao D, et al. Three dimensional printed macroporous polylactic acid/hydroxyapatite composite scaffolds for promoting bone formation in a critical-size rat calvarial defect model. *Sci Technol Adv Mater.* 2016;17(1):136–48.

260. Sukegawa S, Kanno T, Kawai H, Shibata A, Takahashi Y, Nagatsuka H, et al. Long-term bioresorption of bone fixation devices made from composites of unsintered hydroxyapatite particles and poly-L-lactide. *J Hard Tissue Biol.* 2015;24(2):219–24.

261. Frohbergh ME, Katsman A, Botta GP, Lazarovici P, Schauer CL, Wegst UGK, et al. Electrospun hydroxyapatite-containing chitosan nanofibers crosslinked with genipin for bone tissue engineering. *Biomaterials.* 2012;33(36):9167–78.

262. Pati F, Song T-H, Rijal G, Jang J, Kim SW, Cho D-W. Ornamenting 3D printed scaffolds with cell-laid extracellular matrix for bone tissue regeneration. *Biomaterials.* 2015;37:230–41.

263. Liao SS, Cui FZ, Zhang W, Feng QL. Hierarchically biomimetic bone scaffold materials: nano-HA/collagen/PLA composite. *J Biomed Mater Res B Appl Biomater.* 2004;69(2):158–65.

264. Russias J, Saiz E, Nalla RK, Gryn K, Ritchie RO, Tomsia AP. Fabrication and mechanical properties of PLA/HA composites: A study of in vitro degradation. *Mater Sci Eng C.* 2006;26(8):1289–95.

265. Xu X, Chen X, Liu A, Hong Z, Jing X. Electrospun poly(l-lactide)-grafted hydroxyapatite/poly(l-lactide) nanocomposite fibers. *Eur Polym J.* 2007;43(8):3187–96.

266. Wan Y, Wu C, Xiong G, Zuo G, Jin J, Ren K, et al. Mechanical properties and cytotoxicity of nanoplate-like hydroxyapatite/polylactide nanocomposites prepared by intercalation technique. *J Mech Behav Biomed Mater.* 2015;47:29–37.

267. Akindoyo JO, Beg MDH, Ghazali S, Heim HP, Feldmann M. Effects of surface modification on dispersion, mechanical, thermal and dynamic mechanical properties of injection molded PLA-hydroxyapatite composites. *Compos Part Appl Sci Manuf.* 2017;103:96–105.

268. Wu D, Spanou A, Diez-Escudero A, Persson C. 3D-printed PLA/HA composite structures as synthetic trabecular bone: A feasibility study using fused deposition modeling. *J Mech Behav Biomed Mater*. 2020;103:103608.

269. Tayton E, Purcell M, Aarvold A, Smith JO, Briscoe A, Kanczler JM, et al. A comparison of polymer and polymer-hydroxyapatite composite tissue engineered scaffolds for use in bone regeneration. An in vitro and in vivo study. *J Biomed Mater Res A.* 2014;102(8):2613–24.

270. Kim H-W, Lee H-H, Knowles JC. Electrospinning biomedical nanocomposite fibers of hydroxyapatite/poly(lactic acid) for bone regeneration. *J Biomed Mater Res A.* 2006;79A(3):643–9.

271. Rizwan M, Hamdi M, Basirun WJ. Bioglass® 45S5-based composites for bone tissue engineering and functional applications. *J Biomed Mater Res A.* 2017;105(11):3197–223.

272. Maquet V, Boccaccini AR, Pravata L, Notingher I, Jérôme R. Preparation, characterization, and in vitro degradation of bioresorbable and bioactive composites based on Bioglass-filled polylactide foams. *J Biomed Mater Res A.* 2003;66(2):335–46.

273. Zhang K, Wang Y, Hillmyer MA, Francis LF. Processing and properties of porous poly(L-lactide)/bioactive glass composites. *Biomaterials.* 2004;25(13):2489–500.

274. Helen W, Merry CLR, Blaker JJ, Gough JE. Three-dimensional culture of annulus fibrosus cells within PDLLA/Bioglass® composite foam scaffolds: Assessment of cell attachment, proliferation and extracellular matrix production. *Biomaterials.* 2007;28(11):2010–20.

275. Liu A, Hong Z, Zhuang X, Chen X, Cui Y, Liu Y, et al. Surface modification of bioactive glass nanoparticles and the mechanical and biological properties of poly(l-lactide) composites. *Acta Biomater*. 2008;4(4):1005–15.

276. Eldesoqi K, Henrich D, El-Kady AM, Arbid MS, Abd El-Hady BM, Marzi I, et al. Safety Evaluation of a Bioglass–Polylactic Acid Composite Scaffold Seeded with Progenitor Cells in a Rat Skull Critical-Size Bone Defect. *PLoS One.* 2014;9(2):e87642.
DOI: 10.1371/journal.pone.0087642. eCollection 2014.

277. Barbeck M, Serra T, Booms P, Stojanovic S, Najman S, Engel E, et al. Analysis of the in vitro degradation and the in vivo tissue response to bi-layered 3D-printed scaffolds combining PLA and biphasic PLA/bioglass components – Guidance of the inflammatory response as basis for osteochondral regeneration. *Bioact Mater*. 2017;2(4):208–23.

278. Xiao W, Zaeem MA, Li G, Bal BS, Rahaman MN. Tough and strong porous bioactive glass-PLA composites for structural bone repair. *J Mater Sci.* 2017;52(15):9039-9054. DOI: 10.1007/s10853-017-0777-3.

279. Qiu QQ, Ducheyne P, Ayyaswamy PS. New bioactive, degradable composite microspheres as tissue engineering substrates. *J Biomed Mater Res.* 2000;52(1):66–76.

280. Roether JA, Boccaccini AR, Hench LL, Maquet V, Gautier S, Jérĵme R. Development and in vitro characterisation of novel bioresorbable and bioactive composite materials based on polylactide foams and Bioglass for tissue engineering applications. *Biomaterials*. 2002;23(18):3871–8.

281. Yang XB, Webb D, Blaker J, Boccaccini AR, Maquet V, Cooper C, et al. Evaluation of human bone marrow stromal cell growth on biodegradable polymer/bioglass composites. *Biochem Biophys Res Commun.* 2006;342(4):1098–107.

282. Tsigkou O, Hench LL, Boccaccini AR, Polak JM, Stevens MM. Enhanced differentiation and mineralization of human fetal osteoblasts on PDLLA containing Bioglass® composite films in the absence of osteogenic supplements. *J Biomed Mater Res A.* 2007;80A(4):837–51.

283. Lu W, Ji K, Kirkham J, Yan Y, Boccaccini AR, Kellett M, et al. Bone tissue engineering by using a combination of polymer/Bioglass composites with human adipose-derived stem cells. *Cell Tissue Res.* 2014;356(1):97–107.

284. Gerhardt L-C, Widdows KL, Erol MM, Burch CW, Sanz-Herrera JA, Ochoa I, et al. The pro-angiogenic properties of multi-functional bioactive glass composite scaffolds. *Biomaterials.* 2011;32(17):4096–108.

285. Miron RJ, Zhang YF. Osteoinduction: a review of old concepts with new standards. *J Dent Res.* 2012;91(8):736–44.

286. Urist MR, Silverman BF, Büring K, Dubuc FL, Rosenberg JM. The bone induction principle. *Clin Orthop.* 1967 Aug;53:243–83.

287. Firschein HE, Urist MR. The induction of alkaline phosphatase by extraskeletal implants of bone matrix. *Calcif Tissue Res.* 1971;7(2):108–13.

288. García-Gareta E, Coathup MJ, Blunn GW. Osteoinduction of bone grafting materials for bone repair and regeneration. *Bone.* 2015;81:112–21.

289. Hammarstrom L, Blomlof L, Lindskog S. Composition inducing a binding [Internet]. US5071958A, 1991 [cited 2021 Mar 20]. Available from: https://patents.google.com/patent/US5071958A/en

290. Lyngstadaas SP, Wohlfahrt JC, Brookes SJ, Paine ML, Snead ML, Reseland JE. Enamel matrix proteins; old molecules for new applications. *Orthod Craniofac Res.* 2009;12(3):243–53.

291. Chan RC, Marino V, Bartold PM. The effect of Emdogain® and platelet-derived growth factor on the osteoinductive potential of hydroxyapatite tricalcium phosphate. *Clin Oral Investig.* 2012;16(4):1217-27. DOI: 10.1007/s00784-011-0629-5.

292. Birang R, Shah Abouei M, Mohammad Razavi S, Zia P, Soolari A. The Effect of an Enamel Matrix Derivative (Emdogain) Combined with Bone Ceramic on Bone Formation in Mandibular Defects: A Histomorphometric and Immunohistochemical Study in the Canine. *Sci World J.* 2012;2012:e196791.

293. Miron RJ, Sculean A, Cochran DL, Froum S, Zucchelli G, Nemcovsky C, et al. Twenty years of enamel matrix derivative: the past, the present and the future. *J Clin Periodontol.* 2016;43(8):668–83.

294. Laaksonen M, Sorsa T, Salo T. Emdogain in carcinogenesis: a systematic review of in vitro studies. *J Oral Sci.* 2010;52(1):1–11.

295. Tatakis DN, Chambrone L, Allen EP, Langer B, McGuire MK, Richardson CR, et al. Periodontal soft tissue root coverage procedures: a

consensus report from the AAP Regeneration Workshop. *J Periodontol.* 2015;86(2):52-5.

296. Maymon-Gil T, Weinberg E, Nemcovsky C, Weinreb M. Enamel Matrix Derivative Promotes Healing of a Surgical Wound in the Rat Oral Mucosa. *J Periodontol.* 2016;87(5):601–9.

297. Mohamed RN, Basha S, Al-Thomali Y, Tawfik Enan E. Enamel matrix derivative (Emdogain) in treatment of replanted teeth - a systematic review. *Acta Odontol Scand.* 2019;77(3):168–72.

298. Wang HH, Sarmast ND, Shadmehr E, Angelov N, Shabahang S, Torabinejad M. Application of Enamel Matrix Derivative (Emdogain) in Endodontic Therapy: A Comprehensive Literature Review. *J Endod.* 2018;44(7):1066–79.

299. Cochran DL, King GN, Schoolfield J, Velasquez-Plata D, Mellonig JT, Jones A. The effect of enamel matrix proteins on periodontal regeneration as determined by histological analyses. *J Periodontol.* 2003;74(7):1043–55.

300. Esposito M, Grusovin MG, Papanikolaou N, Coulthard P, Worthington HV. Enamel matrix derivative (Emdogain) for periodontal tissue regeneration in intrabony defects. A Cochrane systematic review. *Eur J Oral Implantol.* 2009;2(4):247–66.

301. Intini G, Andreana S, Buhite RJ, Bobek LA. A Comparative Analysis of Bone Formation Induced by Human Demineralized Freeze-Dried Bone and Enamel Matrix Derivative in Rat Calvaria Critical-Size Bone Defects. *J Periodontol.* 2008;79(7):1217–24.

302. Esposito M, Grusovin MG, Papanikolaou N, Coulthard P, Worthington HV. The Effect of Enamel Matrix Derivative (Emdogain®) on Bone Formation: A Systematic Review. *Eur J Oral Implantol.* Winter 2009;2(4):247-66.

303. Kim SY, You CK, Jeong JH, Park EK, Kim SY, Shin HI. Influence of Emdogain® Treatment onto K2O Incorporated Calcium Metaphosphate on Osteogenic Activation. *Key Eng Mater.* 2005;284–286:631–4.

304. Triplett RG, Nevins M, Marx RE, Spagnoli DB, Oates TW, Moy PK, et al. Pivotal, randomized, parallel evaluation of recombinant human bone morphogenetic protein-2/absorbable collagen sponge and autogenous

bone graft for maxillary sinus floor augmentation. *J Oral Maxillofac Surg Off J Am Assoc Oral Maxillofac Surg.* 2009;67(9):1947–60.

305. Bessa PC, Casal M, Reis RL. Bone morphogenetic proteins in tissue engineering: the road from the laboratory to the clinic, part I (basic concepts). *J Tissue Eng Regen Med.* 2008;2(1):1–13.

306. Bragdon B, Moseychuk O, Saldanha S, King D, Julian J, Nohe A. Bone morphogenetic proteins: a critical review. *Cell Signal.* 2011;23(4):609–20.

307. Dimitriou R, Tsiridis E, Giannoudis PV. Current concepts of molecular aspects of bone healing. *Injury.* 2005;36(12):1392–404.

308. James AW, LaChaud G, Shen J, Asatrian G, Nguyen V, Zhang X, et al. A Review of the Clinical Side Effects of Bone Morphogenetic Protein-2. *Tissue Eng Part B Rev.* 2016;22(4):284–97.

309. Lykissas M, Gkiatas I. Use of recombinant human bone morphogenetic protein-2 in spine surgery. *World J Orthop.* 2017 18;8(7):531–5.

310. Zara JN, Siu RK, Zhang X, Shen J, Ngo R, Lee M, et al. High doses of bone morphogenetic protein 2 induce structurally abnormal bone and inflammation in vivo. *Tissue Eng Part A.* 2011;17(9–10):1389–99.

311. Katagiri T, Watabe T. Bone Morphogenetic Proteins. *Cold Spring Harb Perspect Biol.* 2016 1;8(6).

312. Garrison KR, Donell S, Ryder J, Shemilt I, Mugford M, Harvey I, et al. Clinical effectiveness and cost-effectiveness of bone morphogenetic proteins in the non-healing of fractures and spinal fusion: a systematic review. *Health Technol Assess Winch Engl.* 2007;11(30):1–150, iii–iv.

313. Kim IG, Hwang MP, Du P, Ko J, Ha C, Do SH, Park K. Bioactive cell-derived matrices combined with polymer mesh scaffold for osteogenesis and bone healing. *Biomaterials.* 2015;50:75–86.

314. Ferretti C, Mattioli-Belmonte M. Periosteum derived stem cells for regenerative medicine proposals: Boosting current knowledge. *World J Stem Cells.* 2014; 26;6:266–77.

315. Eğri S, Eczacıoğlu N. Sequential VEGF and BMP-2 releasing PLA-PEG-PLA scaffolds for bone tissue engineering: I. Design and in vitro tests. *Artif Cells Nanomedicine Biotechnol.* 2017;45(2):321–9.

316. Hori M, Sawai H, Tsuji Y, Okamura H, Koyama K. Bone morphogenetic protein-2 counterregulates interleukin-18 mRNA and protein in MC3T3-E1 mouse osteoblastic cells. *Connect Tissue Res.* 2006;47(3):124–32.

317. Tasca A, Stemig M, Broege A, Huang B, Davydova J, Zwijsen A, et al. Smad1/5 and Smad4 expression are important for osteoclast differentiation. *J Cell Biochem.* 2015;116(7):1350–60.

318. Calcei JG, Rodeo SA. Orthobiologics for Bone Healing. *Clin Sports Med.* 2019;38(1):79–95.

319. Feigin K, Shope B. Use of Platelet-Rich Plasma and Platelet-Rich Fibrin in Dentistry and Oral Surgery: Introduction and Review of the Literature. *J Vet Dent.* 2019;36(2):109–23.

320. Leo MS, Kumar AS, Kirit R, Konathan R, Sivamani RK. Systematic review of the use of platelet-rich plasma in aesthetic dermatology. *J Cosmet Dermatol.* 2015;14(4):315–23.

321. Mathew J, Sankar P, Varacallo M. Physiology, Blood Plasma. In: StatPearls [Internet]. Treasure Island (FL): StatPearls Publishing; 2021 [cited 2021 Apr 21]. Available from: http://www.ncbi.nlm.nih.gov/books/NBK531504/

322. Dohan Ehrenfest DM, Andia I, Zumstein MA, Zhang C-Q, Pinto NR, Bielecki T. Classification of platelet concentrates (Platelet-Rich Plasma-PRP, Platelet-Rich Fibrin-PRF) for topical and infiltrative use in orthopedic and sports medicine: current consensus, clinical implications and perspectives. *Muscles Ligaments Tendons J.* 2014;4(1):3–9.

323. Ghanaati S, Booms P, Orlowska A, Kubesch A, Lorenz J, Rutkowski J, et al. Advanced platelet-rich fibrin: a new concept for cell-based tissue engineering by means of inflammatory cells. *J Oral Implantol.* 2014;40(6):679–89.

324. Choi B-H, Im C-J, Huh J-Y, Suh J-J, Lee S-H. Effect of platelet-rich plasma on bone regeneration in autogenous bone graft. *Int J Oral Maxillofac Surg.* 2004;33(1):56–9.

325. Miron RJ, Zucchelli G, Pikos MA, Salama M, Lee S, Guillemette V, et al. Use of platelet-rich fibrin in regenerative dentistry: a systematic review. *Clin Oral Investig.* 2017;21(6):1913–27.

326. Giovanini AF, Grossi JRA, Gonzaga CC, Zielak JC, Göhringer I, Vieira J de S, et al. Leukocyte-platelet-rich plasma (L-PRP) induces an abnormal histophenotype in craniofacial bone repair associated with changes in the immunopositivity of the hematopoietic clusters of differentiation, osteoproteins, and TGF-β1. *Clin Implant Dent Relat Res.* 2014;16(2):259–72.

327. Portela GS, Cerci DX, Pedrotti G, Araujo MR, Deliberador TM, Zielak JC, et al. L-PRP diminishes bone matrix formation around autogenous bone grafts associated with changes in osteocalcin and PPAR-γ immunoexpression. *Int J Oral Maxillofac Surg.* 2014;43(2):261–8.

328. Chahla J, Cinque ME, Piuzzi NS, Mannava S, Geeslin AG, Murray IR, et al. A Call for Standardization in Platelet-Rich Plasma Preparation Protocols and Composition Reporting: A Systematic Review of the Clinical Orthopaedic Literature. *J Bone Joint Surg Am.* 2017 18;99(20):1769–79.

329. Dohan Ehrenfest DM, de Peppo GM, Doglioli P, Sammartino G. Slow release of growth factors and thrombospondin-1 in Choukroun's platelet-rich fibrin (PRF): a gold standard to achieve for all surgical platelet concentrates technologies. *Growth Factors Chur Switz.* 2009;27(1):63–9.

330. Witek L, Tian H, Tovar N, Torroni A, Neiva R, Gil LF, et al. The effect of platelet-rich fibrin exudate addition to porous poly(lactic-co-glycolic acid) scaffold in bone healing: An in vivo study. *J Biomed Mater Res B Appl Biomater.* 2020;108(4):1304–10.

331. Blau HM, Brazelton TR, Weimann JM. The evolving concept of a stem cell: entity or function? *Cell.* 2001; 29;105(7):829–41.

332. Zhang Z. Bone regeneration by stem cell and tissue engineering in oral and maxillofacial region. *Front Med.* 2011;5(4):401–13.

333. Sonomoto K, Yamaoka K, Kaneko H, Yamagata K, Sakata K, Zhang X, Kondo M, Zenke Y, Sabanai K, Nakayamada S, Sakai A, Tanaka Y. Spontaneous Differentiation of Human Mesenchymal Stem Cells on Poly-Lactic-Co-Glycolic Acid Nano-Fiber Scaffold. *PLoS ONE*. 2016;11(4):e0153231.

334. Alksne M, Simoliunas E, Kalvaityte M, Skliutas E, Rinkunaite I, Gendviliene I, et al. The effect of larger than cell diameter polylactic acid surface patterns on osteogenic differentiation of rat dental pulp stem cells. *J Biomed Mater Res A*. 2019;107(1):174–86.

335. Mauney JR, Volloch V, Kaplan DL. Role of adult mesenchymal stem cells in bone tissue engineering applications: current status and future prospects. *Tissue Eng.* 2005;11(5–6):787–802.

336. Tatullo M, Falisi G, Amantea M, Rastelli C, Paduano F, Marrelli M. Dental pulp stem cells and human periapical cyst mesenchymal stem cells in bone tissue regeneration: comparison of basal and osteogenic differentiated gene expression of a newly discovered mesenchymal stem cell lineage. *J Biol Regul Homeost Agents.* 2015;29(3):713–8.

337. Chen F-M, Gao L-N, Tian B-M, Zhang X-Y, Zhang Y-J, Dong G-Y, et al. Treatment of periodontal intrabony defects using autologous periodontal ligament stem cells: a randomized clinical trial. *Stem Cell Res Ther*. 2016;7:33.

338. Granz CL, Gorji A. Dental stem cells: The role of biomaterials and scaffolds in developing novel therapeutic strategies. *World J Stem Cells.* 2020;12(9):897–921.

339. Caplan AI. The Mesengenic Process. *Clin Plast Surg.* 1994;21(3):429–35.

340. Caplan AI. Mesenchymal Stem Cells: Time to Change the Name! *Stem Cells Transl Med.* 2017;6(6):1445–51.

341. Bruder SP, Jaiswal N, Haynesworth SE. Growth kinetics, self-renewal, and the osteogenic potential of purified human mesenchymal stem cells during extensive subcultivation and following cryopreservation. *J Cell Biochem.* 1997;64(2):278–94.

342. Banfi A, Muraglia A, Dozin B, Mastrogiacomo M, Cancedda R, Quarto R. Proliferation kinetics and differentiation potential of ex vivo expanded human bone marrow stromal cells: Implications for their use in cell therapy. *Exp Hematol.* 2000;28(6):707–15.

343. Devine SM. Mesenchymal stem cells: Will they have a role in the clinic? *J Cell Biochem.* 2002;85(38):73–9.

344. Hosseinpour S, Ghazizadeh Ahsaie M, Rezai Rad M, Baghani M taghi, Motamedian SR, Khojasteh A. Application of selected scaffolds for bone tissue engineering: a systematic review. *Oral Maxillofac Surg.* 2017;21(2):109–29.

345. Moreno Sancho F, Leira Y, Orlandi M, Buti J, Giannobile WV, D'Aiuto F. Cell‐Based Therapies for Alveolar Bone and Periodontal Regeneration: Concise Review. *Stem Cells Transl Med.* 2019;8(12):1286–95.

346. Kaigler D, Pagni G, Park CH, Braun TM, Holman LA, Yi E, et al. Stem Cell Therapy for Craniofacial Bone Regeneration: A Randomized, Controlled Feasibility Trial. *Cell Transplant.* 2013;22(5):767–77.

347. da Costa CES, Pelegrine AA, Fagundes DJ, Simoes M de J, Taha MO. Use of corticocancellous allogeneic bone blocks impregnated with bone marrow aspirate: a clinical, tomographic, and histomorphometric study. *Gen Dent.* 2011;59(5):e200-205.

348. Pelegrine AA, Teixeira ML, Sperandio M, Almada TS, Kahnberg KE, Pasquali PJ, et al. Can bone marrow aspirate concentrate change the mineralization pattern of the anterior maxilla treated with xenografts? A preliminary study. *Contemp Clin Dent.* 2016;7(1):21–6.

349. Lavareda Corrêa SC, Elias de Sousa J, Pasquali PJ, Scavone de Macedo LG, Aloise AC, Teixeira ML, et al. Use of Bone Allograft With or Without Bone Marrow Aspirate Concentrate in Appositional Reconstructions: A Tomographic and Histomorphometric Study. *Implant Dent.* 2017;26(6):915–21.

350. Sauerbier S, Rickert D, Gutwald R, Nagursky H, Oshima T, Xavier SP, et al. Bone marrow concentrate and bovine bone mineral for sinus floor augmentation: a controlled, randomized, single-blinded clinical and histological trial--per-protocol analysis. *Tissue Eng Part A.* 2011;17(17–18):2187–97.

351. Weir JC, Osinga R, Reid A, Roditi G, MacLean AD, Lo SJ. Free vascularised medial femoral condyle periosteal flaps in recalcitrant long bone non-union: a systematic review. *Arch Orthop Trauma Surg.* 2020;140(11):1619–31.

352. Wang T, Zhang X, Bikle DD. Osteogenic Differentiation of Periosteal Cells During Fracture Healing. *J Cell Physiol.* 2017;232(5):913–21.

353. Jacobsen FS. Periosteum: its relation to pediatric fractures. *J Pediatr Orthop Part B.* 1997;6(2):84–90.

354. Colnot C, Zhang X, Knothe Tate ML. Current insights on the regenerative potential of the periosteum: molecular, cellular, and endogenous engineering approaches. *J Orthop Res Off Publ Orthop Res Soc.* 2012;30(12):1869–78.

355. De Bari C, Dell'Accio F, Luyten FP. Human periosteum-derived cells maintain phenotypic stability and chondrogenic potential throughout expansion regardless of donor age. *Arthritis Rheum.* 2001;44(1):85–95.

356. Ceccarelli G, Graziano A, Benedetti L, Imbriani M, Romano F, Ferrarotti F, et al. Osteogenic Potential of Human Oral-Periosteal Cells (PCs) Isolated From Different Oral Origin: An In Vitro Study. *J Cell Physiol.* 2016;231(3):607–12.

357. Isogai N, Landis WJ, Mori R, Gotoh Y, Gerstenfeld LC, Upton J, et al. Experimental use of fibrin glue to induce site-directed osteogenesis from cultured periosteal cells. *Plast Reconstr Surg.* 2000;105(3):953–63.

358. Zhu S-J, Choi B-H, Huh J-Y, Jung J-H, Kim B-Y, Lee S-H. A comparative qualitative histological analysis of tissue-engineered bone using bone marrow mesenchymal stem cells, alveolar bone cells, and periosteal cells. *Oral Surg Oral Med Oral Pathol Oral Radiol Endod*. 2006 ;101(2):164–9.

359. Ribeiro FV, Suaid FF, Ruiz KGS, Salmon CR, Paparotto T, Nociti FH, et al. Periosteum-derived cells as an alternative to bone marrow cells for bone tissue engineering around dental implants. A histomorphometric study in beagle dogs. *J Periodontol.* 2010;81(6):907–16.

360. Nagata M, Hoshina H, Li M, Arasawa M, Uematsu K, Ogawa S, et al. A clinical study of alveolar bone tissue engineering with cultured autogenous periosteal cells: coordinated activation of bone formation and resorption. *Bone*. 2012;50(5):1123–9.

361. Ogawa S, Hoshina H, Nakata K, Yamada K, Uematsu K, Kawase T, et al. High-Resolution Three-Dimensional Computed Tomography Analysis of the Clinical Efficacy of Cultured Autogenous Periosteal Cells in Sinus Lift Bone Grafting. *Clin Implant Dent Relat Res.* 2016;18(4):707–16.

362. De Francesco F, Ricci G, D'Andrea F, Nicoletti GF, Ferraro GA. Human Adipose Stem Cells: From Bench to Bedside. *Tissue Eng Part B Rev.* 2015;21(6):572–84.

363. Maqsood M, Kang M, Wu X, Chen J, Teng L, Qiu L. Adult mesenchymal stem cells and their exosomes: Sources, characteristics, and application in regenerative medicine. *Life Sci.* 2020;256:118002.

364. Strioga M, Viswanathan S, Darinskas A, Slaby O, Michalek J. Same or not the same? Comparison of adipose tissue-derived versus bone marrow-derived mesenchymal stem and stromal cells. *Stem Cells Dev.* 2012;21(14):2724–52.

365. Zhu X, Shi W, Tai W, Liu F. The comparition of biological characteristics and multilineage differentiation of bone marrow and adipose derived Mesenchymal stem cells. *Cell Tissue Res.* 2012;350(2):277–87.

366. Gimble J, Guilak F. Adipose-derived adult stem cells: isolation, characterization, and differentiation potential. *Cytotherapy.* 2003;5(5):362–9.

367. Melief SM, Zwaginga JJ, Fibbe WE, Roelofs H. Adipose tissue-derived multipotent stromal cells have a higher immunomodulatory capacity than their bone marrow-derived counterparts. *Stem Cells Transl Med.* 2013;2(6):455–63.

368. Lee JA, Parrett BM, Conejero JA, Laser J, Chen J, Kogon AJ, et al. *Ann Plast Surg.* 2003;50(6):610–7.

369. Cowan CM, Shi Y-Y, Aalami OO, Chou Y-F, Mari C, Thomas R, et al. Adipose-derived adult stromal cells heal critical-size mouse calvarial defects. *Nat Biotechnol.* 2004;22(5):560–7.

370. Hayashi O, Katsube Y, Hirose M, Ohgushi H, Ito H. Comparison of osteogenic ability of rat mesenchymal stem cells from bone marrow, periosteum, and adipose tissue. *Calcif Tissue Int.* 2008;82(3):238–47.

371. Stockmann P, Park J, von Wilmowsky C, Nkenke E, Felszeghy E, Dehner J-F, et al. Guided bone regeneration in pig calvarial bone defects using autologous mesenchymal stem/progenitor cells - a comparison of different tissue sources. *J Cranio-Maxillo-fac Surg Off Publ Eur Assoc Cranio-Maxillo-fac Surg.* 2012;40(4):310–20.

372. Prins H-J, Schulten EAJM, Ten Bruggenkate CM, Klein-Nulend J, Helder MN. Bone Regeneration Using the Freshly Isolated Autologous Stromal Vascular Fraction of Adipose Tissue in Combination With Calcium Phosphate Ceramics. *Stem Cells Transl Med.* 2016;5(10):1362–74.

373. Gronthos S, Mankani M, Brahim J, Robey PG, Shi S. Postnatal human dental pulp stem cells (DPSCs) in vitro and in vivo. *Proc Natl Acad Sci U S A.* 2000;97(25):13625–30.

374. Luzuriaga J, Polo Y, Pastor-Alonso O, Pardo-Rodríguez B, Larrañaga A, Unda F, Sarasua JR, Pineda JR, Ibarretxe G. Advances and Perspectives in Dental Pulp Stem Cell Based Neuroregeneration Therapies. *Int J Mol Sci.* 2021 Mar 29;22(7):3546. DOI: 10.3390/ijms22073546.

375. Graziano A, d'Aquino R, Laino G, Papaccio G. Dental pulp stem cells: a promising tool for bone regeneration. *Stem Cell Rev.* 2008;4(1):21–6.

376. Casagrande L, Cordeiro MM, Nör SA, Nör JE. Dental pulp stem cells in regenerative dentistry. *Odontology.* 2011;99(1):1–7.

377. Tomic S, Djokic J, Vasilijic S, Vucevic D, Todorovic V, Supic G, Colic M. Immunomodulatory properties of mesenchymal stem cells derived from dental pulp and dental follicle are susceptible to activation by toll-like receptor agonists. *Stem Cells Dev.* 2011;20(4):695–708. DOI: 10.1089/scd.2010.0145.

378. Paino F, La Noce M, Giuliani A, De Rosa A, Mazzoni S, Laino L, Amler E, Papaccio G, Desiderio V, Tirino V. Human DPSCs fabricate vascularized woven bone tissue: a new tool in bone tissue engineering. *Clin Sci Lond Engl 1979.* 2017;131(8):699–713. DOI: 10.1042/CS20170047.

379. Leyendecker Junior A, Gomes Pinheiro CC, Lazzaretti Fernandes T, Franco Bueno D. The use of human dental pulp stem cells for in vivo bone tissue engineering: A systematic review. *J Tissue Eng.* 2018;9:2041731417752766. DOI: 10.1177/2041731417752766.

380. Miura M, Gronthos S, Zhao M, Lu B, Fisher LW, Robey PG, Shi S. SHED: Stem cells from human exfoliated deciduous teeth. *Proc Natl Acad Sci U S A.* 2003;100(10):5807–12.

381. de Mendonça Costa A, Bueno DF, Martins MT, Kerkis I, Kerkis A, Fanganiello RD, Cerruti H, Alonso N, Passos-Bueno MR. Reconstruction

of large cranial defects in nonimmunosuppressed experimental design with human dental pulp stem cells. *J Craniofac Surg.* 2008;19(1):204–10.

382. Lorusso F, Inchingolo F, Dipalma G, Postiglione F, Fulle S, Scarano A. Synthetic Scaffold/Dental Pulp Stem Cell (DPSC) Tissue Engineering Constructs for Bone Defect Treatment: An Animal Studies Literature Review. *Int J Mol Sci.* 2020;21(24).

383. Wongsupa N, Nuntanaranont T, Kamolmattayakul S, Thuaksuban N. Assessment of bone regeneration of a tissue-engineered bone complex using human dental pulp stem cells/poly(ε-caprolactone)-biphasic calcium phosphate scaffold constructs in rabbit calvarial defects. *J Mater Sci Mater Med.* 2017;28(5):77.

384. Giuliani A, Manescu A, Langer M, Rustichelli F, Desiderio V, Paino F, et al. Three years after transplants in human mandibles, histological and in-line holotomography revealed that stem cells regenerated a compact rather than a spongy bone: biological and clinical implications. *Stem Cells Transl Med.* 2013;2(4):316–24.

385. Kular JK, Basu S, Sharma RI. The extracellular matrix: Structure, composition, age-related differences, tools for analysis and applications for tissue engineering. *J Tissue Eng.* 2014;5:2041731414557112.

386. Frantz C, Stewart KM, Weaver VM. The extracellular matrix at a glance. *J Cell Sci.* 2010;123(24):4195–200.

387. Gentili C, Cancedda R. Cartilage and bone extracellular matrix. *Curr Pharm Des.* 2009;15(12):1334–48.

388. Papadimitropoulos A, Scotti C, Bourgine P, Scherberich A, Martin I. Engineered decellularized matrices to instruct bone regeneration processes. *Bone.* 2015;70:66–72.

389. Kutys ML, Doyle AD, Yamada KM. Regulation of cell adhesion and migration by cell-derived matrices. *Exp Cell Res.* 2013;319(16):2434–9.

390. Hutter H, Vogel BE, Plenefisch JD, Norris CR, Proenca RB, Spieth J, et al. Conservation and novelty in the evolution of cell adhesion and extracellular matrix genes. *Science.* 2000;287(5455):989–94.

391. Hoshiba T, Chen G, Endo C, Maruyama H, Wakui M, Nemoto E, et al. Decellularized Extracellular Matrix as an In Vitro Model to Study the

Comprehensive Roles of the ECM in Stem Cell Differentiation. *Stem Cells Int.* 2016;2016:6397820.

392. Zimmermann G, Moghaddam A. Allograft bone matrix versus synthetic bone graft substitutes. *Injury.* 2011;42:S16–21.

393. Crapo PM, Gilbert TW, Badylak SF. An overview of tissue and whole organ decellularization processes. *Biomaterials.* 2011;32(12):3233–43.

394. Kim JY, Ahn G, Kim C, Lee JS, Lee IG, An SH, Yun WS, Kim SY, Shim JH. Synergistic Effects of Beta Tri-Calcium Phosphate and Porcine-Derived Decellularized Bone Extracellular Matrix in 3D-Printed Polycaprolactone Scaffold on Bone Regeneration. *Macromol Biosci.* 2018;18(6):e1800025.

395. Mohiuddin OA, Campbell B, Poche JN, Ma M, Rogers E, Gaupp D, Harrison MAA, Bunnell BA, Hayes DJ, Gimble JM. Decellularized Adipose Tissue Hydrogel Promotes Bone Regeneration in Critical-Sized Mouse Femoral Defect Model. *Front Bioeng Biotechnol.* 2019;7:211.

396. Kim YS, Majid M, Melchiorri AJ, Mikos AG. Applications of decellularized extracellular matrix in bone and cartilage tissue engineering. *Bioeng Transl Med.* 2018;4(1):83–95.

397. Noh YK, Du P, Kim IG, Ko J, Kim SW, Park K. Polymer mesh scaffold combined with cell-derived ECM for osteogenesis of human mesenchymal stem cells. *Biomater Res.* 2016;20:6.

398. Wu Y-HA, Chiu Y-C, Lin Y-H, Ho C-C, Shie M-Y, Chen Y-W. 3D-Printed Bioactive Calcium Silicate/Poly-ε-Caprolactone Bioscaffolds Modified with Biomimetic Extracellular Matrices for Bone Regeneration. *Int J Mol Sci.* 2019;20(4):942. DOI: 10.3390/ijms20040942.

399. Sokolova M, Putnins A, Kreicbergs I, Locs J. Scale-up of wet precipitation calcium phosphate synthesis. *Key. Eng. Mater.* 2014;604, 216-9. https://DOI.org/10.4028/www.scientific.net/KEM.604.216.

400. Alksne M, Kalvaityte M, Simoliunas E, Rinkunaite I, Gendviliene I, Locs J, et al. In vitro comparison of 3D printed polylactic acid/hydroxyapatite and polylactic acid/bioglass composite scaffolds: Insights into materials for bone regeneration. *J Mech Behav Biomed Mater.* 2020;104:103641.

401. Rueden CT, Schindelin J, Hiner MC, DeZonia BE, Walter AE, Arena ET, Eliceiri KW. ImageJ2: ImageJ for the next generation of scientific image data. *BMC Bioinformatics*. 2017; 18(1):529. DOI: 10.1186/s12859-017-1934-z.

402. Loh QL, Choong C. Three-dimensional scaffolds for tissue engineering applications: role of porosity and pore size. *Tissue Eng Part B Rev.* 2013;19(6):485–502.

403. Cignoni P, Callieri M, Corsini M, Dellepiane M, Ganovelli F, Ranzuglia G. MeshLab: an Open-Source Mesh Processing Tool [Internet]. *The Eurographics Association;* 2008 [cited 2021 Jan 8].

404. Dey N, Blanc-Feraud L, Zimmer C, Roux P, Kam Z, Olivo-Marin J-C, et al. Richardson-Lucy algorithm with total variation regularization for 3D confocal microscope deconvolution. *Microsc Res Tech.* 2006;69(4):260–6.

405. Sage D, Donati L, Soulez F, Fortun D, Schmit G, Seitz A, Guiet R, Vonesch C, Unser M. DeconvolutionLab2: An open-source software for deconvolution microscopy. *Methods San Diego Calif.* 2017;115:28–41.

406. Tsai W-H. Moment-preserving thresolding: A new approach. *Comput Vis Graph Image Process.* 1985;29(3):377–93.

407. Marsell R, Einhorn TA. The biology of fracture healing. *Injury.* 2011;42(6):551–5.

408. Ultimaker Original+ Specifications, 2019. https://ultimaker.com/en/products/ultimaker-original/specifications (accessed 4 July 2019).

409. High Resolution Desktop 3D Printer, 2018. https://massportal.com/wp-content/uploads/2018/05/MP_XD-Series.pdf (accessed 4 July 2019).

410. Soriano Heras E, Blaya Haro F, de Agustín del Burgo JM, Islán Marcos ME. Plate auto-level system for fused deposition modelling (FDM) 3D printers. *Rapid Prototyp J*. 2017;23(2):401–13.

411. Hernandez D. Factors Affecting Dimensional Precision of Consumer 3D Printing. *Int J Aviat Aeronaut Aerosp*. 2015;2(4). Available from: https://commons.erau.edu/ijaaa/vol2/iss4/2

412. Goyanes A, Kobayashi M, Martínez-Pacheco R, Gaisford S, Basit AW. Fused-filament 3D printing of drug products: Microstructure analysis and drug release characteristics of PVA-based caplets. *Int J Pharm.* 2016;514(1):290–5.

413. Tümer EH, Erbil HY. Extrusion-Based 3D Printing Applications of PLA Composites: A Review. *Coatings.* 2021;11(4):390.

414. Sui T, Salvati E, Zhang H, Nyaza K, Senatov FS, Salimon AI, Korsunsky AM. Probing the complex thermo-mechanical properties of a 3D-printed polylactide-hydroxyapatite composite using in situ synchrotron X-ray scattering. *J Adv Res.* 2019;16:113–22.

415. Shilo D, Emodi O, Blanc O, Noy D, Rachmiel A. Printing the Future-Updates in 3D Printing for Surgical Applications. *Rambam Maimonides Med J.* 2018;9(3).

416. Hulsart-Billström G, Dawson JI, Hofmann S, Müller R, Stoddart MJ, Alini M, Red H, Haj AE, Brown R, Salih V, Hilborn J, Larsson S, Oreffo RO. A surprisingly poor correlation between in vitro and in vivo testing of biomaterials for bone regeneration: results of a multicentre analysis. *Eur Cell Mater.* 2016;31:312–22.

417. Gomes PS, Fernandes MH. Rodent models in bone-related research: the relevance of calvarial defects in the assessment of bone regeneration strategies. *Lab Anim.* 2011;45(1):14–24.

418. Strube P, Mehta M, Baerenwaldt A, Trippens J, Wilson CJ, Ode A, Perka, Duda GN, Kasper G. Sex-specific compromised bone healing in female rats might be associated with a decrease in mesenchymal stem cell quantity. *Bone.* 2009;45(6):1065–72.

419. Hughes PC, Tanner JM, Williams JP. A longitudinal radiographic study of the growth of the rat skull. *J Anat.* 1978;127(Pt 1):83–91.

420. Spicer PP, Kretlow JD, Young S, Jansen JA, Kasper FK, Mikos AG. Evaluation of Bone Regeneration Using the Rat Critical Size Calvarial Defect. *Nat Protoc.* 2012;7(10):1918–29.

421. Trejo-Iriarte CG, Serrano-Bello J, Gutiérrez-Escalona R, Mercado-Marques C, García-Honduvilla N, Buján-Varela J, Medina LA. Evaluation of bone regeneration in a critical size cortical bone defect in rat mandible

using microCT and histological analysis. *Arch Oral Biol.* 2019;101:165–71.

422. McGovern JA, Griffin M, Hutmacher DW. Animal models for bone tissue engineering and modelling disease. *Dis Model Mech.* 2018;11(4):dmm033084.

423. Vajgel A, Mardas N, Farias BC, Petrie A, Cimões R, Donos N. A systematic review on the critical size defect model. *Clin Oral Implants Res.* 2014;25(8):879–93.

424. Cooper GM, Mooney MP, Gosain AK, Campbell PG, Losee JE, Huard J. Testing the critical size in calvarial bone defects: revisiting the concept of a critical-size defect. *Plast Reconstr Surg.* 2010;125(6):1685–92.

425. DeNicolo PJ, Guyton MK, Cuenin MF, Hokett SD, Sharawy M, Borke J, McPherson 3rd JC. Histologic Evaluation of Osseous Regeneration Following Combination Therapy With Platelet-Rich Plasma and Bio-Oss in a Rat Calvarial Critical-Size Defect Model. *J Oral Implantol.* 2015;41(5):543–9.

426. Yao X, Carleton SM, Kettle AD, Melander J, Phillips CL, Wang Y. Gender-dependence of bone structure and properties in adult osteogenesis imperfecta murine model. *Ann Biomed Eng*. 2013;41(6):1139–49.

427. Beery AK, Zucker I. Sex bias in neuroscience and biomedical research. *Neurosci Biobehav Rev.* 2011;35(3):565–72.

428. Stavropoulos A, Kostopoulos L, Nyengaard JR, Karring T. Deproteinized bovine bone (Bio-Oss) and bioactive glass (Biogran) arrest bone formation when used as an adjunct to guided tissue regeneration (GTR): an experimental study in the rat. *J Clin Periodontol.* 2003;30(7):636–43.

429. Reddy MSB, Ponnamma D, Choudhary R, Sadasivuni KK. A Comparative Review of Natural and Synthetic Biopolymer Composite Scaffolds. *Polymers.* 2021;13(7):1105.

430. Sponer P, Kučera T, Diaz-Garcia D, Filip S. The role of mesenchymal stem cells in bone repair and regeneration. *Eur J Orthop Surg Traumatol Orthop Traumatol.* 2014;24(3):257–62.

431. Rai NK, Tripathi K, Sharma D, Shukla VK. Apoptosis: a basic physiologic process in wound healing. *Int J Low Extrem Wounds.* 2005;4(3):138–44.

432. Kang S-H, Park J-B, Kim I, Lee W, Kim H. Assessment of stem cell viability in the initial healing period in rabbits with a cranial bone defect according to the type and form of scaffold. *J Periodontal Implant Sci.* 2019;49(4):258–67.

SANTRAUKA

SANTRUMPŲ SĄRAŠAS

Bio-Oss – Geistlich Bio-Oss®

BS – biostiklas 45S5

DFB – Dulbeco fosfatinis buferis

DPKL – dantų pulpos kamieninės ląstelės

EDTA – etilendiamintetraacto rūgštis

FB – fosfatinis buferis

FVS – fetalinis veršelio serumas

HA – hidroksiapatitas

IMDT – Iskovo modifikuota Dulbeco terpė

JSA – jaučio serumo albuminai

KLE – karšto lydymosi ekstruzija

LNM – lydyto nusėdimo modeliavimas

MikroKT – mikrokompiuterinė tomografija

P – porėtumas

PLR – polilaktinė rūgštis

SEM – skenuojantis elektroninis mikroskopas

TU – tarpląstelinis užpildas

3D – trimatis

1. ĮVADAS

1.1. TYRIMO AKTUALUMAS

Pastaraisiais metais dėl pagerėjusios gyvenimo kokybės ir pailgėjusios gyvenimo trukmės didėja kaulinio audinio priauginimo operacijų poreikis įvairiose medicinos srityse[1,2]. Vienos iš dažniausių procedūrų, kurioms reikalingi kauliniai pakaitalai ir bioaktyvios medžiagos, yra: kranioplastikos ar stuburo fiksacijos neurochirurgijoje, lūžių nesugijimai ar pėdos ir kulkšnies operacijos ortopedijoje-traumatologijoje, žandikaulių alveolinių ataugų kaulo priauginimo operacijos burnos, veido ir žandikaulių chirurgijoje [3–5].

Šiuo metu klinikinėje praktikoje kaulo priauginimas yra atliekamas naudojant įvairius kaulo pakaitalus. Siekiama, kad jie užpildytų kaulinio audinio defekto tūrį ir struktūrą, užtikrintų gerą kaulo mechaninį stabilumą ir skatintų reikiamą naujai besiformuojančio kaulo kraujagyslių tinklo formavimąsi (vaskuliarizaciją)[6]. Iki šiol tokio tipo operacijų auksiniu standartu yra autologiniai transplantai. Tačiau šie natūralūs kaulinio audinio pakaitalai turi nemažai trūkumų: pooperacinis diskomfortas, lėtinis donorinės vietos skausmas, lūžiai, infekcija, išvaržos susidarymas, jutimo sutrikimai, kraujavimas, kraujosruvos, ribotas tūris ir donorinių vietų skaičius[5,7,8]. Klinikinėje praktikoje pažeistiems kauliniams defektams užpildyti yra naudojami alogeniniai, ksenogeniniai ir aloplastiniai kaulo pakaitalai, tačiau ir jie neatitinka visų idealiam kaulo transplantui keliamų reikalavimų. Jie pasižymi tik osteokonduktyvumu, bet neužtikrina osteoinduktyvumo [9,10]. Todėl visame pasaulyje kaulų priauginimo srityje yra vykdomi aktyvūs moksliniai tyrimai, kurių metu pasitelkiant pagrindinius audinių inžinerijos principus siekiama sukurti naujus kaulinio audinio pakaitalus, tenkinančius visus idealiam kaulo transplantui keliamus reikalavimus[11,12].

Viena iš pažangiausių iki šiol sukurtų kaulo pakaitalų alternatyvų – trimatis (3D) kompozitinis karkasas. Jo dėka sukuriama mikroaplinka, kuri yra patraukli naują kaulinį audinį formuojančių ląstelių gyvenimui, dauginimuisi ir migracijai[13,14]. Tokių karkasų gamybai yra naudojamos įvarios organinės ir neorganinės medžiagos ar jų mišiniai[14,15]. Karkasų osteoindukcinėms savybėms pagerinti jie papildomi / dekoruojami įvairiomis ląstelėmis ar augimo veiksniais[1]. Tačiau ne vien karkasų gamybai naudojamos medžiagos ir pasirinktos jų paviršiaus dekoravimo technikos yra svarbios norint pagaminti kaulinio audinio regeneracijai tinkamą produktą. Tyrimų parodyta, kad karkasų mechaninės savybės, nulemtos jų morfologijos (porėtumo, porų dydžio, susisiekiamumo), taip pat moduliuoja jų osteoregeneracinį pajėgumą[16]. Manoma, kad lydyto nusėdimo modeliavimo

(LNM) 3D spausdinimo technologija yra viena iš perspektyviausių, norint sąlygiškai lengvai, greitai ir pigiai pagaminti karkasus, kurių morfologija ir mechaninės savybės tenkins kaulo transplantui keliamus reikalavimus[17]. Tačiau iki šiol idealaus, turinčio sertifikuotas klinikines indikacijas ir kaulo regeneracijai tinkamo karkaso vis dar nėra sukurta [5,18]. Manome, kad ir toliau turi būti aktyviai vystomi moksliniai tyrimai, vertinantys karkasų gamybai tinkamas naujas biomedžiagas, inovatyvius gamybos metodus ir skirtingas karkasų paviršių dekoravimo technologijas.

1.2. TYRIMO TIKSLAS

Sukurti inovatyvų tvarkų karkasą kaulo regeneravimui ir įvertinti jo savybes *in vitro* ir *in vivo* sąlygomis.

1.3. TYRIMO UŽDAVINIAI

1. Įvertinti karkasų, atspausdintų skirtingais 3D spausdintuvais iš gamyklinių PLR filamentų, morfologiją, spausdinimo tikslumą ir porėtumą.
2. Pagaminti tinkamo skersmens filamentus iš PLR mikrogranulių, kompozitinius filamentus iš PLR ir hidroksiapatito (HA) bei PLR ir biostiklo 45S5 (BS) karšto lydymosi ekstruzijos būdu.
3. Įvertinti sukurtų PLR, PLR/HA ir PLR/BS karkasų morfologiją, spausdinimo tikslumą, porėtumą ir palyginti rezultatus su karkasais, pagamintais iš gamyklinių PLR filamentų.
4. Pirmuoju *in vivo* etapu nustatyti inovatyvių osteokondukcinių karkasų indukuojamą kaulinio audinio regeneraciją Wistar žiurkių kaukolių kritinio dydžio defektuose.
5. Antruoju *in vivo* etapu įvertinti inovatyvių konstruktų, pagamintų iš osteokondukcinių karkasų, papildytų dantų pulpos kamieninėmis ląstelėmis (DPKL) ar jų išskirtu tarpląsteliniu užpildu (TU), indukuojamą kaulinio audinio regeneraciją Wistar žiurkių kaukolių kritinio dydžio defektuose. Palyginti gautus osteoindukcinės grupės rezultatus su pirmojo *in vivo* etapo mėginiais.

1.4. TYRIMO AKTUALUMAS

Dauguma kaulo priauginimo operacijų klinikinėje praktikoje yra atliekamos naudojant autogeninius, alogeninius ar ksenogeninius kaulinius pakaitalus, nes vis dar nėra sukurto tvarkaus 3D spausdinto karkaso, kuris galėtų atitikti daugumą idealiam kauliniam pakaitalui keliamų reikalavimų.

Šio tyrimo metu sukurti inovatyvūs tvarkūs 3D karkasai buvo atspausdinti naudojant LNM technologiją, derinamą su karšto lydymosi ekstruzijos (KLE) metodu. Pateikta įžvalgų ir rekomendacijų, kuriose atkreipiama dėmesio, kokie parametrai turi įtakos spausdinimo tikslumui, kaip būtų galima jį patobulinti ir gauti norimus karkasų morfologijos parametrus.

Tyrime pirmą kartą palyginti skirtingų 3D spausdintų osteokondukcinių karkasų ir tų pačių medžiagų biodekoruotų konstruktų indukuojamos kaulinio audinio regeneracijos mikrokompiuterinės tomografijos (mikroKT) ir kaulinio audinio histologinio ištyrimo rezultatai kritinio dydžio Wistar žiurkių kaukolių defektuose su viena iš labiausiai žinomų ir klinikinėje praktikoje naudojamų ksenogeninių medžiagų – Geistlich Bio-Oss® (Bio-Oss). Šios žinios yra svarbios siekiant įvertinti, ar tiriamųjų karkasų rezultatai yra konkurencingi dabar klinikinėje praktikoje naudojamoms medžiagoms. Rasta, kad PLR/HA TU, PLR/BS, PLR/BS DPKL, PLR/BS TU turi teigiamą įtaką naujo kaulo formavimuisi kritinio dydžio defektuose ir gaunami rezultatai yra panašūs į Bio-Oss grupės rezultatus.

Naujausiuose tyrimuose ypač palankiai yra vertinama osteokondukcinių karkasų dekoravimo technologija ląstelėmis ar jų TU, tačiau mes nustatėme, kad praėjus 8 savaitėms po operacijos nebuvo statistiškai reikšmingo skirtumo tarp tos pačios medžiagos osteokondukcinio karkaso ir biodekoruotų konstruktų mikroKT ir kaulinio audinio histologinio ištyrimo rezultatų. Tačiau buvo matomas intensyvesnis naujo kaulo formavimasis kritinio dydžio defektuose biodekoruotų konstruktų grupėse. Šios žinios yra svarbios ateities tyrimams, nes mokslininkai turi įvertinti, ar šios dekoravimo technologijos pakankamai reikšmingai pagerina kaulo regeneracijos rezultatus ir yra verta toliau tobulinti inovatyvius karkasus šia kryptimi, atsižvelgiant į padidėjusias procedūros išlaidas, laiką, technologijas. Reikia tolesnių tyrimų, kad būtų galima vertinti 3D spausdintų karkasų įtaką kaulo regeneravimui praėjus ilgesniam laikotarpiui po operacijos ir su stambesniais gyvūnais.

Šio tyrimo metu gautos *in vitro* ir *in vivo* žinios yra svarbios audinių inžinerijos pažangai ir dirbtiniam kauliniam audiniui „OSSEUM 4D“ kurti ir tobulinti.

1.5. GINAMIEJI TEIGINIAI

1. 3D karkasų morfologija ir tikslumas priklauso nuo 3D LNM technologijos ir parinktų spausdinimo parametrų.

2. Karšto lydymosi ekstruzijos būdu pagamintais kompozitiniais filamentais galima atspausdinti 3D karkasus, morfologija ir tikslumu prilygstančius gamyklinių PRL karkasų rezultatams.

3. Biokompozitiniai 3D karkasai teigiamai veikia naujo kaulo formavimąsi žiurkių kritinio dydžio defektuose.

4. 3D konstruktai, biodekoruoti DPKL ar jų TU, padidina naujo susiformavusio kaulo tūrį žiurkių kritinio dydžio defektuose.

5. Sukurti 3D karkasai yra tinkami kaulinio audinio regeneracijai ir toliau kuriant dirbtinį kaulą.

2. MEDŽIAGOS IR METODAI

2.1. MEDŽIAGOS

Medžiagos naudotos 3D karkasams kurti ir spausdinti: PLR1 filamentas (PLR filamentas; DR3D Filament Ltd, skersmuo 2,85 mm), PLR2 filamentas (PLR filamentas; DR3D Filament Ltd, skersmuo 1,75 mm). Kompozitinių filamentų gamybai karšto lydymosi ekstruzijos būdu buvo naudotos 100–800 μm dydžio, 42,700 g/mol molekulinės masės PLR granulės (STP Chem Solutions Co., Ltd.), 50 μm dydžio hidroksiapatito (HA; Riga Technical University [399]) milteliai bei 38– 75 μm biostiklo 45S5 (BS; XL Sci-Tech, Inc.) dalelės. Geistlich Bio-Oss® (Geistlisch Pharmaceutical, Wolhusen, Šveicarija) 0,25–1 mm granulės buvo naudotos kaip teigiama kontrolė *in vivo* tyrime.

Medžiagos ląstelių tyrimams: Iskovo modifikuota Dulbeco terpė (IMDM; Gibco); fetalinis veršelio serumas (FVS; Gibco); antibiotikų penicilino ir streptomicino (atitinkamai 100,000 vnt./ml ir 100,000 μg/ml) mišinys (Gibco); fosfatinis buferis (FB; Gibco); etilendiamintetraacto rūgštis (EDTA; Sigma-Aldrich Co.); tripsinas (Gibco); deksametazonas (Sigma-Aldrich Co.); β-glicerofosfatas (Sigma-Aldrich Co.); L-Askorbo rūgšties 2- fosfatas (Sigma-Aldrich Co.); 96 proc. etanolis (Vilniaus degtinė); 10 proc. vandeninis amonio hidroksido tirpalas (Sigma-Aldrich Co.); I tipo kolagenazė (Sigma-Aldrich Co.); hialuronidazė (Sigma-Aldrich Co.); jaučio serumo albuminai (JSA; AppliChem GmbH); Dulbeco fosfatinio buferio tirpalas (DFB; Gibco); magnetinės dalelės, padengtos ožkos IgG antriniais antikūnais, atpažįstančiais pelės antikūno Fc domeną (New England Biolabs, Inc.); pirminiai pelės antikūnai, atpažįstantys CD45, CD54, CD14, CD90 (Merck Millipore), CD44 (Cell Signaling Technology), CD13 (Santa Cruz Biotechnology, Inc.), CD31 (Abcam, Inc.); ožkos IgG antriniai antikūnai, atpažįstantys pelės antikūno Fc domeną, konjuguoti su RPE (Invitrogen); pelės IgG2a izotipinė kontrolė (Abcam, Inc.). Visos medžiagos tyrime naudotos kaip gautos.

2.2. FILAMENTO PARUOŠIMAS

Kompozitiniams filamentams gaminti masės santykiu 9:1 tarpusavyje buvo maišomos PLR ir HA arba PLR ir BS granulės. Grynos PLR filamentui gaminti naudoti tik PLR milteliai. Drėgmei panaikinti medžiagų mišiniai buvo laikomi uždaruose maišeliuose su silicio gelio granulėmis. Filamentas buvo ruošiamas karšto lydymosi ekstruzijos būdu naudojant stalinį ekstruderį su 1,75 mm antgaliu (Filabot Original, Filabot HQ). Prieš naudojimą ekstruderis buvo įkaitinamas iki 140–145 °C. Medžiagų mišinys įpiltas į talpą, filamento ekstruzijos metu buvo palaikoma 137–145 °C temperatūra. Gautas filamentas buvo susuktas į ritę naudojant savadarbį reguliuojamo greičio suktuką. Proceso metu ekstruderio temperatūra buvo rankiniu būdu sureguliuota iki 140 °C PLR filamentui, 140–145 °C PLR/HA gijoms ir 137 – 142 °C PLR/BS gijoms kurti. Gauto PLR filamento skersmuo svyravo nuo 1,67 iki 1,75 mm, kompozitinių PLR/HA gijų – nuo 1,28 iki 1,45 mm, o PLR/BS gijų skersmuo – nuo 1,6 iki 1,75 mm.

2.3. TERMOGRAVIMETRINĖ PLR/HA FILAMENTŲ ANALIZĖ

Papildomas tyrimas skirtas HA koncentracijai sukurtame kompozitiniame filamente įvertinti. Aliuminio oksido tigliai buvo kaitinami iki pastovaus svorio 4x5 val. 1000 °C temperatūroje, kaitinimo greitis – 5 °C/min. 10 PLR/HA filamento mėginių buvo dedama į tiglius ir 5 val. kaitinama 800 °C temperatūroje, kaitinimo greitis – 1 °C/min.

2.4. KARKASŲ GAMYBA

Darbe tirtų karkasų struktūros buvo sukurtos naudojant AutoCAD 2017 programinį paketą, modeliai išsaugoti STL formatu. Karkasų porų dydis buvo 450 μm, porėtumas 58 proc. Kiekvieną karkasą sudarė 8 gijų sluoksniai, kiekvienos gijos plotis 0,4 mm, aukštis 0,2 mm (1 A ir B pav.).

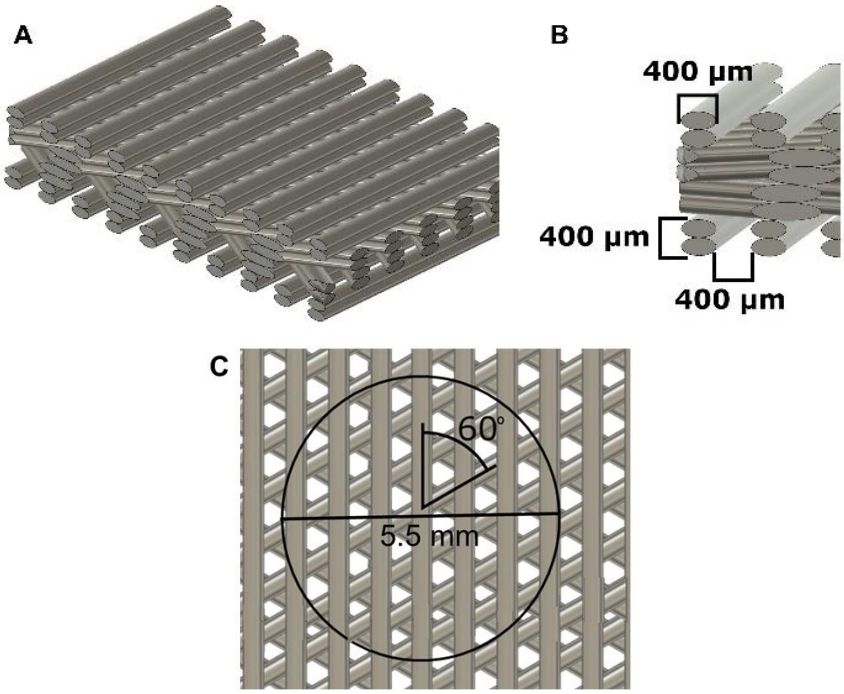

1 pav. Karkaso modelis: A – karkaso vaizdas iš šono; B – gijų skersmenys; C – karkaso vaizdas iš viršaus: kiekvieno sluoksnio gijos susikirsdamos sudarydavo 60° kampą, 5,5 mm apvali *in vivo* mėginių išpjovimo sritis

Karkasų mikroarchitektūra buvo sudaryta rotuojant kiekvieną karkaso sluoksnį, kad jie susikirsdami suformuotų 60° kampą. Tokiu būdu gaunamos šešiakampio formos poros (1 C pav). Atspausdintų karkasų dydis buvo 3 cm x 3 cm x 0,16 cm, jie naudoti *in vitro* tyrimuose. Naudojant lazerio šviesos filamentų fabrikacijos technologiją, išpjauti 5,5 mm skersmens apvalūs karkasai (1 C pav.), kurie naudoti *in vivo* tyrimams. Darbe naudotos iš skirtingų medžiagų pagamintos penkios tokių karkasų grupės: PLR, PLR1, PLR2, PLR/HA ir PLR/BS.

PLR1 karkasai buvo gaminami naudojant LNM 3D spausdintuvą „Ultimaker Original“ (Ultimaker, JAV). Spausdinimo parametrai: ekstruderio skersmuo 0,4 mm; 200 – 210 °C temperatūra; 50 mm/s greitis; šildomo pagrindo temperatūra 50 °C. STL formato modeliai 3D spausdintuvo programinėje įrangoje Ultimaker Cura 3.6 (Ultimaker, JAV) konvertuoti į g kodą.

PLR, PLR2, PLR/HA ir PLR/BS karkasai buvo gaminami naudojant LNM 3D spausdintuvą „Pharaoh XD 20“ (Mass Portal, Latvija). Spausdinimo parametrai: ekstruderio skersmuo 0,4 mm, 200–210 °C temperatūra ir 35 mm/s greitis. STL formato modeliai į g kodą konvertuoti atviros prieigos programa Slic3r 1.2.8.

2.5. SKENUOJANČIO ELEKTRONINIO MIKROSKOPO ANALIZĖ

Spausdinimo tikslumo ir karkasų morfologijos analizė (naudojant penkis nepriklausomus mėginius iš kiekvienos tiriamosios karkasų grupės: PLR, PLR1, PLR2, PLR/HA ir PLG/BS) buvo atlikta naudojant skenuojantį elektroninį mikroskopą (SEM) (Hitachi TM-1000). Karkasų (3 cm×3 cm×0,16 cm) šoniniai pjūviai (2 pav.) atlikti naudojant lazerio šviesos pluošto technologiją, pjauta 10 mm atstumu nuo karkaso krašto.

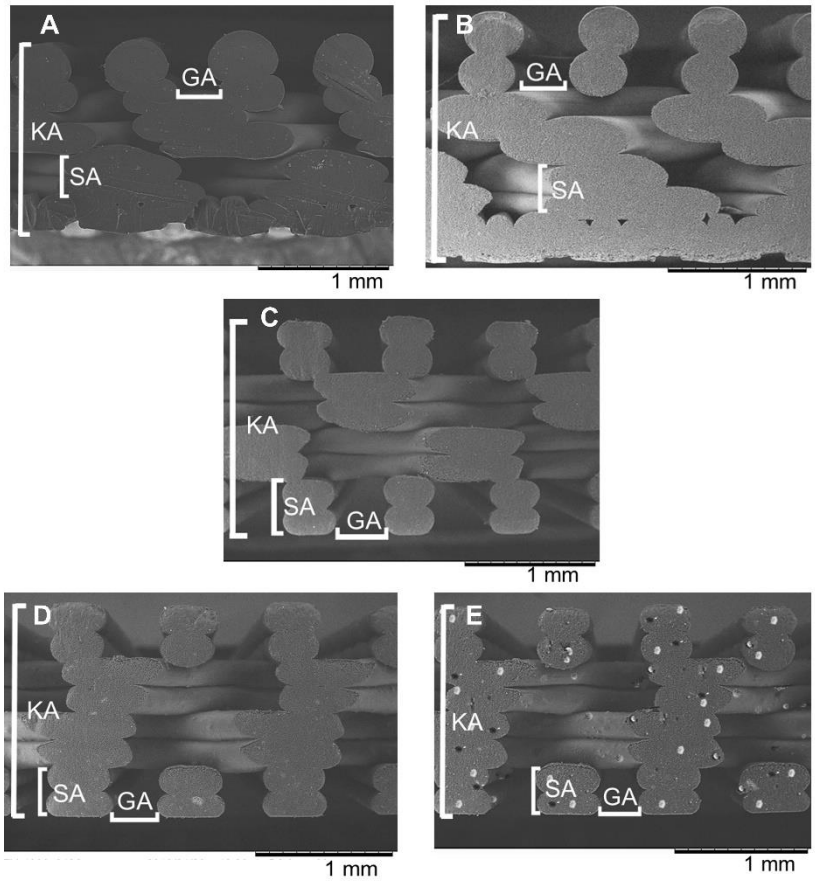

2 pav. Karkasų šoninių pjūvių vaizdai: A – PLR; B – PLR1; C – PLR2; D – PLR/HA; E – PLR/BS

Karkasų nuotraukos gautos skenuojant mėginio šoną (iš viso buvo gautos 25 kiekvienos karkasų grupės nuotraukos, kiekvieną karkasą fotografuojant po 5 kartus). Naudojant programą ImageJ (ImageJ 1.8.0_11 [402]) gautose nuotraukose buvo išmatuotas karkasų aukštis (KA), sluoksnio aukštis (SA) ir atstumas tarp gijų (GA)

2.6. PORĖTUMO VERTINIMAS GRAVIMETRINIU METODU

PLR1, PLR2 ir PLR/HA karkasų porėtumas (P) buvo vertinamas gravimetriniu metodu, skaičiavimams naudojant karkasų tūrį ir tankį. Mėginio tankis (ρ karkaso) apskaičiuotas Archimedo metodu. Karkasų tūris gautas išmatavus jų ilgį, plotį ir aukštį. Porėtumo vertinimas buvo atliktas naudojant šias formules:

$$\text{Porėtumas}_{\text{karkaso}} = \frac{masė}{tūris}$$

$$\text{Porėtumas} = 1 - \frac{\rho_{karkaso}}{\rho_{medžiagos}}$$

2.7. SUSISIEKIANČIO PORĖTUMO VERTINIMAS SKYSČIO IŠSTŪMIMO METODU

Susisiekiantis PLR1, PLR2 ir PLR/HA karkasų porėtumas buvo vertinamas skysčių išstūmimo metodu naudojant etanolį. Karkasai buvo panardinami į žinomą etanolio kiekį, paskui iš jo ištraukiami. Vertintas etanolio tūrio pokytis. Porėtumui apskaičiuoti naudota formulė:

$$\text{Susisiekiantis porėtumas} = \frac{v_1 - v_3}{v_2 - v_3}$$

V_1 – žinomas etanolio tūris, į kurį buvo panardinamas mėginys; V_2 – etanolio ir į jį įmerkto mėginio tūris; V_3 –mėginį ištraukus likusio etanolio tūris.

2.8. MIKROKOMPIUTERINĖS TOMOGRAFIJOS IR SUPERIMPOZICIJOS *IN VITRO* ANALIZĖ

PLR1, PLR2 ir PLR/HA karkasų grupių mikroKT tyrimai atlikti mikrokompiuteriniu tomografu „Skyscan 1178“ (Bruker microCT, Belgija). Matavimai atlikti naudojant 65 kV įtampos ir 615 µA srovės rentgeno spindulių šaltinį. Naudotas lėtas skenavimo režimas – 80 µm pikseliai, 82 mm FOV. Gauto atvaizdo dimensijos: 1024x1024 XY ašyje su 400–500 Z ašies

pjūvių. Kiekvieno karkaso dydis pikseliais buvo 360x360x20. Dėl žemos skenavimo raiškos (vokselio dydis – 0,08495x0,08495x0,08495 mm) lyginant su karkasų struktūrų matmenimis (~ 5 pikselius vienam sluoksniui) gauti mikroKT vaizdai buvo papildomai skaitmeniškai apdoroti. Naudojant Fiji programą, paremtą ImageJ[401], MeshLab[402] ir Geomagic Control X (3D Systems, Kanada) programomis buvo atliekama gautų atvaizdų dekonvuliacija ir segmentacija (3 pav.). Atlikus šiuos žingsnius mikroKT analizės metu gauti vaizdai buvo konvertuoti į STL formatą, dėl to juos buvo galima palyginti su originaliais, 3D spausdinti sukurtais modeliais.

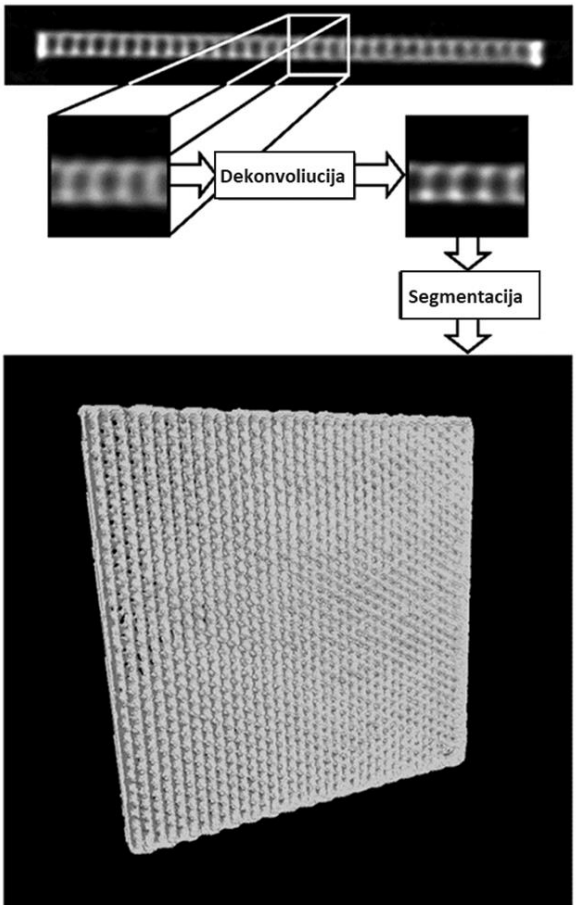

3 pav. MikroKT atvaizdo dekonvuliacija ir segmentacija

Vėliau naudojant 3D Geomagic Control X (3D Systems, Kanada) programą buvo vertinami skirtumai tarp originalių, 3D spausdinti sukurtų karkasų STL modelių bei mikroKT analizės metu gautų 3D karkasų STL

vaizdų. Šių modelių superimpozicija buvo atlikta rankiniu N taškų metodu, siekiant geriausios vaizdų atitikties.

2.9. KAMIENINIŲ LĄSTELIŲ IŠSKYRIMAS

Eksperimentiniam darbui, kuriame naudoti bandomieji gyvūnai, buvo gautas Lietuvos Respublikos valstybinės maisto ir veterinarijos tarnybos Etikos komisijos leidimas Nr. G2-40, 2016-03-18.

DPKL buvo išskirtos iš 3 mėn. amžiaus Wistar klono bandomųjų žiurkių priekinių kandžių pulpų (n = 4 pulpos mėginiai kiekvieno skyrimo metu). Detali ląstelių išskyrimo procedūra aprašyta Alksne ir kt. straipsnyje[334]. Pulpos mėginiai buvo keletą kartų išplauti IMDM terpe, praturtinta 100 µg/mL primocino, paskui buvo mechaniškai sukarpyti į <1 mm^3 gabalėlius. Ant susmulkintų audinio gabalėlių buvo pilama fermentų mišinio (0,5 proc. I tipo kolagenazės, 0,3 proc. hialuronidazės, 0,25 proc. tripsino ir 0,02 proc. EDTA), inkubuota 30–45 min. 37 °C temperatūroje, purtant 300 aps./min. greičiu (Eppendorf Thermomixer comfort). Praėjus numatytam laikui, mišinys iki 10 ml buvo praskiedžiamas auginimo terpe (IMDM praturtinta 10 proc. FVS, 100 VV/ml penicilinu ir 100 µg/ml streptomicinu). Po to mėginiai centrifuguoti 10 min. 1500 rpm greičiu (CL10 Centrifuge Thermo Scientific). Supernatantas nupiltas, ląstelės dar kartą plautos 10 ml auginimo terpe ir centrifuguotos 10 min. 1500 rpm greičiu. Pašalinus supernatantą, ant nuosėdų užpilta nauja auginimo terpė, ląsteliu suspensija kartu su likusiais audinių fragmentais perkelta į auginimo flakonus.

Ląstelėms suformavus 70–80 proc. monosluoksnį, jos buvo papildomai gryninamos naudojant magnetines daleles, dengtas ožkos antikūnais, gebančiais jungtis prie pelės pirminių antikūnų, atitinkamai atpažįstančių ląstelių paviršiuje esantį CD44 žymenį. Gryninimo procedūra buvo vykdyta naudojant prietaisą KingFisher™ mL (Thermo Scientific). Visi gryninimo žingsniai atlikti pagal magnetinių dalelių gamintojo BioLab's rekomendacijas. Vėliau ląstelės augintos 37 °C temperatūroje, aplinkoje esant 5 proc. CO_2. Eksperimentams naudotos ne didesnio kaip 12 pasažo ląstelės.

2.10. BIODEKORUOTŲ KONSTRUKTŲ GAMYBA

Detali karkasų gamyba aprašyta Alksne ir kt. straipsnyje[400]. 4000 cells/cm^2 DPKL suspensija buvo sėjama ant PLR, PLR/HA ir PLR/BS karkasų. Po 24 val. nuo ląstelių išsėjimo augimo terpė buvo pakeista osteogeninę diferenciaciją indukuojančia terpe (augimo terpė papildyta 50 nM

deksametazonu, 25 μg/ml L-Askorbo rūgšties 2-fosfatu ir 10 mM β-glicerofosfatu), inkubuota 21 dieną, pusę terpės tūrio pakeičiant kas 2–3 dienas (4 pav.).

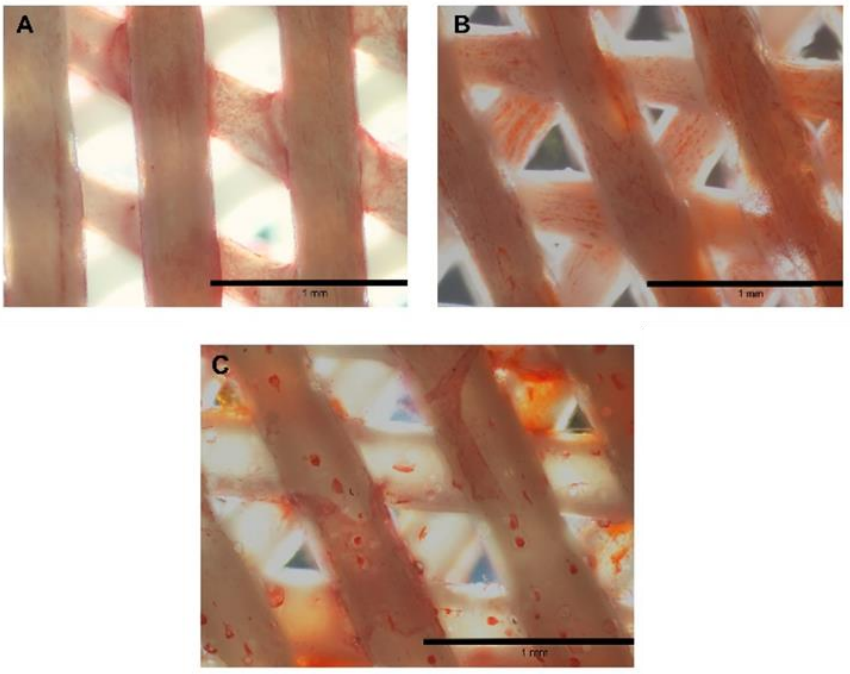

4 pav. Osteogenine kryptimi diferencijuotos DPKL ląstelės ant karkasų augintos 21 dieną. Raudona spalva rodo kalcio sankaupas, susidariusias DPKL suformuotame mineralizuotame TU (dažyta Alizarin Red S dažu): A – PLR karkasas; B – PLR/HA karkasas; C – PLR/BS karkasas

Po numatyto laiko dalis karkasų buvo tiesiogiai naudojami *in vivo* eksperimentuose (ląstelėmis padengtų karkasų grupė). Likę mėginiai buvo du kartus plauti FB ir užšaldomi –80 ° C šaldiklyje. Išėmus iš šaldiklio karkasams buvo leista atšilti, jie išplauti dejonizuotu vandeniu ir vėl užšaldyti. Tokie šaldymo-šildymo ciklai buvo kartoti 5 kartus. Paskui mėginiai 20 min. inkubuoti 25 mM amonio hidroksido tirpale bei šešis kartus plauti dejonizuotu vandeniu. Taip paruošti mėginiai buvo naudojami *in vivo* eksperimentuose kaip TU baltymais padengti karkasai.

2.11. GYVŪNAI

Tyrimui leidimą išdavė Gyvūnų tyrimų etikos komitetas, licencijos Nr. G2-40, 2016-03-18 (1 priedas). Wistar klono bandomosios žiurkės buvo veistos ir chirurginė procedūra atlikta Vilniaus universiteto Gyvybės mokslų centro Biochemijos institute Biologinių modelių skyriuje.

Tiriamoji imtis – 48 Wistar klono bandomosios žiurkės (amžius 4 mėn., vidutinis svoris 300 g). Tiriamoji imtis buvo apskaičiuota *a-priori*, naudojant Gpower programą (vieno faktoriaus ANOVA, α – 0,05, galingumas – 0,8, efekto dydis f – 0,75). Kiekvieną tiriamąją grupę sudarė 8 gyvūnai (n = 8), iš kurių buvo 4 patelės ir 4 patinėliai. Viso eksperimento metu gyvūnai buvo laikomi kontroliuojamoje aplinkoje (21 °C; 12:12 valandų šviesos cikle), maitinami standartizuotu pašaru, vandens gavo *ad libitum*.

In vivo tyrimas buvo išskirtas į dvi stadijas. Pirmojoje stadijoje buvo tiriamas 6 skirtingų medžiagų poveikis naujo kaulinio audinio formavimuisi kritinio dydžio defektuose (5 pav). Neigiama ir teigiama (Bio-Oss) kontrolės sudarė pirmą grupę, PLR ir PLR/HA karkasai – antrąją, PLR2 ir PLR/BS mėginiai – trečiąją.

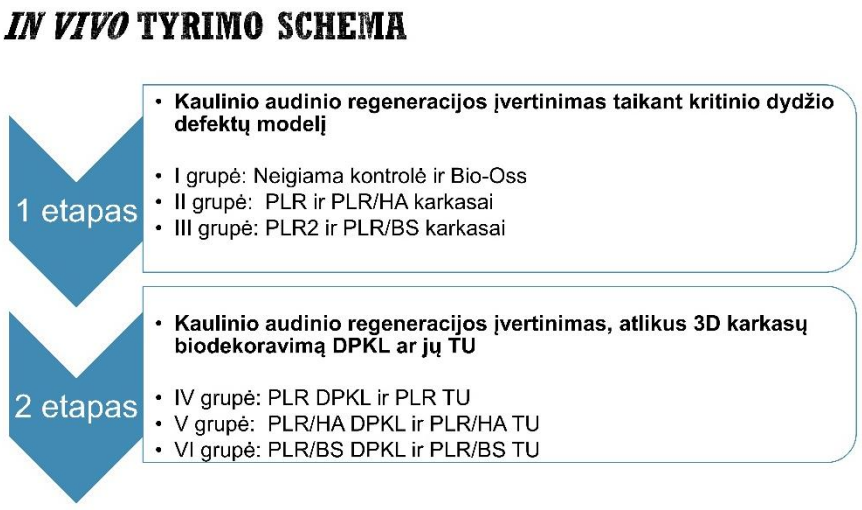

5 pav. *In vivo* tyrimo schema

Antrojo etapo metu PLR, PLR/HA ir PLR/BS karkasai buvo praturtinami DPKL arba jų suformuotu TU bei vertinamas jų poveikis naujo kaulo formavimuisi. PLR karkasai su ląstelėmis (PLR DPKL) ir PLR mėginiai su DPKL suformuotu TU (PLR TU) buvo priskirti ketvirtai grupei, PLR/HA

DPKL ir PLR/HA TU – penktai, o PLR/BS DPKL ir PLR/BS TU šeštai tyrimo grupėms.

2.12. CHIRURGINĖ OPERACIJA

Gyvūnams buvo atlikta bendroji anestezija į pilvaplėvės ertmę suleidžiant ketamino hidrochlorido 2,4 ml/kg (100 mg/ml; Rotex Medica GMBH, Tritau) ir ksilazino 5 mg/kg (2 proc.; Alfasan, Woerden). Žiurkių skalpo kailis buvo nuskustas, operacinė vieta dezinfekuota oktanidino dihidrochloridu (Octenisept, Schülke & Mayr GmbH). Atlikta vietinė aplikacinė ir infiltracinė nejautra, išilgai sagitalinės vidurinės kaukolės linijos, po oda, suleidžiant 2 proc. lidokaino tirpalo (20 mg/ml; Baxter Holding B.V., Utrecht). Toliau buvo padarytas 1,5 cm ilgio pjūvis per odą, paodį, antkaulį išilgai sagitalinės siūlės nuo nosikaulių iki lambdinės siūlės. Ties pjūvio kraštais atlikti 0,5 cm ilgio atpalaiduojantys horizontalūs pjūviai. Atkeltas odos – antkaulio lopas (6 A pav.). Suformuoti du kritinio dydžio defektai žiurkės kaukolėje naudojant 5,5 mm išorinio skersmens trepaną (Hager & Meisinger GmbH) 800 apsisukimų per minutę greičiu, aušinant steriliu fiziologiniu tirpalu (1 lašas per 1 sekundę). Tarp kiekvieno defekto buvo paliekamas bent 1,5 mm tarpas. Sukurtas kaulinis defektas išplautas steriliu fiziologiniu tirpalu, pašalinti kauliniai fragmentai, atplaišos (6 B pav.). Kaulinis pakaitalas arba tiriamieji karkasai įdėti į defektus atsitiktiniu būdu. Neigiamos kontrolės grupėje defektas buvo paliktas tuščias (6 C, E pav.). Po implantacijos antkaulis ir oda buvo susiūti pasluoksniui pavienėmis siūlėmis besirezorbuojančiu siūlu (Vicryl 5/0 Ethicon®, Johnson & Johnson, Amersfoort) (6 D pav.).

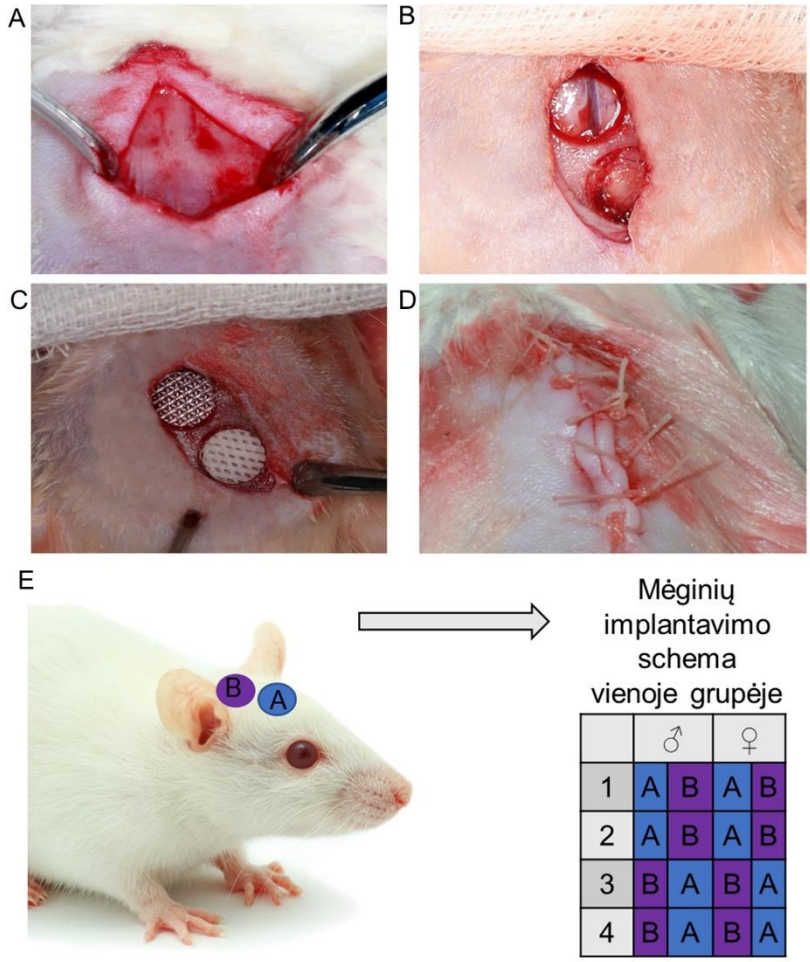

6 pav. Chirurginė operacija: A – atkeltas odos – antkaulio lopas; B – suformuoti du 5,5 mm skersmens kauliniai defektai; C – defektai užpildyti PLR ir PLR/HA karkasais; D – susiūta žaizda; E – vienos grupės mėginių išdėstymo kaukolėje schema. I grupė: A – neigiama kontrolė, B – Bio-Oss; II grupė: A – PLR, B – PLR/HA karkasai; III grupė: A – PLR2, B – PLR/BS karkasai; IV grupė: A – PLR DPKL, B – PLR TU karkasai; V grupė: A – PLR/HA DPKL, B – PLR/HA TU karkasai; VI grupė: A – PLR/BS DPKL, B – PLR/BS TU karkasai.

Pooperacinė priežiūra: žiurkės laikytos atskiruose narveliuose, kur laisvai galėjo pasiekti vandens ir maisto. Praėjus 3 val. po operacijos ir kitas tris dienas du kartus per dieną po oda buvo leidžiami Buprenorphine HCl 0,01 mg/kg (0,3 mg/mL; Richter Pharma AG, Wels) nesteroidiniai priešuždegiminiai vaistai. Gyvūnai eutanazuoti po 8 sav., išimti mėginiai iš

karto buvo perkeliami į 10 proc. (v/v) formalino tirpalą. Toliau defektai buvo vertinami mikroKT ir histologinės analizės metodais.

2.13. MIKROKT ANALIZĖ *IN VIVO*

MikroKT tyrimai buvo atlikti bendradarbiaujant su Kauno technologijos universiteto Prof. K. Baršausko ultragarso mokslo instituto mokslo darbuotojais, panaudojus 3D mikrokompiuterinį tomografą RayScan 250 E (RayScan Technologies GmbH). Tomografijai atlikti buvo pasirinktas 10–230 kV mikrofokusinis rentgeno spindulių šaltinis ir plokščias 2048x2048 pikselių detektorius. Naudoti pastovūs parametrai: 100 kV įtampa, 200 mA srovė, 666 ms integracijos laikas, vieno vokselio dydis 20 µm. Kiekvieno skenavimo metu atlikta 1800 projekcijų (7 pav).

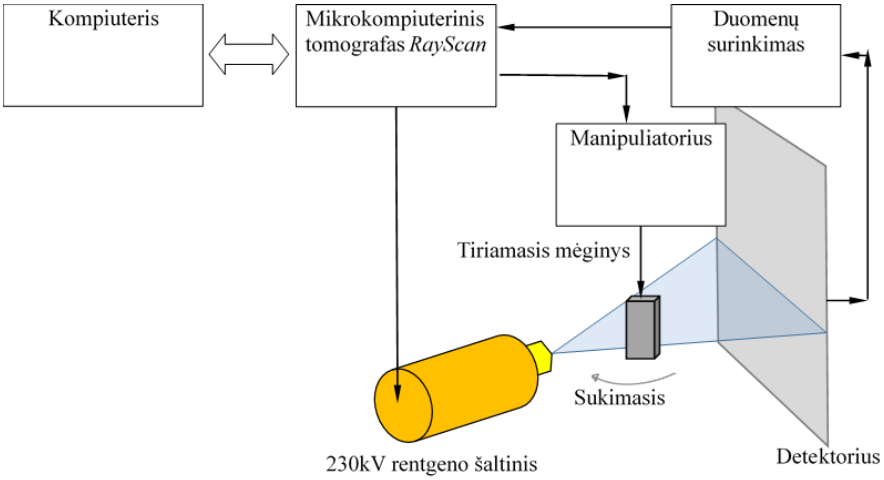

7 pav. MikroKT atlikimo schema *in vivo*

Naujo kaulo tūris (mm^3) buvo apskaičiuotas naudojant Avizo 3D for Industrial Inspection 9.70 (FEI-SAS, Thermo Fischer Scientific Inc.) programą. Naujai susiformavusio kaulo kiekiui apskaičiuoti buvo sukurtas specialus algoritmas. Operacijos metu suformuoto kaulinio defekto vieta buvo apibrėžiama 5,5 mm skersmens apskritimu. Apskritimo centre kaukolės plokštumoje brėžiami statmeni vektoriai, pagal kuriuos skaičiuojamas naujai susidariusio kaulo kiekis. Minkštieji audiniai, kaulo pakaitalų granulės ir karkasai nuo regeneravusio kaulo buvo atskiriami atsižvelgiant į skirtingus pilkumo skalės (angl. *grey values*) parametrus. Minkštųjų audinių ir PLR pilkumo skalės parametrai buvo < 20 000; naujai susiformavusio kaulo – 20 000–44 000; karkasuose naudotų keramikų tankis – > 44 000.

2.14. KAULINIO AUDINIO HISTOLOGINIS IŠTYRIMAS

Atlikus mikroKT analizę, kaulo mėginiai dvi savaites buvo dekalcifikuojami 10 proc. EDTA – 10 proc. formalino tirpale (pH 7,0–7,4). Tada kiekvienas mėginys buvo padalytas į 5 dalis: per centrą, nuo centro į abi puses nutolus per 1,3 mm ir 2,6 mm, po to padalytos dalys buvo įtvirtintos parafine. Kiekviename tiriamosios medžiagos segmente buvo atlikti 3 µm storio 5 išilginiai pjūviai. Tiriamieji mėginiai nudažyti hematoksilino ir eozino dažų mišiniu. Gauti pjūviai analizuoti šviesiniu mikroskopu „Olympus BX41TF“ (Olympus Optical Co. LTD). Kokybinės analizės metu buvo vertintas kaulinis defektas, naujo kaulo formavimasis, jungiamojo audinio formavimasis, uždegimo požymiai. Kiekybinė analizė buvo atlikta Aperio ImageScope (Leica Biosystems Imaging) programa, apskaičiuojant naujai susiformavusio kaulo plotą (mm^2).

2.15. STATISTINĖ ANALIZĖ

Duomenų analizė buvo atlikta naudojant R programų paketą (RStudio v1.1.442). Eksperimentuose, kuriuose buvo naudojama SEM analizė, tyrimai atlikti su 5 nepriklausomais mėginiais. *In vitro* mikroKT analizei buvo naudoti 22 mėginiai. Gautų duomenų normalumas ir variacija buvo vertinti naudojant Shapiro-Wilk bei Levene’s testus. Duomenys pateikti kaip vidurkis ± standartinė paklaida. *In vitro* rezultatai buvo vertinami atliekant vieno faktoriaus ANOVA testą. Statistiškai patikimi rezultatų skirtumai buvo nustatomi naudojant Tukey HSD testą. Statistiškai patikimi *in vivo* rezultatų skirtumai tarp skirtingų gyvūnų lyčių buvo nustatyti naudojant Student t testą, o tarp skirtingų grupių – vieno faktoriaus ANOVA bei Tukey HSD testus. Manyta, kad tarp duomenų yra statistiškai patikimas skirtumas, kai $p < 0,05$.

3. REZULTATAI IR JŲ APTARIMAS

3.1. *IN VITRO* REZULTATAI

Kaulų defektų atkūrimas yra vienas iš didžiausių iššūkių įvaririose medicinos šakose: neurochirurgijoje, ortopedijoje ir traumatologijoje ar burnos, veido ir žandikaulių chirurgijoje[19]. Remiantis šiuolaikinėmis technologijomis tikimasi, kad tokius pažeidimus greitai bus galima gydyti taikant daug žadančius, audinių inžinerijos principais sukurtus kaulinio audinio pakaitalus[262]. Kaulas yra mineralizuotas jungiamasis audinys[114], kuriam būdinga specializuota organinė-neorganinė struktūra. Tokį kaulinį

audinį galima suprasti kaip mikro- ir nanokompozitinį junginį[257]. Būtent tokia audinio struktūra ir sudėtis (porėtumas, trabekulinė ir kortikalinė audinio architektūra, kolageno fibrilių išsidėstymas, TU mineralizacija ir kt.) nulemia kaulo mechanines savybes[257]. Kuriant karkasus, skirtus kaulo regeneracijai, stengiamasi kuo labiau atkartoti natūralią kaulinio audinio sandarą.

Įvairūs kaulinio audinio priauginimo operacijų būdai yra pagrįsti natūraliais, po pažeidimo vykstančiais kaulo gijimo ir regeneracijos procesais. Po traumos kaulo gijimas prasideda ir visiška kaulo regeneracija yra galima tik tuo atveju, jei yra teisinga lūžio galų anatominė pozicija ir stabili jų fiksacija[407]. Jei tarpas tarp lūžusio kaulo galų yra mažesnis nei 0,01 mm, vyksta kontaktinis gijimas. Jei tarpas tarp kaulo galų yra mažesnis nei 0,8–1 mm, tačiau yra stabili kaulo galų fiksacija, kaulinis audinys dar geba regeneruoti tokį defektą savaime[407]. Taigi, norint dirbtinio kaulinio audinio gamybai naudoti 3D spausdintus karkasus, svarbu užtikrinti naudojamos spausdinimo technologijos tikslumą, nes pagamintas konstruktas turi kuo labiau atitikti paciento kaulo defektą.

Visų pirma šiam darbui buvo pasirinkti du LNM 3D spausdintuvai – „ Ultimaker Original“ ir „Pharaoh XD 20“. Pagal nurodytus techninius parametrus spausdinti struktūras abu gali naudojant PLR filamentus. „Ultimaker Original“ spausdintuvas naudoja 2,85 mm skersmens filamentus spausdinti ir jo didžiausia sluoksnio skiriamoji geba yra nuo 20 iki 200 μm[408]. „Pharaoh XD 20“ spausdintuvo sluoksnio skiriamoji geba yra 100 μm[409], o spausdinti naudojami 1,75 mm skersmens filamentai. Siekiant sukonstruoti struktūrą, skirtą dirbtiniam kaului konstruoti, buvo nuspręsta įvertinti, ar LNM spausdintuvų parametrai turi įtakos spausdinimo tikslumui, kai yra spausdinami mėginiai naudojant tos pačios įmonės, tos pačios medžiagos filamentus. PLR1 karkasai buvo pagaminti spausdintuvu „Ultimaker Original“, PLR2 – „Pharaoh XD 20“. Buvo vertinama, kaip tiksliai abu įrenginiai atspausdina tame pačiame STL faile esantį 3D mikrostruktūrizuotą karkaso modelį SEM, gravimetriniu ir skysčio išstūmimo metodais, mikroKT.

Atlikus SEM matavimų analizę nustatyta, kad iš gamyklinio PLR polimero tiksliau karkasų sluoksnius atspausdino spausdintuvas „Pharaoh XD“ (PLR2 mėginiai), palyginti su „Ultimaker Original“ atspausdintais mėginiais (PLR1) (8 pav).

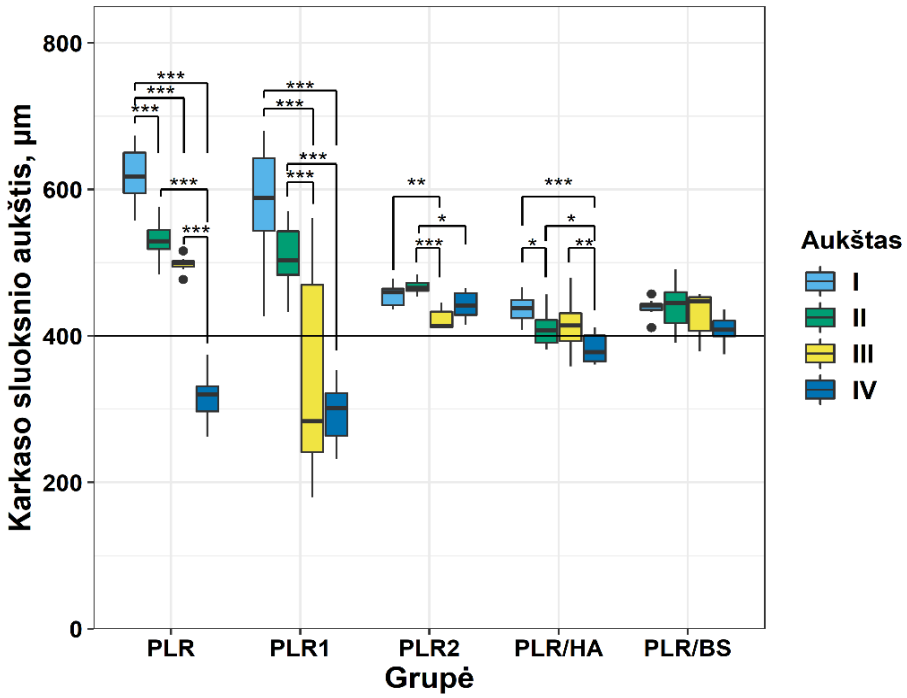

8 pav. Karkasų sluoksnių aukštis. Juoda horizontali linija žymi teorinį sluoksnio aukštį – 400 µm. Statistiškai reikšmingi skirtumai tarp grupių pažymėti kaip „*“, kai $p < 0,05$, „**“, kai $p < 0,01$, ir „***“, kai $p < 0,001$.

Reikia pažymėti, kad su spausdintuvu „Ultimaker Original“ buvo sudėtinga atspausdinti sluoksnius, kurių aukštis buvo net 20 kartų didesnis (400 µm) nei minimali jo skiriamoji geba (20 µm). Atstumas tarp gijų buvo taip pat tiksliau išlaikytas PLR2 grupėje, kurios matmenys mažiau nukrypo nuo STL failo nei PLR1 grupės. Rastas statistiškai reikšmingas skirtumas tarp PLR1 ir PLR2 grupių (9 pav.).

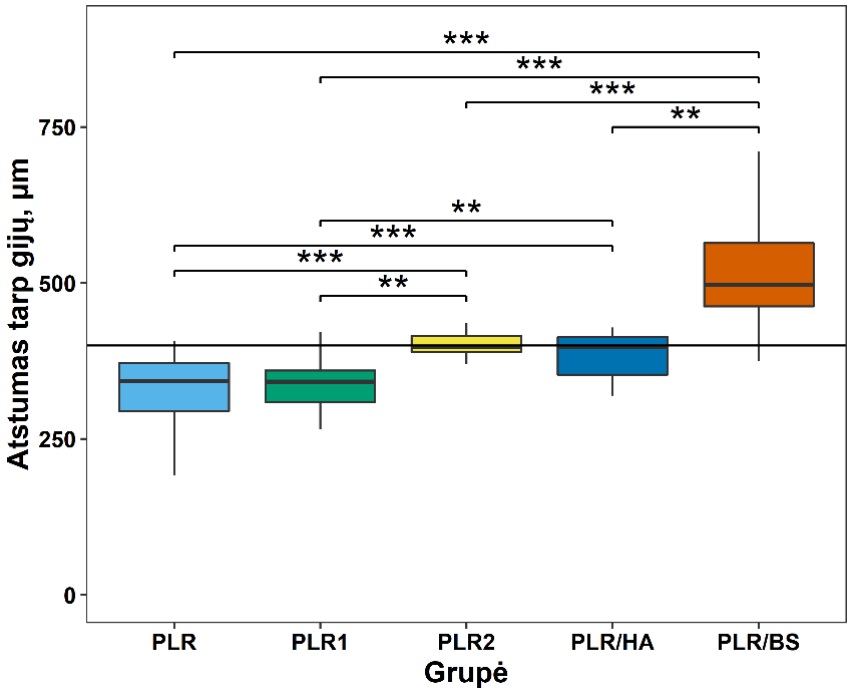

9 pav. Atstumas tarp karkasų gijų. Juoda horizontali linija žymi teorinį atstumą tarp gijų – 400 µm. Statistiškai reikšmingi skirtumai tarp grupių pažymėti kaip „*“, kai $p < 0,05$, „**“, kai $p < 0,01$, ir „***“, kai $p < 0,001$.

Nepaisant didelių sluoksnių aukščių skirtumų tarp PLR1 ir PLR2 grupių, „Ultimaker Original“ ir „Pharaoh XD“ spausdintuvai pagamino panašaus aukščio karkasus, tarp kurių nebuvo statistiškai reikšmingo skirtumo (10 pav.).

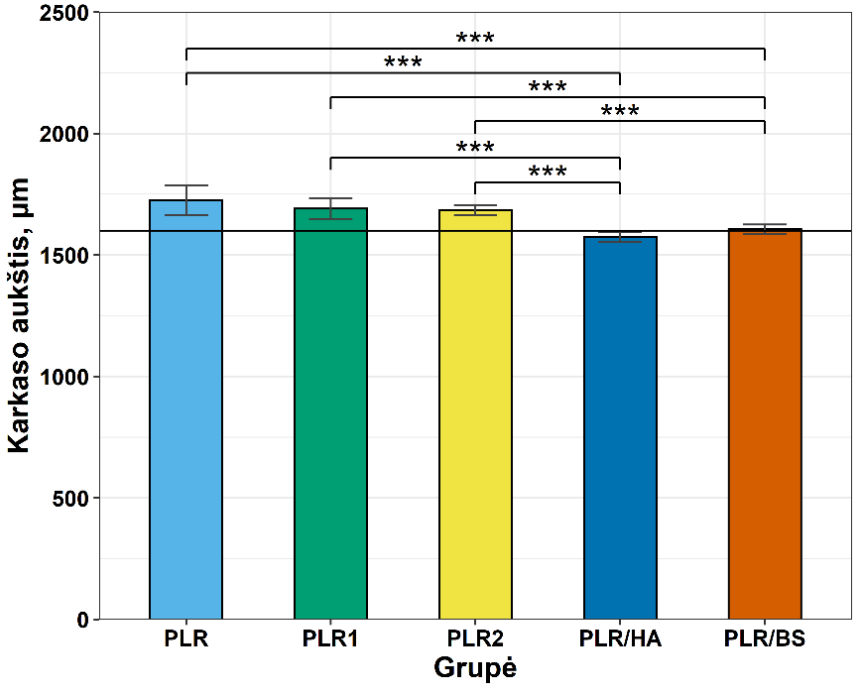

10 pav. Karkasų aukštis. Statistiškai reikšmingi skirtumai tarp grupių pažymėti kaip „***“, kai $p < 0,001$

Įvertinus gautus gravimetrinio ir skysčio išstūmimo metodų duomenis, nerasta statistiškai reikšmingo skirtumo tarp PLR1 ir PLR2 karkasų, taip pat ir su teoriniu karkasų porėtumu (11 pav.). Tačiau PLR2 grupės vidutinis porėtumas buvo didesnis nei PLR1, o tai lemia geresnes karkaso savybes kaulo regeneracijai.

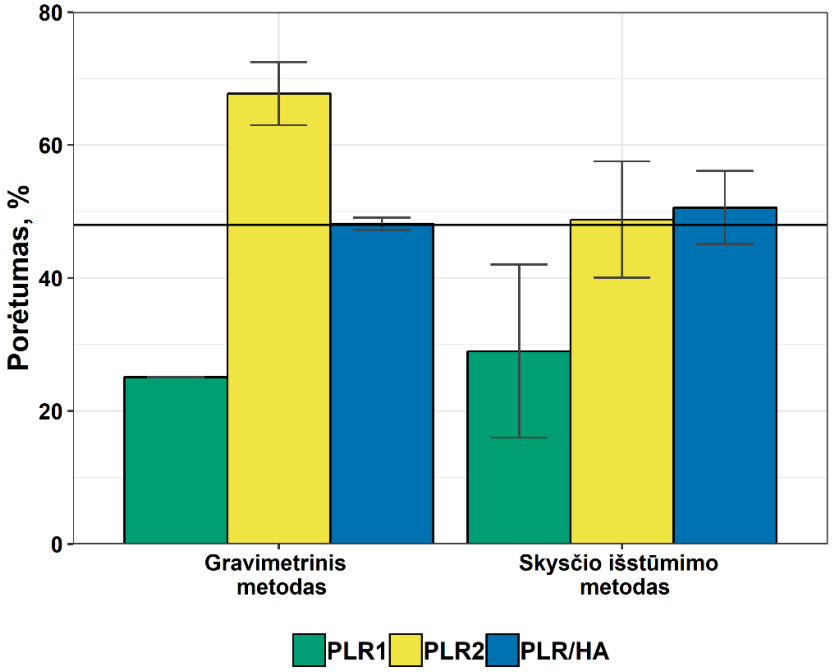

11 pav. Skirtingų tyrimų vidutinis karkasų porėtumas (proc.). Juoda linija žymi teorinį porėtumą – 48 proc.

Apskaičiavus vidutinį karkasų tūrį pagal mikroKT duomenis, rastas statistiškai reikšmingas skirtumas tarp PLR1 ir PLR2 grupių (12 pav.).

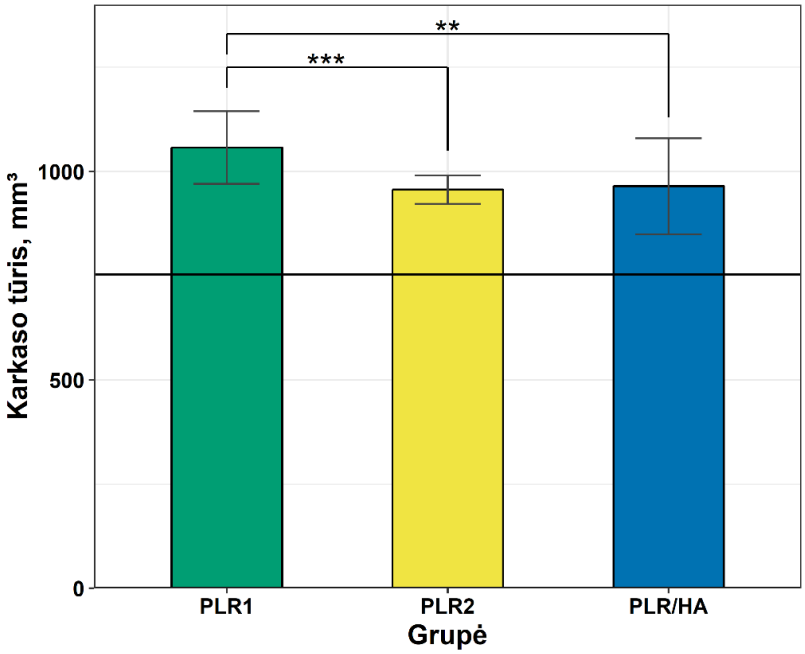

12 pav. Karkasų tūris (mm^3) pagal mikroKT ir superimpoziciją. Juoda horizontali linija žymi teorinį karkaso tūrį – 753,23 mm^3. Statistiškai reikšmingi skirtumai tarp grupių pažymėti kaip „*“, kai $p < 0,05$, „**“, kai $p < 0,01$, ir „***“, kai $p < 0,001$

Apibendrinant „Ultimaker Original“ ir „Pharaoh XD 20“ spausdinimo tikslumo rezultatus, galima teigti, kad tikslesnis yra įrenginys „Pharaoh XD 20“. Skirtumų tarp abiejų 3D spausdintuvų spausdinimo kokybės galėjo atsirasti dėl skirtingos jų aparatinės ir programinės įrangos. „Pharaoh XD“ spausdintuvas turėjo automatinį kalibravimą, kuris padėjo išlaikyti tikslesnį atstumą tarp spausdinimo galvutės ir paviršiaus pagrindo, ant kurio buvo spausdinamas karkasas. Yra žinoma, kad automatinis kalibravimas pagerina spausdinimo tikslumą[410]. Be to, su „Pharaoh XD 20“ spausdintuvu buvo naudojama „Slicer 1.2.8“ programinė įranga, o su „Ultimaker Original“ spausdintuvu – „Ultimaker Cura 3.6“. Nors literatūroje nėra duomenų, kad šios programinės įrangos skirtųsi, tačiau yra žinoma, kad naudojant skirtingas pjaustymo programas tokiam pačiam modeliui sukurti, po jo gamybos proceso gaunamas skirtingas rezultatas[411]. Remiantis šio tyrimo rezultatais, abu tirti spausdintuvai gebėjo atspausdinti karkasus taip tiksliai, kad pakaktų užtikrinti kaulinio audinio regeneraciją. Tačiau tolesniems darbams buvo pasirinktas geresnius rezultatus parodęs „Pharaoh XD 20“ spausdintuvas ir KLE būdu buvo gaminami 1,75 mm skersmens filamentai.

Plastiko, gumos, maisto ir farmacijos pramonėje viena iš plačiausiai naudojamų gamybos technologijų yra KLE [412]. Neseniai šį metodą imta taikyti ir filamentų, skirtų kaulinio audinio karkasams 3D spausdinti, gamybai[413]. Šiame darbe, taikant KLE technologiją, buvo gaminami kompozitiniai PLR ir 10 proc. HA bei PLR ir 10 proc. BS filamentai. Filamentų gamybai naudota Filabot Original KLE sistema. Tolygus HA ir BS dalelių pasiskirstymas kompozitiniame filamente buvo užtikrinamas pasirenkant vienodo dydžio PLR bei HA arba BS granules, kurios tarpusavyje buvo nuolat maišomos. Literatūros duomenimis, 5 proc. BS koncentracijos pakanka sėkmingam naujo kaulinio audinio[283], kraujotakos [277] bei mineralizuoto TU formavimuisi[282] *in vivo*. Be to, manoma, kad didesnė BS koncentracija gali pagerinti minėtas savybes[282]. HA atveju, norint užtikrinti osteogeninių procesų iniciaciją ląstelėse bei aktyvinti sėkmingą kaulo regeneraciją *in vivo,* reikia didesnės šios medžiagos koncentracijos kompozite – bent 10 proc. Remiantis literatūroje pateiktomis aptartų medžiagų savybėmis, šiame darbe buvo pasirinkta tirti kompozitus, turinčius 10 proc. neorganinių komponentų (HA arba BS). Kartu su kompozitiniais filamentais buvo gaminami ir kontroliniai – grynos PLR mėginiai. Pagaminus skirtingus filamentus buvo matuojami jų skersmenys. Priklausomai nuo medžiagos rūšies gautų filamentų skersmenys buvo skirtingi: PLR – 1,67–1,75 mm, PLR/HA – 1,28–1,45 mm, PLR/BS – 1,6–1,75 mm. Tyrimo metu buvo pastebėta, kad vidurinės sukurtų filamentų dalys turėjo mažiausius skersmens nuokrypius ir buvo gana tolygios eksperimentiniams mėginiams gaminti. Tačiau, remiantis literatūra, kintamas filamentų skersmuo gali sukelti netolygumus išstūmimo iš spausdintuvo galvutės metu, tačiau diskutuotina, ar nedideli skersmens nuokrypiai gali turėti įtakos 3D spausdinimo tikslumui ir sukurtų karkasų morfologijai[150].

Toliau vertinome, ar KLE technologija pagaminti (PLR, PLR/HA arba PLR/BS) filamentai nekeičia „Pharaoh XD 20“ spausdinimo tikslumo. Visų pirma iš pasiruošto PLR filamento spausdintuvu buvo pagaminti PLR karkasai, naudojant tokį patį karkaso modelio STL failą kaip ir anksčiau įvertintose grupėse. Kaip ir LNM technologijos tikslumo vertinimo eksperimentuose, atspausdinti mėginiai buvo fotografuojami SEM ir vertinamas bendras karkaso aukštis, kiekvieno jo sluoksnio aukštis ir atstumas tarp sluoksnį sudarančių gijų. Įvertinus visus PLR grupės SEM rezultatus (8–10 pav.), buvo pastebėta, kad yra liejami netolygūs sluoksniai, o SEM rezultatai buvo panašūs į PLR1 grupės. Remiantis pasiektais rezultatais, prieš spausdinant karkasus iš PLR/HA ir PLR/BS gijų, rankiniu būdu buvo papildomai sureguliuoti „Pharaoh XD 20“ spausdintuvo parametrai (atstumas

tarp spausdintuvo galvutės ir spausdinamo objekto, pirmojo sluoksnio aukštis).

Vėliau atspausdinti kompozitiniai PLR/HA ir PLR/BS karkasai buvo įvertinti SEM ir jų rezultatai palyginti su visų anksčiau spausdintų PLR grupių rezultatais. Remiantis SEM rezultatais, kompozitiniai karkasai, atspausdinti iš PLR/HA ir PLR/BS gijų, turėjo tokius pačius ar net tikslesnius sluoksnių (8 pav.) ir karkasų aukščius (10 pav.) nei visos PLR grupės. Įdomu , kad SEM vaizdai parodė, jog PLR/BS karkasų grupėje sluoksniai buvo atspausdinti tolygiausiai. Šioje vienintelėje grupėje nebuvo statistiškai reikšmingo skirtumo tarp sluoksnių (8 pav). Galbūt šis efektas padėjo išlaikyti ir didžiausius atstumus tarp gijų PLR/BS karkasuose (9 pav.). Šie pasiekti PLR/BS karkasų spausdinimo parametrai lėmė, kad buvo galima apskaičiuoti šios grupės teorinį porėtumą, todėl šių karkasų nebuvo atlikti gravimetriniai ir skysčių išstūmimo vertinimo metodai, mikro-KT įvertinimas.

Tolesnė morfologijos analizė buvo atlikta vertinant PLR/HA karkasų rezultatus, kurie buvo palyginti su PLR2 grupės rezultatais. PLR/HA karkasus buvo sunkiausia atspausdinti dėl gijų trapumo ir labiausiai besiskiriančio filamento skersmens. Be to, SEM vaizdai parodė statistiškai reikšmingus skirtumus tarp skirtingų PLR/HA karkasų sluoksnių. Įdomu, kad, nepaisant PLR/HA karkasų spausdinimo sunkumų, porėtumo įvertinimas skirtingais būdais parodė artimiausias vertes (48 ir 50 proc.) originaliam STL modelio porėtumui, palyginti su PLR2 grupe (11 pav.). Literatūroje atlikti tyrimai patvirtina, kad 50 proc. karkasų porėtumas skatina ląstelių dauginimąsi ir migraciją bei teigiamai veikia kaulo regeneraciją[152], taigi PLR/HA karkasų porėtumas yra tinkamas kurti dirbtinį kaulinį audinį. Įvertinus mikroKT rezultatus, rasta, kad šių grupių PLR2 ir PLR/HA karkasų tūriai buvo panašūs , tačiau neatitiko teorinio STL failo tūrio (12 pav.).

Apibendrinus tikslumo rezultatus, galima patvirtinti, kad KLE yra vertinga priemonė individualiems kompozitiniams filamentams kurti, tačiau reikia tolesnių tyrimų, kaip pagerinti kuriamų filamentų skersmens tolygumą. Manome, kad šį tikslą būtų galima pasiekti naudojant išmaniuosius gijų ekstruderius su internetiniu filamento skersmens valdymu, kuris matuoja kaitinamojo filamento skersmenį ir atitinkamai koreguoja ekstruzijos parametrus (temperatūrą, greitį ir kt.). Kita vertus, sunku pasakyti, kuris iš šių parametrų (netolygus skersmuo ar filamentų sudėtis) turėjo didesnį poveikį galutinei karkasų morfologijai. Manome, kad dėl HA ar BS dalelių kompozitiniai filamentai turėjo aukštesnę savitąją šiluminę talpą ir lėčiau vėso. Kompozitinio filamento klampa taip pat buvo didesnė nei grynos PLR. Tikriausiai tai ir nulėmė, kad PLR/HA ir PLR/BS mėginiuose sluoksnių gijos

buvo atspausdintos lygiau, o bendri tūriniai karkasų matmenys buvo tikslesni (labiau atitiko STL faile esantį modelį).

Šio tyrimo rezultatai yra svarbūs norint geriau suprasti 3D spausdinimo procesą. Svarbi žinia, pagrįsta šio tyrimo rezultatais, yra ta, kad 3D spausdintų karkasų matmenys ir morfologija gali skirtis nuo pradinio STL failo. Tokie skirtumai yra ypač svarbūs gaminant medicinos reikmenis – chirurginius gidus, individualius pacientui skirtus implantus ir kt. [413]. Rekomenduojame pirmą kartą spausdinant 3D objektus, skirtus kaulinei regeneracijai ar reikalaujančius ypatingo spausdinimo tikslumo, įvertinti atspausdintų 3D objektų parametrus ir palyginti su originaliomis STL failo vertėmis. Esant statistiškai reikšmingų skirtumų, reikėtų pritaikyti STL modelį norimam pasiekti rezultatui, ypač medicinos reikmėms[407].

3.2. *IN VIVO* REZULTATAI

Kaulų regeneracija yra sudėtingas procesas, kurio metu naujos bioaktyvios medžiagos padeda užpildyti kaulinius defektus ir atkurti prarastas ar sutrikusias kaulinio audinio funkcijas[11]. Pastaruoju metu manoma, kad 3D spausdinti kompozitiniai kaulų karkasai yra viena iš perspektyviausių kaulų persodinimo strategijų[13, 14]. Tačiau jų veiksmingumas turėtų būti įvertintas patikimais ir palyginamais metodais prieš perkeliant juos naudoti klinikinėje praktikoje[416]. Nemažai 3D spausdintų karkasų savybių galima įvertinti *in vitro* esamais metodais[417, 418]. Tačiau norint geriau suprasti šeimininko atsaką į tam tikrą bioaktyvią medžiagą bei įvertinti regeneracinį efektyvumą, būtini tyrimai *in vivo*.

Graužikų modeliai yra vieni iš populiariausių ir geriausiai aprašytų kaulų regeneraciją ir gijimą tiriančių modelių literatūroje[417]. Šiame tyrime buvo pasirinktos Wistar klono žiurkės, kurios yra genetiškai panašios, dėl to į išorinius ir vidinius stimulus reaguoja panašiai, o tai leidžia patikimiau įvertinti naujas kaulo regeneracijos strategijas[417]. Be to, tokių beveik identiškų gyvūnų naudojimas leido sumažinti reikiamą žiurkių skaičių DPKL išskirti bei karkasų su ląstelėmis ar jų TU gamybai. Svarbu paminėti, kad šiame tyrime kaulo regeneracijos galimybės buvo įvertintos abiejų lyčių gyvūnų organizme. Yra žinoma, kad žiurkių patelių regeneracinis pajėgumas yra mažesnis nei patinų, nes jų kaulų čiulpuose yra mažiau mezenchiminių kamieninių ląstelių[418]. Vienodas gyvūnų skaičius pagal lytis mėginių grupėse taip pat yra labai svarbus, nes patinėliai, matuojant neurokranijinį ilgį ir plotį, auga greičiau nei patelės ir nuo 120 gyvenimo dienos šis skirtumas tik

didėja[419]. Neišlaikant vienodo gyvūnų skaičiaus pagal lytį grupėse, tyrimo rezultatai galėjo būti paveikti ir netikslūs dėl skirtingo gyvūnų augimo.

Šiame darbe kaulo regeneracijai įvertinti buvo pasirinktas žiurkių kaukolės skliauto kritinio dydžio defekto modelis. Šios anatominės srities pasirinkimą lėmė tai, kad yra daug duomenų literatūroje, su kuriais galima palyginti gautus rezultatus[417]. Šis modelis yra tinkamas tirti intramembraninį naujo kaulo formavimąsi[420]. Nereikia papildomos bioaktyvių medžiagų fiksacijos, nesudėtinga atlikti chirurginę operaciją[417]. Sukurtuose defektuose galima tirti įvairios konsistencijos medžiagas (birias, karkasus) ir lyginti gautus rezultatus[417]. Šis aspektas buvo labai svarbus renkantis tyrimo modelį, nes teigiamai kontrolei naudota medžiaga Bio-Oss yra biri, o tiriamosios medžiagos – karkasai. Svarbu paminėti, kad literatūroje yra prieštaravimų, kokio skersmens defektas yra kritinio dydžio žiurkių kaukolėse. Vieni šaltiniai teigia, kad 5 mm, kiti – 8 mm[417,423]. Šiame tyrime buvo atlikti maksimaliai dideli 5,5 mm skersmens kauliniai defektai, paliekant bent 1,5 mm kaulinį tiltą tarp jų. Remiantis bandomojo tyrimo duomenimis, mažesnis nei 1,5 mm kaulinis tiltas turėjo neigiamą įtaką kaulo regeneracijai. Buvo nuspręsta atlikti 5,5 mm skersmens defektus, nes norėta vienoje žiurkės kaukolėje talpinti du defektus, taip sumažinti reikalingą gyvūnų skaičių ir labiau atitikti 3Rs taisyklę. Įprasta, kad kritinio dydžio defekto terminą[423] galima vartoti, jei suformuotas defektas nesugijo savaime per tiriamąjį laikotarpį.

Gyvūnų eutanazijos atlikimo laikas, kuris rodo transplanto buvimo organizme trukmę, įvairiuose tyrimuose skiriasi[422]. Šiame darbe kaulo regeneracija buvo vertinta mikroKT ir kaulinio audinio histologinio tyrimais praėjus aštuonioms savaitėms po operacijos, nes tai yra geriausias laikas ištirti naują kaulo formavimąsi žiurkės modelyje[425]. Jei būtume kaulinius defektus palikę ilgesniam pooperaciniam gijimui, tikėtina, kad dėl besikaupiančių PLR degradavimo produktų[261] būtų išryškėję statistiškai reikšmingų skirtumų tarp visų PLR grupių ir kompozitinių arba Bio-Oss. Remiantis literatūra, abu neorganiniai komponentai (HA ir BS) sukurtuose kompozitiniuose karkasuose sumažina karkasų skilimo greitį ir neutralizuoja PLR degradavimo produktų rūgštingumą[261,263,272,277]. Be to, tikėtina, kad biodekoruoti konstruktai su DPKL arba jų TU būtų parodę geresnius gijimo rezultatus nei gryni kompozitiniai karkasai dėl šių medžiagų osteoinduktyvumo[338].

Bio-Oss yra vienas iš dažniausiai naudojamų gyvūninės kilmės kaulinių pakaitalų kaulo priauginimo operacijose dėl puikių osteokondukcinių savybių, mažo rezorbcijos greičio ir pakaitinės laipsninės kaulo remodeliacijos[156]. Be to, neseniai atliktas tyrimas vertinant kaulo regeneracinį potencialą burnos, veido ir žandikaulių srityje parodė, kad Bio-Oss teigiamai veikia naujo kaulo formavimąsi, prilygstantį autogeninio transplanto, kuris laikomas auksiniu

standartu, naujo kaulo indukavimui sukurtuose kauliniuose defektuose[106]. Dėl šių Bio-Oss savybių jis buvo pasirinktas teigiama kontrole šiame tyrime. Buvo svarbu išsiaiškinti, ar kuriami 3D karkasai yra konkurencingi šiuo metu klinikinėje praktikoje naudojamoms medžiagoms. Remiantis šio tyrimo kaulinio audinio histologinio ištyrimo ir mikroKT rezultatais nustatyta, kad tik Bio-Oss ir neigiamos kontrolės grupėse nebuvo statistiškai reikšmingo skirtumo tarp abiejų lyčių, vertinant naujo kaulo formavimosi intensyvumą (13 ir 14 pav.).

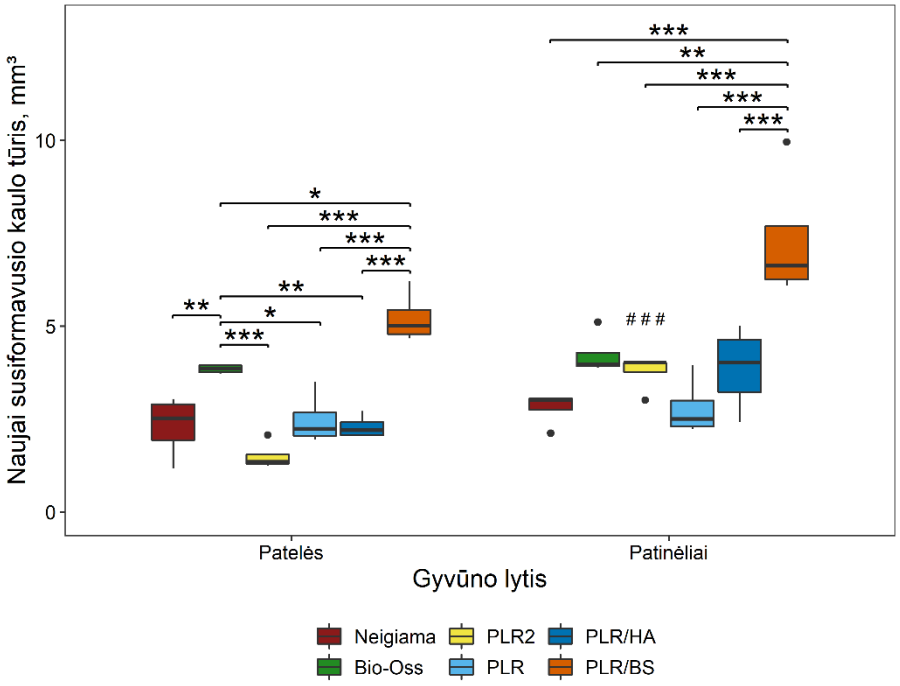

13 pav. *In vivo* I etapo mikroKT rezultatai, pavaizduoti histograma su pasikliautinių intervalų grafiniu vaizdu naujai susiformavusiam kaulo tūriui (mm^3) pagal mėginių grupes ir gyvūnų lytį. *, ** ir *** rodo statistiškai reikšmingus grupių skirtumus, atitinkamai $p < 0,05$, $p < 0,01$ ir $p < 0,001$. #, ## ir ### žymi statistiškai reikšmingus skirtumus tarp lyčių toje pačioje imties grupėje, atitinkamai $p < 0,05$, $p < 0,01$ ir $p < 0,001$.

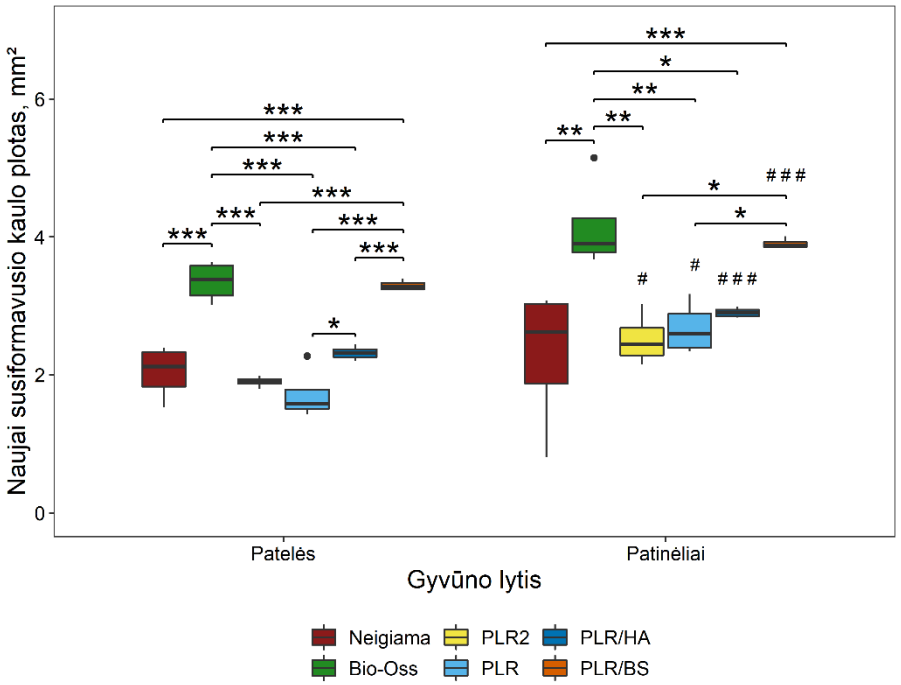

14 pav. *In vivo* I etapo kiekybinio kaulinio audinio histologinio ištyrimo rezultatai naujai suformuotam kaulo plotui (mm^2) pagal mėginių grupes ir gyvūnų lytį. *, ** ir *** rodo statistiškai reikšmingus grupių skirtumus, atitinkamai $p < 0,05$, $p < 0,01$ ir $p < 0,001$. #, ## ir ### žymi statistiškai reikšmingus skirtumus tarp lyčių toje pačioje imties grupėje, atitinkamai $p < 0,05$, $p < 0,01$ ir $p < 0,001$

Įdomu, kad remiantis kiekybinio kaulinio audinio histologinio ištyrimo I etapo rezultatais, visose eksperimentinėse grupėse buvo rasta statistiškai reikšmingų skirtumų tarp abiejų lyčių kauliniame audinyje naujai suformuoto kaulo ploto. Buvo padaryta prielaida, kad šiuos skirtumus tarp abiejų lyčių kauliniame audinyje naujai suformuotų kaulų plotų dažniausiai lėmė mažesnis mezenchiminių kamieninių ląstelių skaičius moteriškos lyties žiurkių kaulų čiulpuose[418]. Dėl to buvo nuspręsta pagerinti osteoindukcines eksperimentinių karkasų (PLR, PLR/HA ir PLR/BS) savybes DPKL ar jų TU. Tačiau remiantis II etapo rezultatais statistiškai reikšmingi skirtumai tarp abiejų lyčių kauliniame audinyje naujai suformuoto kaulo ploto išliko visose eksperimentinėse grupėse, išskyrus PLR/DPKL ir PLR/TU grupes ($p = 0,07$). (15 ir 16 pav.).

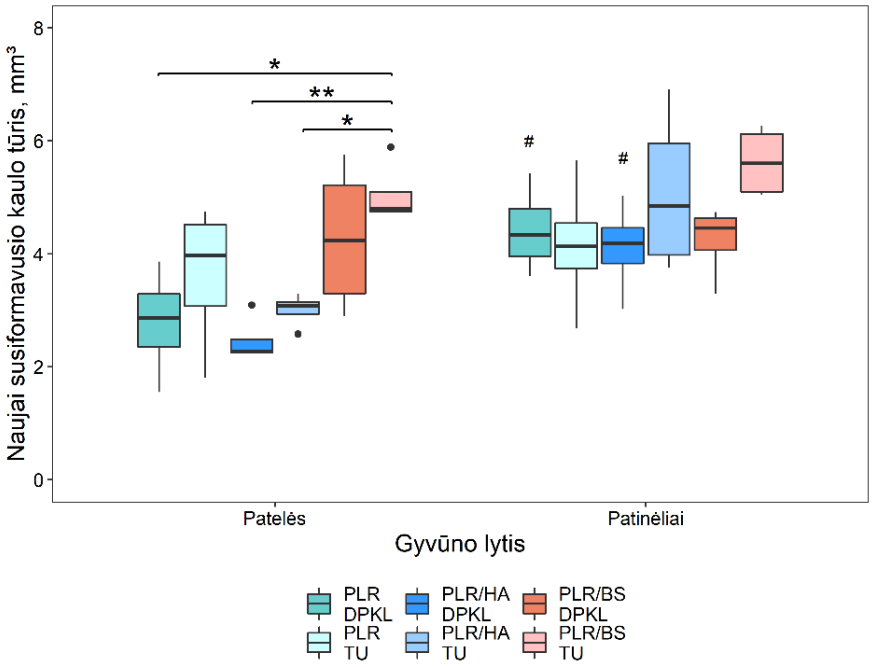

15 pav. *In vivo* II etapo mikroKT rezultatai, pavaizduoti histograma su pasikliautinių intervalų grafiniu vaizdu naujai susiformavusiam kaulo tūriui (mm^3) pagal mėginių grupes ir gyvūnų lytį. *, ** ir *** rodo statistiškai reikšmingus grupių skirtumus, atitinkamai $p < 0,05$, $p < 0,01$ ir $p < 0,001$. #, ## ir ### žymi statistiškai reikšmingus skirtumus tarp lyčių toje pačioje imties grupėje, atitinkamai $p < 0,05$, $p < 0,01$ ir $p < 0,001$

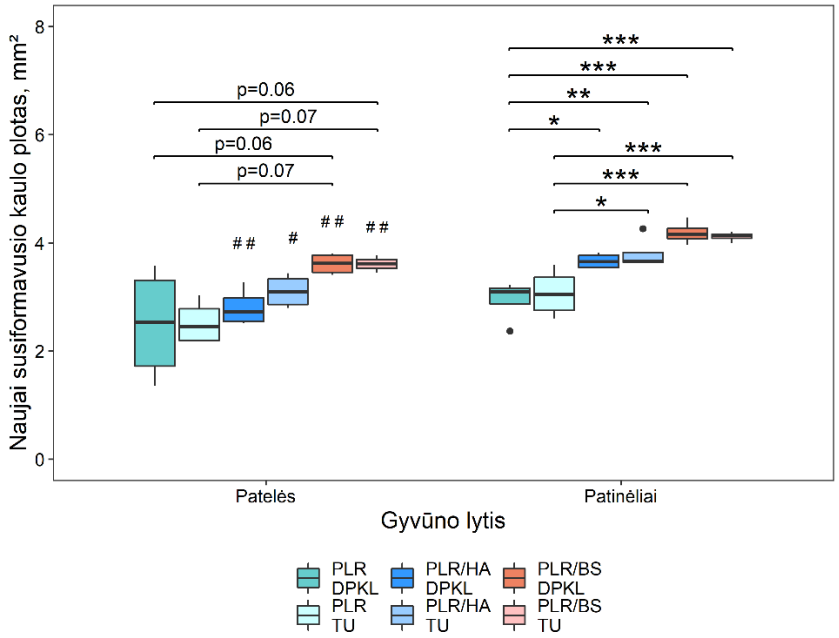

16 pav. *In vivo* II etapo kiekybinio kaulinio audinio histologinio ištyrimo rezultatai naujai suformuotam kaulo plotui (mm^2) pagal mėginių grupes ir gyvūnų lytis. *, ** ir *** rodo statistiškai reikšmingus grupių skirtumus, atitinkamai $p < 0,05$, $p < 0,01$ ir $p < 0,001$. #, ## ir ### žymi statistiškai reikšmingus skirtumus tarp lyčių toje pačioje imties grupėje, atitinkamai $p < 0,05$, $p < 0,01$ ir $p < 0,001$

Literatūroje yra duomenų, kurie rodo, kad lytinių ir augimo hormonų kiekio skirtumai taip pat gali lemti moteriškos lyties žmonių ir gyvūnų silpnesnę kaulo regeneraciją[426]. Reikia tolesnių tyrimų, vertinant šių priežasčių poveikį šeimininko ir bioaktyvių medžiagų sąveikai bei kaulo regeneracijai, naudojant kaulinius pakaitalus. Šiame darbe nebuvo sukurta universalaus kaulo karkaso, vienodai gerai veikiančio naujo kaulo formavimąsi kritinio dydžio defektuose abiejų lyčių žiurkių organizmuose. Tačiau pasiektus rezultatus būtų galima pagerinti padidinus neorganinių medžiagų procentinę dalį 3D karkasuose osteokondukcinėms savybėms pagerinti ar praturtinant 3D karkasus kitomis osteoindukcinėmis medžiagomis, pavyzdžiui, trombocitų papildyta plazma ar kaulo morfogenetiniais baltymais[1]. Ši svarbi informacija apie skirtingą kaulo regeneracinį potencialą kritinio dydžio defektuose skirtingų lyčių žiurkių organzime būtų praleista, jei šiame tyrime nebūtų įtraukti abiejų lyčių gyvūnai, tada PLR/BS ir PLR/HA karkasai bei jų konstruktai būtų parodę labai konkurencingus ar net geresnius rezultatus nei Bio-Oss grupės rezultatai (17 ir 18 pav.).

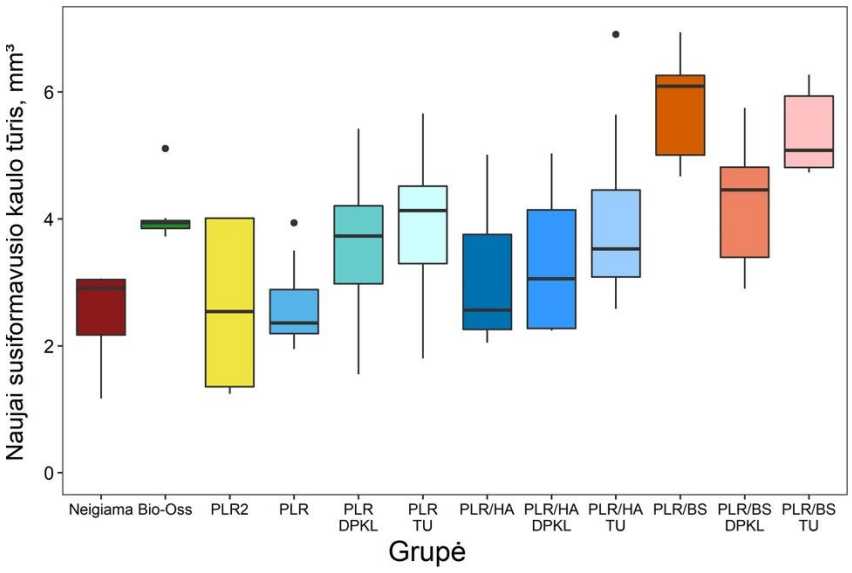

	Neigiama	Bio-Oss	PLR2	PLR	PLR DPKL	PLR TU	PLR/HA	PLR/HA DPKL	PLR/HA TU	PLR/BS	PLR/BS DPKL	PLR/BS TU
Neigiama												
Bio-Oss	-											
PLR2	-	-										
PLR	-	-	-									
PLR DPKL	-	-	-	-								
PLR TU	-	-	-	-	-							
PLR/HA	-	-	-	-	-	-						
PLR/HA DPKL	-	-	-	-	-	-	-					
PLR/HA TU	-	-	-	-	-	-	-	-				
PLR/BS	***	**	***	***	***	**	***	***	**			
PLR/BS DPKL	-	-	-	-	-	-	-	-	-	*		
PLR/BS TU	***	-	***	***	0.09	-	**	*	-	-	-	

17 pav. *In vivo* mikroKT rezultatai naujai susiformavusio kaulo tūriui (mm^3) pagal mėginių grupes. *, ** ir *** rodo statistiškai reikšmingus grupių skirtumus, atitinkamai $p < 0,05$, $p < 0,01$ ir $p < 0,001$

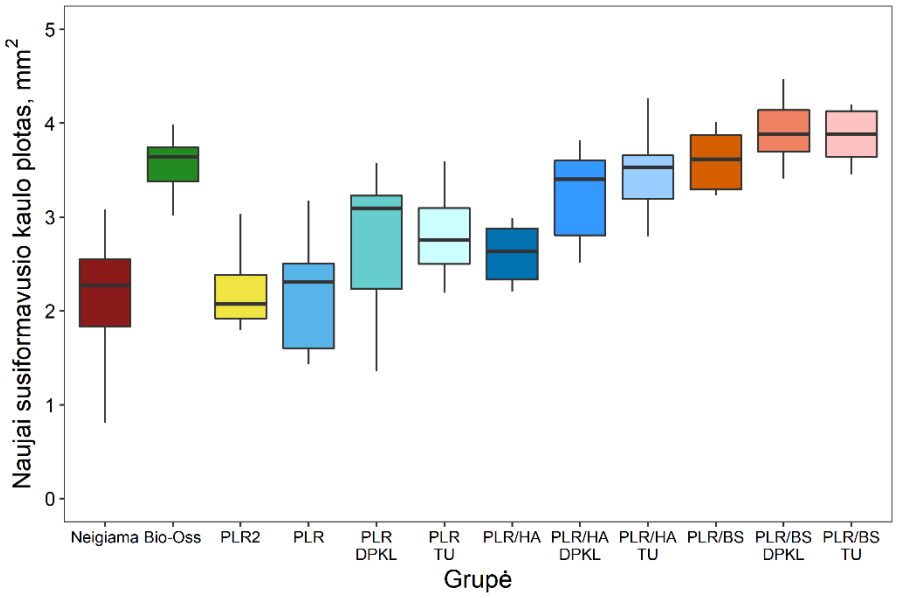

Grupė	Neigiama	Bio-Oss	PLR2	PLR	PLR DPKL	PLR TU	PLR/HA	PLR/HA DPKL	PLR/HA TU	PLR/BS	PLR/BS DPKL	PLR/BS TU
Neigiama												
Bio-Oss	***											
PLR2	-	***										
PLR	-	***	-									
PLR DPKL	-	**	-	-								
PLR TU	-	*	-	-	-							
PLR/HA	-	**	-	-	-	-						
PLR/HA DPKL	**	-	**	**	-	-	-					
PLR/HA TU	***	-	***	***	-	-	0.07	-				
PLR/BS	***	-	***	***	*	-	*	-	-			
PLR/BS DPKL	***	-	***	***	**	**	***	-	-	-		
PLR/BS TU	***	-	***	***	**	**	***	-	-	-	-	

18 pav. Kiekybinio kaulinio audinio histologinio ištyrimo rezultatai naujai susiformavusio kaulo plotui (mm^2) pagal mėginių grupes. *, ** ir *** rodo statistiškai reikšmingus grupių skirtumus, atitinkamai $p < 0,05$, $p < 0,01$ ir $p < 0,001$.

Literatūroje taip pat diskutuojama, kad duomenys, kurie gauti tyrimų metu tik vertinant vyriškosios lyties gyvūnus, negali atspindėti tam tikrų gyvūnų rūšių tikro rezultato[427]. Deja, net 80 proc. visų mokslinių straipsnių tiriami tik vyriškosios lyties gyvūnai ir tik 1 proc. straipsnių analizuoja rezultatus pagal lytį gyvūnų chirurginiuose modeliuose[427]. Remdamiesi mūsų gautais rezultatais, taip pat rekomenduojame atlikti tyrimus kaulo regeneracijai vertinti kritinio dydžio graužikų modeliuose abiejų lyių išlaikant vienodą skaičių grupėse.

Nepaisant gautų statistiškai reikšmingų skirtumų tos pačios imties grupės, indukuojančios kaulo regeneraciją, gyvūnų lyčių skirtumų, kartu apskaičiuoti I ir II *in vivo* etapų mikroKT duomenys parodė, kad geriausius kaulų regeneracijos sugebėjimus parodė PLR/BS ir PLR/BS TU grupės (17 pav.). Naujo kaulo statistiškai reikšmingai daugiau susiformavo PLR/BS karkasų grupėje ne tik pavienuose 3D osteokondukciniuose karkausuose (13 pav.), bet ir sukurtuose PLR/BS konstruktuose (15 pav.), išskyrus II etapo vyriškos lyties gyvūnų organizme. Tikėtina, kad PLR/BS grupėje gauti tokie geri naują kaulinį audinį indukuojantys rezultatai, nes BS yra labai aktyvus nuo pirmojo kontakto su recipientinio kaulo defektu. BS paviršius pritraukia hidroksikarbonato apatito kristalus per pirmą valandą po implantacijos[243]. Antrą valandą po implantacijos BS sužadina augimo faktorių, kurie skatina osteoblastų proliferaciją, gamybą[237,248]. Įvairūs *in vivo* tyrimai, vertinantys graužikų kaulo regeneraciją po skirtingų karkasų implantacijos, taip pat parodė PLR/BS pranašumus PLR atžvilgiu. PLR/BS grupių buvo geresni rezultatai ne tik vertinant kaulų regeneraciją[276], bet ir ektopinio kaulo formavimąsi[283], vaskuliarizaciją[277, 284]. Tolesni moksliniai tyrimai turėtų būti atliekami siekiant įvertinti kaulų regeneraciją, bioaktyvios medžiagos ir hormonų sąveiką, augimo faktorių ir recipientinio kaulinio defekto atsaką ilgalaikiuose *in vivo* stambiųjų gyvūnų kaulų regeneracijos modeliuose.

Remiantis šiame tyrime gautais kaulinio audinio histologinio ištyrimo duomenimis (18 pav.), geriausius naujų kaulų formavimosi indukavimo rezultatus parodė PLR/HA TU, PLR/BS, PLR/BS DPKL, PLR/BS TU karkasų grupės. Šių grupių pasiekti rezultatai buvo panašūs į Bio-Oss grupės ir nebuvo rasta statistiškai reikšmingų skirtumų tarp minėtų grupių. Karkasai, dekoruoti TU, sulaukia vis didėjančio susidomėjimo kaulinio audinio regeneracijoje ir audinių inžinerijoje dėl gebėjimo išsaugoti natūralias biologiškai aktyvias molekules, kurios pagerina ląstelių sukibimą, proliferaciją, migraciją ir diferenciaciją[398]. Histologiškai TU padengtų karkasų kaulų regeneracija buvo geresnė nei grynų 3D karkasų ar 3D karkasų su DPKL grupėse. Tačiau statistiškai reikšmingų skirtumų tarp osteokondukcinėmis savybėmis pasižyminčių karkasų ir jų biologiškai dekoruotų konstruktų,

vertinant naujo kaulo formavimąsi kritinio dydžio kauliniuose defektuose praėjus aštuonioms savaitėms po operacijos, nebuvo. Manome, kad kamieninėms ląstelėms, esančioms kaulo defekto kraštuose, buvo sunku migruoti į karkasų centrą dėl po nuląstelinimo proceso likusio kolageno skaidulų tinklo karkasų viduje, kuris galėjo veikti kaip prisitvirtinimą skatinantis, bet migraciją stabdantis barjeras[385]. Tolesni tyrimai tuėtų būti atliekami keičiant karkasų morfologiją (porėtumą, porų dydį, formą) ir stebint, kaip tai veikia TU formavimąsi bei ieškant tinkamiausios 3D karkasų morfologijos ir TU sąveikos su osteokondukciniais karkasais kaulo regeneracijai skatinti.

Šiame tyrime TU konstruktai buvo šiek tiek geresni nei tos pačios medžiagos 3D karkasai su DPKL, nors teoriškai implantacijos metu 3D karkasai su DPKL turėjo labai panašų TU. Kaulo regeneracijos skirtumų galėjo atsirasti dėl DPKL žūties, kurią lėmė nepakankama mityba karkasų viduje[432], mechaninis DPKL pažeidimas implantacijos metu[431]. Yra žinoma, kad ląstelių žūties metu atpalaiduotos bioaktyvios medžiagos skatina uždegimo procesus gretimuose audiniuose, o tai lėtina kaulo regeneraciją[430]. Tačiau dar daugelis kamieninių ląstelių transplantacijos dalykų yra nežinoma, pavyzdžiui, implantuotų ir recipientinių kamieninių ląstelių, esančių pažeidimo kraštuose, tarpusavio sąveika. Taip pat tyrėjai turėtų įvertinti, kurias iš biodekoravimo technologijų yra verta toliau tobulinti, atsižvelgiant į padidėjusias procedūros išlaidas, laiką, reikalingas technologijas.

Šiame tyrime gryni PLR karkasai buvo prasčiausi naujo kaulo formavimuisi sukurtuose kritinio dydžio kaulų defektuose dėl rūgštinių produktų, kurie išsiskyrė PLR degradacijos metu[158]. Tuo tarpu HA ir BS, kurie buvo įvesti į kompozitinius filamentus, lėmė didesnį naujo kaulo formavimąsi, nes yra geri buferiai, neleidžiantys rūgštėti aplinkiniams audiniams PLR skilimo metu ir didinantys karkasų osteokondukcines savybes[261,263,272,277]. Nors literatūroje yra tyrimų, patvirtinančių, kad kompozitiniai PLR/HA ir PLR/BS 3D karkasai santykiu 9:1 turi teigiamą įtaką kaulų regeneracijos tyrimuose *in vitro* ir *in vivo*[269,276], tačiau yra manoma, kad padidinus neorganinės dalies procentinę dalį kompozitiniuose karkasuose, karkasų osteokondukcinės savybės būtų pagerintos, indukuojant spartesnį naujo kaulo formavimąsi kritinio dydžio defektuose[159,372]. Tolesni tyrimai turėtų įvertinti tikslią DPKL TU charakteristiką, pagerinti karkasų morfologiją ir medžiagų sudėtį, ištirti 3D spausdintų karkasų mechanines savybes ir rezorbcijos greitį. Tai padėtų atsakyti į šio tyrimo metu rastus neapibrėžtumus ir prisidėtų prie audinių inžinerijos pažangos bei dirbtinio kaulinio audinio kūrimo ir tobulinimo.

4. IŠVADOS

1. Remiantis SEM, mikroKT ir porėtumo nustatymo metodų rezultatais, gamykliniai PLR karkasai, atspausdinti „Pharaoh XD“, pasižymėjo statistiškai reikšmingai didesniu tikslumu spausdinant skirtingus karkaso sluoksnius, išlaikant tikslesnius tarpus tarp gijų ir bendrą karkaso aukštį, tikslesnį tūrį ir didesnį porėtumą nei PLR karkasai, atspausdinti „Ultimaker Original“. 3D spausdintuvo parametrai turi įtakos 3D PLR karkasų morfologijai ir tikslumui.

2. Karšto lydymosi ekstruzijos būdu galima pagaminti filamentus iš PLR mikrogranulių, kompozitinius filamentus (9:1 santykiu) iš PLR ir HA, PLR ir BS mikrogranulių. Pagamintų filamentų skersmenys buvo netolygūs ir svyravo nuo 1,28 iki 1,75 mm, tačiau buvo tinkami 3D karkasams gaminti LNM 3D technologija.

3. Kompozitinių 9:1 PLR/BS ir PLR/HA karkasų morfologiniai parametrai statistiškai patikimai nesiskyrė nuo teorinių STL modelio duomenų ir buvo tiek pat tikslūs ar net tikslesni už gamyklinių PLR karkasų, atspausdintų „Pharaoh XD 20“.

4. Remiantis mikroKT rezultatais, PLR/BS karkasų grupėje susiformavo statistiškai reikšmingai daugiau naujo kaulo abiejų lyčių gyvūnuose nei kitose I etapo tiriamosiose grupėse. Kiekybinės histologijos rezultatai parodė, kad PLR/BS ir Bio-Oss grupės turi teigiamą įtaką naujo kaulo formavimuisi, gaunami šių grupių rezultatai yra panašūs ir statistiškai reikšmingo skirtumo nėra. Tačiau naujai susiformavusio kaulo plotas statistiškai reikšmingai besiskiria tarp lyčių visose I etapo tiriamosiose grupėse.

5. Įvertinus mikroKT ir kaulinio audinio histologinio ištyrimo rezultatus II etapo tiriamosiose grupėse, nustatyta, kad PLR/HA TU, PLR/BS DPKL, PLR/BS TU turi teigiamą įtaką naujo kaulo formavimuisi kritinio dydžio defektuose. Gaunami rezultatai yra panašūs į Bio-Oss ir PLR/BS. Kiekybinio kaulinio audinio histologinio ištyrimo rezultatai parodė, kad naujai susiformavusio kaulo plotas statistiškai reikšmingai besiskiria tarp lyčių kompozitiniuose karkasuose, biodekoruotuose DPKL ar jų TU. Remiantis kokybinio kaulinio audinio histologinio ištyrimo duomenimis, tik Bio-Oss, PLR/HA TU ir PLR/BS TU grupėse buvo matomos besiformuojančios atskiros kaulinės salelės, nesusijusios su defektų kraštais. MikroKT ir kiekybinio kaulinio audinio histologinio ištyrimo rezultatai parodė, kad nėra statistiškai reikšmingo skirtumo tarp tos pačios medžiagos osteokondukcinio karkaso ir biodekoruotų konstruktų, nors matomas didesnis naujo kaulo formavimasis kritinio dydžio defektuose.

5. PRAKTINĖS REKOMENDACIJOS IR ATEITIES PERSPEKTYVOS

1. Spausdinant 3D karkasus, skirtus kaulinei regeneracijai, yra svarbu įvertinti, kiek gautas karkasas pagal dimensijas ir porėtumo parametrus atitinka gamybinį (pvz., STL) failą ir, esant statistiškai reikšmingų skirtumų nuo originalių parametrų, pritaikyti STL modelį, atsižvelgiant į dimensines neatitiktis.

2. Tolesni *in vivo* tyrimai turėtų būti atliekami su abiejų lyčių gyvūnais, norint išvengti klaidingo rezultatų interpretavimo.

3. Šio tyrimo rezultatai yra svarbūs kurti ir tobulinti 3D dirbtinį kaulinį audinį „OSSEUM 4D“.

6. PUBLIKACIJŲ SĄRAŠAS

Publikacijos disertacijos tema:

1. Gendviliene I., Simoliunas E., Rekstyte S., Malinauskas M., Zaleckas L., Jegelevicius D., Bukelskiene V., Rutkunas V. Assessment of the morphology and dimensional accuracy of 3D printed PLA and PLA/HAp scaffolds. *J Mech Behav Biomed Mater*. 2020;104:103616. DOI:10.1016/j.jmbbm.2020.103616. https://www.sciencedirect.com/science/article/abs/pii/S1751616119309361?via%3Dihub
2. Gendviliene I., Simoliunas E., Alksne M., Dibart S., Jasiuniene E., Cicenas V., Jacobs R., Bukelskiene V., Rutkunas V. Effect of extracellular matrix and dental pulp stem cells on bone regeneration with 3D printed PLA/HA composite scaffolds. *Eur Cell Mater*. 2021; 41:204-215. DOI: 10.22203/eCM.v041a15. https://www.ecmjournal.org/papers/vol041/vol041a15.php.

Kitos publikacijos:

1. Alksne M., Simoliunas E., Kalvaityte M., Skliutas E., Rinkunaite I., Gendviliene I., Baltriukiene D., Rutkunas V., Bukelskiene V.The effect of larger than cell diameter polylactic acid surface patterns on osteogenic differentiation of rat dental pulp stem cells. *J Biomed Mater Res A.* 2018; 107(1):174-186. DOI: 10.1002/jbm.a.36547. https://onlinelibrary.wiley.com/DOI/10.1002/jbm.a.36547

2. Alksne M., Kalvaityte M., Simoliunas E., Rinkunaite I., Gendviliene I., Locs J., Rutkunas V., Bukelskiene V. In vitro comparison of 3D printed polylactic acid/hydroxyapatite and polylactic acid/bioglass composite scaffolds: Insights into materials for bone regeneration. *J Mech Behav Biomed Mater*. 2020;104:103641. DOI: 10.1016/j.jmbbm.2020.103641. https://www.sciencedirect.com/science/article/abs/pii/S1751616119316613?via%3Dihub
3. Gendviliene I., Legrand P., Nicolielo LFP., Sinha D., Spaey Y., Politis C., Jacobs R. Conservative management of large mandibular dentigerous cysts with a novel approach for follow up: Two case reports. *Stomatologija* 2017; 19 (1):23-32. https://sbdmj.lsmuni.lt/171/171-04.pdf
4. Zaleckas L., Peciuliene V., Gendviliene I., Puriene A., Rimkuviene J. Prevalence and etiology of midfacial fractures: A study of 799 cases. *Medicina*, 2015;51(4):222-227. DOI: 10.1016/j.medici.2015.06.005. https://www.sciencedirect.com/science/article/pii/S1010660X15000506?via%3Dihub.

NOTES

NOTES

Vilniaus universiteto leidykla
Saulėtekio al. 9, III rūmai, LT-10222 Vilnius
El. p.: info@leidykla.vu.lt, www.leidykla.vu.lt
Tiražas 20 egz.